



HAL
open science

Silicon surface passivation and epitaxial growth on c-Si by low temperature plasma processes for high efficiency solar cells

Martin Labrune

► **To cite this version:**

Martin Labrune. Silicon surface passivation and epitaxial growth on c-Si by low temperature plasma processes for high efficiency solar cells. Micro and nanotechnologies/Microelectronics. Ecole Polytechnique X, 2011. English. NNT: . pastel-00611652

HAL Id: pastel-00611652

<https://pastel.hal.science/pastel-00611652>

Submitted on 26 Jul 2011

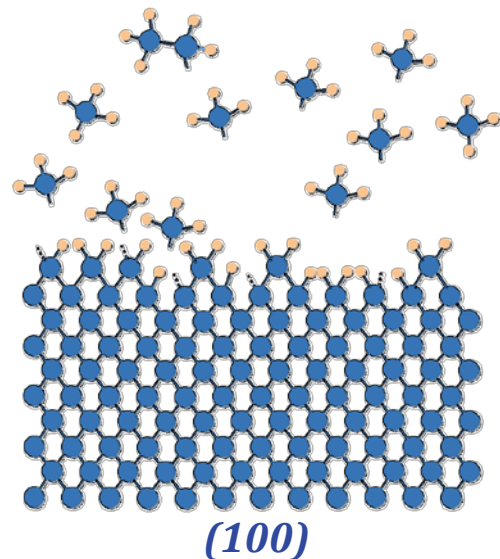
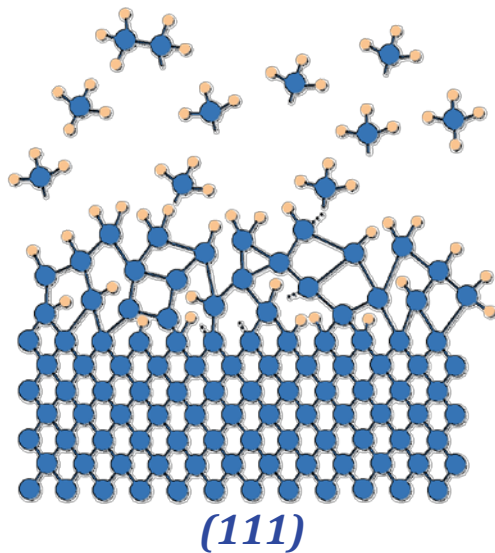
HAL is a multi-disciplinary open access archive for the deposit and dissemination of scientific research documents, whether they are published or not. The documents may come from teaching and research institutions in France or abroad, or from public or private research centers.

L'archive ouverte pluridisciplinaire **HAL**, est destinée au dépôt et à la diffusion de documents scientifiques de niveau recherche, publiés ou non, émanant des établissements d'enseignement et de recherche français ou étrangers, des laboratoires publics ou privés.

Martin Labrune

***Silicon surface passivation and epitaxial growth
on c-Si by low temperature plasma processes
for high efficiency solar cells***

Doctoral thesis in Materials Science





THÈSE

présentée en vue d'obtenir le grade de

Docteur de l'École Polytechnique

Spécialité "Science des Matériaux"

par

MARTIN LABRUNE

martin.labrune@polytechnique.edu

SILICON SURFACE PASSIVATION AND EPITAXIAL GROWTH ON C-SI BY LOW TEMPERATURE PLASMA PROCESSES FOR HIGH EFFICIENCY SOLAR CELLS

Thèse soutenue le 20 Mai 2011 devant le jury composé de :

Prof.	HENRI-JEAN DROUHIN	Président du jury
Prof.	RAMON ALCUBILLA	Rapporteur
Prof.	MUSTAPHA LEMITI	Rapporteur
Prof.	PERE ROCA i CABARROCAS	Directeur de thèse
Dr.	JEAN-PAUL KLEIDER	Examineur
Dr.	LARS KORTE	Examineur
Dr.	VINCENT SCHACHTER	Examineur
Prof.	RICHARD VAN DE SANDEN	Examineur

Ils disent tous: "C'est une rose, ma jolie!"
Je dis : "Elle est tulipe, ma jolie!"
"La rose est belle, la tulipe est belle et jolie;
"Pour une belle avoir cœur dans la beauté, c'est être jolie!"

Omar Khayam

à Marie-Claire, ma jolie

REMERCIEMENTS

CES trois années de thèse se sont déroulées au sein du Laboratoire de Physique des Interfaces et Couches Minces dans lequel j'étais détaché par la R&D solaire de la branche Gaz & Power de Total. À ce titre, je remercie le directeur du laboratoire, Bernard Drévilion qui, par la grâce de sa signature, m'a permis de rester (au moins) 3 années consécutives au LPICM. Je remercie aussi mes premiers interlocuteurs industriels, Philippe Costerg et Gilles Cochevelou, pour m'avoir aidé à rejoindre le groupe. Merci à Marc Vermeersch et Loïc Francke qui furent mes tuteurs industriels. Je remercie également Vincent Schachter pour avoir accepté de faire partie de mon jury et pour avoir toujours prêté une oreille attentive aux doctorants. Je remercie tous les autres membres du jury: Henri-Jean Drouhin, Ramon Alcubilla, Mustapha Lemiti, Lars Korte, Jean-Paul Kleider, Lars Korte et Richard van de Sanden.

Je remercie bien évidemment mon directeur de thèse, Pere Roca i Cabarrocas, qui a rapidement su me faire confiance tout en m'encadrant judicieusement. Je suis et resterai toujours impressionné par sa capacité de travail: il en était presque embarrassant d'être son étudiant! Son intelligence, son intuition et son sens inné des rapports humains m'ont été précieux.

Il convient également de remercier ici un certain nombre de personnes de la confrérie des utilisateurs de l'ARCAM.¹ Outre Pere lui-même, je tiens à saluer Alexey Abramov, qui ne fût pas seulement un excellent collègue de bureau,² amateur de *friggin in the riggin'*, mais qui m'a également transmis les maigres connaissances que j'ai aujourd'hui de la PECVD et du silicium amorphe: une masse de travail et de gentillesse. Il me serait impossible de chiffrer les changements d'électrode ou les pre-coatings dont il m'a dispensé! Je pense aussi à Erik "Vancouver" Johnson,³ Ka-Hyun (aka James) Kim ainsi qu'à Benedict O'Donnell (pour tellement plus encore, notamment d'avoir fait de ce laboratoire un endroit si vivant) et Romain Cariou, qui m'ont tous, à un moment ou un autre, grandement aidé sur ce réacteur. Il ne me semble pas inutile de rappeler que sans Cyril Jadaud ou Garry Rose, à qui je suis infiniment redevable, ce réacteur, qui m'a précédé sur cette planète, ne fonctionnerait pas (du tout). Un grand merci également à Jérôme Charliac pour avoir approvisionné le laboratoire en substrats et microbillé tant d'électrodes.

J'ai une pensée pour tous mes collègues de bureau, outre Alexey. Yasmine Djeridane qui m'a aidé dans mes premiers pas au laboratoire et qui a su conserver en toutes occasions sa bonne humeur, sa sympathie et sa

¹Definitely not a *confederacy of dunces*.

²"from time to time you are joking too much"

³All the leaves are brown and the sky is gray

disponibilité. Laurent Kroely, sérieux, rigoureux, intelligent et drôle, sauf quand il veut fermer la fenêtre... Ning Ning pour sa bonne humeur, sa gentillesse, et ses si charmantes fautes de français. Merci aussi à David Éon qui m'a initié à l'ARCAM et à DeltaPsi2, et qui, en plus, a dû partager son bureau avec moi, et notre ami américain Jonathan "King" Mapel. J'en profite pour remercier Jacqueline Tran qui a toujours réparé cet UVISEL de bonne grâce quand il m'empêchait de m'enfoncer plus avant dans la spirale infernale des dépôts! Merci aussi à ces stagiaires qui ont (plus que) rythmé la vie du laboratoire: Mathieu Boccard,¹ Stefano Granata dont je ne saurais atteindre le dramatisme de ses remerciements, Mun-Ho Song, Ana Klimovic, Lizi George, Xavier Brill, Vincent Loumi, Bon-Min Koo, Romain Mailhes, et d'autres encore.

Bien sûr, sans Laurence Corbel, Chantal Geneste et Carine Roger-Roullin côté LPICM ou bien Christiane Boroniec-Coriou, Valérie Bernier et Myriam Altot côté TOTAL, il n'y a finalement pas grand chose que j'aurais pu faire durant cette thèse. Un grand merci à elles.

Je ne saurai pas ne pas penser à mes "camarades" des "algécos" avec qui j'ai vécu presque deux années, sur notre petit coin de parking, au rythme des saisons, avec qui j'ai appris à choisir mes grosses chaussettes ou à calfeutrer les interstices entre le boîtier de climatisation et la paroi. Plus particulièrement, merci à Antoine Salomon. Merci aussi à Samir Kasout, Ludovic Hudanski, Guillaume Courtois, Jérôme Damon-Lacoste, Patricia Prod'homme et bien sûr Jeff Donut (aka Jean-François Besnier). Enfin, merci aux indispensables Nada Habka et Coralie Charpentier. Merci à Coralie pour m'avoir accordé toute sa sympathie et fait de moi le récepteur de ses inépuisables, mais toujours bienvenues, confidences.

Je resterai longtemps marqué par l'ambiance chaleureuse et internationale qui pouvait régner au LPICM. En vrac, quelques responsables: Maher Oudwan dont l'amitié et la cuisine ne furent jamais mises en défaut, Oumkelthoum Mint Moustapha, Omid Yaghmazadeh, Emmanuel Lefeuvre, Clément Fallet, Evgeny Norman, Mario Moreno (Moreno), Serguey Abolmasov, Nans Pham, Roelene Botha, Jinyoun Cho, Chang Seok Lee, Rosa Antonelli, Marc Chaigneau, Fatima Bouanis, Feng Yang, Alfonso (tcc Poncho) Torres-Rios, Junzhuan Wang et Linwei Yu, Tatiana Novikova et Pavel Bulkin dont je n'oublierai ni la gentillesse, ni la cuisine, ni le vin, ni ses connaissances en plasma, pompes, physique, et sans doute plein d'autres domaines que je n'ai pas eu le temps de découvrir, Dmitri Daineka, Enric Garcia-Caurel, Laurent Baraton, Aurélien Gohier, Kenji Hirata et Emi Sugimura, Denis Tondelier, Yvan Bonnassieux, Aurélien Gohier, Bicher Haj Ibrahim, Joaquim Nassar, Veinardi Suendo, François Moreau, Holger Vach, Frédéric Farci et ses dessins et ses pièces, Eric Paillassa, Frédéric Liège, Rachida Boubekri, Parsathi Chatterjee, Jean-Eric Bourrée, et toutes celles et ceux que j'ai malencontreusement oubliés.

Bien sûr je pense aussi à toutes les personnes que j'ai rencontrées lors de projets ou qui m'ont toutes aidé à un moment ou à un autre: Isidro Martin, Delfina Muñoz, Thibaut Desrues, Aurélie Vandeneynde, Christine Denis, Yannick Veschetti, Pierre-Jean Ribeyron, Wilfried Favre, Djicknoum

¹ Ces blind tests et ces courses échevelés vers le Sinton du LGEP... Merci!

Diouf, Rémy Chouffot,¹ François Jomard (indispensables SIMS), Gilles Patriarche (impeccables TEM), Ludovic Largeau (XRD), Jacques et Jonathan Méot (entre autres, gracieux dépôts d'ITO).

Enfin je veux remercier ici mes amis, ma famille et Marie-Claire, qui m'ont en tous points soutenu tout au long de cette thèse. Merci à Linna Bun, Alexandre Bredimas, Diane Chan, Damien Devillers, Etienne Espagne, Damien Granger, Sylvie Lam Macé, Romain Nguyen, François Rosenberg (ça inclut Julie, Marie et P.E.R.), Martin Du Vachat, et pour tous ces papiers demandés, un gros merci à Antoine "Berkeley" Hervier et Véronique "Harvard" Izard.

¹ J'ai beaucoup appris de lui et regretterai longtemps encore de ne pas avoir eu son manuscrit sous la main pendant ma thèse...

CONTENTS

CONTENTS	viii
LIST OF FIGURES	ix
LIST OF TABLES	xv
LIST OF ACRONYMS	xvii
INTRODUCTION	1
REFERENCES	5
1 BASICS OF PHOTOVOLTAICS	9
1.1 Solar energy	10
1.1.1 Solar spectrum	10
1.2 Semiconductor principles involved in PV	12
1.2.1 Electrons and holes in the dark	13
1.2.2 Quasi-Fermi level distributions	14
1.2.3 Transport	15
1.2.4 Junctions	17
1.3 Crystalline silicon (c-Si)	20
1.3.1 Lifetimes in c-Si	20
1.4 Hydrogenated amorphous silicon (a-Si:H)	26
1.5 Indium Tin Oxide (ITO)	28
1.6 Conclusions	30
REFERENCES	33
2 EXPERIMENTAL — THEORETICAL	37
2.1 Fabrication and characterisation of thin films and solar cell precursors	38
2.1.1 Heterojunction solar cell	38
2.1.2 Plasma enhanced chemical vapour deposition (PECVD)	41
2.1.3 Thermal evaporation	48
2.1.4 Spectroscopic ellipsometry (SE)	49
2.1.5 Effective lifetime measurements	54
2.2 Surface passivation	57
2.2.1 Theoretical point of view	57
2.2.2 Practical point of view	58
2.3 Physics of heterojunction solar cells	61
2.3.1 Interest, drawbacks	61
2.3.2 Band offsets	61

2.3.3	Intrinsic layer	64
2.3.4	Doped layers	66
2.3.5	ITO contact	67
2.4	Conclusions	68
REFERENCES		69
3	AMORPHOUS/CRYSTALLINE HETEROJUNCTION SOLAR CELLS	81
3.1	Undoped layer : avoiding epitaxy	82
3.1.1	Low temperature approach	83
3.1.2	Plasma treatments	88
3.1.3	The alloy way	92
3.2	Doped layers	100
3.2.1	Passivation	100
3.2.2	Light soaking	107
3.2.3	Annealing	111
3.3	Heterojunction solar cells	114
3.3.1	Intrinsic layer	115
3.3.2	p-type layers	118
3.4	Inside and outside collaborations on heterojunctions	121
3.4.1	Multicrystalline silicon wafers	121
3.4.2	Plasma cleaning	125
3.4.3	Laser Fired Contacts (LFC)	129
3.5	Conclusions	134
REFERENCES		137
4	EPITAXY	147
4.1	Undoped and doped silicon thin films	148
4.1.1	Precedents in RF PECVD	149
4.1.2	Early results	150
4.1.3	Does someone know what happens ?	157
4.1.4	Intrinsic epitaxy: towards a wafer equivalent approach	162
4.1.5	Epitaxial growth of doped layers	168
4.2	Germanium films	176
4.2.1	Precedents	177
4.2.2	Preliminary studies	178
4.2.3	Multilayer samples	179
4.3	Conclusions	188
REFERENCES		189
CONCLUSION		197
LIST OF PUBLICATIONS		199

LIST OF FIGURES

1	World cumulative photovoltaic power installed, from Ref. [3]	2
2	Solar cell technology shares in 2010, from PHOTON (March 2011)	3
1.1	AM0 and AM1.5 spectral irradiance as well as the maximum energy for different absorbing materials	10
1.2	Best research solar cell efficiencies plotted against time for various PV technologies	12
1.3	Electron affinity (χ) and work function (ϕ) of a semiconductor	14
1.4	Electron and hole distributions after thermalization Ref. [10]	15
1.5	Band diagrams of metal ohmic contacts with n-type (left) and p-type (right) semiconductor materials	17
1.6	Band diagrams of metal Schottky contacts with n-type (left) and p-type (right) semiconductor materials	17
1.7	Schematic band diagram of a pn homojunction made of crystalline silicon	18
1.8	Electrical model used to described an illuminated diode . .	19
1.9	Typical current-voltage characteristic of a heterojunction solar cell	20
1.10	Radiative recombination in a semiconductor	21
1.11	Auger recombination in a semiconductor	22
1.12	Four possible interactions between charge carriers and a defect. For electrons we can have trapping (1) or detrapping (2). For holes we can have trapping (3) or detrapping (4) . .	23
1.13	Radiative, Auger and SRH recombination lifetimes plotted against the excess carrier density. The resulting bulk lifetime is also plotted	25
1.14	Example of the a-Si:H network	27
1.15	Density of states of a-Si:H (from Ref. [27])	27
1.16	Transmission spectra of ITO films deposited on glass substrate for various oxygen (in argon) flow rates. We also plotted the transmission spectrum of a bare glass substrate for a more comprehensible comparison	31
1.17	Resistivity and Hall mobility of ITO films deposited on glass substrate plotted against the Ar+O ₂ flow rate	31
2.1	Comparison of the structure of the PERL and standard heterojunction solar cell	38
2.2	Reflectance of a bare flat c-Si wafer, of a 80 nm ITO film on flat c-Si wafer and of 80 nm of ITO on a textured c-Si wafer	40

2.3	Completed solar cells when a screen-printed grid (left) from INES or an evaporated silver grid (right) from LPICM was applied.	41
2.4	Picture of the opened ARCAM reactor	42
2.5	Schematic view of the plasma box used in the ARCAM reactor	43
2.6	Schematic view of the potential distribution in a RF discharge where the substrate is grounded and the RF voltage applied to the RF electrode	44
2.7	Schematic views of the SiH_4 dissociation and plasma reactions involved in a-Si:H depositions	45
2.8	Schematic representation of the surface reactions involved during the growth of a-Si:H in the MGP model where the SiH_3 radical is the only growth precursor.	46
2.9	Schematic view of the thermal evaporator	49
2.10	Picture of the UVISEL based at LPICM	49
2.11	Schematic view of the phase modulated ellipsometers From http://www.horiba.com	50
2.12	Imaginary part of the dielectric function of hydrogenated amorphous silicon, small and large grain polysilicon and monocrystalline silicon	51
2.13	Imaginary part of the pseudo-dielectric functions of a typical a-Si:H layer on c-Si (grey line), an epitaxial Si film on c-Si (green squares), the fit of the epitaxial film (red line) and a crystalline silicon wafer (black line)	53
2.14	Imaginary part of the pseudo-dielectric functions of the measurement of an epitaxial film, the modelled stack and of a c-Si wafer, zoomed in the low photon energy part of the spectrum	53
2.15	Picture of the WCT-120 Sinton based at LPICM	55
2.16	Schematic band diagram of the heterojunction solar cell on a (n) c-Si wafer. The different energy levels are not at scale.	62
3.1	Effective lifetimes in (n) c-Si wafers passivated by a (i) a-Si:H layer with buffer epitaxial layer of various thicknesses . . .	83
3.2	Defect density and atomic hydrogen content of a-Si:H films as a function of the deposition temperature [9]	84
3.3	Effective lifetime at 1 sun in symmetrical BSF structures on (n) c-Si with or without a buffer layer made of an amorphous or a polymorphous undoped layer. As a reference we also show the result obtained by a thick and symmetrical layer of 40 nm of (i) a-Si:H	86
3.4	Effective lifetime at 1 sun in symmetrical emitter structures on (n) c-Si with or without a buffer layer made of an amorphous or a polymorphous undoped layer.	87
3.5	Effective lifetimes at 1 sun illumination of symmetrical emitters deposited on (n) c-Si wafers at different substrate temperatures (150, 175 and 200°C) plotted against the annealing temperature	89

3.6	Current-voltage characteristics of small solar cells on (n) c-Si using emitters deposited at low temperature after a short NH ₃ plasma treatment, in the as deposited state and after successive annealings at different temperatures	90
3.7	Effective lifetimes various BSF stacks deposited on (111) or (100), with or without argon plasma treatment	91
3.8	Effective lifetimes in symmetrical samples deposited at 200°C on (100) with different CH ₄ gas presence time during the deposition	94
3.9	Ellipsometric spectra of the samples deposited with the presence of CH ₄ during the following times: 15", 30", 1'30" and 10'	95
3.10	Effective lifetimes of symmetrical samples deposited at 200°C on (111) and (100) orientations with different dilutions and in the presence or not of CH ₄	97
3.11	Effective lifetimes of symmetrical samples deposited at 200°C on (111) orientation from SiH ₄ , SiH ₄ +H ₂ and SiH ₄ +Ar	99
3.12	Imaginary part of the pseudo-dielectric function of a (n) a-Si:H layer grown in the same conditions on (100) for sample 1001209 and on (111) for sample 1002177, and of a (i)+(n) a-Si:H stack.	101
3.13	Effective lifetime in symmetrical samples on (n) c-Si consisting of two (n) a-Si:H layers grown in the same conditions on (111) c-Si for sample 1001209 and on (111) for sample 1002177 and of a different (i)+(n) a-Si:H stacks	102
3.14	Effective lifetime from (p) and (i)+(p) a-Si:H passivation stacks grown under various conditions detailed in the text and in Tab. 3.7	103
3.15	Imaginary part of the pseudo-dielectric function of (i) a-Si:H + (p) μc-Si:H stacks with different deposition times for both layers on (100) c-Si substrates.	106
3.16	Imaginary part of the pseudo-dielectric function of (i) a-Si:H + (p) μc-Si:H stacks deposited entirely at 175°C, or with the i-layer at 200°C and the p-layer at 175°C. The SiH ₄ flow rate is indicated in the legend.	107
3.17	Effective lifetimes in all the (i) a-Si:H + (p) μc-Si:H stacks	108
3.18	Effective lifetime at 10 ¹⁵ cm ⁻³ in a symmetrical sample passivated by a 22 nm (i) a-Si:H layer as a function of time	110
3.19	Effective lifetime at 10 ¹⁵ cm ⁻³ of a symmetrical sample passivated by a 15 nm (i)+(p) a-Si:H stack as a function of time	111
3.20	Effective lifetime at 10 ¹⁵ cm ⁻³ of a symmetrical sample passivated by a 15 nm (i)+(n) a-Si:H stack as a function of the light soaking time	112
3.21	Effective lifetimes in symmetrical (i/n) and (i/p) stacks for various consecutive micro-wave annealing times.	113
3.22	Atomic concentrations in the (i/n) and (i/p) stacks, in their as-deposited or final annealed state as a function of depth as obtained by SIMS	113
3.23	Current-voltage characteristic of our best in-house 4 cm ² solar cell measured with or without a shadow mask	115

3.24	Open-circuit voltage and short-circuit current density plotted against the deposition time for the (i) a-Si:H layer	116
3.25	Current-voltage characteristics in the dark of heterojunction solar cells with various (i) a-Si:H thicknesses	117
3.26	Current-voltage characteristics of silicon heterojunction solar cells obtained during this doctoral work.	120
3.27	Effective lifetimes in solar cell structures deposited on various mono and multicrystalline wafers	122
3.28	SEM picture of a HETSI mc-Si sample	124
3.29	μ W-PCD mapping of the effective lifetime in monocrystalline (left) and multicrystalline (right) silicon substrates capped by a thick (i) a-Si:H layer. Note the difference in the colour scales	125
3.30	Effective lifetimes in symmetrical samples with 20 nm of a-Si:H for various powers and durations of SiF ₄ etching plasma.	128
3.31	Schematic view of the future Laser Fired Contacts solar cell structure before the laser firing of the thick dielectric back surface passivation layer	130
3.32	Schematic view of the Laser Fired Contacts solar cell structure after the laser firing of the thick dielectric back surface passivation layer	130
3.33	Effective lifetimes in the heterojunction and LFC samples measured in the as-deposited state, before any ITO deposition or laser firing	131
3.34	V _{oc} and FF of the solar cells as a function of the pitch value for the 0.8 Ω .cm wafers (closed symbols) and for the 1–5 Ω .cm (open symbols). HJ refers to the full heterojunction sample	132
3.35	External quantum efficiency of the samples made on 0.8 Ω .cm wafer for a full heterojunction and for LFC samples with pitches of 0.4, 0.7, 1 and 1.5 mm.	133
3.36	Electro-luminescence of a LFC solar cell on a 0.8 Ω .cm wafer	133
4.1	Optically polished multicrystalline silicon samples on which we used two different plasma conditions known to lead to amorphous silicon	150
4.2	Imaginary part of the pseudo-dielectric function of silicon thin films co-deposited on various substrates (111) Si, (100) Si and Corning glass	151
4.3	Imaginary part of the pseudo-dielectric functions of Si stacks deposited at 200°C on (111) and (100) wafers, consisting of a first layer deposited in the conditions of pm-Si:H and of a second layer deposited in the condition of a-Si:H from pure silane (red) or from a silane+hydrogen gas mixture. We also plotted the dielectric function of a crystalline silicon wafer (black line)	153
4.4	Imaginary part of the pseudo-dielectric functions of films deposited in H ₂ dilution at 100°C (red squares) and at room temperature (RT) (blue triangles), or in pure SiH ₄ at 100°C (green circles), and a crystalline silicon wafer (black line)	154

4.5	SIMS profiles of H atoms along silicon thin films grown on (111) and (100), with or without a 2' H ₂ plasma treatment. Films on (100) are epitaxial in both cases, films on (111) are amorphous.	156
4.6	H concentration from SIMS along silicon thin films grown on (111) and (100) for which the $\frac{H_2}{SiH_4+H_2}$ ratio varied (unintentionally) during the deposition from 80% to 0%.	156
4.7	On the left, regrowth rate of an amorphous silicon on crystalline silicon at 550°C as a function of the crystalline orientation of the a-Si/c-Si interface. On the right, section looking down the [01 $\bar{1}$] axis in Si. Indices denote intersections of the named plane with the [01 $\bar{1}$] plane. Assuming atoms can be transferred from the amorphous to crystalline phase at positions where at least two nearest-neighboring atoms are already in crystalline positions, the atoms marked A will occupy the crystalline position first, then B, C, etc. Images and legends from Ref. [48]	160
4.8	Si atoms in the unit cell of the diamond lattice in (100), left, or (111) positions for two alternate planes and the possible bonds perpendicular to these planes.	161
4.9	Imaginary part of the pseudo-dielectric function of epitaxial films grown with different SiH ₄ flow rates, close-up view in the photon energy range of interest for crystalline films . . .	164
4.10	Maximum of the pseudo-dielectric function and deposition rate plotted against the SiH ₄ flow rate	166
4.11	Maximum of the pseudo-dielectric function and percentage of monocrystalline silicon in the model of the bulk layer plotted against the SiH ₄ flow rate	166
4.12	Schematic view of the structure of the epitaxial cells we used	167
4.13	Current-voltage characteristics of epitaxial solar cells deposited at 165°C with different base thicknesses	167
4.14	Imaginary part of the pseudo-dielectric function of silicon thin films grown on (100) Si substrates for various flow rates for B ₂ H ₆ . We added the pseudo-dielectric function of the film grown without dopant (undoped) and the dielectric function of silicon for comparison	169
4.15	Imaginary part of the pseudo-dielectric function of silicon thin films grown on (100) Si substrates for various substrate temperatures at fixed flow rates for B ₂ H ₆ and TMB (B(CH ₃) ₃). We added the pseudo-dielectric function of the film grown without dopant (undoped) and the dielectric function of silicon for comparison	170
4.16	Carrier concentration and mobilities as a function of the sample temperature as deduced from Hall effect measurements for epitaxial films grown at various substrate temperatures and at fixed flow rates for B ₂ H ₆ and TMB (B(CH ₃) ₃).	171
4.17	Current-voltage of our homojunction and heterojunction solar cell	173

4.18	Imaginary part of the pseudo-dielectric function of silicon thin films grown on (100) Si substrates with various PH ₃ flow rates. We added the pseudo-dielectric function of the film grown without dopant (undoped) and the dielectric function of silicon for comparison	174
4.19	Carrier concentration and mobilities as a function of the sample temperature as deduced from Hall effect measurements from several PH ₃ flow rates	175
4.20	Raman spectra around the 300 cm ⁻¹ of Ge films deposited at two different GeH ₄ flow rate on (100) Si and Corning Glass.	178
4.21	Imaginary part of the pseudo-dielectric function of Ge films grown on (100) Si substrates under different process conditions.	179
4.22	Imaginary part of the pseudo-dielectric function of the Ge/Si stack co-deposited onto various substrates as deduced from SE measurements, the black line corresponds to the fits obtained by modelling the stack deposited on the (100) Si and (111) Si substrates using the optical model described in Tab. 4.7 on (100) Si or in Tab. 4.8 for (111) Si	180
4.23	Raman scattering intensity of the Ge/Si stack co-deposited on (100) Si and (111) Si	182
4.24	Imaginary part of the pseudo-dielectric function of the multi layer stack co-deposited onto various substrates as deduced from SE measurements, the black line corresponds to the fit obtained by modelling the stack deposited on the (100) Si substrate using the optical model described in Tab. 4.9	183
4.25	Raman scattering intensity as a function of the Raman shift for the multi layer samples (905071) co-deposited on various substrates ((100) GaAs, (100) Si and (111) Si)	184
4.26	TEM image of the Ge/Si/Ge/Si stack grown on (100) GaAs	186
4.27	HRTEM images of the Ge ₁ /Si ₂ /Ge ₂ /Si ₂ stack on (100) GaAs at different interfaces	186
4.28	HAADF STEM image of the Si ₁ /Ge ₂ /Si ₂ interfaces	187
4.29	SIMS profiles of Si, Ge, C and O against the sputtering time	187

LIST OF TABLES

1.1	Electron and hole densities in n and p-type semiconductors (in the dark)	13
2.1	Optical model used to describe an a-Si:H film on a c-Si substrate: it consists of a semi-infinite substrate with a bulk layer of a-Si:H and a surface roughness.	52

3.1	Description and passivation results of various BSF stacks deposited on (111) and (100), with or without an argon plasma treatment	91
3.2	Description of different layers deposited at 200°C on (100) with different CH ₄ gas presence time during the deposition	93
3.3	SE model of the sample deposited with 15" presence of CH ₄	95
3.4	Description of different layers deposited at 200°C on (111) and (100) orientations with different dilutions and in the presence or not of CH ₄ gas	96
3.5	Optical parameters of the a-Si:H layers deposited in various hydrogen dilution on c-Si wafers from pure silane and hydrogen gas mixture (upper part) or with the presence of methane at the beginning of the deposition (lower part).	97
3.6	Description of different layers deposited at 200°C on (111) and (100) orientation from SiH ₄ , SiH ₄ +H ₂ and SiH ₄ +Ar	99
3.7	Description of (p) and (i)+(p) a-Si:H stacks and their passivation properties at 1 sun. Unless stated the power of the plasma was 1 Watt, the substrate temperature set at 200°C and no H ₂ was used for the deposition.	103
3.8	Solar cell parameters of heterojunction solar cells with various (i) a-Si:H thicknesses indicated by their deposition time	116
3.9	One diode model parameters of heterojunction solar cells with various (i) a-Si:H thicknesses indicated by their deposition time.	118
3.10	Solar cell parameters of heterojunction solar cells with various (i) and (p) a-Si:H thicknesses indicated by their deposition time	118
3.11	Best solar cells obtained on flat c-Si wafers, of p and n-type	120
3.12	Solar cell parameters on (n) mc-Si substrates of different surface states on 25 cm ² , thin (i) a-Si:H series	123
3.13	Solar cell parameters on (n) mc-Si substrates of different surface states on 25 cm ² , thick (i) a-Si:H series	123
3.14	Solar cell parameters of two cells whose native oxide was removed by a SiF ₄ plasma etching.	128
3.15	Implicit V _{oc} of the heterojunction and LFC samples measured in the as-deposited state, before any ITO deposition or laser firing step	131
3.16	Efficiencies comparison between the full heterojunction and the best LFC solar cell made on 0.8 Ω.cm wafers	134
4.1	Deposition conditions of Si films deposited at low substrate temperatures	153
4.2	Sample name and corresponding flow rate of the B ₂ H ₆ series	168
4.3	Sample name and corresponding growth temperature of the Boron-doping series	170
4.4	Sample name and corresponding flow rate of the PH ₃ series	173
4.5	Process parameters for different Ge films grown on (100) Si, (111) Si and Glass	178
4.6	Plasma conditions used to grow Ge and Si epitaxial film, at 175°C	180

4.7	SE model of the Ge/Si stack deposited on the (100) Si wafer	180
4.8	SE model of the Ge/Si stack deposited on the (111) Si wafer	181
4.9	SE model of the multilayer stack deposited on the (100) Si and GaAs wafers	183

LIST OF ACRONYMS

Acronym		Unit
a-Si:H	hydrogenated amorphous silicon	
a-SiC:H	hydrogenated amorphous silicon carbide	
a-SiN:H	hydrogenated amorphous silicon nitride	
BSF	Back Surface Field	
c-Si	monocrystalline Silicon	
c-Ge	monocrystalline Germanium	
E_F	Fermi level energy	eV
E_{FC}	quasi Fermi level energy for electrons	eV
E_{FV}	quasi Fermi level energy for holes	eV
E_g	optical bandgap energy	eV
E_i	intrinsic Fermi energy	eV
FF	fill factor	%
HWCVD	Hot Wire Chemical Vapor Deposition	
ITO	Indium Tin Oxide (Tin doped Indium Oxide)	
J_{sc}	short-circuit current	mA.cm ⁻²
MBE	Molecular Beam Epitaxy	
μc-Si:H	hydrogenated microcrystalline silicon	
μ_h	hole mobility	cm ⁻² .V ⁻¹ .s ⁻¹
μ_n	electron mobility	cm ⁻² .V ⁻¹ .s ⁻¹
mc-Si	multicrystalline silicon	
nc-Si:H	hydrogenated nanocrystalline silicon	
PECVD	Plasma Enhanced Chemical Vapor Deposition	
pm-Si:H	hydrogenated polymorphous silicon	
PV	Photovoltaics	
R_S	series resistance	Ω.cm ²
R_{Sh}	shunt resistance	Ω.cm ²
SE	Spectroscopic ellipsometry	
SEM	Scanning electron microscopy	
SIMS	Secondary Ion Mass Spectrometry	
sccm	standard cubic centimeter per minute	cm ³ .min ⁻¹
S_{rec}	surface recombination velocity	cm ² .s ⁻¹
STEM	Scanning Electron Microscopy	
τ_{eff}	effective lifetime	s
TEM	Transmission Electron Microscopy	
V_{oc}	open-circuit voltage	mV
Impl. V_{oc}	implicit open-circuit voltage	mV

INTRODUCTION

OUR world is growing faster and faster and so is its energy demand. In 2010, the annual world consumption has reached more than 5×10^{20} J and is expected to have increased by 25% or 50% by 2035, depending on the policy scenario chosen.¹ To address such a growing demand, exhausting all available fossil fuels is a possible option, that seems now unavoidable since many countries rely on them for heating and electricity production and since no other energy vector could successfully be implemented for transports. However, even if such an exhaust is very likely to occur, due to the forthcoming peak-oil,² it is neither wise nor perennial. Indeed, it will be very difficult to rely exclusively on fossil fuels to meet our needs in terms of transports, plastic elaboration, etc, since these fossil fuels resources, that we have depleted in less than two centuries, would need a few hundred million years to form.

Even though nuclear energy may appear as an attractive alternative way to be independent from conventional fossil fuels in terms of electricity production, it should be remembered that such a technology suffers from several major drawbacks: uranium itself is in limited amount, handling nuclear wastes remains an issue, and safety issues are consubstantial to it. Besides, it is not adapted to every country since it cannot be implemented in rural situations where a decentralized production makes more sense.

Most renewable energies can provide a decentralized production. Among them, solar energy conversion has the advantage of being possibly implemented in both centralized (plants) and decentralized (roofs, etc) production centers. Within solar energy field, photovoltaic energy is the one used to convert light from the sun into electricity. On the one side, silicon, the base material of most solar cell technologies is one of the most abundant materials of the Earth's crust. On the other side, the annual solar irradiation received at the surface of the Earth can provide a lot more energy than the global annual consumption. One may question about the energy payback time of photovoltaic modules. It is now about 1.5 year and always shorter than 3 years: it depends a little on the technology used to fabricate the cells of the module and also on the illumination level, e.g. middle or south of Europe.³ Therefore, in this frame, photovoltaic energy conversion is a valid candidate. This is confirmed

¹, *World Energy Outlook, 2010* [1]

²Such a peak oil is ill-defined in time since the amount of recoverable fossil fuels, by definition limited, depends the available resources but also on the demand, or in other words the costs at which oil companies will extract oil profitably. Both constraints are ill-defined and hard to predict, even if for the most pessimistic "predictions" it has already occurred.

³Alsema, de Wild-Scholten, and Fthenakis, "Environmental impacts of PV electricity generation - a critical comparison of energy supply options", 2006 [2]

by the interest it has gained over the last decade. Indeed, Fig. 1 shows the world cumulative photovoltaic power installed. Over the last decade

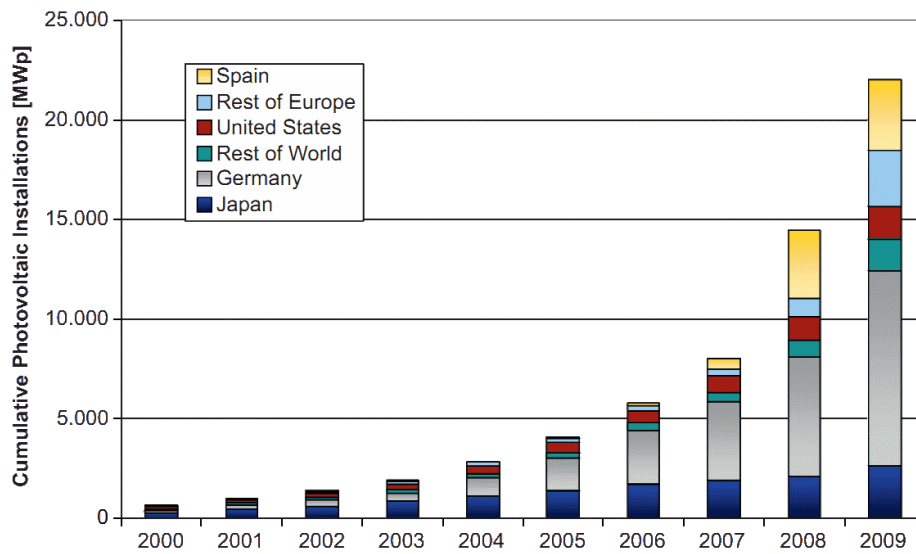


Figure 1 – World cumulative photovoltaic power installed, from Ref. [3]

this market has exhibited an exponential growth and most predictions confirm this tendency, with various exponential coefficients, for the next years [3]. Before 2000, the market was very small, quiet, and increased very slowly, even though it was already a proven technology. Indeed, the photovoltaic effect is generally considered to originate from the early experimental observations by *Alexandre-Edmond Becquerel* in 1839. After these first experimental observations, many researchers have worked, directly or not, on such an effect,¹ but it was not before 1954 that the Bell laboratories designed a photovoltaic device based on a crystalline silicon p-n junction with an efficiency of about 6%.² Continuous efforts devoted to the optimization of crystalline silicon solar cells allowed laboratories to reach a 25% efficiency,³ close to the theoretical maximum for this material in the 29% range.⁴ Crystalline silicon technology is often referred to as the “first generation” of solar cells. Huge progress has been made in increasing the efficiency but also in terms of costs’ reduction. Meanwhile, the “second generation” which refers to thin film technologies has gained in importance. The “third generation”, is often associated with technological and scientific breakthroughs and thus is still at the laboratory scale. Fig. 2 shows the different technology shares in 2008. It shows that the “first generation”, which includes all the crystalline silicon materials, represents more than 87% of the market shares, even if thin-film modules are increasing faster.

The need for a diversification and the attractiveness of such a growing market has led many oil companies to invest in photovoltaic manufac-

¹Petrova-Koch, “Milestones of Solar Conversion and Photovoltaics”, 2009 [4]

²Chapin, Fuller, and Pearson, “A New Silicon p – n Junction Photocell for Converting Solar Radiation into Electrical Power”, 1954 [5]

³Green, Emery, Hishikawa, and Warta, “Solar cell efficiency tables (version 36)”, 2010 [6]

⁴Shockley and Queisser, “Detailed Balance Limit of Efficiency of p – n Junction Solar Cells”, 1961 [7]

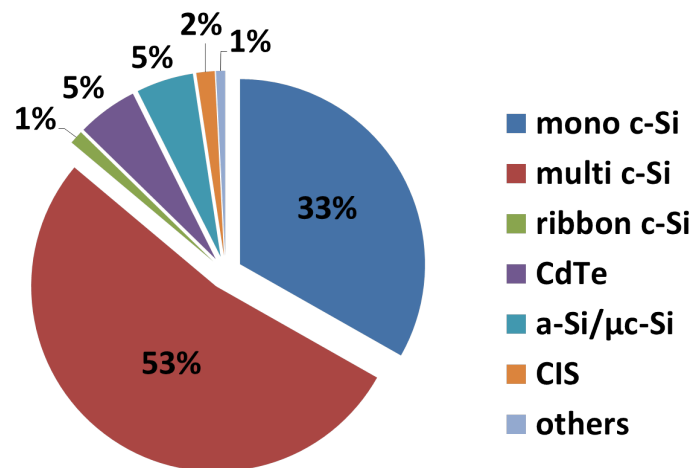


Figure 2 – Solar cell technology shares in 2010, from PHOTON (March 2011)

turers, if not directly into research on photovoltaic energy. Among them, TOTAL S.A.¹ showed some interest in thin-film technology based on amorphous silicon as well as on heterojunction solar cells. Therefore they decided, in the frame of a 3-year French “Cifre” contract which involves the financial partnership of the ANRT association,² to fund this doctoral work, from March 2008 to the end of February 2011.

This thesis was partly devoted to the study of amorphous/crystalline (a-Si:H/c-Si) silicon heterojunction solar cells. Such a technology does not fit into a well-defined technology generation since it combines crystalline materials with thin films. In such solar cells, the absorber material is a crystalline wafer whereas the surface passivation and the junction are formed during the deposition of doped amorphous silicon layers. The main challenge is to obtain a good diode while minimizing the number of interface defect states. The motivation for such a work came from the validation of this concept by the Japanese corporation Sanyo, which has been able to fabricate and commercialize efficient modules based on this technology. They started in the early 90’s to develop such structures on (n) c-Si,³ starting from efficiencies in the 10% range to reach a 23% efficiency.^{4,5} The key point to achieve both goals at the same time is to insert a very thin (< 5 nm) undoped a-Si:H layer in order to decrease the interface defect density, the reason for such high open-circuit voltages (≥ 730 mV). Such a concept started to attract a lot of attention during the last decade and many PV research groups started to work on such structures, on p and n-type c-Si wafers: LPICM [11], HZB [12], NREL [13, 14], IMT [15, 16], INES [17], AIST [18], Fraunhofer ISE [19], and many others not cited

¹<http://www.total.com/en/home-page-940596.html>

²<http://www.anrt.asso.fr/>

³Tanaka, Taguchi, Matsuyama, Sawada, Tsuda, Nakano, Hanafusa, and Kuwano, “Development of New a-Si/c-Si Heterojunction Solar Cells: ACJ-HIT (Artificially Constructed Junction-Heterojunction with Intrinsic Thin-Layer)”, 1992 [8]

⁴Tsunomura, Yoshimine, Taguchi, Baba, Kinoshita, Kanno, Sakata, Maruyama, and Tanaka, “Twenty-two percent efficiency HIT solar cell”, 2009 [9]

⁵Mishima, Taguchi, Sakata, and Maruyama, “Development status of high-efficiency HIT solar cells”, 2011 [10]

here. Our laboratory had already started to study this topic [20, 21], but it was only devoted to p-type c-Si whereas we will here report mostly on n-type silicon materials, including multicrystalline wafers. Many texturing and cleaning processes, materials and structures have been investigated and a lot has been understood. As it can appear from the above list, many groups are involved and some collaborations exist. Indeed, this work has been done within a few collaboration programs with supports from the French Agence Nationale de la Recherche (ANR) (PHARE, polySiverre, QC-Passi, MULTIXEN, SolarNanocrystal) or from the European Commission (HETSI).

Another part of this doctoral work was devoted to the investigation of the epitaxial growth of silicon (and germanium) on (100) silicon substrates, a side-effect for heterojunction solar cells, that could be exploited for photovoltaic applications.

In this manuscript, the **first chapter** will introduce the most useful concepts of solid state physics needed to describe and understand the physical phenomena involved in solar cells: Fermi and quasi Fermi levels, doping, contacts and junctions. The semiconductor materials used during this work will also be introduced and described with respect to their optical and electrical properties, such as crystalline silicon (c-Si), hydrogenated amorphous silicon (a-Si:H) and indium tin oxide (ITO). The **second chapter** will introduce and describe the structure of the heterojunction solar cell itself. The band diagram and its specificities with respect to conventional crystalline silicon homojunction solar cells will be discussed. The surface passivation will also be discussed and the conventional passivation scheme introduced. Also, the experimental process will be presented and the experimental set-ups dedicated to the elaboration and the characterisation of the materials or devices will be described such as Spectroscopic Ellipsometry (SE), Plasma Enhanced Chemical Vapour Deposition (PECVD) and effective lifetime measurements (Sinton lifetime tester based on photoconductance decay). The **third chapter** presents and discusses the results obtained in terms of surface passivation and solar cell efficiency. The **fourth chapter** deals with the epitaxial growth of silicon and germanium thin films on (100) c-Si substrates and its investigation by Raman spectroscopy, Spectroscopic Ellipsometry, TEM, and their application to several photovoltaic devices.

REFERENCES

- [1] *World Energy Outlook*. International Energy Agency, 2010. ISBN: 978-92-64-08624-1 (cit. on p. 1).
- [2] E.A. Alsema, M.J. de Wild-Scholten, and V.M. Fthenakis. "Environmental impacts of PV electricity generation - a critical comparison of energy supply options". In: *21st European Photovoltaic Energy Conference, Dresden*. 2006 (cit. on p. 1).
- [3] Arnulf Jäger-Waldau. *PV Status Report 2010*. Tech. rep. European Commission, Joint Research center, 2010. DOI: 10.2788/87966 (cit. on p. 2).
- [4] V. Petrova-Koch. "Milestones of Solar Conversion and Photovoltaics". In: *High-Efficient Low-Cost Photovoltaics*. Ed. by Vesselinka Petrova-Koch, Rudolf Hezel, and Adolf Goetzberger. Vol. 140. Springer Series in Optical Sciences. Springer Berlin / Heidelberg, 2009, pp. 1–5. DOI: 10.1007/978-3-540-79359-5_1 (cit. on p. 2).
- [5] D. M. Chapin, C. S. Fuller, and G. L. Pearson. "A New Silicon $p - n$ Junction Photocell for Converting Solar Radiation into Electrical Power". In: *Journal of Applied Physics* 25 (1954), pp. 676–677. DOI: 10.1063/1.1721711 (cit. on p. 2).
- [6] M. A. Green, K. Emery, Y. Hishikawa, and W. Warta. "Solar cell efficiency tables (version 36)". In: *Progress in photovoltaics: Research & applications* 18 (2010), p. 346. DOI: 10.1002/pip.1021 (cit. on p. 2).
- [7] W. Shockley and H. J. Queisser. "Detailed Balance Limit of Efficiency of $p - n$ Junction Solar Cells". In: *Journal of Applied Physics* 32 (1961), pp. 510–519. DOI: 10.1063/1.1736034 (cit. on p. 2).
- [8] M. Tanaka, M. Taguchi, T. Matsuyama, T. Sawada, S. Tsuda, S. Nakano, H. Hanafusa, and Y. Kuwano. "Development of New a-Si/c-Si Heterojunction Solar Cells: ACJ-HIT (Artificially Constructed Junction-Heterojunction with Intrinsic Thin-Layer)". In: *Japanese Journal of Applied Physics* 31 (1992), pp. 3518–3522. DOI: 10.1143/JJAP.31.3518 (cit. on p. 3).
- [9] Y. Tsunomura, Y. Yoshimine, M. Taguchi, T. Baba, T. Kinoshita, H. Kanno, H. Sakata, E. Maruyama, and M. Tanaka. "Twenty-two percent efficiency HIT solar cell". In: *Solar Energy Materials and Solar Cells* 93 (2009), pp. 670–673. DOI: 10.1016/j.solmat.2008.02.037 (cit. on p. 3).

- [10] T. Mishima, M. Taguchi, H. Sakata, and E. Maruyama. "Development status of high-efficiency HIT solar cells". In: *Solar Energy Materials & Solar Cells* 95 (2011), pp. 18–21. DOI: 10.1016/j.solmat.2010.04.030 (cit. on p. 3).
- [11] J. Damon-Lacoste and P. Roca i Cabarrocas. "Toward a better physical understanding of a-Si:H/c-Si heterojunction solar cells". In: *Journal of Applied Physics* 105, 063712 (2009), p. 063712. DOI: 10.1063/1.3091283 (cit. on p. 3).
- [12] H. Angermann, L. Korte, J. Rappich, E. Conrad, I. Siebera, M. Schmidt, K. Hübener, and J. Hauschild. "Optimisation of electronic interface properties of a-Si:H/c-Si hetero-junction solar cells by wet-chemical surface pre-treatment". In: *Thin Solid Films* 516 (2008), pp. 6775–6781. DOI: 10.1016/j.tsf.2007.12.033 (cit. on p. 3).
- [13] M.R. Page, E. Iwaniczko, Y. Xu, Q. Wang, Y. Yan, L. Roybal, H. M. Branz, and T.H. Wang. "Well-Passivated a-Si:H Back Contacts for Double-Heterojunction Solar cells". In: *IEEE 4th World Conference on Photovoltaic Energy Conversion, Waikoloa, Hawaii, May 7-12, 2006*. DOI: 10.1109/WCPEC.2006.279750 (cit. on p. 3).
- [14] Q. Wang, M. R. Page, E. Iwaniczko, Y. Xu, L. Roybal, R. Bauer, B. To, H.-C. Yuan, A. Duda, F. Hasoon, Y. F. Yan, D. Levi, D. Meier, H. M. Branz, and T. H. Wang. "Efficient heterojunction solar cells on p-type crystal silicon wafers". In: *Applied Physics Letters* 96, 013507 (2010), p. 013507. DOI: 10.1063/1.3284650 (cit. on p. 3).
- [15] S. Olibet, C. Monachon, A. Hessler-Wyser, E. Vallat-Sauvain, S. De Wolf, L. Fesquet, J. Damon-Lacoste, and C. Ballif. "Textured silicon heterojunction solar cells with over 700 mV open-circuit voltage studied by Transmission Electron Microscopy". In: *23rd European Photovoltaic Solar Energy Conference, 1-5 September, Valencia, Spain, 2008* (cit. on p. 3).
- [16] S. De Wolf et al. "High-efficiency silicon heterojunction solar cells: From physics to production lines". In: *Solid-State and Integrated Circuit Technology (ICSICT), 2010 10th IEEE International Conference on*. 2010, pp. 1986–1989. DOI: 10.1109/ICSICT.2010.5667849 (cit. on p. 3).
- [17] D. Muñoz et al. "Towards high efficiency on full wafer a-Si:H/c-Si heterojunction solar cells: 19.6% on 14 8cm²". In: *Photovoltaic Specialists Conference (PVSC), 2010 35th IEEE*. 2010, pp. 000039–000043. DOI: 10.1109/PVSC.2010.5614179 (cit. on p. 3).
- [18] H. Fujiwara and M. Kondo. "Effects of a-Si:H layer thicknesses on the performance of a-Si:H/c-Si heterojunction solar cells". In: *Journal of Applied Physics* 101, 054516 (2007), p. 054516. DOI: 10.1063/1.2559975 (cit. on p. 3).
- [19] D. Pysch, M. Bivour, M. Hermle, and S. W. Glunz. "Amorphous silicon carbide heterojunction solar cells on p-type substrates". In: *Thin Solid Films* 519 (2011), pp. 2550–2554. DOI: 10.1016/j.tsf.2010.12.028 (cit. on p. 3).

- [20] Y. Veschetti, J.-C. Muller, J. Damon-Lacoste, P. Roca i Cabarrocas, A.S. Gudovskikh, J.-P. Kleider, P.-J. Ribeyron, and E. Rolland. "Optimisation of amorphous and polymorphous thin silicon layers for the formation of the front-side of heterojunction solar cells on p-type crystalline silicon substrates". In: *Thin Solid Films* 511-512 (2006), pp. 543-547. DOI: 10.1016/j.tsf.2005.12.166 (cit. on p. 4).
- [21] Jérôme Damon-Lacoste. "Vers une ingénierie de bandes des cellules solaires à hétérojonctions a-Si:H/c-Si. Rôle prépondérant de l'hydrogène." PhD thesis. École Polytechnique, 2007. URL: http://tel.archives-ouvertes.fr/docs/00/25/95/75/PDF/Damon-Lacoste_These_protege.pdf (cit. on p. 4).

BASICS OF PHOTOVOLTAICS



Contents

1.1	Solar energy	10
1.1.1	Solar spectrum	10
1.2	Semiconductor principles involved in PV	12
1.2.1	Electrons and holes in the dark	13
1.2.2	Quasi-Fermi level distributions	14
1.2.3	Transport	15
1.2.4	Junctions	17
1.3	Crystalline silicon (c-Si)	20
1.3.1	Lifetimes in c-Si	20
1.4	Hydrogenated amorphous silicon (a-Si:H)	26
1.5	Indium Tin Oxide (ITO)	28
1.6	Conclusions	30

The photovoltaic energy is based on the conversion of the photons' energy, coming from the sun, into electrical energy. Therefore it is necessary to know what this source of energy (the sun) is and obviously how a photovoltaic device works. Therefore, we will first introduce the solar energy, and in the next section explain the physics governing this energy conversion.

1.1 Solar energy

1.1.1 Solar spectrum

The sun is a very strong light emitter that can be approximated by a black body whose temperature would be close to 5800 K. However, the actual solar spectrum slightly differs from that of a black body. Indeed, on Fig. 1.1, we have plotted the $AM0^1$ and $AM1.5^2$ spectra. These spectra have been obtained by collecting a huge amount of experimental data and are now the standard solar spectral irradiance distributions.³ The $AM0$ spectrum is to be used by the spatial industry and is the irradiation spectrum received from the sun by the Earth before this light crosses the atmosphere.

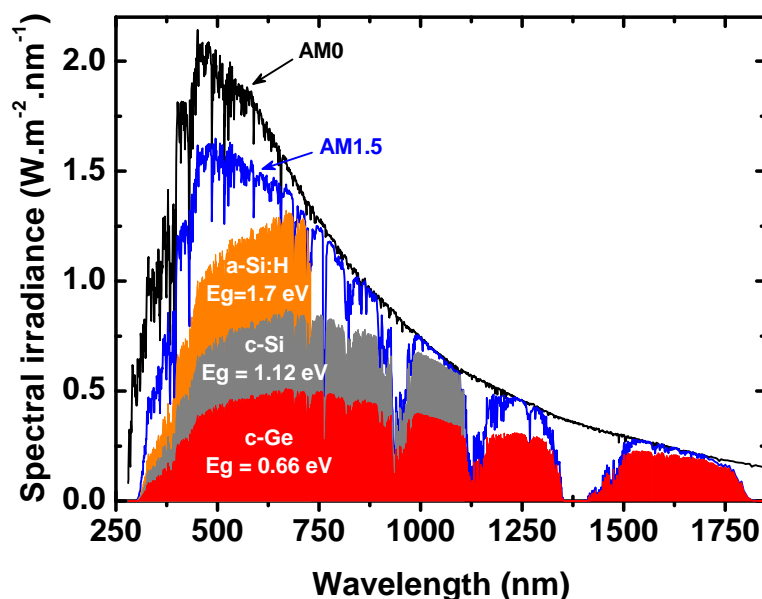


Figure 1.1 – $AM0$ and $AM1.5$ spectral irradiance as well as the maximum energy for different absorbing materials

On Fig. 1.1 we have also filled some areas under the $AM1.5$ spectrum in order to show, for various absorbing materials important in the PV field and studied during this doctoral work, what is the maximum recoverable

¹<http://rredc.nrel.gov/solar/spectra/am0/>

²<http://rredc.nrel.gov/solar/spectra/am1.5/>

³The 1.5 factor indicates that it has been assumed that the light had to go through one and a half of the vertical atmosphere thickness to reach the ground, which is relatively close to the Europe solar irradiance. Other standards exist, e.g. for the cells working under concentrated light.

energy. The energy collection losses arise from two mechanisms. The first one is the fact that when one photon has an energy higher than the bandgap energy of the material, it can move one electron from the valence band to the conduction band at an energy level higher than the edge of the conduction band, and this electron is extremely fast to release its extra energy via phonon scattering. This means that, no matter what the original photon energy which promoted the electron from the valence band to the conduction band was, the theoretically available energy will always be very close to the one of the bandgap of the material and all the extra energy is lost for today's solar cells. The main limitation which prevents us from collecting these "hot electrons" when they are in the excited state, is their relaxation time, which is very short compared to the one needed to collect them. The second one arises from the simple fact that when the photon energy is smaller than the bandgap energy, the photon is not absorbed by the material and its energy is lost.

These two constraints have opposite effects: increasing the bandgap reduces the thermalization losses, or in other terms increases the energy per absorbed photon, whereas it also increases the number of photons that will not be absorbed because of their too low energy. Therefore, some optimum must exist. *Shockley and Queisser*¹ have carried out a study, which was not involving any junction but was merely based on thermodynamic principles, which resulted in a concave function representing the efficiency as a function of the bandgap of the absorbing material. According to their study, for a single material (single junction), the maximum efficiency is reached at a bandgap of 1.4 eV, close to that of GaAs, and has a value of 30%.

However, independently from this optimum bandgap, various PV technologies have been developed as shown on Fig. 1.2, which represents the best research solar cell's efficiency for most of the existing PV technologies plotted against time. Interestingly enough, one can see on Fig. 1.2 that one of the most powerful and straightforward way to overcome the Shockley-Queisser limit is to develop multi-junction solar cells where we have not only one absorber but several absorbers of different bandgap energies. On Fig. 1.2, it appears that such multi-junction solar cells have been mostly developed with III-V materials for spatial applications, but also with amorphous or nanostructured silicon materials for terrestrial applications. The LPICM laboratory, within its PV activities, has focused on p-i-n solar cells based on a-Si:H² and $\mu\text{c-Si:H}$ materials,³ including alloys with Ge,⁴ and more recently has studied devices based

¹Shockley and Queisser, "Detailed Balance Limit of Efficiency of $p - n$ Junction Solar Cells", 1961 [1]

²Poissant, Chatterjee, and Roca i Cabarrocas, "Analysis and optimization of the performance of polymorphous silicon solar cells: Experimental characterization and computer modeling", 2003 [2]

³Kalache, "Rôle des ions dans les mécanismes de croissance du silicium microcristallin obtenu par voie plasma: Applications aux dispositifs photovoltaïques", 2003 [3]

⁴Gueunier, Kleider, Brüggemann, Lebib, Roca i Cabarrocas, Meaudre, and Canut, "Properties of polymorphous silicon-germanium alloys deposited under high hydrogen dilution and at high pressure", 2002 [4]

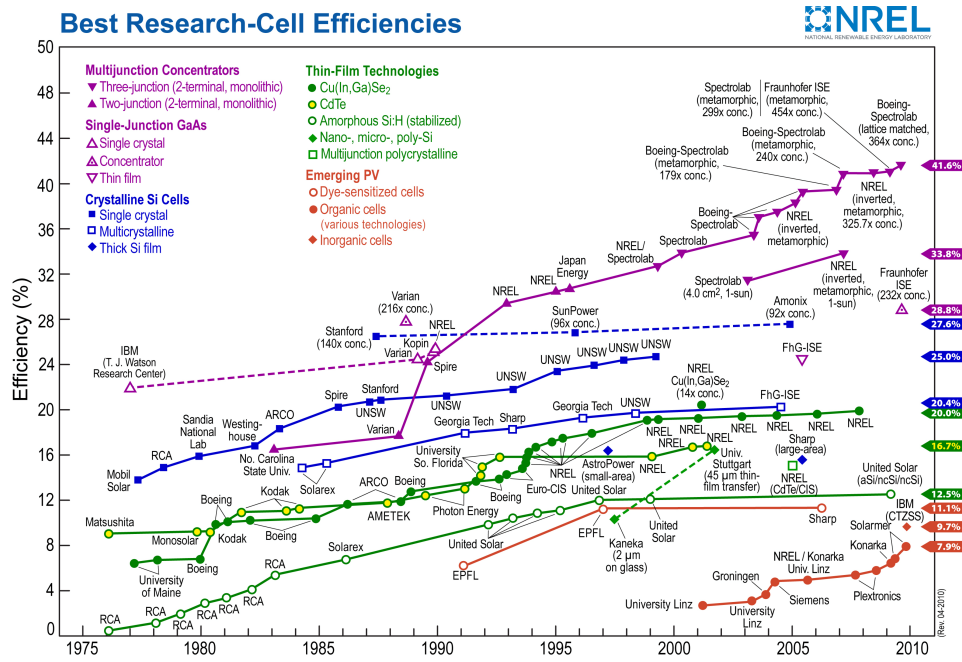


Figure 1.2 – Best research solar cell efficiencies plotted against time for various PV technologies

on silicon nanowires,¹ including some hybrid cells with organic materials,² and silicon heterojunction cells.³

1.2 Semiconductor principles involved in PV

In this section we will present a few concepts from the solid state physics that we need in order to understand how our solar cells work. The concepts presented here are based on several textbooks where one can find more detailed explanations.⁴ These reference textbooks are listed here by the name of their author: *Stephen Fonash*,⁵ *Jenny Nelson*,⁶ and *Peter Würfel*.⁷ The reader will find in these references detailed calculations and assumptions done to obtain the equations presented in this section. We will not repeat them, but merely focus on the fundamental definitions.

¹Yu, O'Donnell, Alet, and Roca i Cabarrocas, "All-in-situ fabrication and characterization of silicon nanowires on TCO/glass substrates for photovoltaic application", 2010 [5]

²Alet, P.-J. Palacin, S. Roca i Cabarrocas, P. Kalache, B. Firon, M. And de Bettignies, R. "Hybrid solar cells based on thin-film silicon and P₃HT", 2006 [6]

³Damon-Lacoste, "Vers une ingénierie de bandes des cellules solaires à hétérojonctions a-Si:H/c-Si. Rôle prépondérant de l'hydrogène.", 2007 [7]

⁴Also, in a very interactive and visual way, a huge amount of information on theoretical and technical questions regarding semiconductors can be found on this website, created by STUART BOWDEN and CHRISTIANA HONSBURG: <http://www.pveducation.org/pvcdrom>

⁵Fonash, *Solar Cell Device Physics, 2nd Edition*, 2010 [8]

⁶Nelson, *The physics of solar cells*, 2003 [9]

⁷Würfel, *Physics of Solar Cells: From Basic Principles to Advanced Concepts, 2nd edition*, 2009 [10]

1.2.1 Electrons and holes in the dark

As semiconductors are the base materials of our solar cells, we need to know a few quantities in order to understand and design photovoltaic devices. First, we have n_e , the density of electrons (in the conduction band), which is given by Eq. 1.1.

$$n_e = N_C \exp\left(\frac{E_C - E_F}{kT}\right) \quad (1.1)$$

Here N_C is the effective density of states of the conduction band and equals $2 \times 10^{19} \text{ cm}^{-3}$ in c-Si, assuming that the effective mass of the electron equals its mass. Similarly, we have n_h , the density of holes (in the valence band), which is given by Eq. 1.2.

$$n_h = N_V \exp\left(-\frac{E_F - E_V}{kT}\right) \quad (1.2)$$

From these two equations arises a condition on the product of these two quantities that is given by Eq. 1.3.

$$n_e \times n_h = N_C N_V \exp\left(-\frac{E_g}{kT}\right) = n_i^2 \quad (1.3)$$

n_i is called the intrinsic carrier concentration. In the case of crystalline silicon, we usually consider $n_i = 10^{10} \text{ cm}^{-3}$, experimentally determined by Sproul and Green.¹

One can selectively increase the concentration of one type of carriers by adding impurity atoms to our semiconductor, called dopants, at a low concentration. Basically, in the case of crystalline silicon which has a valence of four, we can have donors (most common: P, As) that have an extra valence electron compared to what is necessary for the bonding whereas we also have acceptors (most common: B, In) that lack of a valence electron to satisfy for the bonding. In both cases, the energy necessary to donate an electron (a hole) to the conduction (valence) band from the donor (acceptor) atom is low at room temperature, compared to $k \times T$, so that adding dopants to the semiconductor changes the distribution of electrons (and holes through Eq. 1.3). At room temperature, the dopants are almost all ionized so that the density of electrons and holes in doped semiconductors can be summarized by Tab. 1.1.

	n_e	n_h
n-type	$n_e \approx n_D$	$n_h = \frac{n_i^2}{n_e} = \frac{n_i^2}{n_D}$
p-type	$n_e = \frac{n_i^2}{n_h} = \frac{n_i^2}{n_A}$	$n_h = n_A$

Table 1.1 – Electron and hole densities in n and p-type semiconductors (in the dark)

In Tab. 1.1, n_A and n_D refer to the acceptor or donor atom density.

¹Sproul and Green, "Improved value for the silicon intrinsic carrier concentration from 275 to 375 K", 1991 [11]

These results apply to the case of shallow donors that have energies close to the conduction band. If their energy is close to the middle of the gap they act as recombination centers and are inefficient as donors. The same applies for acceptor impurities that must have energies close to the valence band.

Here, it is necessary to introduce two properties of semiconductors: electron affinity (χ) and work function (ϕ). These properties are graphically defined on Fig. 1.3. The electron affinity is the amount of energy

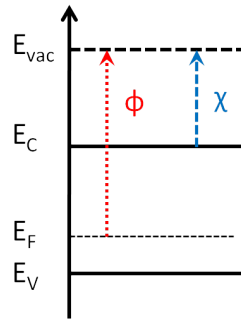


Figure 1.3 – Electron affinity (χ) and work function (ϕ) of a semiconductor

needed to move an electron from the lowest occupied energy level of the conduction band to the vacuum level (E_{vac}) where it is free from forces (from the solid). The work function is the energy difference between the vacuum level and the Fermi level. In the case of metals, for which there is no bandgap, we have $\chi = \Phi$.

1.2.2 Quasi-Fermi level distributions

The above results apply only to a semiconductor in the dark. However, solar cells aim at converting photons' energy into electrical energy and need, by definition, to be illuminated. We will describe here the new distributions of electrons and holes under these new conditions. When photons are absorbed, they create electron-hole pairs. As mentioned earlier, right after their generation, the electrons and holes have a rather broad energy distribution over the conduction and valence band states. However, they lose their energy by phonon scattering very quickly so that within a 10^{-12} s range they form electron and hole distributions that are expected to remain so for their lifetime in the band, that we will describe later but which is of the order of μs to ms in the case of crystalline silicon. This process is schematized on Fig. 1.4.

From Fig. 1.4, it appears that n_e and n_h can be much higher than their equilibrium value and that both of them will be much increased, what doping could not do, so that $n_e \times n_h \gg n_i^2$. In this case it is necessary to introduce two Fermi distributions to describe each of the distributions with two different Fermi energies: E_{FC} and E_{FV} . Each of these two quasi Fermi levels is closer to the conduction and valence band to describe the electron and hole densities respectively and to account for the fact that both densities are greatly increased. Hence, we can write the density of electrons (in the conduction band) and of holes (in the valence band) in

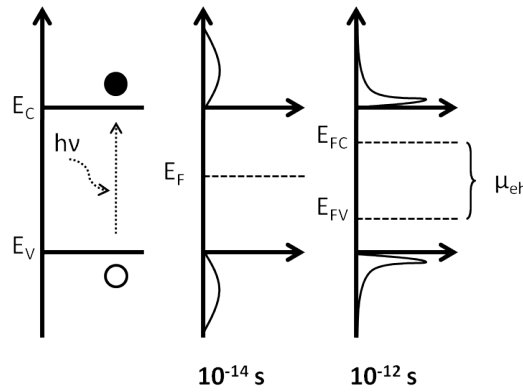


Figure 1.4 – Electron and hole distributions after thermalization Ref. [10]

Eq. 1.4 and 1.5 respectively.

$$n_e = N_C \exp\left(-\frac{E_C - E_{FC}}{kT}\right) \quad (1.4)$$

$$n_h = N_V \exp\left(-\frac{E_{FV} - E_V}{kT}\right) \quad (1.5)$$

μ_{eh} ($= E_{FC} - E_{FV}$) is referred to as the quasi Fermi levels splitting and has some importance regarding the properties of solar cells, namely their open-circuit voltage, as it will be seen later. We can obtain from Eq. 1.4 and Eq. 1.5 the following relation:

$$n_h \times n_e = n_i^2 \exp\left(\frac{E_{FC} - E_{FV}}{kT}\right) \quad (1.6)$$

We know a little bit more about semiconductors but in order to obtain solar cells we need to bring into contact different materials: semiconductors with semiconductors or metals. We will briefly review here what kind of junctions can be involved and how they basically work.

1.2.3 Transport

One of the first things to understand, before going into the details of the different kinds of junctions, is what makes electrons and holes, called charge carriers, move. They are particles and they are charged, therefore, they are sensitive to gradients in the electrical potential and in particle concentrations.

The gradient in the electrical potential results in an electric field that results in a *field current* or *drift current*. This is what happens when there is a gradient in the work function or in the vacuum level. This field current for electrons and holes can be expressed, as follows:

$$\vec{J}_{e,drift} = -qn_e\mu_e \vec{E} \quad (1.7)$$

$$\vec{J}_{h,drift} = qn_h\mu_h \vec{E} \quad (1.8)$$

\vec{E} is the electric field, μ_e, μ_h are the mobility for electrons and holes respectively. Or as follows:

$$\vec{J}_{e,drift} = \frac{\sigma_e}{e} \times \nabla(eV(x)) \quad (1.9)$$

$$\vec{J}_{h,drift} = -\frac{\sigma_h}{e} \times \nabla(eV(x)) \quad (1.10)$$

The gradient in the chemical potential results in a *diffusion current*. This is the case for instance when we have a non-uniform carrier concentration (in the absence of any electrical field). The diffusion current obeys the Fick's law and the resulting current can be expressed as follows:

$$\vec{J}_{e,diff} = e \times D_e \times \nabla(n_e(x)) \quad (1.11)$$

$$\vec{J}_{h,diff} = -e \times D_h \times \nabla(n_h(x)) \quad (1.12)$$

We have the Einstein relation $\frac{\mu_e}{D_n} = \frac{e}{kT}$. Besides, we know that we have for the chemical potential for electrons the following equation:

$$\nabla(\mu_{chem,e}) = \nabla(kT \times \ln(\frac{n_e}{N_C}))$$

Based on that and acknowledging the mathematical equality:

$$\nabla(kT \times \ln(\frac{n_e}{N_C})) = kT \times \nabla(\ln(n_e)) = kT \times \frac{\nabla(n_e)}{n_e}$$

we can rewrite Eq. 1.11 as follows:

$$\vec{J}_{e,diff} = \frac{en_e(x)kT\mu_e}{e} \times \nabla(n_e(x)) \frac{n_e(x)}{n_e(x)} \quad (1.13)$$

$$\vec{J}_{e,diff} = \frac{e\mu_e n_e(x)}{e} \times \nabla(\mu_{chem,e}) \quad (1.14)$$

An finally, noting that $en\mu_e = \sigma_e$:

$$\vec{J}_{e,diff} = \frac{\sigma_e}{e} \times \nabla(\mu_{chem,e}) \quad (1.15)$$

Similarly we can write for holes:

$$\vec{J}_{h,diff} = -\frac{\sigma_h}{e} \times \nabla(\mu_{chem,h}) \quad (1.16)$$

The net resulting currents of electrons and holes is the result of the addition of these two currents (drift and diffusion) which can be expressed as follows:

$$\vec{J}_e = \frac{\sigma_e}{e} \nabla(eV(x)) + \frac{\sigma_e}{e} \times \nabla(\mu_{chem,e}) \quad (1.17)$$

$$\vec{J}_e = \frac{\sigma_e}{e} \nabla(eV(x) + \mu_{chem,e}) = \frac{\sigma_e}{e} \nabla(E_{FC}) \quad (1.18)$$

$$\vec{J}_h = -\frac{\sigma_h}{e} \nabla(eV(x)) - \frac{\sigma_h}{e} \times \nabla(\mu_{chem,h}) \quad (1.19)$$

$$\vec{J}_h = -\frac{\sigma_h}{e} \nabla(eV(x) + \mu_{chem,h}) = \frac{\sigma_h}{e} \nabla(E_{FV}) \quad (1.20)$$

1.2.4 Junctions

1.2.4.1 Ohmic contact

When we bring into contact a metal and a semiconductor, what we usually want is a good transport, i.e. no potential barrier for the majority carriers to flow into the metal. In this case we have an *ohmic contact*. This can happen when the work function of a metal is smaller (higher) than the work function of a n-type (p-type) semiconductor. The band diagrams of such contacts are summarized on Fig. 1.5.

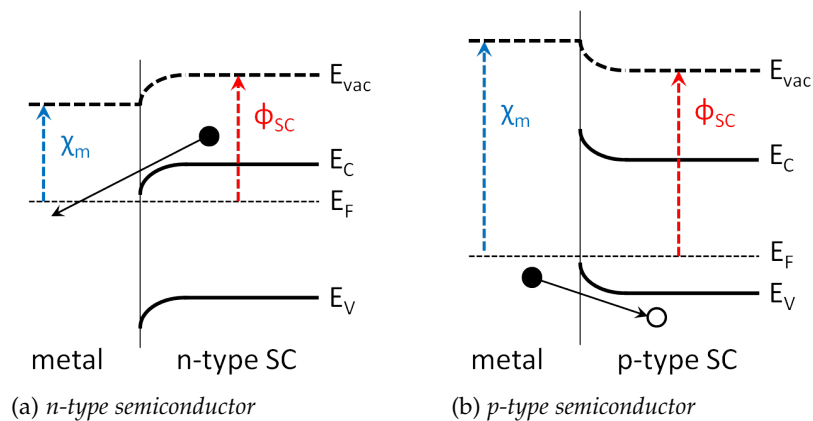


Figure 1.5 – Band diagrams of metal ohmic contacts with n-type (left) and p-type (right) semiconductor materials

1.2.4.2 Schottky contact

When we have opposite conditions to the ones necessary to establish an ohmic contact, so that the majority carriers face a potential barrier, resulting in a rectifying behaviour, we have a Schottky contact. This happens when the work function of a metal is higher (smaller) than the work function of a n-type (p-type) semiconductor. The band diagrams of such contacts are summarized on Fig. 1.6.

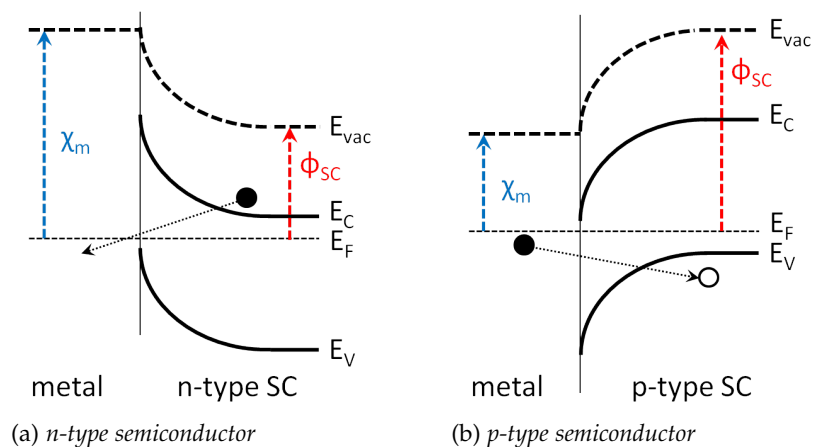


Figure 1.6 – Band diagrams of metal Schottky contacts with n-type (left) and p-type (right) semiconductor materials

1.2.4.3 p-n junction

There is also another type of junction that occurs when two semiconductors are brought into contact. The p-n junction is the basis of crystalline silicon solar cells and of many other electronic devices. Such a junction is formed when we contact a n-type semiconductor with a p-type semiconductor. When both semiconductors have the same bandgap energy, which is the general case, this junction is called homojunction. A particular case is the heterojunction: the bandgap of the two semiconductors is not the same, which results in a more complex band diagram that will be presented and discussed in the next chapter. When the two semiconductors are brought into contact, electrons and holes diffuse from the region where they are in a high concentration towards the region where there are in a low concentration. By doing so, they leave fixed ionized donors or acceptors. These ionized atoms, that remain in a free carrier depopulated zone (depletion zone) and therefore quasi intrinsic will create an increasing electric field until it reaches the value needed to stop any further charge transfer. Such a field opposed to diffusion gives its name to a voltage called diffusion voltage qV_d that corresponds to the band bending on each side of the junction. On Fig. 1.7, we have drawn the schematic band diagram of a pn junction in the dark at thermal equilibrium. The

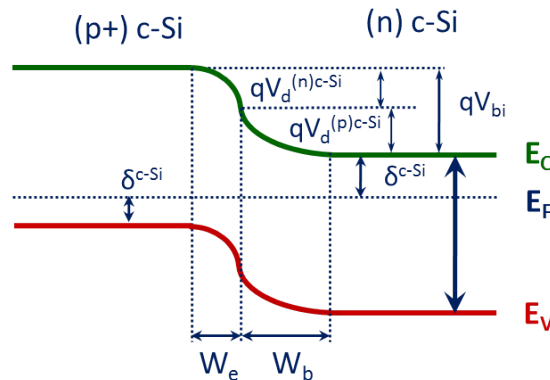


Figure 1.7 – Schematic band diagram of a pn homojunction made of crystalline silicon

depletion region has a width of $W_e + W_b$. The width on each side of the junction, W_e on the emitter side and W_b on the base side, depends on the doping concentration. The more doped the semiconductor, the shorter the width. Indeed, when a semiconductor is highly doped, the dopant atom concentration is very high so that it can create the same fixed charge on a much shorter length. The qV_{bi} voltage is called the built-in potential of the junction.

In the dark, the current can be expressed as a function of the voltage as follows in Eq. 1.21, called *Shockley's law*:

$$J(V) = J_0 \left(\exp \left(\frac{eV}{n k T} \right) - 1 \right) \quad (1.21)$$

Here J_0 is called the diode saturation current and n is the ideality factor. It should be equal to unity in a perfect diode or at least be comprised between 1 and 2. This is in the dark but when the diode is illuminated,

we should add to this equation a photogeneration (J_{ph}) current flowing in the opposite direction. However, this is the case of a perfect diode and does not take into account some parasitic effects. Indeed, a more realistic model for the diode is shown on Fig. 1.8.

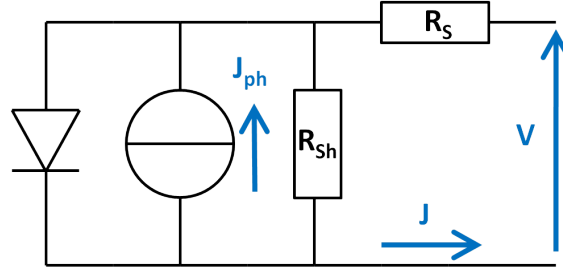


Figure 1.8 – Electrical model used to describe an illuminated diode

The diode equation can be then replaced by the following one, where R_{sh} and R_s are the shunt and the series resistances:

$$J(V) = J_0 \left(\exp \left(\frac{q(V - R_s J)}{nkT} \right) - 1 \right) + \frac{V - R_s J}{R_{sh}} - J_{ph} \quad (1.22)$$

The I-V measurement is the most basic, and the most important, characterization tool for photovoltaic devices. Even though quite simple, it is the one that gives the most information on the device quality. This measurement can be performed in the dark or under illumination. Working in the dark allows to determine J_0 and n . When working under illumination, we get information on the solar cell parameters (V_{oc} , J_{sc} and FF), which might differ from the simple superimposition of a photocurrent and the diode obtained in the dark, as well as the solar cell efficiency. The set-up used to perform this measurement is usually a lamp giving an incident (on the sample) power density of $100 \text{ mW}\cdot\text{cm}^{-2}$ and a spectral distribution supposed to match closely to that of the AM1.5 spectrum and thus that of the sun. When performing the measurements at LPICM we used a set-up provided by Newport. On Fig. 1.9, we have plotted a typical current-voltage characteristic obtained when measuring a solar cell under illumination. On the curve of Fig. 1.9, three points are of great importance:

- where no current flows, the voltage equals the open-circuit voltage V_{oc}
- where there is no voltage, the current density equals the short-circuit current density J_{sc}
- where the product current times voltage reaches its maximum and called maximum power point (MPP)

The maximum power point determines a parameter called *fill factor* (FF), which is defined as $FF = \frac{I_{MPP} \times V_{MPP}}{J_{sc} \times V_{oc}}$. This parameter is the ratio between the areas of two rectangles: the one formed by the origin and the maximum power point (gray) and the one formed by the origin and the point whose coordinates are $(V_{oc}; J_{sc})$ (light gray). R_s and R_{sh} are parasitic resistances and are responsible for losses reducing the efficiency. R_s accounts

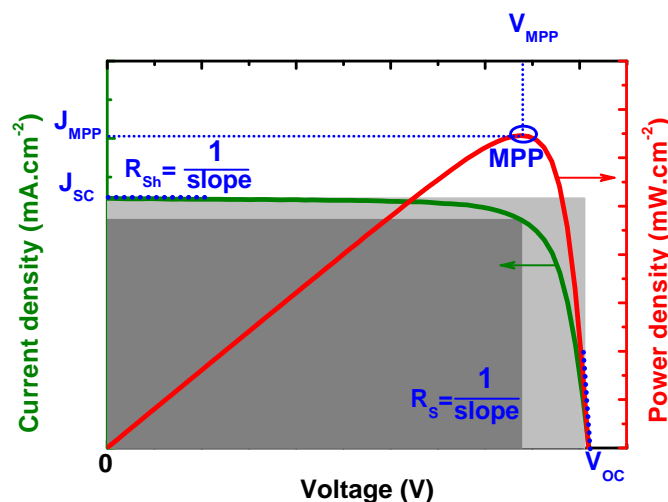


Figure 1.9 – Typical current-voltage characteristic of a heterojunction solar cell

for all the resistive losses in the solar cell (e.g. contact resistances, resistivity of the layers) and should be kept as low as possible. R_{sh} is called the shunt resistance and accounts for shunt losses and should be as high as possible.

The efficiency (η) of a solar cell is defined as the ratio between the photogenerated electrical power and the incident light power. Therefore it is very easy to write Eq. 1.23.

$$\eta = \frac{J_{MPP} \times V_{MPP}}{P_{incident}} = \frac{J_{sc} \times V_{oc} \times F.F.}{P_{incident}} \quad (1.23)$$

1.3 Crystalline silicon (c-Si)

Crystalline silicon is a semiconducting material with a diamond crystal structure and an indirect bandgap of 1.12 eV at 300 K. The consequence is that the light needs a lot more material, compared to direct bandgap materials like a-Si:H, to be effectively absorbed. Typically, a-Si:H based pin solar cells require a total thickness of less than 500 nm whereas the standards of the c-Si industry are close to 180 μm .

1.3.1 Lifetimes in c-Si

c-Si is a semiconductor, hence all the carriers contained in the material are subject to recombination processes that will be described in this section. Understanding these processes, and avoiding them to occur, is a key factor to achieve the highest device efficiencies. Inside the bulk crystalline silicon, carriers have three possible recombination paths, each of them is to be described in the following sections:

1. radiative recombination (§1.3.1.1, page 21)
2. Auger recombination (§1.3.1.2, page 22)
3. Shockley-Read-Hall recombination (§1.3.1.3, page 23)

We will quickly describe these recombination processes but a lot more details can be found in the textbooks written by *Jenny Nelson*¹ and *Stephen Fonash*,² as well as in *Isidro Martin*'s PhD thesis.³

1.3.1.1 Radiative recombination

This is an unavoidable process and it exists in all the semiconductors. We have represented on Fig. 1.10 the recombination paths involved. Path 1 is the band to band recombination of an electron from the conduction band with a hole in the valence band. During this recombination some energy, equal to the bandgap value, is lost and is transferred to an emitted photon. Path 2 is the opposite path for which an electron in the valence band is promoted to the conduction band. These processes require a certain

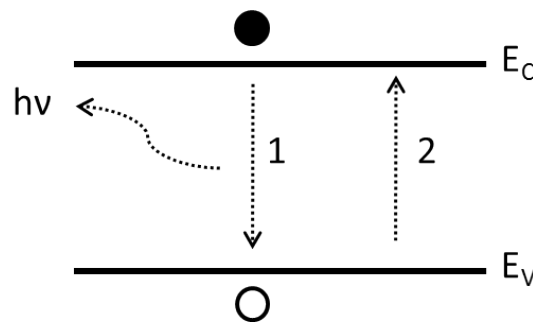


Figure 1.10 – Radiative recombination in a semiconductor

concentration of electrons in the conduction band (n) as well as a hole concentration in the valence band (p). The net recombination rate of the radiative recombination can be expressed by the Eq. 1.24.

$$R_{rad} = B_{rad} \times (n \times p - n_i^2) \quad (1.24)$$

In the case of a n-type c-Si material in which extra carriers have been generated (e.g. via illumination or charge injection), and by naming Δn and Δp the numbers of extra electrons and holes respectively, we can rewrite Eq. 1.24 to obtain the following equality:

$$R_{rad} = B_{rad} \times ((N_D + \Delta p) \times \Delta p - n_i^2) \quad (1.25)$$

One should note that c-Si being an indirect bandgap semiconductor, the conservation of the momentum imposes that phonons should be involved to balance the momentum change. This phonon interaction is responsible for the very low radiative recombination rate and makes it a negligible process regarding the recombination of the photogenerated carriers. In all these equations, the term B_{rad} is a parameter depending on the temperature. Quantitative data can be found in the work of *Schlengenotto et al.*⁴ Based on this work we can estimate this B_{rad} coefficient to be close

¹Nelson, *The physics of solar cells*, 2003 [9]

²Fonash, *Solar Cell Device Physics, 2nd Edition*, 2010 [8]

³Martin, "Silicon surface passivation by Plasma Enhanced Chemical Vapor Deposited amorphous silicon carbide films", 2001 [12]

⁴Schlengenotto, Maeder, and Gerlach, "Temperature dependence of the radiative recombination coefficient in silicon", 1974 [13]

to $9.5 \times 10^{-15} \text{ cm}^3 \cdot \text{s}^{-1}$. We can also define the radiative lifetime contribution as the inverse of the recombination rate multiplied by the minority carrier concentration: $\tau_{rad} = \frac{\Delta p}{R_{rad}}$. During our work, we used n-type c-Si with a resistivity of $3 \text{ } \Omega \cdot \text{cm}$ (i.e. a donor concentration N_D of $1.55 \times 10^{15} \text{ cm}^{-3}$) so that at a minority carrier density of 10^{15} cm^{-3} we have a radiative recombination lifetime: $\tau_{rad} = \frac{\Delta p}{R_{rad}} \approx \frac{1}{B_{rad} \times (N_D + \Delta p)} = \frac{1}{9.5 \cdot 10^{-15} \times (10^{15} + 1.55 \cdot 10^{15})} > 41 \text{ ms}$ quite high, much higher than the lifetime associated to the other recombination processes described below.

1.3.1.2 Auger recombination

Auger recombination also is an unavoidable recombination process. It involves band-to-band recombination between an electron and a hole, but in this case there is no photon emission since the extra energy is transferred to or taken from a third carrier. On Fig. 1.11 we have schematized the Auger recombination processes involving two electrons and one hole (case a) or one electron and two holes (case b). The third carrier which gained extra energy will afterwards loose this extra energy by slowly moving from its excited state to the band edge.

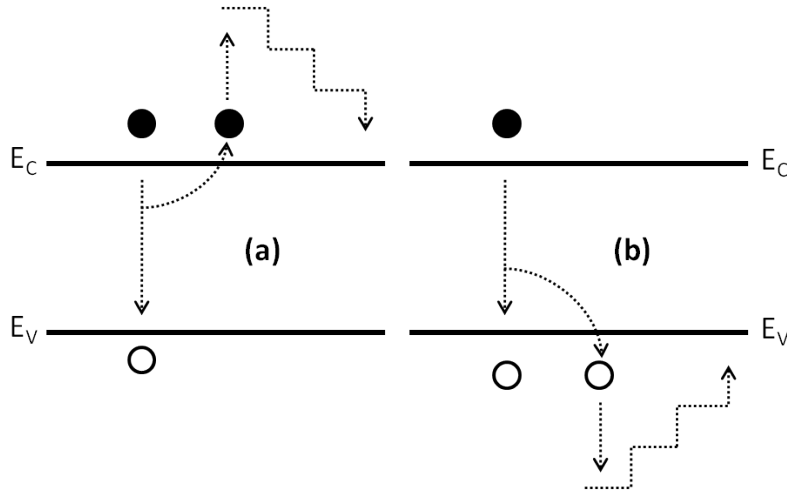


Figure 1.11 – Auger recombination in a semiconductor

The consequence of such a recombination mechanism is that the recombination rate will depend on product of one type of carrier concentration with the square of the other type of carrier concentration. Indeed, the recombination rate of such processes can be expressed by the Eq. 1.26.

$$R_{Aug} = C_n \times (p \times n^2 - p_0 \times n_0^2) + C_p \times (n \times p^2 - n_0 \times p_0^2) \quad (1.26)$$

In Eq. 1.26, the coefficients C_n and C_p are called the Auger coefficients. Many papers have been written on the determination of these coefficients. So far, the most complete parametrization comes from the work by *Kerr and Cuevas*.¹ This very interesting paper includes a comprehensive discussion about the previous parametrizations and gives a general parametrization of the Auger recombination rate, given in Eq. 1.27. One can also find

¹Kerr and Cuevas, "General parameterization of Auger recombination in crystalline silicon", 2002 [14]

a similar interesting discussion about the different parametrizations in the thesis of *Isidro Martin* (Ref. [12]). From the *Kerr and Cuevas* paper we can obtain the Auger recombination rate, defined in Eq. 1.27.

$$R_{Aug} = n \times p \times (1.8 \cdot 10^{-24} \cdot n_0^{0.65} + 6 \cdot 10^{-25} \cdot p_0^{0.65} + 3 \cdot 10^{-27} \cdot \Delta n^{0.8}) \quad (1.27)$$

This process appears to be the dominant recombination one as soon as we are dealing with highly doped semiconductors or operating at high¹ injection levels, as it is the case under concentration for instance.

1.3.1.3 Shockley-Read-Hall recombination

Also frequently abbreviated SRH recombination, this phenomenon is the defect assisted recombination that can occur in bulk materials and that has been formalized by the works of *Hall*,² *Shockley and Read*.³ This recombination is based on the trapping and consequent recombination of two charge carriers. On Fig. 1.12, we show the four possible interactions that a defect, with an energy of E_t , can have with the charge carriers. They are listed here:

1. an electron from the conduction band gets trapped
2. a trapped electron gets released to the conduction band
3. a hole from the valence band gets trapped
4. a trapped hole gets released to the valence band

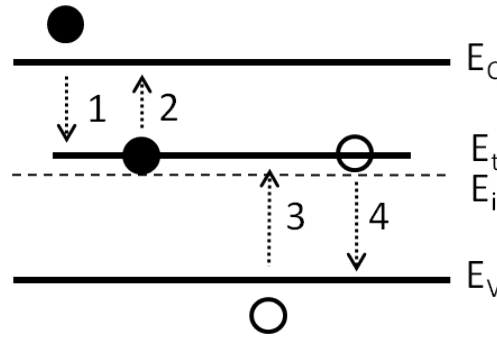


Figure 1.12 – Four possible interactions between charge carriers and a defect. For electrons we can have trapping (1) or detrapping (2). For holes we can have trapping (3) or detrapping (4)

Once they are at the same energy level, electron and hole recombine. The net recombination rate can be expressed as follows (Eq. 1.28).

$$R_{SRH} = \frac{n \times p - n_i^2}{\tau_{n,SRH}(p + p_t) + \tau_{p,SRH}(n + n_t)} \quad (1.28)$$

The electron ($\tau_{n,SRH}$) and hole ($\tau_{p,SRH}$) capture lifetimes can be expressed as the inverse of the products of the trap density (N_t), the mean thermal

¹For our substrates, this will typically be more than a few 10^{15} cm^{-3}

²Hall, "Electron-Hole Recombination in Germanium", 1952 [15]

³Shockley and Read, "Statistics of the Recombinations of Holes and Electrons", 1952 [16]

velocity of the charge carrier (v_n or v_p) and the capture cross section of the trap for electrons or holes (σ_n or σ_p):

$$\tau_{n,SRH} = \frac{1}{N_t \times \sigma_n \times v_n}$$

$$\tau_{p,SRH} = \frac{1}{N_t \times \sigma_p \times v_p}$$

Considering that we have a density N_t of defects located at an energy of E_t , the n_t and p_t can be expressed:

$$n_t = n_i e^{\frac{E_t - E_i}{k_B T}}$$

$$p_t = p_i e^{\frac{E_i - E_t}{k_B T}}$$

We should stress the fact that when the defect energy is located close to the conduction (valence) band, the defect acts more like a trap for electrons (holes) rather than like a recombination center. Indeed, if the defect is located close to the conduction band, time constants for trapping and detrapping will be much smaller than the time constants needed to trap a hole. These traps can slow down the transport of charge carriers but they do not remove them from the material. Contrariwise, it has also been demonstrated that the closer to the Fermi level the defects are located, the higher the recombination rate will be. Unlike Auger and radiative recombination, the SRH recombination is not unavoidable and is due to defects induced by elaboration or processing steps.

Finally, all these recombination processes lead to an effective bulk lifetime described as: $\tau_{bulk} = \left(\frac{1}{\tau_{Radiative}} + \frac{1}{\tau_{Auger}} + \frac{1}{\tau_{SRH}} \right)^{-1}$. On Fig. 1.13 we have plotted the Auger (\cdots), the radiative ($—$) and the SRH ($- -$) recombination lifetime as a function of the excess carrier density. We have also plotted the bulk lifetime ($—$). On this graph, for Auger recombination, we considered a $3 \Omega \cdot \text{cm}$, n-type wafer since this is the wafer we used the most during my doctoral research. For the SRH recombination we considered a defect located at the middle of the bandgap so that $E_t = E_i$, and considered that we had $\tau_{n,SRH} = \tau_{p,SRH} = 10 \text{ms}$. This graph highlights very well the different contributions of the different recombination paths. The radiative recombination is not significant. The bulk lifetime is imposed by the SRH recombination in the low injection level whereas in the high injection level, the bulk lifetime is determined by the Auger recombination.

1.3.1.4 Surface recombination

All these lifetimes describe bulk phenomena. However, a solar cell is a finite device. Using industrial equipments, we can obtain highly efficient c-Si solar cells with thicknesses ranging from only $50 \mu\text{m}$,¹ $98 \mu\text{m}^2$ or

¹Reuter, Brendle, Tobail, and Werner, "50 μm thin solar cells with 17.0% efficiency", 2009 [17]

²Mishima, Taguchi, Sakata, and Maruyama, "Development status of high-efficiency HIT solar cells", 2011 [18]

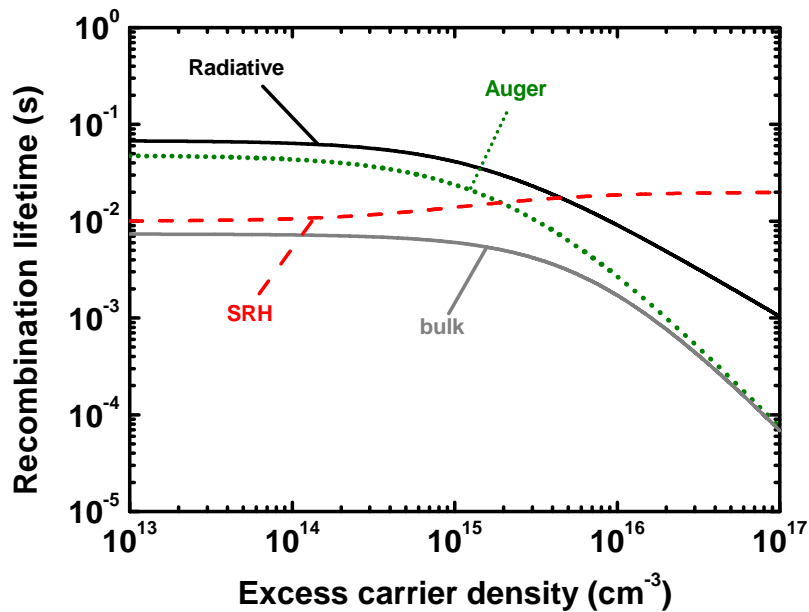


Figure 1.13 – Radiative, Auger and SRH recombination lifetimes plotted against the excess carrier density. The resulting bulk lifetime is also plotted

120 μm^1 to 180 μm^2 . During our work we mostly used wafers of 280 μm . Having said that, we should note that at the surface of the crystal, the network symmetry is broken so that recombination at the surface states can occur if they are not passivated. Thus, to fully characterize our devices, we have to introduce another recombination term which is the surface recombination. This leads us to define a new global lifetime called “effective lifetime” (τ_{eff}) which takes into account all the recombination processes, as defined in Eq. 1.29.

$$\frac{1}{\tau_{bulk}} = \frac{1}{\tau_{Auger}} + \frac{1}{\tau_{SRH}} + \frac{1}{\tau_{rad}} + \frac{1}{\tau_{surface}} \quad (1.29)$$

These recombinations are defect assisted and in our case the defects are dangling bonds, in the ideal case.³ The surface recombination is a recombination process via defects for which we can extend the SRH recombination formalism introduced earlier (§1.3.1.3). However, it can be more meaningful to introduce some parameters per unit of surface rather than per unit of volume. Indeed, introducing N_s , S_n and S_p as the number of traps per unit area and the surface recombination velocity of electrons and holes we can write the recombination rate per unit area in Eq. 1.30.

$$R_s = \frac{n_s \times p_s - n_i^2}{\frac{p_s + p_i}{S_n} + \frac{n_s + n_i}{S_p}} \quad (1.30)$$

¹Gautero, Hofmann, Rentsch, Lemke, Mack, Seiffe, Nekarda, Biro, Wolf, Bitnar, Sallese, and Preu, “All-screen-printed 120 μm thin large area silicon solar cells applying dielectric rear passivation and laser-fired contacts reaching 18% efficiency”, 2009 [19]

²Datasheets can be found on <http://www.photovolttech.com>

³As mentioned, recombination can also be induced by process based defects like chemical or mechanical etching, impurities concentrated at the surface during growth, chemical residuals, etc.

n_s and p_s are the carriers concentrations at the surface, which are generally (much) different from the carriers concentration in the wafer. Unlike the other recombination processes, it is rather difficult to determine since the carrier concentrations at the interface, and the recombination surface velocities, all depend on the film deposited at the surface of the wafer.

1.4 Hydrogenated amorphous silicon (a-Si:H)

Hydrogenated amorphous silicon is the major research topic of LPICM where a-Si:H is used to fabricate semiconductor-based devices: p-i-n solar cells,¹ Light Emitting Diodes,² Thin Film Transistors,³... Indeed, a-Si:H is a semiconductor material that has been thoroughly investigated. The most important textbooks on this material are the ones from *R.A. Street*⁴ and the one edited by *T. Searle*.⁵ Most of the material structure or properties we talk about later are extensively covered in these books.

Silicon can also exist in a non crystalline structure called amorphous silicon (a-Si). Unlike c-Si, a-Si does not possess a long range order. a-Si does possess some short range order in the way that each silicon atom is covalently bonded to its four neighbouring atoms. However, beyond a few atomic distances the structural order is lost. When the material is obtained by the dissociation of silane in a plasma, hydrogen can be incorporated to the film resulting in a different material called hydrogenated amorphous silicon (a-Si:H). On Fig. 1.14, we have represented the random a-Si:H network on which one can see that most of the Si atoms have a coordination of four, sometimes three or two. Dangling bonds and hydrogen-passivated dangling bonds are also represented. We can also have the presence of atomic hydrogen or molecular hydrogen.

Even though a-Si and a-Si:H are not crystals, a band structure exists in such materials. Indeed, *Thorpe and Weaire* have shown that the short-range order plays a very important role so that many features of the density of states we know from crystalline solids are still valid.⁶ It has also been shown that increasing the disorder of a network can lead to localized states.⁷ Thus, this material possesses localized states in an energy range close to its conduction and valence band edges that are called Urbach tails and also in the middle of the energy gap that are called deep states. The Urbach tails are due to the bonding disorder (eg. variations of the bonding angle), whereas the deep states are due to structural defects, dangling bonds (DB) that are unsatisfied Si bonds. The Urbach tail states are

¹Poissant, Chatterjee, and Roca i Cabarrocas, "Analysis and optimization of the performance of polymorphous silicon solar cells: Experimental characterization and computer modeling", 2003 [2]

²Stenger, Abramov, Barthou, Nguyen-Tran, Frigout, and Roca i Cabarrocas, "Strong orange/red electroluminescence from hydrogenated polymorphous silicon carbon light-emitting devices", 2008 [20]

³Oudwan, Moustapha, Abramov, Daineka, Bonnassieux, and Roca i Cabarrocas, "Threshold voltage shift under electrical stress in amorphous, polymorphous, and microcrystalline silicon bottom gate thin-film transistors", 2010 [21]

⁴Street, *Hydrogenated Amorphous Silicon*, 1991 [22]

⁵Searle, *Properties of Amorphous Silicon and Its Alloys*, 1998 [23]

⁶Thorpe and Weaire, "Electronic Density of States of Amorphous Si and Ge", 1971 [24]

⁷Anderson, "Absence of Diffusion in Certain Random Lattices", 1958 [25]

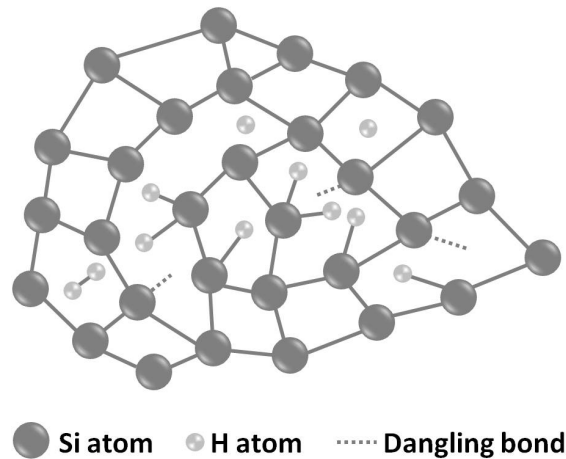


Figure 1.14 – Example of the a-Si:H network

donor-type when they are close to the conduction band and acceptor-like when they are close to the valence band.

In a-Si the density of the deep states is very high and impedes the doping of this material. However, it has been shown that the incorporation of hydrogen to the a-Si network can passivate these dangling bonds and by doing so greatly reduce the density of deep states and allow for its doping, as demonstrated by Spear and Le Comber.¹ One way to represent the density of states of a-Si:H is shown on Fig. 1.15. We make a distinction

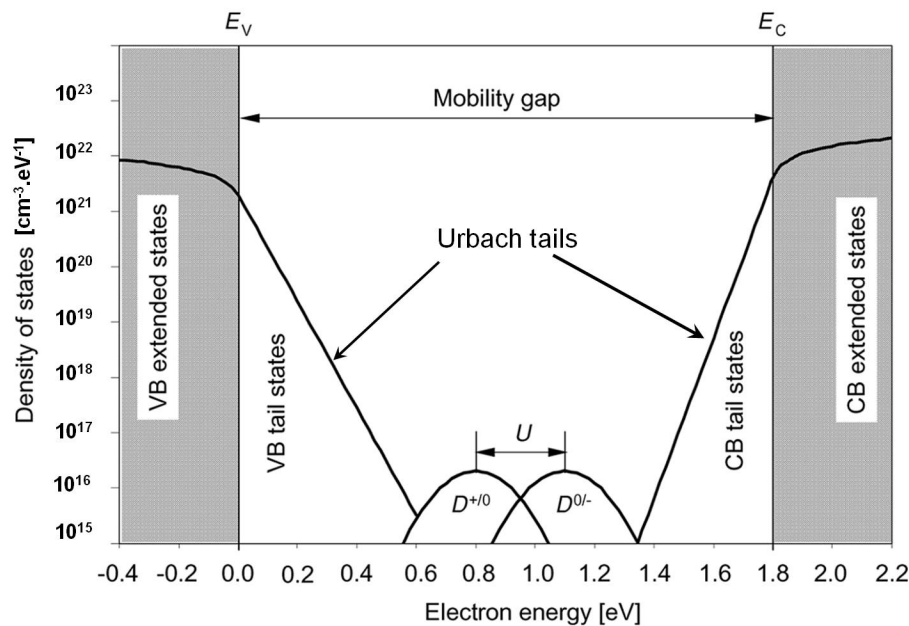


Figure 1.15 – Density of states of a-Si:H (from Ref. [27])

between the mobility gap (E_{μ}) which is taken at the end of the parabolic density of states of the valence or conduction band, that is the border between localized and extended states, and the optical bandgap (E_g), which is smaller since the localized states can contribute to the absorption. It is

¹Spear and Le Comber, "Substitutional doping of amorphous silicon", 1975 [26]

commonly considered that $E_{\mu} \approx E_g + 0.15 \text{ eV}$.¹ In the middle of the gap we have two Gaussian distributions of defects, due to the dangling bonds. The dangling bonds are commonly referred to as amphoteric defects since they can act as donor or acceptor defects. When they are acceptor defects the DB can have zero electron (+q) or one electron (o). When they are donor defects they can have one electron (o) or two electron (-q). This corresponds to the $D^{+/o}$ and $D^{o/-}$ Gaussians respectively on Fig. 1.15. The energy difference between the centers of these two Gaussians is called U , correlation energy, and it corresponds to the energy needed to add one electron to a DB occupied by one electron.

There is also another description of the defects of a-Si:H called the Defect-Pool Model. It has been proposed by *Winer, Powell and Deane*.^{2,3,4} The idea is that there is a thermodynamical equilibrium between the weak Si-Si bonds and the dangling bonds in the material and that this equilibrium depends on the Fermi level energy (the doping). The dangling bonds can be broken by the hydrogen present in the material. Roughly, if the material is n-doped, there will be an excess of electrons in the material and the material will “respond” to this increase by breaking weak Si-Si bonds. These dangling bonds will be able to trap some of these electrons and therefore become acceptor-like. By doing so the material will have a higher density of states in the gap close to the valence band. The opposite applies for holes.

We will not describe the recombination processes in a-Si:H since they have been described in the section on c-Si. One of the most common ways to obtain a-Si:H is to deposit it by Plasma Enhanced Chemical Vapour Deposition (PECVD). This deposition technique and the obtained materials are described in the next chapter, partly devoted to experimental aspects (§2.1.2, p. 41).

1.5 Indium Tin Oxide (ITO)

A third material of importance for heterojunction solar cells is ITO.⁵ ITO belongs to a material family called the TCOs (Transparent Conductive Oxides). These materials are high bandgap semiconductors ($\geq 3.3 \text{ eV}$), thus transparent (at least in the visible range), but also conductive. Example of reviews of the existing TCOs and their range of possible use can be found in *Fortunato et al*,⁶ or in *Gordon*.⁷ This material is needed since our doped a-Si:H layers are not conductive enough to allow for an efficient lateral collection. Hence we need to add at the front of our solar cell, where the grid

¹Chen and Wronski, “Internal photoemission on a-Si:H Schottky barrier structures revisited”, 1995 [28]

²Winer, “Defect formation in a-Si:H”, 1990 [29]

³Powell and Deane, “Improved defect-pool model for charged defects in amorphous silicon”, 1993 [30]

⁴Powell and Deane, “Defect-pool model and the hydrogen density of states in hydrogenated amorphous silicon”, 1996 [31]

⁵Indium Tin Oxide even if a more correct description of such a material would be Tin-doped Indium Oxide

⁶Fortunato, Ginley, Hosono, and Paine, “Transparent Conducting Oxides for Photovoltaics”, 2007 [32]

⁷Gordon, “Criteria for Choosing Transparent Conductors”, 2000 [33]

is, another material that will improve the carrier collection. The requirement for this layer is that it should be transparent to let the incident light be absorbed in the active layers of the cell and conductive to allow for the carrier collection. ITO can fulfill these two requirements. Additionally, as it has a refractive index close to 2 it can be used as an anti-reflection coating for our solar cells. It has a bandgap energy of about 3.5 eV or higher and a work function close to 4.6 eV.¹ ITO is an oxide material (In_2O_3) that can be doped in two ways:²

1. addition of tetravalent tin (Sn) atoms that will release one electron
2. oxygen vacancies that are expected to release two electrons

Generally speaking, ITO films are obtained by magnetron sputtering from a ceramic target made up of a mixture of In_2O_3 and SnO_2 . The optimum ratio of the two oxides in the target, as deduced by years of optimization, is found to be $\frac{\text{In}_2\text{O}_3}{\text{SnO}_2} = \frac{9}{1}$ and is used in our target. Magnetron sputtering means that a radial magnet is attached behind the ceramic target: a magnetic field exists close to the target that forces the electrons of the plasma to have an helical trajectory along the field lines. By doing so we increase the mean free path of the electrons and increase the probability of collision with other particles of the plasma so that the density of ionized atoms is higher close to the target. Thus, we can sustain a plasma at lower gas pressures and also increase the deposition rate. The gas is a mixture of argon and oxygen. The oxygen was in our case provided by a cylinder in which O_2 was 3%-diluted in Ar. Oxygen and substrate temperature play an important role during the deposition since it was shown that crystallization of ITO films could occur at a substrate temperature of about 150°C .³ and that oxygen incorporation to the gas mixture could strongly modify the electrical and optical properties of the material. Indeed, it results in a U-shape dependence of the resistivity when plotted against the oxygen flow rates,^{4,5} that can be even more dramatic when the deposition is made from metal alloys target such as In:Sn targets with a 9:1 ratio.⁶

On Fig. 1.16 we have plotted the transmission spectra of ITO films deposited on glass for various oxygen (in argon) flow rates. The working pressure was $5 \cdot 10^{-3}$ mbar and we had to slightly adjust the argon flow rate to keep the same total pressure. The deposition time was 2 minutes, resulting in 75 nm films, and the substrate temperature was set at 180°C .

¹Minami, Miyata, and Yamamoto, "Work function of transparent conducting multicomponent oxide thin films prepared by magnetron sputtering", 1998 [34]

²Shigesato and Paine, "Study of the effect of Sn doping on the electronic transport properties of thin film indium oxide", 1993 [35]

³Lee, Kim, Cho, and Lee, "Effect of process parameters on the characteristics of indium tin oxide thin film for flat panel display application", 1997 [36]

⁴Bender, Seelig, Daube, Frankenberger, Ocker, and Stollenwerk, "Dependence of oxygen flow on optical and electrical properties of DC-magnetron sputtered ITO films", 1998 [37]

⁵Terzini, Nobile, Loreti, Minarini, Polichetti, and Thilakan, "Influences of Sputtering Power and Substrate Temperature on the Properties of RF Magnetron Sputtered Indium Tin Oxide Thin Films", 1999 [38]

⁶Mientus and Ellmer, "Reactive magnetron sputtering of tin-doped indium oxide (ITO): influence of argon pressure and plasma excitation mode", 2001 [39]

Apart from the sample with the lowest oxygen flow rate they all show very similar results in the visible and near IR. However, the spectra are different in the IR part of the spectrum. Indeed, adding a small amount of oxygen to the gas mixture is beneficial since it reduces the number of free carriers, as shown by the decrease of the free-carrier absorption in the IR part of the spectrum on Fig. 1.16, and increases the mobility (Fig. 1.17).

On Fig. 1.17, we have plotted the resistivity and Hall mobility as obtained from hall effect measurements. We can indeed observe the U-shape dependence of the resistivity of the ITO films. Indeed, when increasing the oxygen flow rate, we expect to have a beneficial effect on the electrical properties, resistivity and mobility, as observed. However, beyond a certain oxygen content, the oxygen vacancies will start to decrease, so that the resistivity will increase.

As we have to comply with a low square resistance condition for our ITO films, we have used during my doctoral work the 3 sccm flow rate for the Ar+O₂ gas mixture since it gives the lowest resistivity and could produce an efficient anti-reflective coating and a good transparency in the range of interest for c-Si solar cells. However, the final optimization of heterojunction solar cells will require to go back to the ITO optimization since we found a current density limitation that need to be overcome by a subsequent ITO improvement of both the transparency and the reflectivity of such films.

1.6 Conclusions

This chapter has introduced some of the most important concepts of solid state physics needed to understand and thus design photovoltaic devices. Radiative, Auger and Shockley-Read-Hall recombination processes have been described, and some orders of magnitude given. The charge transport has also been described in terms of drift and diffusion. Also, we have introduced the main materials that have been investigated or used during this doctoral work, namely crystalline silicon (c-Si), hydrogenated amorphous silicon (a-Si:H) and indium tin oxide (ITO).

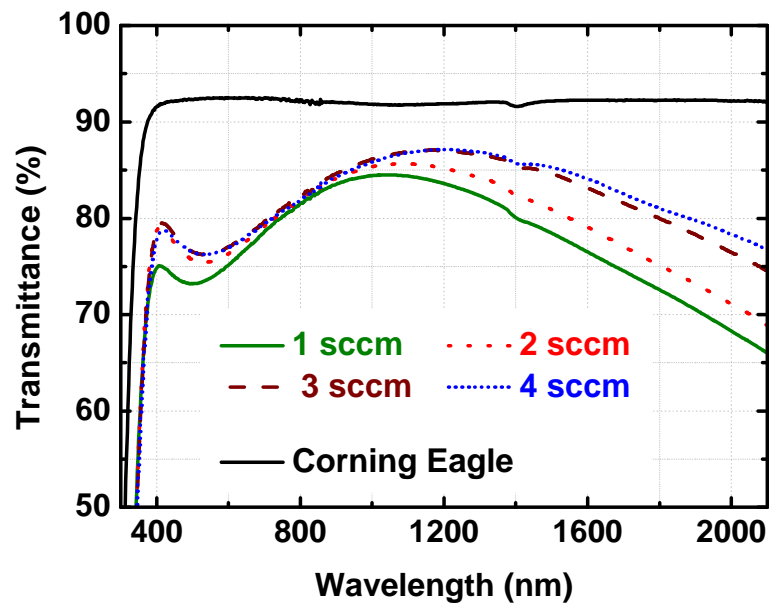


Figure 1.16 – Transmission spectra of ITO films deposited on glass substrate for various oxygen (in argon) flow rates. We also plotted the transmission spectrum of a bare glass substrate for a more comprehensible comparison

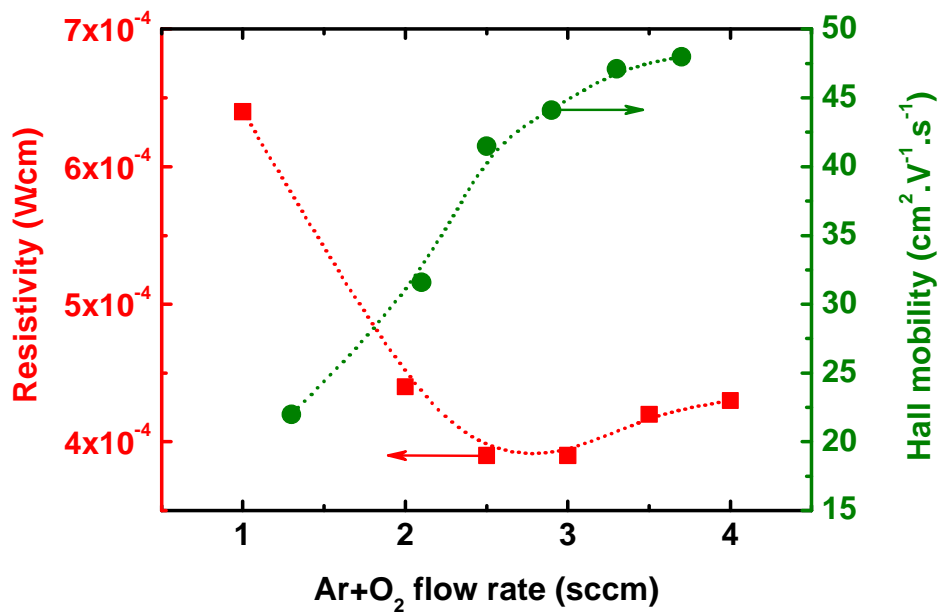


Figure 1.17 – Resistivity and Hall mobility of ITO films deposited on glass substrate plotted against the Ar+O₂ flow rate

REFERENCES

- [1] W. Shockley and H. J. Queisser. “Detailed Balance Limit of Efficiency of $p - n$ Junction Solar Cells”. In: *Journal of Applied Physics* 32 (1961), pp. 510–519. DOI: 10.1063/1.1736034 (cit. on p. 11).
- [2] Y. Poissant, P. Chatterjee, and P. Roca i Cabarrocas. “Analysis and optimization of the performance of polymorphous silicon solar cells: Experimental characterization and computer modeling”. In: *Journal of Applied Physics* 94 (2003), pp. 7305–7316. DOI: 10.1063/1.1623610 (cit. on pp. 11, 26).
- [3] Billel Kalache. “Rôle des ions dans les mécanismes de croissance du silicium microcristallin obtenu par voie plasma: Applications aux dispositifs photovoltaïques”. PhD thesis. École Polytechnique, 2003 (cit. on p. 11).
- [4] M. E. Gueunier, J.P. Kleider, R. Brüggemann, S. Lebib, P. Roca i Cabarrocas, R. Meaudre, and B. Canut. “Properties of polymorphous silicon–germanium alloys deposited under high hydrogen dilution and at high pressure”. In: *Journal of Applied Physics* 92 (2002), pp. 4959–4967. DOI: 10.1063/1.1508429 (cit. on p. 11).
- [5] L. Yu, B. O’Donnell, P.-J. Alet, and P. Roca i Cabarrocas. “All-in-situ fabrication and characterization of silicon nanowires on TCO/glass substrates for photovoltaic application”. In: *Solar Energy Materials and Solar Cells* 94 (2010), pp. 1855–1859. DOI: 10.1016/j.solmat.2010.06.021 (cit. on p. 12).
- [6] Alet, P.-J., Palacin, S., Roca i Cabarrocas, P., Kalache, B., Firon, M., and de Bettignies, R. “Hybrid solar cells based on thin-film silicon and P₃HT”. In: *Eur. Phys. J. Appl. Phys.* 36 (2006), pp. 231–234. DOI: 10.1051/epjap:2006145 (cit. on p. 12).
- [7] Jérôme Damon-Lacoste. “Vers une ingénierie de bandes des cellules solaires à hétérojonctions a-Si:H/c-Si. Rôle prépondérant de l’hydrogène.” PhD thesis. École Polytechnique, 2007. URL: http://tel.archives-ouvertes.fr/docs/00/25/95/75/PDF/Damon-Lacoste_These_protege.pdf (cit. on p. 12).
- [8] Stephen J. Fonash. *Solar Cell Device Physics, 2nd Edition*. Academic Press, Elsevier, 2010 (cit. on pp. 12, 21).
- [9] Jenny Nelson. *The physics of solar cells*. Imperial College Press, 2003 (cit. on pp. 12, 21).
- [10] Peter Würfel. *Physics of Solar Cells: From Basic Principles to Advanced Concepts, 2nd edition*. Wiley, 2009 (cit. on pp. 12, 15).

- [11] A. B. Sproul and M. A. Green. "Improved value for the silicon intrinsic carrier concentration from 275 to 375 K". In: *Journal of Applied Physics* 70 (1991), pp. 846–854. DOI: 10.1063/1.349645 (cit. on p. 13).
- [12] Isidro Garcia Martin. "Silicon surface passivation by Plasma Enhanced Chemical Vapor Deposited amorphous silicon carbide films". PhD thesis. Universitat Politecnica de Catalunya, 2001 (cit. on pp. 21, 23).
- [13] H. Schlangenotto, H. Maeder, and W. Gerlach. "Temperature dependence of the radiative recombination coefficient in silicon". In: *physica status solidi (a)* 21 (1974), pp. 357–367. DOI: 10.1002/pssa.2210210140 (cit. on p. 21).
- [14] Mark J. Kerr and Andres Cuevas. "General parameterization of Auger recombination in crystalline silicon". In: *Journal of Applied Physics* 91 (2002), p. 2473. DOI: 10.1063/1.1432476 (cit. on p. 22).
- [15] R. N. Hall. "Electron-Hole Recombination in Germanium". In: *Phys. Rev.* 87 (1952), p. 387. DOI: 10.1103/PhysRev.87.387 (cit. on p. 23).
- [16] W. Shockley and W. T. Read. "Statistics of the Recombinations of Holes and Electrons". In: *Phys. Rev.* 87 (1952), pp. 835–842. DOI: 10.1103/PhysRev.87.835 (cit. on p. 23).
- [17] M. Reuter, W. Brendle, O. Tobail, and J. H. Werner. "50 μm thin solar cells with 17.0% efficiency". In: *Solar Energy Materials & Solar Cells* 93 (2009), pp. 704–706. DOI: 10.1016/j.solmat.2008.09.035 (cit. on p. 24).
- [18] T. Mishima, M. Taguchi, H. Sakata, and E. Maruyama. "Development status of high-efficiency HIT solar cells". In: *Solar Energy Materials & Solar Cells* 95 (2011), pp. 18–21. DOI: 10.1016/j.solmat.2010.04.030 (cit. on p. 24).
- [19] L. Gautero, M. Hofmann, J. Rentsch, A. Lemke, S. Mack, J. Seiffe, J. Nekarda, D. Biro, A. Wolf, B. Bitnar, J.-M. Sallese, and R. Preu. "All-screen-printed 120 μm thin large area silicon solar cells applying dielectric rear passivation and laser-fired contacts reaching 18% efficiency". In: *34th IEEE Photovoltaic Specialist Conference, 7-12 June, Philadelphia, USA*. 2009. DOI: 10.1109/PVSC.2009.5411562 (cit. on p. 25).
- [20] I. Stenger, A. Abramov, C. Barthou, Th. Nguyen-Tran, A. Frigout, and P. Roca i Cabarrocas. "Strong orange/red electroluminescence from hydrogenated polymorphous silicon carbon light-emitting devices". In: *Applied Physics Letters* 92, 241114 (2008), p. 241114. DOI: 10.1063/1.2948852 (cit. on p. 26).
- [21] M. Oudwan, O. Moustapha, A. Abramov, D. Daineka, Y. Bonnassieux, and P. Roca i Cabarrocas. "Threshold voltage shift under electrical stress in amorphous, polymorphous, and microcrystalline silicon bottom gate thin-film transistors". In: *physica status solidi (a)* 207 (2010), pp. 1245–1248. DOI: 10.1002/pssa.200925403 (cit. on p. 26).

- [22] R.A. Street. *Hydrogenated Amorphous Silicon*. Ed. by Cambridge University Press. 1991 (cit. on p. 26).
- [23] Tim Searle. *Properties of Amorphous Silicon and Its Alloys*. INSPEC, 1998 (cit. on p. 26).
- [24] M. F. Thorpe and D. Weaire. "Electronic Density of States of Amorphous Si and Ge". In: *Phys. Rev. Lett.* 27 (1971), pp. 1581–1584. DOI: 10.1103/PhysRevLett.27.1581 (cit. on p. 26).
- [25] P. W. Anderson. "Absence of Diffusion in Certain Random Lattices". In: *Phys. Rev.* 109 (1958), pp. 1492–1505. DOI: 10.1103/PhysRev.109.1492 (cit. on p. 26).
- [26] W.E. Spear and P.G. Le Comber. "Substitutional doping of amorphous silicon". In: *Solid State Communications* 17 (1975), pp. 1193–1196. DOI: 10.1016/0038-1098(75)90284-7 (cit. on p. 27).
- [27] Jef Poortmans and Vladimir Arkhipov. *Thin Film Solar Cells: Fabrication, Characterization, And Applications*. Wiley, 2006 (cit. on p. 27).
- [28] I.-S. Chen and C. R. Wronski. "Internal photoemission on a-Si:H Schottky barrier structures revisited". In: *Journal of Non-Crystalline Solids* 190 (1995), pp. 58–66. DOI: 10.1016/0022-3093(95)00257-X (cit. on p. 28).
- [29] K. Winer. "Defect formation in a-Si:H". In: *Phys. Rev. B* 41 (1990), pp. 12150–12161. DOI: 10.1103/PhysRevB.41.12150 (cit. on p. 28).
- [30] M. J. Powell and S. C. Deane. "Improved defect-pool model for charged defects in amorphous silicon". In: *Phys. Rev. B* 48 (1993), pp. 10815–10827. DOI: 10.1103/PhysRevB.48.10815 (cit. on p. 28).
- [31] M. J. Powell and S. C. Deane. "Defect-pool model and the hydrogen density of states in hydrogenated amorphous silicon". In: *Phys. Rev. B* 53 (1996), pp. 10121–10132. DOI: 10.1103/PhysRevB.53.10121 (cit. on p. 28).
- [32] E. Fortunato, D. Ginley, H. Hosono, and D. C. Paine. "Transparent Conducting Oxides for Photovoltaics". In: *MRS Bulletin* 32 (2007), pp. 242–247 (cit. on p. 28).
- [33] Roy G. Gordon. "Criteria for Choosing Transparent Conductors". In: *MRS Bulletin* (2000), pp. 52–57 (cit. on p. 28).
- [34] T. Minami, T. Miyata, and T. Yamamoto. "Work function of transparent conducting multicomponent oxide thin films prepared by magnetron sputtering". In: *Surface and Coatings Technology* 108-109 (1998), pp. 583–587. DOI: 10.1016/S0257-8972(98)00592-1 (cit. on p. 29).
- [35] Y. Shigesato and D. C. Paine. "Study of the effect of Sn doping on the electronic transport properties of thin film indium oxide". In: *Applied Physics Letters* 62 (1993), pp. 1268–1270. DOI: 10.1063/1.108703 (cit. on p. 29).

- [36] B. H. Lee, I. G. Kim, S. W. Cho, and S.-H. Lee. "Effect of process parameters on the characteristics of indium tin oxide thin film for flat panel display application". In: *Thin Solid Films* 302 (1997), pp. 25–30. DOI: 10.1016/S0040-6090(96)09581-8 (cit. on p. 29).
- [37] M. Bender, W. Seelig, C. Daube, H. Frankenberger, B. Ocker, and J. Stollenwerk. "Dependence of oxygen flow on optical and electrical properties of DC-magnetron sputtered ITO films". In: *Thin Solid Films* 326 (1998), pp. 72–77. DOI: 10.1016/S0040-6090(98)00521-5 (cit. on p. 29).
- [38] E. Terzini, G. Nobile, S. Loreti, C. Minarini, T. Polichetti, and P. Thilakan. "Influences of Sputtering Power and Substrate Temperature on the Properties of RF Magnetron Sputtered Indium Tin Oxide Thin Films". In: *Japanese Journal of Applied Physics* 38 (1999), pp. 3448–3452. DOI: 10.1143/JJAP.38.3448 (cit. on p. 29).
- [39] R. Mientus and K. Ellmer. "Reactive magnetron sputtering of tin-doped indium oxide (ITO): influence of argon pressure and plasma excitation mode". In: *Surface and Coatings Technology* 142-144 (2001), pp. 748–754. DOI: 10.1016/S0257-8972(01)01160-4 (cit. on p. 29).

EXPERIMENTAL — THEORETICAL INTRODUCTION TO SILICON PASSIVATION AND HETEROJUNCTIONS

2

Contents

2.1	Fabrication and characterisation of thin films and solar cell precursors	38
2.1.1	Heterojunction solar cell	38
2.1.2	Plasma enhanced chemical vapour deposition (PECVD)	41
2.1.3	Thermal evaporation	48
2.1.4	Spectroscopic ellipsometry (SE)	49
2.1.5	Effective lifetime measurements	54
2.2	Surface passivation	57
2.2.1	Theoretical point of view	57
2.2.2	Practical point of view	58
2.3	Physics of heterojunction solar cells	61
2.3.1	Interest, drawbacks	61
2.3.2	Band offsets	61
2.3.3	Intrinsic layer	64
2.3.4	Doped layers	66
2.3.5	ITO contact	67
2.4	Conclusions	68

AFTER having introduced in the previous chapter the most relevant elements of semiconductor physics, we will address here the heterojunction solar cell itself, trying to figure out what the fundamental parameters are and the main requirements to achieve high efficiencies. We will review the state of the art as well as the main findings and challenges regarding crystalline surface passivation by a-Si:H materials for heterojunction solar cells. We will also describe a few techniques used to fabricate and characterize our devices and assess their quality through the entire fabrication sequence.

2.1 Fabrication and characterisation of thin films and solar cell precursors

This section will be devoted to the description of the experimental setups dedicated to the fabrication and the characterization of our solar cells. Here, by “precursor” we refer to unborn solar cells where only the a-Si:H layers have been deposited but neither the ITO nor the metal contacts.

2.1.1 Heterojunction solar cell

We have introduced many semiconductor materials needed to fabricate heterojunction solar cells. Before we start to describe the deposition and characterization techniques we used during this work to obtain these materials, we need to introduce the structure of the standard heterojunction solar cell of this work, which is schematized on Fig. 2.1b. On Fig. 2.1 we show the schematic views of:

- Fig. 2.1a, the PERL record cell with an efficiency of 25%
- Fig. 2.1b, our standard heterojunction solar cell

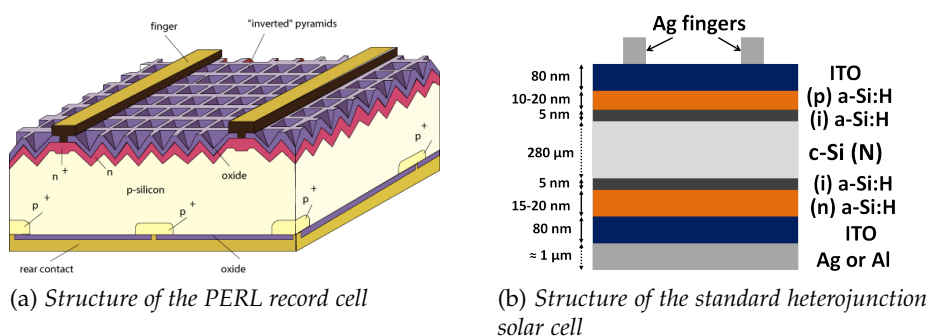


Figure 2.1 – Comparison of the structure of the PERL and standard heterojunction solar cell

The PERL¹ cell has been developed over the years by Prof. Martin A. Green from the UNSW group. It consists of a p-type silicon wafer

¹Passivated Emitter Rear Locally-diffused

processed using microelectronics techniques to provide the most efficient silicon-based device that has now¹ reached a 25% efficiency.²

Contrariwise, our solar cell is based on a n-type c-Si wafer absorber material. The emitter is a thin undoped a-Si:H layer capped by a thicker p-type a-Si:H layer. The BSF consists of a thin undoped a-Si:H layer capped by a n-type a-Si:H layer. On the front side of the solar cell a sputtered ITO layer acts as both anti-reflection coating and transparent electrode. However, given the conductivity of the ITO layer we have to use a metal grid to enhance the collection of carriers. On the back side of the solar cell we also use an ITO layer whose role is to increase the reflection of the light on the rear surface. As the solar cell is illuminated only from the front side, we could put metal on the entire surface of the back side to collect the carriers in the most effective way.

In this section we will describe all the steps involved in the fabrication of an heterojunction solar cell and introduce some of the characterization tools we used on a daily basis. The silicon wafers we used were almost always provided by Topsil and had a resistivity of 1–5 $\Omega\cdot\text{cm}$ for a thickness of 280 μm . Unless stated, they were all n-type and polished on both sides. The fabrication sequence started by wetting the surface of our c-Si wafers, that are hydrophilic in their oxidized state, with deionized water in order to remove possible dust. Consecutively, there was a 30 seconds dip in a HF solution previously diluted in deionized water³ to reach a concentration of 5% (starting from 40%). H-terminated c-Si surfaces are hydrophobic so that upon removal from the PTFE beaker⁴ the very few, if any, droplets left on the wafer could be blown away towards the sink by the nitrogen blower. The wafers were then immediately loaded into the ARCAM PECVD reactor that was closed and pumped down. Depending on the reactor temperature, the time needed to load the substrate and achieve a “good” vacuum could vary between 30 to 60 minutes. Usually, we started the deposition after 30 minutes of pumping for we would get a base pressure of $5\text{--}9 \times 10^{-7}$ mbar. This reactor was used for the growth of all of our silicon based thin films and is described below, as well as the PECVD technique itself (§2.1.2, page 41). The reactor has no load-lock facility so that when we had deposited on one side of the wafer, we had to open the reactor, flip the sample, without performing any additional HF-dip, to allow for the deposition of the other side. Once deposited, the optical properties and thicknesses of the films were checked by spectroscopic ellipsometry, a technique described below (§2.1.4, p. 49). The passivation of the solar cells was characterized by photoconductance decay, using a Sinton lifetime tester as explained below (§2.1.5, p. 54). On Fig. 2.2, we have plotted the integrated reflectance of c-Si wafers, flat and textured, covered by an ITO film, to show the decrease of the reflectivity compared to a flat bare c-Si wafer. For an ITO thickness of 80 nm we have

¹Thanks to a new definition of the AM1.5 spectrum

²Green, Emery, Hishikawa, and Warta, “Solar cell efficiency tables (version 36)”, 2010 [1]

³The water’s resistivity was measured on the purifier itself and was expected to be of 18 $\text{M}\Omega\cdot\text{cm}$

⁴PTFE stands for PolyTetraFluoroEthylene. It is commercialized by the American company DuPont under the Teflon trademark. This plastic-like material is hydrophobic and known to resist to hydrofluoric acid, unlike glass.

an anti-reflection coating, with a minimum of reflectivity around 630 nm, which is the maximum of the AM1.5 irradiance. The sputtering technique used here has already been introduced in the first chapter (§1.5, p. 28).

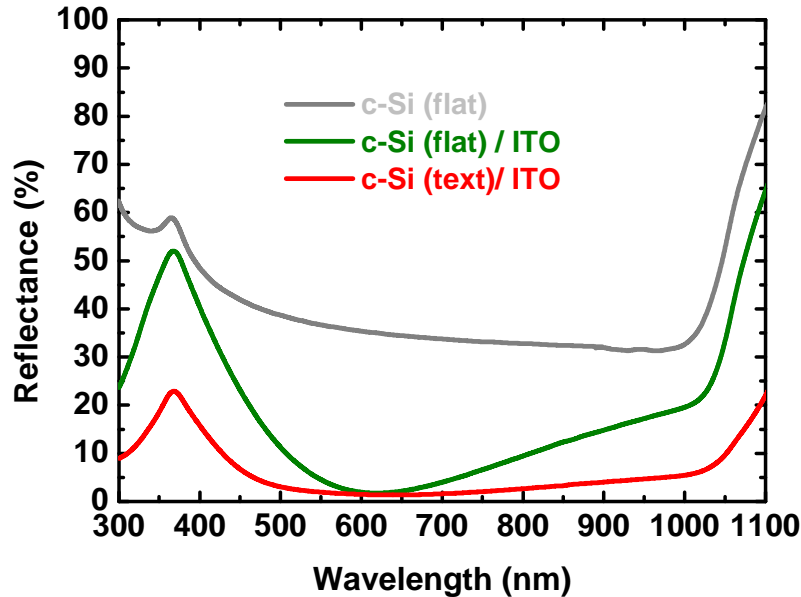


Figure 2.2 – Reflectance of a bare flat c-Si wafer, of a 80 nm ITO film on flat c-Si wafer and of 80 nm of ITO on a textured c-Si wafer

Finally, at the back side of the solar cell we evaporated some metal on the entire surface since only optical reflection and electrical conductivity matter. On the front (illuminated) side of the solar cell it is important to have an efficient carrier collection while minimizing the optical losses due to the metal on the front side. At this point we had the possibility to choose between two options:

1. Complete the cells at LPICM. For that purpose we thermally evaporated a silver grid through a shadow mask. The description of the thermal evaporator is to be found below (§2.1.3, page 48). In that case the ITO was also sputtered through a shadow mask. The resulting cells are shown on the right part of Fig. 2.3 and were squares of 1 or 4 cm².
2. Send the samples with ITO and back metallization to INES where an aluminium silver paste would be screen-printed onto the front ITO resulting in 25 cm² square cells that were cleaved by laser to define more precisely the surface and avoid lateral effects. The resulting cell is shown on the left part of Fig. 2.3.

When a solar cell was completed a current-voltage measurement was performed at 25°C and under an AM1.5 illumination. This measurement allowed one to get access to the solar cell parameters, particularly its efficiency.

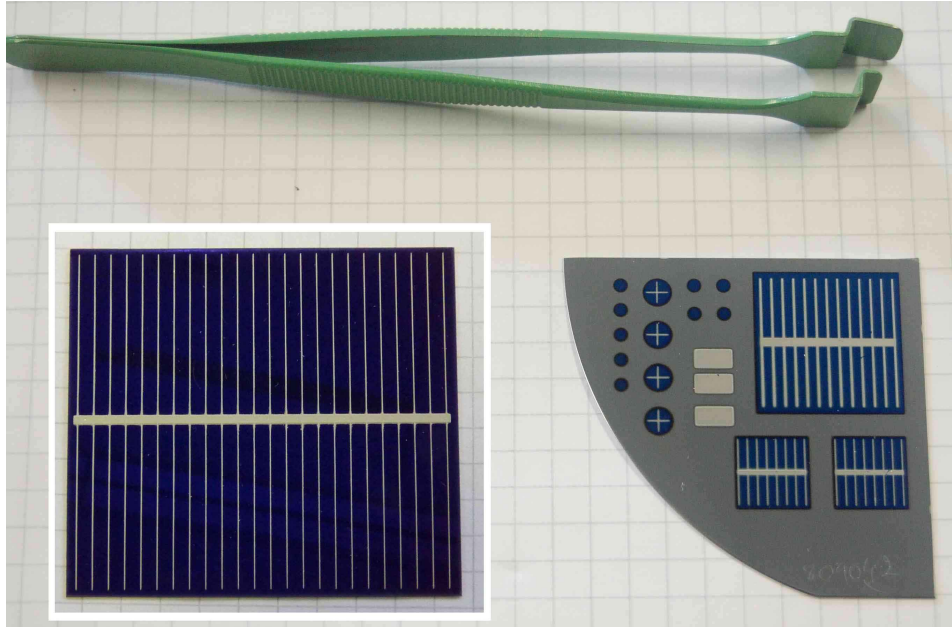


Figure 2.3 – Completed solar cells when a screen-printed grid (left) from INES or an evaporated silver grid (right) from LPICM was applied.

2.1.2 Plasma enhanced chemical vapour deposition (PECVD)

The LPICM has a very long history on silicon thin films deposition, mostly based on silane plasmas. The laboratory has used various sources like Photo-CVD, multipolar DC, Hot Wire CVD (also frequently referred to by Cat-CVD, i.e. Catalytic CVD) to produce device grade $\mu\text{-Si:H}$,¹ and more recently it has adapted sources pioneered by *Pelletier*² to develop its own Matrix Distributed Electron Cyclotron Resonance (MDECR) plasmas³ to produce optical coatings,⁴ a-Si:H,⁵ or $\mu\text{-Si:H}$.^{6,7,8} However, most of its background comes from the extensive use of capacitively coupled RF PECVD.

In this doctoral work, RF PECVD was widely used to deposit our films

¹Niikura, Poissant, Gueunier, Kleider, and Bourée, “Transport properties of hot-wire CVD $\mu\text{-Si:H}$ layers for solar cells”, 2002 [2]

²Lacoste, Lagarde, Béchu, Arnal, and Pelletier, “Multi-dipolar plasmas for uniform processing: physics, design and performance”, 2002 [3]

³Daineka, Bulkin, Girard, Bourée, and Drévilion, “High density plasma enhanced chemical vapor deposition of optical thin films”, 2004 [4]

⁴Botha, Haj Ibrahim, Bulkin, and Drévilion, “Deposition of dielectrics using a matrix distributed electron cyclotron resonance plasma enhanced chemical vapor deposition system”, 2007 [5]

⁵Gueunier-Farret, Bazin, Kleider, Longeaud, Bulkin, Daineka, Dao, Roca i Cabarrocas, Descamps, Kervyn de Meerendre, Leempoel, Meaudre, and Meaudre, “Device quality a-Si:H deposited from electron cyclotron resonance at very high deposition rates”, 2006 [6]

⁶Roca i Cabarrocas, Bulkin, Daineka, Dao, Leempoel, Descamps, Kervyn de Meerendré, and Charliac, “Advances in the deposition of microcrystalline silicon at high rate by distributed electron cyclotron resonance”, 2008 [7]

⁷Kroely, “Process and material challenges in the high rate deposition of microcrystalline silicon thin films and solar cells by Matrix Distributed Electron Cyclotron Resonance plasma”, 2010 [8]

⁸Ram, Kroely, Bulkin, and Roca i Cabarrocas, “Effect of ion energy on structural and electrical properties of intrinsic microcrystalline silicon layer deposited in a matrix distributed electron cyclotron resonance plasma reactor”, 2010 [9]

and even though they have been studied for their passivation properties and their ability to produce good devices, the plasma itself has not been investigated. In the frame of this work, the reactor that we used was a capacitively coupled RF PECVD reactor named ARCAM that we used to grow a-Si:H films that we could alloy with carbon (a-SiC:H) to widen its band gap, or with germanium (a-Si:Ge:H) to narrow its band gap (not done). We could also synthesize doped films using phosphorous atoms to produce a n-type material or boron atoms to produce a p-type material. Alternatively, other kinds of materials could also be occasionally elaborated such as polymorphous silicon (pm-Si:H), microcrystalline silicon ($\mu\text{c-Si:H}$), silicon nitride (a-SiN_x:H) or epitaxial films of silicon and germanium as will be detailed in chapter 4.

2.1.2.1 ARCAM reactor

ARCAM¹ reactor is the only PECVD reactor that we used during our doctoral work. This reactor was designed and build in the early 80's. A lot of details regarding the design of this reactor can be found in *Roca i Cabarrocas et al.*² Additional information as well as experimental results dealing with materials and devices produced can be found in the thesis of *Pere Roca i Cabarrocas*.³

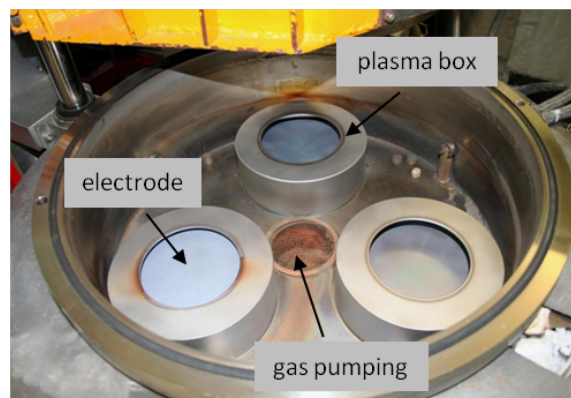


Figure 2.4 – Picture of the opened ARCAM reactor

Let us briefly describe the ARCAM reactor shown in Fig. 2.4. The reactor can be described as an oven-like structure since it is made up of a single vessel in which all the elements are kept, via the use of three Thermo-coax wires, at the same temperature. This means that the walls, the electrodes and the substrate holders are kept at the same temperature. We do have a single vessel, without any load-lock capability, but this reactor has been designed in such a way that even though the gas injected into the reactor, through a gas inlet that arrives below the electrode, “sees” the entire vessel, the plasma itself, and thus the reactive species, is confined

¹Action de Recherche Coordonnée sur les Matériaux Amorphes

²Roca i Cabarrocas, Chévrier, Huc, Lloret, Parey, and Schmitt, “A fully automated hot-wall multiplasma-monochamber reactor for thin film deposition”, 1991 [10]

³Roca i Cabarrocas, “Science des matériaux et techniques du réacteur dans le dépôt par procédé plasma RF de photopiles et d’autres dispositifs en silicium amorphe hydrogéné”, 1988 [11]

inside a plasma box as one can see on Fig. 2.4 as well as on the schematic view we displayed on Fig. 2.5.

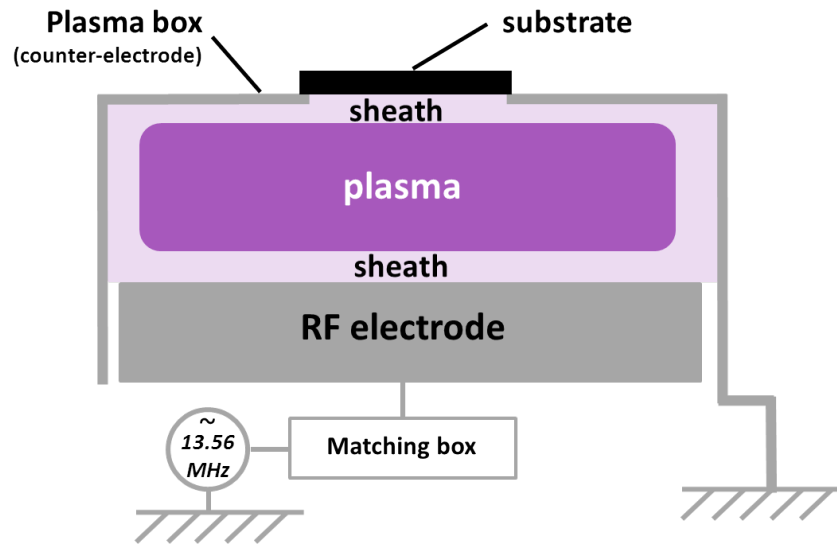


Figure 2.5 – Schematic view of the plasma box used in the ARCAM reactor

The design of this reactor aimed at avoiding cross contamination between P, I and N layers as in multichamber systems while keeping simplicity of single chamber reactors. This reactor can be therefore described as a multiplasma monochamber reactor. Indeed, the samples are located on a rotating plate which allows us to start the plasma on a blank sample before rotating the substrate holder and put it in front of the plasma. Thus, we can use one plasma box for one material, e.g. one for (p) a-Si:H, one for (n) a-Si:H and one for (i) a-Si:H. This design has already been proved to be efficient in decreasing the cross contamination and in producing sharp interfaces and device grade materials [10, 11]. Regarding the pumping system, the base pressure of 2.9×10^{-7} mbar is reached within about 30 minutes at a working temperature of 200°C and is ensured by a turbomolecular pump, backed by a rotary vane pump. The pumping of the process gases is ensured by a roots pump backed by a rotary vane pump.

2.1.2.2 Basics of PECVD

In this section, we will briefly describe some general principles of the deposition technique we used even though a more comprehensive study of plasma processes was beyond the scope of this work and can be found in some excellent textbooks such as the ones by *Chapman*,¹ or *Lieberman*.²

That said, the basic principle of this process is that we deposited films from reactive species created in a plasma, at temperatures where these gases would not thermally dissociate.³ This is due to the ionization of the neutral gas molecules by the electrons accelerated in an oscillating electric field caused by a sinusoidal voltage applied to the RF electrode (called

¹Chapman, *Glow Discharge Processes: Sputtering and Plasma Etching*, 1980 [12]

²Lieberman and Lichtenberg, *Principles of Plasma Discharges and Materials Processing, Second Edition*, [13]

³The special case of diborane B_2H_6 will be seen later in chapter 4.

cathode even if not DC). As mentioned earlier, we created our plasma inside a plasma box (Fig. 2.5) where the substrate holder is grounded. Most of the time we used conductive substrates (doped crystalline silicon) so that the substrate was grounded too. Otherwise, when using glass substrates for instance, the substrate was at floating potential. As the plasma behaves as a variable load, we need to insert a *matching box* between the RF voltage source and the plasma whose goal is to adapt the impedance of the plasma to that of a $50\ \Omega$ load for the generator that will minimize the reflected power. Such plasmas are called Capacitively Coupled Plasmas (CCP) for the discharge can be considered as capacitive. The matching box includes a blocking capacitor. Ions are much heavier than electrons so that they are more difficult to move. The result of that is that electrons can be more easily accelerated towards, and reach the anode and the cathode, which is not the case for the ions that have a too low mobility to “follow” the electric field. This will result in a potential distribution that is represented on Fig. 2.6, where the blocking capacitor will allow a self bias on the RF electrode (V_{DC}) to be created. Indeed, at each near surface

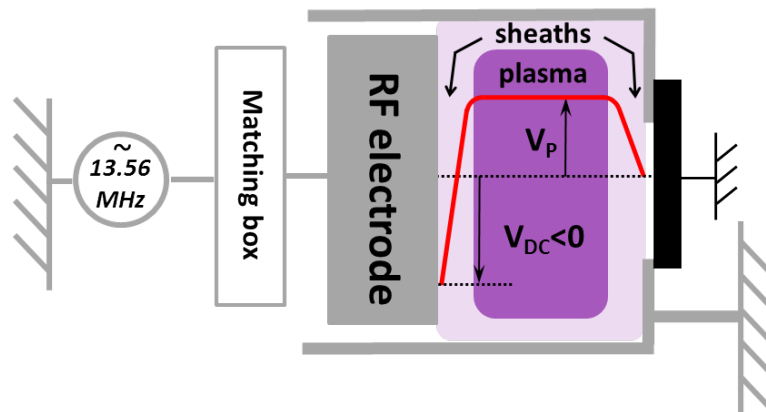


Figure 2.6 – Schematic view of the potential distribution in a RF discharge where the substrate is grounded and the RF voltage applied to the RF electrode

region there will be a deficit of electrons and therefore an accumulation of positive charges that are called *sheaths*. In a RF discharge there are generally two electrodes, the one on which the voltage is applied and the other, generally grounded. The potential drop from the plasma potential to the electrode potential is thus different. A relationship has been established [13] between the electrode areas and their voltage drops:

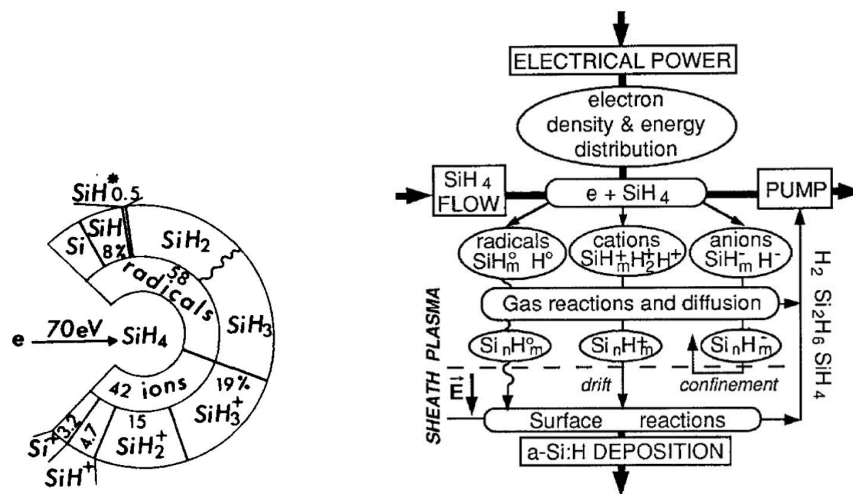
$$\frac{V_1}{V_2} = \left(\frac{A_2}{A_1} \right)^q$$

Where q is experimentally close to $\frac{5}{2}$. Unlike laboratory scaled reactors, industrial reactors are generally much larger and the difference in areas is much smaller leading to more symmetrical reactors, reducing V_{DC} . This is one of the major causes of difficulties met by engineers when trying to transfer processes from laboratory to industry. Also we usually have the following relationship which allows to have an idea of the plasma potential from easily measurable values:

$$V_p \approx \frac{V_{RF} + V_{DC}}{2}$$

where V_p , V_{RF} and V_{DC} are the plasma potential, the electrode peak to peak voltage and the self bias voltage respectively.

We have briefly described the discharge but not yet what happens to the gas. Upon impact with an electron, a monosilane molecule (SiH_4) can be dissociated into various species. On Fig. 2.7a, we have represented a pie chart showing the main species that can be generated by the dissociation of a silane molecule from the impact with an electron with an energy of 70 eV.¹ We have also inserted a very general synopsis of a-Si:H deposition mechanisms from silane glow discharges. The glow discharge is named after the fact that excited species in the plasma can recover to their fundamental energy level by emitting a photon that gives its visible light to a plasma. As one can easily see from Fig. 2.7b, a lot of species exist



(a) Probability pie chart for the silane dissociative channels due to a 70 eV electron impact (Ref. [14])

(b) Synopsis of a-Si:H deposition mechanisms from SiH_4 glow discharge (Ref. [15])

Figure 2.7 – Schematic views of the SiH_4 dissociation and plasma reactions involved in a-Si:H depositions

in the plasma. Neutral and positive ions can take part in the deposition whereas negative ions are trapped inside the bulk plasma by the repulsive forces arising from the sheaths. It is not easy to describe comprehensively the mechanisms leading to the growth of a-Si:H from such a synopsis and there is a need for a growth model, even if some complex simulation involving hundreds of reactions have been proposed.²

2.1.2.3 a-Si:H deposition

The mechanisms of the a-Si:H growth by PECVD have been studied for more than two decades. The model that appears to have emerged, but which does not address all the questions, is often referred to as the “MGP

¹Schmitt, “Fundamental mechanisms in silane plasma decompositions and amorphous silicon deposition”, 1983 [14]

²Kushner, “A model for the discharge kinetics and plasma chemistry during plasma enhanced chemical vapor deposition of amorphous silicon”, 1988 [16]

model".¹ This model has been studied a lot,^{2,3,4} and recently a paper comprehensively reviewed such a model in the frame of new experimental results, in which one can find useful references.⁵ On Fig. 2.8, we have drawn a schematic representation of the processes involved in the growth of a-Si:H in PECVD. The main assumption of this model is that the growth

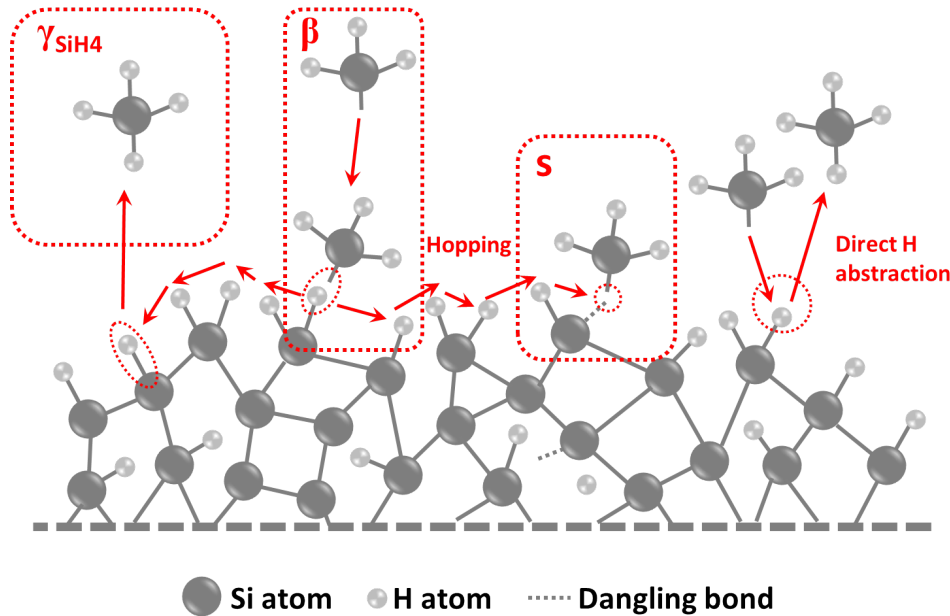


Figure 2.8 – Schematic representation of the surface reactions involved during the growth of a-Si:H in the MGP model where the SiH_3 radical is the only growth precursor.

occurs via only one precursor: the SiH_3 radical. This assumption is based on the fact that other radicals can react very quickly to form neutral gas molecules or ions or SiH_3 so that SiH_3 becomes the dominant radical, as observed experimentally by *Itabashi et al.*⁶ and predicted by *Gallagher*.⁷ When a SiH_3 radical arrives at the growth surface, it can remain on the surface and create a weak Si–H– SiH_3 bond. This is called physisorption, and the probability of this event equals β . Then it can diffuse on the surface until it either removes a H atom going back to the gas phase under the form of a SiH_4 molecule (this is H abstraction with a probability γ) or finds a dangling bond (DB) site and creates a Si– SiH_3 bond, this is the sticking with a probability s . We have $\beta = \gamma + s$. One should note that two diffusing SiH_3 radicals can also leave the surface as a disilane molecule (Si_2H_6). Here, $\gamma = \gamma_{\text{SiH}_4} + \gamma_{\text{Si}_2\text{H}_6}$ comprises the probability of leaving as a silane and a disilane. The diffusion of radicals can occur on a distance of a

¹Named after the researchers Akihisa Matsuda, Alan Gallagher and Jérôme Perrin.

²Perrin, "Plasma and surface reactions during a-Si:H film growth", 1991 [15]

³Matsuda, Nomoto, Takeuchi, Suzuki, Yuuki, and Perrin, "Temperature dependence of the sticking and loss probabilities of silyl radicals on hydrogenated amorphous silicon", 1990 [17]

⁴Street, *Hydrogenated Amorphous Silicon*, 1991 [18]

⁵Kessels, Smets, Marra, Aydil, Schram, and van de Sanden, "On the growth mechanism of a-Si:H", 2001 [19]

⁶Itabashi, Nishiwaki, Magane, Naito, Goto, Matsuda, Yamada, and Hirota, "Spatial Distribution of SiH_3 Radicals in RF Silane Plasma", 1990 [20]

⁷Gallagher, "Neutral radical deposition from silane discharges", 1988 [21]

few nanometers, relatively independently from the incident angle of hydrogen surface coverage, as obtained from calculations.¹ However, some experiments have been interpreted as an evidence of the importance of the surface diffusion in the change of the growth regime towards $\mu\text{c-Si:H}$ and that such an enhancement was due to an increased atomic hydrogen flux, for temperatures lower than the desorption temperature where the mobility of species is decreased.² Also, it should be noted that molecular dynamics has shown that direct abstraction of hydrogen by a SiH_3 radical, as described on Fig. 2.8, was possible, resulting in a DB to which other impinging SiH_3 radicals can stick,³ and that about half of the incoming radicals could act so.⁴ Some agreement with experimental work seems to have been found on this matter.⁵

Nevertheless, even if this early model seems to be convincing at describing standard a-Si:H growth at low deposition rates, it fails to account for the deposition of films at high deposition rates. Indeed, higher RF power, pressure, deposition rates or changes in the gas dilution have produced nanoparticles in the plasma,^{6,7,8} that could eventually be incorporated to the film and play an important role in the deposition of polymorphous silicon for instance.⁹ Besides, some authors calculated that the binding of the SiH_3 radical would not occur via the three center Si-H-SiH₃ binding previously assumed in the growth model but rather via the direct binding to a Si atom and the displacement of a H to a Si-Si bond center, but without preventing the diffusion of SiH_3 to the nearest neighbours.¹⁰ Other researchers calculated that SiH_3 radicals could diffuse on a silicon surface thanks to weak bonds with Si atoms, therefore over-coordinated, from the surface, without the breaking of any strong Si-Si bond; the incorporation to the film is done via the creation of a second bond and the transfer of the H atom.¹¹ Other researchers deduced from their calculations that there were no evidence for the existence of the Si-H-SiH₃ ph-

¹Ohira, Ukai, Adachi, Takeuchi, and Murata, "Molecular-dynamics simulations of SiH_3 radical deposition on hydrogen-terminated silicon (100) surfaces", 1995 [22]

²Gerbi and Abelson, "Deposition of microcrystalline silicon: Direct evidence for hydrogen-induced surface mobility of Si adspecies", 2001 [23]

³Ramalingam, Maroudas, Aydil, and Walch, "Abstraction of hydrogen by SiH_3 from hydrogen-terminated Si(001)-(2×1) surfaces", 1998 [24]

⁴Cereda, Ceriotti, Montalenti, Bernasconi, and Miglio, "Quantitative estimate of H abstraction by thermal SiH_3 on hydrogenated Si(001)(2×1)", 2007 [25]

⁵Kessels, Smets, and van de Sanden, "The a-Si:H growth mechanism and the role of H abstraction from the surface by SiH_3 radicals via an Eley-Rideal mechanism", 2004 [26]

⁶Hollenstein, "The physics and chemistry of dusty plasmas", 2000 [27]

⁷Roca i Cabarrocas, Nguyen-Tran, Djeridane, Abramov, Johnson, and Patriarche, "Synthesis of silicon nanocrystals in silane plasmas for nanoelectronics and large area electronic devices", 2007 [28]

⁸Nguyen-Tran, Roca i Cabarrocas, and Patriarche, "Study of radial growth rate and size control of silicon nanocrystals in square-wave-modulated silane plasmas", 2007 [29]

⁹Roca i Cabarrocas, Fontcuberta i Morral, and Poissant, "Growth and optoelectronic properties of polymorphous silicon thin films", 2002 [30]

¹⁰Dewarrat and Robertson, "Surface diffusion of SiH_3 radicals and growth mechanism of a-Si:H and microcrystalline Si", 2003 [31]

¹¹Valipa, Bakos, and Maroudas, "Surface smoothness of plasma-deposited amorphous silicon thin films: Surface diffusion of radical precursors and mechanism of Si incorporation", 2006 [32]

ysisorption state and that H abstraction from the surface was energetically easier than by a SiH_3 radical.¹

There are many other articles providing variations on the initial growth model but it should be noted that all simulations do not agree between them and that some of them may change the microscopic phenomena without changing the results at the macroscopic level. The only conclusion is that the simple MPG model provides a very interesting frame to think on the deposition process but one has to remember that it does not account for all the observed phenomena and that the progress in numerical simulations could help to provide a better and deeper understanding.

2.1.3 Thermal evaporation

Thermal evaporation was used for all of our samples metallization. It is a simple technique that allows to deposit materials, mostly metals, at a relatively high deposition rate (up to $1 \mu\text{m}\cdot\text{min}^{-1}$). However, this technique is not very thrifty as most of the material is not deposited on the sample. The principle of this technique is straightforward. Indeed, it is made up of a vacuum vessel in which we put our sample, facing down, in front of a boat filled with powders of the metal we want to evaporate (Fig. 2.9). The vessel is then pumped down to a base pressure of about 5×10^{-6} mbar. Then a high current (several amperes) is applied on the boat,² which is heated by Joule effect, until the boat temperature reaches the melting temperature of the contained metal. By doing so, we allow the particles to evaporate and condense on the surface of the sample. The vessel having been pumped down, the vapours coming from other sources are very rare and given that this process occurs in vacuum (in a rarefied atmosphere) the particles have a very long mean free path allowing them to reach directly the surface of the sample. Other sources of energy exist for such a process. Among them the most common is the electron beam evaporation, for which an electron beam is directed, thanks to magnets, to a boat containing metal powders. This process allows to reach much higher temperatures and therefore to evaporate metals with a much higher melting temperature. The set-up we used is schematized on Fig. 2.9. The pumping system consists of a turbomolecular pump backed by a rotary vane pump. In our case the thickness was monitored by a quartz crystal microbalance. Indeed, quartz exhibits piezoelectric properties so that when a voltage is applied to it, the crystal responds to this solicitation by a mechanical stress. The resonant frequency of a quartz crystal oscillator depends on its weight so that when the evaporation takes place, and taking into account the metal density, we can determine, in real time, what is the thickness of the evaporated film. Some precautions should be taken regarding the vacuum level since some materials, like aluminium, may form oxides with the residual oxygen atoms. Moreover, some metals can also form alloys with the material used to fabricate the boats.

¹Gupta, Yang, and Parsons, "Ab initio analysis of silyl precursor physisorption and hydrogen abstraction during low temperature silicon deposition", 2002 [33]

²Usually made of a refractory material, in our case tungsten (W)

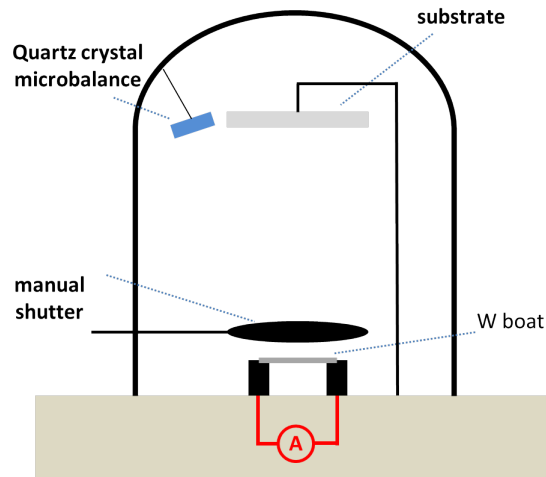


Figure 2.9 – Schematic view of the thermal evaporator

2.1.4 Spectroscopic ellipsometry (SE)

Spectroscopic ellipsometry is a very powerful tool which combines several advantages. It is a fast and non-destructive tool which can be used either in-situ or ex-situ, the latter case shown on Fig. 2.10. We can obtain informations on the thickness and other parameters of the films that will be detailed later. Our set-up is a phase modulated spectroscopic ellipsometer

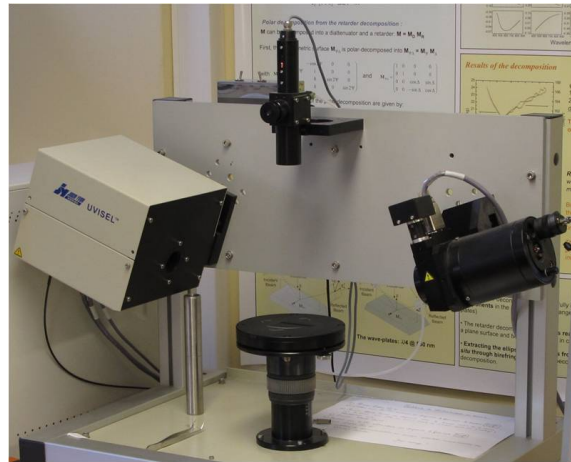


Figure 2.10 – Picture of the UVISEL based at LPICM

with a scanning range going from 1.5 to 4.7 eV. The principle of the measurement is based on the change in the polarization state of the light upon reflection on a surface, this surface generally being a thin film deposited on a substrate. The two parameters that we get from a measurement are Δ and Ψ . They are defined as follows (Eq. 2.1), where r_p and r_s are the complex Fresnel reflection coefficient of the parallel (r_p) and perpendicular (r_s) components of the light in the plane of incidence and ρ is called the complex reflectance ratio.

$$\rho = \frac{r_p}{r_s} = \tan(\Psi) \exp(i\Delta) \quad (2.1)$$

The principle of a phase modulated ellipsometer, as ours, is shown on Fig. 2.11. It consists of:

1. a source of light
2. a polarizer
3. a Photoelastic modulator (PEM)
4. an analyzer (another polarizer)
5. a monochromator and a detection system

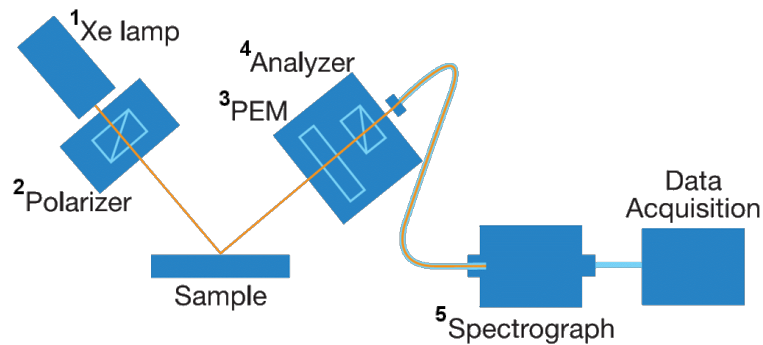


Figure 2.11 – Schematic view of the phase modulated ellipsometers
From <http://www.horiba.com>

The goal of the PEM is to introduce the phase modulation, at a frequency of 50 kHz, and by doing so to avoid the use of a rotating analyzer. A important notion for us is the pseudo-dielectric function, expressed in Eq. 2.2 where ϕ is the angle of incidence.¹ It is a meaningful concept for people familiar with SE measurements but has a different physical meaning with respect to the dielectric function since it takes into account both the film and the substrate. It is only in the case of a bulk, semi-infinite, material that the pseudo-dielectric function equals the dielectric function.

$$\langle \epsilon \rangle = \langle \epsilon_r \rangle + i \langle \epsilon_i \rangle = \sin^2(\phi) \left\{ 1 + \left[\frac{1 - \rho}{1 + \rho} \right]^2 \tan^2(\phi) \right\} \quad (2.2)$$

SE allows for the determination of the thickness and film composition. This determination is done via some modelling where we describe our film or stack and substrate. The model enables for multilayer descriptions were the model inputs are the thickness, the composition and the dielectric function of each layer. The outputs are the same except that the we can ask to fit or not the dielectric function of the materials. Indeed, the choice of the input dielectric function of the materials used in the model can be:

- taken from a library containing the dielectric functions of materials of interest. It is the case for instance of different crystalline, amorphous or oxide materials. In the case of silicon, *Jellison et al.*² have determined the dielectric function of polycrystalline silicon of different grain sizes. Ranging from amorphous silicon to small grain

¹Tompkins and Haber, *Handbook of ellipsometry*, 2006 [34]

²Jellison, Chisholm, and Gorbatskin, "Optical functions of chemical vapor deposited thin-film silicon determined by spectroscopic ellipsometry", 1993 [35]

(SG) and large grain (LG) polysilicon. The dielectric function of crystalline silicon has been published by *Jellison*,¹ or *Aspnes and Studna*.²

- Described by a dispersion law, whose parameters can be adjusted to fit better our experimental data, that is generally a Tauc-Lorentz dispersion law detailed below.

On Fig. 2.12 we show the imaginary part of the dielectric function of a-Si:H, small and large grain polysilicon as well as monocrystalline silicon. Even more interesting, is the fact that we can model our layers using

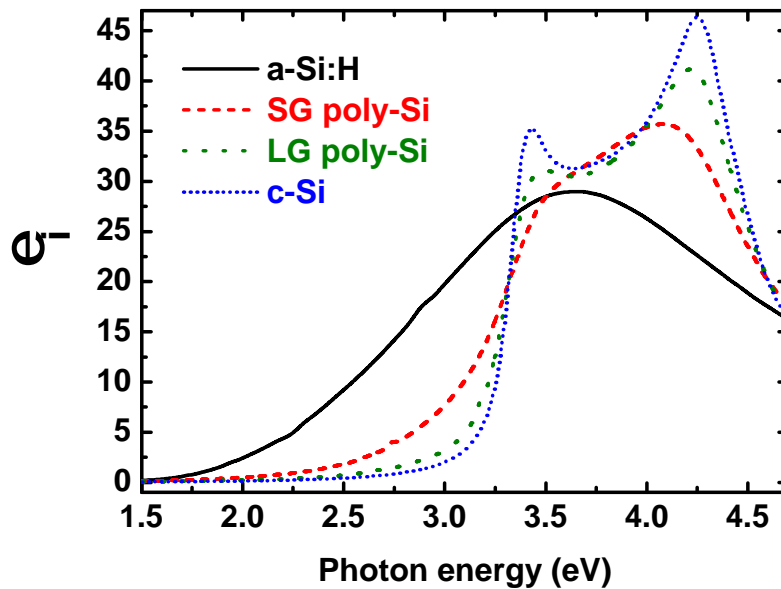


Figure 2.12 – *Imaginary part of the dielectric function of hydrogenated amorphous silicon, small and large grain polysilicon and monocrystalline silicon*

the Bruggeman Effective Medium Approximation (BEMA) that says (see Ref [34] or the original paper, written in German, by *Bruggeman*³) that we can define a new dielectric function (ϵ_h) for a material that we can deduce from a combination of the dielectric functions of the different materials that constitute this layer using the formula of Eq. 2.3.

$$0 = \sum_j f_j \frac{\epsilon_j - \epsilon_h}{\epsilon_j + 2\epsilon_h} \quad (2.3)$$

In Eq. 2.3, ϵ_j is the dielectric function of the material j with a fraction f_j and ϵ_h is the effective medium dielectric function. This BEMA is mostly used when one wants to model microcrystalline films or epitaxial films. In the case of a-Si:H materials, it is very common to use a Tauc-Lorentz

¹Jellison, "Optical functions of silicon determined by two-channel polarization modulation ellipsometry", 1992 [36]

²Aspnes and Studna, "Dielectric functions and optical parameters of Si, Ge, GaP, GaAs, GaSb, InP, InAs, and InSb from 1.5 to 6.0 eV", 1983 [37]

³Bruggeman, "Berechnung verschiedener physikalischer Konstanten von heterogenen Substanzen. I. Dielektrizitätskonstanten und Leitfähigkeiten der Mischkörper aus isotropen Substanzen", 1935 [38]

dispersion law to describe them as explained for instance in a paper by *Jellison et al.*¹ Within this approach, the imaginary part of the dielectric function (ϵ_2) is given by the formula:

$$\epsilon_2(E) = \begin{cases} \frac{AE_0C(E-E_g)^2}{E[(E^2-E_0^2)^2+C^2E^2]} & \text{if } E > E_g \\ 0 & \text{if } E \leq E_g \end{cases} \quad (2.4)$$

Here the fitting parameters are:

E_g the optical gap of the material (eV)

E_0 the energy of maximum absorption (eV)

A a parameter whose value is related to the density of the material (eV)

C a parameter whose value is related to the disorder of the material (eV)

As to the real part (ϵ_1), it is obtained from ϵ_2 by performing a Kramers-Kronig integration of ϵ_2 as defined in Eq. 2.5.

$$\epsilon_1(E) = n^2(E) - k^2(E) = \epsilon_1(\infty) + \frac{2}{\pi} P \int_{E_g}^{\infty} \frac{\zeta \epsilon_2(E)}{\zeta^2 - E^2} d\zeta \quad (2.5)$$

P is the Cauchy principal part of the integral and $\epsilon_1(\infty)$ is another fitting parameter and is usually taken as 1 (therefore not fitted). The simple optical model we used to fit our experimental spectra in the case of a-Si:H films was always the same, except in very few cases involving crystalline phases ($\mu\text{c-Si:H}$ or epitaxial films), and is schematized on Tab. 2.1.

50% a-Si:H	50% voids	↕ 0–2 nm
100% a-Si:H		↕ 1–30 nm
c-Si		↑ semi-infinite

Table 2.1 – Optical model used to describe an a-Si:H film on a c-Si substrate: it consists of a semi-infinite substrate with a bulk layer of a-Si:H and a surface roughness.

This is a three layer model which consists of a semi-infinite c-Si substrate, a bulk a-Si:H layer and a surface roughness layer modelled by a BEMA mixture of 50% of a-Si:H and 50% of voids.

This technique can also be used when we are facing more complex cases such as epitaxial growth or mixed phase growth, i.e. microcrystalline silicon ($\mu\text{c-Si:H}$). On Fig. 2.13, we have plotted the imaginary part of the pseudo-dielectric function of a typical a-Si:H layer on c-Si, an epitaxial Si layer on c-Si as well as the spectrum given by the optical model in the inset after fitting of the experimental data and also the spectrum of a c-Si wafer as obtained by *Aspnes and Studna* [37].

It is very easy to distinguish between amorphous and epitaxial films due to the fact that amorphous materials have a broad absorption peak whereas crystalline silicon has two characteristic peaks at 3.4 eV and 4.2 eV. The modelling of an epi-Si film is done by considering the film as a three layer model (inset of Fig. 2.13):

¹Jellison, Merkulov, Puzetky, Geohegan, Eres, Lowndes, and Caughmans, “Characterization of thin-film amorphous semiconductors using spectroscopic ellipsometry”, 2000 [39]

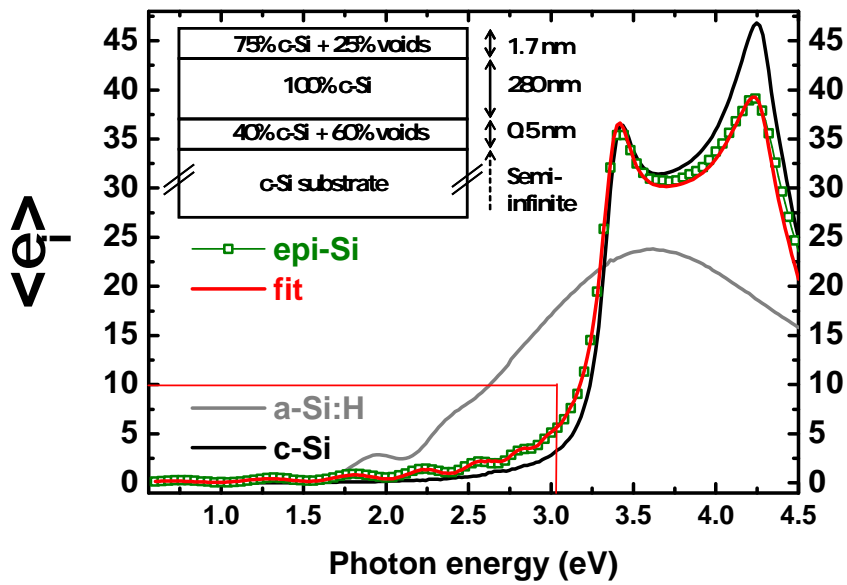


Figure 2.13 – Imaginary part of the pseudo-dielectric functions of a typical *a*-Si:H layer on *c*-Si (grey line), an epitaxial Si film on *c*-Si (green squares), the fit of the epitaxial film (red line) and a crystalline silicon wafer (black line)

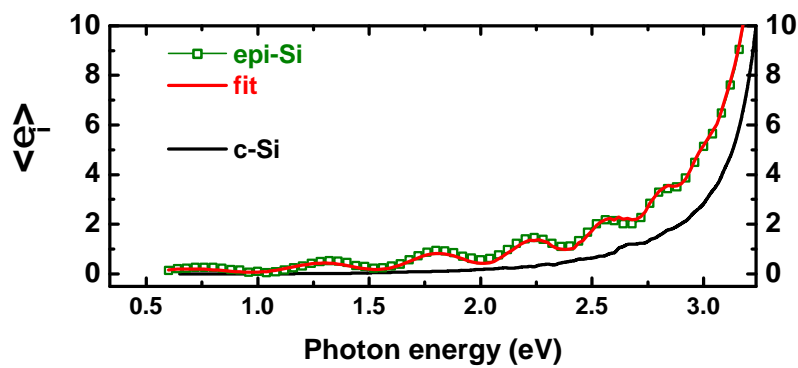


Figure 2.14 – Imaginary part of the pseudo-dielectric functions of the measurement of an epitaxial film, the modelled stack and of a *c*-Si wafer, zoomed in the low photon energy part of the spectrum

1. A very thin (0.5 nm) **interface** layer between the substrate and the film made up of a mixture of c-Si and voids. It accounts for the fact that we do not have a perfect interface between the substrate and the film and that there is a much higher hydrogen content at the interface than in the film thus decreasing the refractive index of this ultra thin layer. This hydrogen “peak” at the interface can be detected by SIMS measurements (see Fig. 4.5). This layer is the reason why we “see” interference fringes (Fig. 2.14) in the low photon energy part (< 3 eV) and is absolutely necessary to determine the thickness of the film.
2. A **bulk** layer modelled by a 100% fraction of c-Si which represents our film
3. A **roughness** layer made up of a mixture of c-Si and voids. It accounts for the fact that we do not have a perfectly flat surface and also for the fact that some native oxide starts to grow as soon as the film is taken out of the reactor. This layer explains why the height of the peak at 4.2 eV is smaller than the one we could expect from a bare c-Si surface as obtained from the database or from a HF cleaned c-Si wafer.

One can always observe some disparities with this model. This happens, for instance, in the work of *Moreno and Roca i Cabarrocas* [40] when a very porous interface appears, as it can be the case when the native oxide is removed by plasma etching before immediate epitaxial growth. This leads to interference fringes of a much higher amplitude, depending on the plasma conditions (mostly H_2 flow rate) used to grow the subsequent layer. Also, it can occur that the epitaxial growth is of poorer quality and that one has to model the bulk layer by a mixture of monocrystalline Si and large grains polycrystalline Si, as it is the case when we are far from the optimum conditions or when we are incorporating dopants to the gas mixture to obtain doped films.

2.1.5 Effective lifetime measurements

SE allows us to determine the optical properties but does not provide information on the electrical properties of our layers nor on their passivation properties. The latter can be determined via the use of the photoconductance decay method. This method is based on the fact that when we illuminate a semiconductor we increase the number of charge carriers. The change in the carrier densities will result in a change of the conductance of the material. Measuring this conductance and its decreasing rate allows us to have access to the effective lifetime of our solar cell precursors. This technique has been described in many papers and a simple description can be found in this paper from *Sinton and Cuevas*.¹ Our measurements were performed on a WCT-120 Sinton lifetime tester (Fig. 2.15) provided by the Sinton Consulting Corporation.

¹Sinton and Cuevas, “Contactless determination of current–voltage characteristics and minority-carrier lifetimes in semiconductors from quasi-steady-state photoconductance data”, 1996 [41]



Figure 2.15 – Picture of the WCT-120 Sinton based at LPICM

As we know, the lifetime we obtain from this measurement method is an effective lifetime that takes into account all recombination lifetimes, including surface recombination lifetimes at both interfaces: $\frac{1}{\tau_{eff}} = \frac{1}{\tau_{bulk}} + \frac{1}{\tau_{interface1}} + \frac{1}{\tau_{interface2}}$. However we do have two interfaces in an heterojunction solar cell so that if we want to separate the values of each of the interface recombination lifetimes, and not only get an information on their mean value, we need to perform this measurement with the same layers on both sides of the wafer. Such samples will be called *symmetrical samples*. Assuming that our deposition conditions are reproducible enough so that we have identical surface states and layers, we have access to the surface recombination velocity induced by this layer.

The Sinton lifetime tester has been thoroughly studied by *Isidro Martín García*.¹ It consists of a flash lamp installed above the sample which is positioned on top of an hidden inductive coil. The flash photogenerates carriers in the wafer. The inductive coil will measure a voltage proportional to the extra conductance of the wafer that can be expressed in Eq. 2.6.

$$\Delta\sigma = q \times W \times \Delta p_{ave} \times (\mu_e + \mu_h) \quad (2.6)$$

W is the thickness of the wafer and μ_e and μ_h are the electron and hole mobilities. All these values are well known and well calibrated. We use Δp_{ave} which is the average excess hole density over the entire thickness of the wafer. We will now consider that we have $\Delta p_{ave} = \Delta n_{ave} = \Delta p$. In the *generalized* mode the effective lifetime can be expressed as follows:

$$\tau_{eff} = \frac{\Delta p}{G - \frac{d\Delta p}{dt}} \quad (2.7)$$

G is the photon generation rate. However, in most cases (high lifetimes), Eq. 2.7 can be simplified since we operate the Sinton lifetime tester in the so-called *transient* mode. In this mode we use a very short pulse² and then

¹Martin, "Silicon surface passivation by Plasma Enhanced Chemical Vapor Deposited amorphous silicon carbide films", 2001 [42]

²Compared to the minority carrier lifetime. In that case the pulse would be in the order of 10 μ s

monitor the decay of the photoconductance. In this case the generation term equals 0 and we can rewrite Eq. 2.7 as Eq. 2.8.

$$\tau_{eff} = \frac{\Delta p}{-\frac{d\Delta p}{dt}} \quad (2.8)$$

However, when we have short lifetimes ($< 200 \mu\text{s}$, see Ref. [42]) and in order to avoid large error measurements, we can operate the Sinton lifetime tester in another mode, QSS mode¹ where the pulse of light is much longer ($\approx 2 \text{ ms}$) so that at any time we have an equilibrium between what is generated and what recombines, so that we can express the lifetime as Eq. 2.9.

$$\tau_{eff} = \frac{\Delta p}{G} \quad (2.9)$$

In this mode, the accuracy of the measurements, for which the illumination is measured at all times, depends on the accuracy of an optical factor (f) which depends on the reflectivity of the surface of the wafer and that determines the generation rate in the wafer. Unlike the transient mode, we can measure at all times (not only at the beginning) the intensity of the light that is shed on the wafer via the use of a calibrated photodiode. In the case of the transient mode, we can only measure the illumination at the beginning since its intensity vanishes extremely fast. Thus, the equivalent illumination is determined by the initial illumination and the recombination rate.

In fact, the Sinton lifetime tester was always used in the so-called generalized mode which does not make any approximation and keep all the terms of Eq. 2.7. This measurement allows us to plot the effective lifetime against the minority carrier density.

Sometimes, people prefer to use, instead of the effective lifetime, another physical quantity that is the surface recombination velocity. In this case you have to replace the interface recombination lifetime by $\frac{W}{S_{int}}$ where W is the thickness of the wafer and S_{int} is the surface recombination velocity of the interface, generally expressed in $\text{cm}\cdot\text{s}^{-1}$. A physical representation of this quantity is the velocity of the carriers to go recombine at the interface and as to be minimized. Just like the effective lifetime, the surface recombination velocity strongly depends on the injection level.

Interestingly enough, we can deduce from this measurement a value called implicit V_{oc} . Indeed, based on the first chapter, using Eq. 1.6, and assuming that V_{oc} should be at best equal to the Fermi level splitting under an illumination of 1 sun, we can obtain a value for the open-circuit voltage of our solar cell precursor that we call implicit V_{oc} for it is not a measured value but merely the value that we expect to get. This value is defined in Eq. 2.10.

$$V_{oc} = \frac{E_{FC} - E_{FV}}{e} = \frac{kT}{e} \ln \left(\frac{n_e n_h}{n_i^2} \right) \quad (2.10)$$

In the case of a n-type wafer we have $n_h = \Delta p$ and $n_e = N_D + \Delta p$. We finally reach the expression Eq. 2.11.

$$V_{oc} = \frac{kT}{q} \ln \left(\frac{(N_D + \Delta p_{|1sun}) \times \Delta p_{|1sun}}{n_i^2} \right) \quad (2.11)$$

¹Quasi Steady State

2.2 Surface passivation

2.2.1 Theoretical point of view

The recombination processes in c-Si have been described in the previous chapter and any improvement of the bulk lifetime was in the hands of the suppliers.¹ The goal of the passivation of crystalline silicon surfaces is to avoid recombination of the minority carriers at the surface of the crystalline silicon. Indeed, all designs of solar cells based on crystalline silicon include a passivation scheme. This means that crystalline silicon, whether it is the base or a highly doped emitter, is always capped by a film whose goal is to provide a passivation of the Si surface. In the previous chapter, where we introduced all the recombination processes, we obtained an equation governing the surface recombination rate (Eq. 1.30):

$$R_s = \frac{n_s \times p_s - n_i^2}{\frac{p_s + p_i}{S_n} + \frac{n_s + n_i}{S_p}}$$

Based on this equality and aiming at reducing the recombination rate U_s , we can establish two strategies:

1. We can reduce the defect density at the interface, or in other words reduce S_n and S_p the surface recombination velocities of electrons and holes
2. We can decrease the surface concentrations of electrons or holes at the surface n_s and p_s

The first strategy is often referred to as *chemical passivation* whereas the second one is referred to as *field effect passivation*. Indeed, the decrease of the concentration of one type of carriers is usually achieved by an internal electric field below the surface (band bending towards the surface). It can be implemented by a doping profile near the interface, resulting in a high-low junction when using the same doping type, often referred to as Front Surface Field or Back Surface Field depending on whether this layer is located on the illuminated or back side of the solar cell respectively. In the case of a p-n junction, we call it an emitter. When not contacted, these junctions are called *floating junctions*. It can also be achieved by the deposition of an insulator layer possessing fixed charges, or that we charge by corona discharge for instance (see below).

However, these two strategies do not provide the same result since it is known that a decrease of the defect density will result in an increase of the effective lifetime on the entire injection level range whereas an increase of the field effect passivation will mostly increase it in the low injection range.^{2,3} The best situation would involve a low surface defect density to reduce the interface defect density, known as being silicon dangling

¹During our work we mostly used wafers from Topsil that were Float Zone and therefore had a very high bulk lifetime

²Schmidt and Dauwe, *Surface Passivation of Silicon Solar Cells using SiN_x:H: The Effect of Space Charge Recombination*, 2005 [43]

³Olibet, Vallat-Sauvain, and Ballif, "Model for a-Si:H/c-Si interface recombination based on the amphoteric nature of silicon dangling bonds", 2007 [44]

bonds,¹ coupled to a strong field effect passivation. The next paragraph will give an overview of the existing passivation films.

During this work, we used the effective lifetime measurements to check the passivation quality. However, some researchers, starting with *Garín et al.*,² have also used these data in order to assess the validity of different recombination models to discriminate the contributions of the defect density and of the field effect passivation. However, SRH recombination is a single defect recombination process whereas we expect to have a distribution of defects at the interface. Generally, following the approach of the model established by *Hubin et al.*³ to describe the bulk a-Si:H recombination, some authors have applied it to the surface recombination like *Olibet et al.*⁴ and later *Bahardoust et al.*⁵ However, recent studies have pointed out some limitations to the aforementioned a-Si:H dangling bonds recombination model [44], acknowledged in the article by the authors, for which the energetic demarcation levels for DB between recombination centers and traps is assumed to be outside the distribution of DB and may reduce the range of validity of the model.⁶ However, in such a case, the differences showed up at extreme low injection levels. Recently, improvements on the simpler *Hubin et al.* model implemented by *Olibet et al.* have been done by *Leendertz et al.*,⁷ who based their work on that of *Sah and Shockley*⁸ which allow them, for instance, to define arbitrary interface defect distributions. This may have some importance since other simulations have pointed out that assuming an asymmetric distribution of interface defects between acceptors and donors could lead to an important decrease in the band bending in the c-Si and reduce solar cells efficiency.⁹

2.2.2 Practical point of view

As we already mentioned, the surface defect density has to be as low as possible and this means making the defects inactive. Indeed, it has been shown by *Yablonoitch et al.*¹⁰ that immersing Si wafers into a hydrofluoric acid (HF) solution would give rise to extremely high effective lifetimes.

¹Biegelsen, Johnson, Stutzmann, Poindexter, and Caplan, "Native defects at the Si/SiO₂ interface-amorphous silicon revisited", 1985 [45]

²Garín, Rau, Brendle, Martín, and Alcubilla, "Characterization of a-Si:H/c-Si interfaces by effective-lifetime measurements", 2005 [46]

³Hubin, Shah, and Sauvain, "Effects of dangling bonds on the recombination function in amorphous semiconductors", 1992 [47]

⁴Olibet, Vallat-Sauvain, and Ballif, "Model for a-Si:H/c-Si interface recombination based on the amphoteric nature of silicon dangling bonds", 2007 [44]

⁵Bahardoust, Chutinan, Leong, Gougam, Yeghikyan, Kostas, Kherani, and Zukotynski, "Passivation study of the amorphous-crystalline silicon interface formed using DC saddle-field glow discharge", 2010 [48]

⁶Li, McIntosh, and Cuevas, "Limitations of a simplified dangling bond recombination model for a-Si:H", 2008 [49]

⁷Leendertz, Stangl, Schulze, Schmidt, and Korte, "A recombination model for a-Si:H/c-Si heterostructures", 2010 [50]

⁸Sah and Shockley, "Electron-Hole Recombination Statistics in Semiconductors through Flaws with Many Charge Conditions", 1958 [51]

⁹Mikolásek, Racko, Harmatha, Gaspierik, and Sutta, "Influence of the broken symmetry of defect state distribution at the a-Si:H/c-Si interface on the performance of heterojunction solar cells", 2010 [52]

¹⁰Yablonoitch, Allara, Chang, Gmitter, and Bright, "Unusually Low Surface-Recombination Velocity on Silicon and Germanium Surfaces", 1986 [53]

The explanation for that is that HF etching of native oxide, always present, results in a H-terminated (and not Si-F even if it is supposed to be more thermodynamically stable) surface with only Si-H bonds and virtually no dangling bonds.¹ Although being very efficient, this passivation technique has no sense to make practical devices since HF is a very hazardous product and the passivation is lost rather quickly when the wafer is taken out of the HF solution. Commonly, we deposit films on the surface of c-Si to achieve surface passivation. By doing so one can first expect to satisfy the bonding requirement which is to minimize the number of dangling bonds. Besides, a film can also induce a band bending towards the surface of the wafer and by doing so can lead to a regime of inversion, or accumulation. We should note that generally speaking the nature of the deposited film has some impact on the defect density *and* the band bending. In the work of *Olibet et al.*,² it is claimed that it is possible to do so by introducing microdoped layers, that are a-Si:H films grown with a very small amount of doping, allowing to change the charge of the film without increasing the defect density. However, even if it allowed them to establish a simple model for the recombination, it is of no practical use. Reducing the number of defects at the surface of c-Si before any deposition can be done for instance by performing a thorough chemical cleaning of the wafer.^{3,4}

There are several techniques to passivate c-Si surfaces. In the c-Si PV industry, the most commonly used material to achieve that is amorphous silicon nitride (a-Si_{1-x}N_x:H).^{5,6,7} It also has the advantage of passivating the bulk defects of defective materials (such as multicrystalline silicon) through the incorporation and diffusion of hydrogen.^{8,9} Besides, the thickness of this layer can be chosen so that it acts as an anti-reflection layer on the illuminated side of the solar cell.¹⁰ However, it has been shown that in silicon nitride the dangling bonds are the main defects,¹¹ and that this defect will result in the creation of what is called "K⁺ centers".¹² This

¹Trucks, Raghavachari, Higashi, and Chabal, "Mechanism of HF etching of silicon surfaces: A theoretical understanding of hydrogen passivation", 1990 [54]

²Olibet, Vallat-Sauvain, and Ballif, "Model for a-Si:H/c-Si interface recombination based on the amphoteric nature of silicon dangling bonds", 2007 [44]

³Angermann, Korte, Rappich, Conrad, Siebera, Schmidt, Hübener, and Hauschild, "Optimisation of electronic interface properties of a-Si:H/c-Si hetero-junction solar cells by wet-chemical surface pre-treatment", 2008 [55]

⁴Page, Iwaniczko, Xu, Wang, Yan, Roybal, Branz, and Wang, "Well-Passivated a-Si:H Back Contacts for Double-Heterojunction Solar cells", 2006 [56]

⁵Aberle, "Surface passivation of crystalline silicon solar cells: a review", 2000 [57]

⁶Aberle, "Overview on SiN surface passivation of crystalline silicon solar cells", 2001 [58]

⁷Kerr and Cuevas, "Recombination at the interface between silicon and stoichiometric plasma silicon nitride", 2002 [59]

⁸Lelièvre, Fourmond, Kaminski, Palais, Ballutaud, and Lemiti, "Study of the composition of hydrogenated silicon nitride SiN_x:H for efficient surface and bulk passivation of silicon", 2009 [60]

⁹Dekkers, Carnel, and Beaucarne, "Carrier trap passivation in multicrystalline Si solar cells by hydrogen from SiN_x:H layers", 2006 [61]

¹⁰Goetzberger, Knobloch, and Voss, *Crystalline silicon solar cells*, 1998 [62]

¹¹Robertson, Warren, and Kanicki, "Nature of the Si and N dangling bonds in silicon nitride", 1995 [63]

¹²Mäckel and Lüdemann, "Detailed study of the composition of hydrogenated SiN_x layers for high-quality silicon surface passivation", 2002 [64]

results in the fact that this material possesses a fixed positive charge,¹ that will make it suitable for (n) c-Si passivation. However, some studies have also been carried out on passivation based on silicon oxide SiO_2 ,^{2,3,4} which gives a superior passivation of (n) c-Si. Another feature of SiO_2 , which possesses positive interface charges, is the possibility we have to change the band bending at the surface by depositing static charge thanks to corona discharge.⁵

More recently, aluminium oxide (Al_2O_3) has attracted a lot of attention because of its negative fixed charge density that allows him to give a good passivation of (p) c-Si.^{6,7,8} This dielectric can be deposited by Atomic Layer Deposition and requires an annealing.

Also, a lot of work has been carried out on hydrogenated amorphous silicon, which had proved very early to be a very efficient passivation layer,^{9,10} as well as on different alloys. For instance, a lot of work has been done on silicon carbide ($\text{a-Si}_{1-x}\text{C}_x\text{:H}$),^{11,12,13} on silicon carbide nitride ($\text{a-Si}_{1-x-y}\text{C}_x\text{N}_y\text{:H}$),¹⁴ as well as on silicon suboxide ($\text{a-Si}_{1-x}\text{O}_x\text{:H}$).¹⁵ All these materials form an interesting family that can be used depending on the needs. Actually, for heterojunction solar cells, one can be interested in forming emitters with wider bandgap energies in order to reduce the parasitic absorption losses. Besides, RF PECVD is not the only deposition

¹Dauwe, Schmidt, Metz, and Hezel, "Fixed charge density in silicon nitride films on crystalline silicon surfaces under illumination", 2002 [65]

²Aberle, "Surface passivation of crystalline silicon solar cells: a review", 2000 [57]

³Lee and Glunz, "Investigation of various surface passivation schemes for silicon solar cells", 2006 [66]

⁴Kerr and Cuevas, "Very low bulk and surface recombination in oxidized silicon wafers", 2002 [67]

⁵Mizsei, "Silicon surface passivation by static charge", 2006 [68]

⁶Agostinelli, Delabie, Vitanov, Alexieva, Dekkers, De Wolf, and Beaucarne, "Very low surface recombination velocities on p-type silicon wafers passivated with a dielectric with fixed negative charge", 2006 [69]

⁷Hoex, Gielis, van de Sanden, and Kessels, "On the c-Si surface passivation mechanism by the negative-charge-dielectric Al_2O_3 ", 2008 [70]

⁸Dingemans, Beyer, van de Sanden, and Kessels, "Hydrogen induced passivation of Si interfaces by Al_2O_3 films and $\text{SiO}_2/\text{Al}_2\text{O}_3$ stacks", 2010 [71]

⁹Dauwe, Schmidt, and Hezel, "Very low surface recombination velocities on p- and n-type silicon wafers passivated with hydrogenated amorphous silicon films", 2002 [72]

¹⁰Dauwe, Mittelstadt, Metz, Schmidt, and Hezel, "Low-temperature rear surface passivation schemes for >20% efficient silicon solar cells", 2003 [73]

¹¹Pysch, Ziegler, Becker, Suwito, Janz, Glunz, and Hermle, "Stretched-exponential increase in the open-circuit voltage induced by thermal annealing of amorphous silicon-carbide heterojunction solar cells", 2009 [74]

¹²Vetter, Martín, Ferre, Garín, and Alcubilla, "Crystalline silicon surface passivation by amorphous silicon carbide films", 2007 [75]

¹³Glunz, Janz, Hofmann, Roth, and Willeke, "Surface passivation of silicon solar cells using amorphous silicon carbide layers", 2006 [76]

¹⁴Ferre, Orpella, Munoz, Martín, Recart, Voz, Puigdollers, Roca i Cabarrocas, and Alcubilla, "Very low surface recombination velocity of crystalline silicon passivated by phosphorus-doped $\text{a-SiC}_x\text{N}_y\text{:H(n)}$ alloys", 2007 [77]

¹⁵Mueller, Schwertheim, and Fahrner, "Crystalline silicon surface passivation by high-frequency plasma-enhanced chemical-vapor-deposited nanocomposite silicon suboxides for solar cell applications", 2010 [78]

method, since it has also been shown that a-Si:H deposition via HWCVD¹ or VHF PECVD² could lead to excellent passivations.

2.3 Physics of heterojunction solar cells

2.3.1 Interest, drawbacks

Silicon heterojunction solar cells are very different from silicon homojunction solar cells, both in the making and in the physical aspects. We will discuss later some physical peculiarities of such devices but we will start by describing the manufacturing differences.

The first thing to remark is that all steps of the heterojunction solar cells are made at low temperature so that there is a low thermal budget. Indeed, there are mainly three steps in making an heterojunction: a-Si:H depositions, TCO deposition and metallization. However, all these processes can be, and have to be, done at about 200°C, whereas in the case of homojunctions the diffusions and contacts' firing steps are usually performed at much higher temperatures (800-1000°C). A low temperature process can reduce the constraints on the electronic quality and thickness of the wafer: no impurity diffusion, no defect creation, no wafer bowing. Also, the sum of the heterojunction steps remains shorter in time. Additionally, it is often said that the formation of the junction and of the passivation scheme at the same time is a great advantage but it should be remembered that it is also at the cost of the deposition of a TCO layer (in fact two), that is not needed in the case of homojunction cells, that are absorbing and quite expensive. Nevertheless, the passivation provided by the a-Si:H layers is excellent, and with regards to current trend of thinning the wafers, the passivation quality becomes more and more important, so that such structures can be even more interesting.

Moreover, a quite interesting feature of heterojunction solar cells is that their high V_{oc} (small J_0), translates into a low temperature coefficient.³ Indeed, certified efficiencies are defined under the AM1.5 spectrum, at 25°C, whereas most operating conditions result in higher temperature values, which result in a decrease of efficiency which is less important for HIT modules.

2.3.2 Band offsets

In this section we give a review on the specificities of heterojunction solar cells (compared to homojunction cells). Indeed, unlike homojunction, heterojunction solar cells use two materials of different bandgap energies to realize the base and the emitter of the solar cell. The main consequence of this is that there is a bandgap mismatch and it is not possible to have both

¹Gielis, van den Oever, Hoex, van de Sanden, and Kessels, "Real-time study of a-Si:H/c-Si heterointerface formation and epitaxial Si growth by spectroscopic ellipsometry, infrared spectroscopy, and second-harmonic generation", 2008 [79]

²Olibet, Vallat-Sauvain, and Ballif, "Model for a-Si:H/c-Si interface recombination based on the amphoteric nature of silicon dangling bonds", 2007 [44]

³Taguchi, Terakawa, Maruyama, and Tanaka, "Obtaining a higher V_{oc} in HIT cells", 2005 [80]

conduction and valence band edge levels continuous through the junction. This results in band offsets. On Fig. 2.16, we have drawn a schematic band diagram of the heterojunction solar cell on a (n) c-Si wafer, as it is generally admitted from several publications.^{1,2,3} On Fig. 2.16, $V_d^{a-Si:H}$ and V_d^{c-Si} refer to the diffusion voltage on the amorphous and crystalline side of the junction respectively. $\delta^{a-Si:H}$ and δ^{c-Si} refer to the doping level of the amorphous and the crystalline silicon respectively. On this band

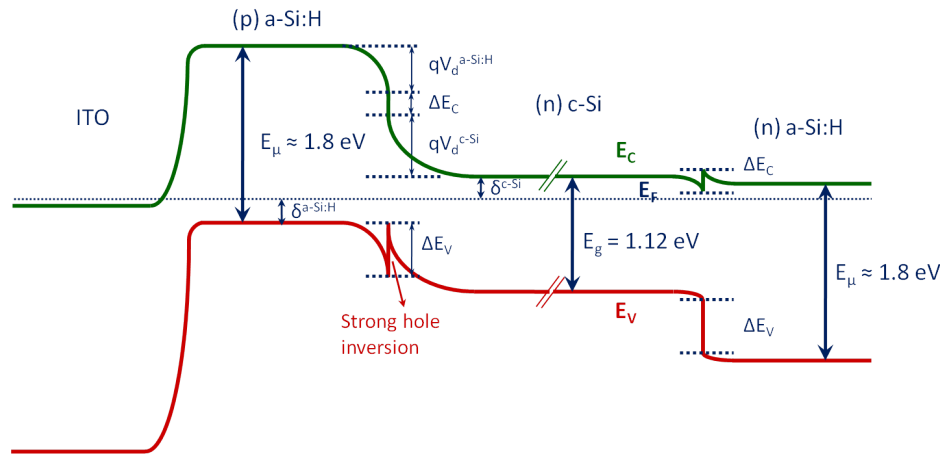


Figure 2.16 – Schematic band diagram of the heterojunction solar cell on a (n) c-Si wafer. The different energy levels are not at scale.

diagram the band offsets are designated ΔE_c and ΔE_v for the conduction and the valence band offset respectively. Such a band diagram suggests that on the (n) a-Si:H side (BSF) holes in the c-Si face a large potential barrier whereas electrons have a very small potential barrier. As it has already been pointed out by several authors, the ohmic contact on the back (n) a-Si:H side is not a problem and does not hinder electron collection.^{4,5}

However, on the emitter side we have a valence band offset that represents a barrier that holes photogenerated in the (n) c-Si wafer will have to cross on their way to the (p) a-Si:H layer. Indeed, some groups have experimentally observed S-shaped current-voltage characteristics, most of the time under standard conditions of light and temperature, a decade ago.^{6,7} None of the authors groups could agree on an explanation which

¹Favre, Labrune, Dadouche, Gudovskikh, Roca i Cabarrocas, and Kleider, "Study of the interfacial properties of amorphous silicon/n-type crystalline silicon heterojunction through static planar conductance measurements", 2010 [81]

²Kanevce and Metzger, "The role of amorphous silicon and tunneling in heterojunction with intrinsic thin layer (HIT) solar cells", 2009 [82]

³Wang, Page, Iwaniczko, Levi, Yan, Branz, Yelundur, Rohatgi, Bunea, Terao, and Wang, "Toward Better Understanding and Improved Performance of Silicon Heterojunction Solar Cells", 2004 [83]

⁴Kanevce and Metzger, "The role of amorphous silicon and tunneling in heterojunction with intrinsic thin layer (HIT) solar cells", 2009 [82]

⁵Wang, Page, Iwaniczko, Levi, Yan, Branz, Yelundur, Rohatgi, Bunea, Terao, and Wang, "Toward Better Understanding and Improved Performance of Silicon Heterojunction Solar Cells", 2004 [83]

⁶van Cleef, Rubinelli, Rath, Schropp, van der Weg, Rizzoli, Summonte, Pinghini, Centurioni, and Galloni, "Photocarrier collection in a-SiC:H/c-Si heterojunction solar cells", 1998 [84]

⁷Fantoni, Vigranenko, Fernandes, Schwarz, and Vieira, "Influence of the band offset on the performance of photodevices based on the c-Si/a-Si:H heterostructure", 2001 [85]

has been ascribed to the valence band offset which is so large that it hinders the hole collection for *Fantoni et al.* [85], whereas an insufficient doping of the (p) a-SiC_x:H layer can explain the poorer collection for *van Cleef et al.* [84]. More recent experiments have led *Page et al.* to conclude to the absence of tunnelling.¹

Also, *Froitzheim et al.*² have shown experimentally and by simulations that the interface defect density could have a great impact on the current-voltage characteristics and lead to S-shaped characteristics when its value was too high. Similar conclusions can be found in the work by *Ghosh et al.*,³ who have shown that the existence of an inversion layer at the interface between the c-Si base and the a-Si:H emitter was very important and dependant on the defect densities.

However, apart from these early results, most of the work on the influence of the valence band offset has been carried out numerically. Indeed, *Kanevce and Metzger* on the one side,⁴ and *Rahmouni et al.* on the other side,⁵ have published comprehensive simulation studies based on Sanyo's solar cells' parameters. These two groups of authors do not agree. *Kanevce and Metzger* main's point is that removing the ITO layer from the modelled devices make things "too easy" as it is a heavily (degenerate) doped n-type semiconductor. Their conclusion is that in the case of heterojunction solar cells on (n) c-Si, tunnelling is necessary at both c-Si/a-Si:H and ITO/a-Si:H interfaces to correctly fit Sanyo's cells. Tunnelling at the (p) a-Si:H/c-Si interface had also been introduced by *van Cleef et al.* to explain the absence of S-shaped current-voltage characteristic despite the large measured valence band offsets.⁶ However, in *Rahmouni et al.*'s simulations where Sanyo's cells, including those from a Sanyo's paper acknowledging the possibility of a tunnelling current in the $0.1 < V < 0.4$ V region,⁷ are modelled, tunnelling is not considered in the model but all of the cells can be correctly fitted.

An interesting feature of this band diagram is the existence at the interface of an inversion layer in the crystalline silicon. The LPICM has collaborated with the LGEP to study this interface. Indeed, the inversion layer had already been investigated for (n) a-Si:H emitters on (p) c-Si wafers by *Kleider et al.*,⁸ who had shown that this inversion layer results

¹Page, Iwaniczko, Xu, Roybal, Hasoon, Wang, and Crandall, "Amorphous/crystalline silicon heterojunction solar cells with varying i-layer thickness", 2011 [86]

²Froitzheim, Brendel, Elstner, Fuhs, Kliefoth, and Schmidt, "Interface recombination in heterojunctions of amorphous and crystalline silicon", 2002 [87]

³Ghosh, Tracy, Herasimenka, Honsberg, and Bowden, "Explanation of the device operation principle of amorphous silicon/ crystalline silicon heterojunction solar cell and role of the inversion of crystalline silicon surface", 2010 [88]

⁴Kanevce and Metzger, "The role of amorphous silicon and tunneling in heterojunction with intrinsic thin layer (HIT) solar cells", 2009 [82]

⁵Rahmouni, Datta, Chatterjee, Damon-Lacoste, Ballif, and Roca i Cabarrocas, "Carrier transport and sensitivity issues in heterojunction with intrinsic thin layer solar cells on N-type crystalline silicon: A computer simulation study", 2010 [89]

⁶van Cleef, Schropp, and Rubinelli, "Significance of tunneling in p⁺ amorphous silicon carbide n crystalline silicon heterojunction solar cells", 1998 [90]

⁷Taguchi, Maruyama, and Tanaka, "Temperature Dependence of Amorphous/Crystalline Silicon Heterojunction Solar Cells", 2008 [91]

⁸Kleider, Gudovskikh, and Roca i Cabarrocas, "Determination of the conduction band offset between hydrogenated amorphous silicon and crystalline silicon from surface inversion layer conductance measurements", 2008 [92]

in a highly conductive channel that disappears when the (n) a-Si:H layer is etched. Using coplanar conductance measurements, coupled to simulations, they had been able to evaluate the ΔE_C which is of 0.15 ± 0.04 eV. More recently, we performed similar experiments on (n) c-Si heterojunction solar cells that resulted in the determination of a lower boundary value: $\Delta E_V \geq 0.28$ eV. In a more elegant way, *Kleider et al.* and *Maslova et al.* have shown that they could perform Conductive-Probe AFM along the junction of a cleaved heterojunction solar cell.^{1,2} By doing so they could evidence the presence of a highly conductive channel in the (n) and (p) c-Si wafers. Again, coupled to some modelling they could refine their previous calculations and obtained a value of $\Delta E_V = 0.4$ eV for (n) c-Si heterojunctions. This value supports their previous calculations and is in good agreement with the value of 0.46 eV obtained by *Schmidt et al.* from HZB,³ recently confirmed by *Korte and Schmidt* at the same value and also claimed to be independent from the doping type of both the c-Si substrate and the capping a-Si:H layer,⁴ or the value 0.44 eV obtained by *Sebastiani et al.*⁵ Also, *Brown et al.* have experimentally obtained the valence band offsets of a-Si_{1-x}C_x:H/c-Si heterostructures.⁶ In the x=0 case they found $\Delta E_V = 0.44$ eV. However, many other measurements exist, using various techniques and various materials resulting in a rather large scattering of this value, as it has been pointed out by *Van de Walle and Yang*,⁷ who have performed numerical calculations and shown that the band offsets were dependent on the H content and the density of the film close to the interface, more hydrogen and less dense materials leading to a higher valence band offset.

2.3.3 Intrinsic layer

As we have already seen, passivation is one of the most crucial and difficult steps in the fabrication of an efficient heterojunction solar cell. This is what is claimed for instance by the Japanese corporation Sanyo which has developed HIT modules, HIT standing for Heterojunction with Intrinsic Thin film. Their original idea was to insert a thin undoped layer between the crystalline silicon substrate and the doped a-Si:H layer. By doing so they showed a decrease in the dark saturation current of their diode, com-

¹Kleider, Alvarez, Andkudinov, Gudovskikh, Gushina, Labrune, Maslova, Favre, Gueunier-Farret, Roca i Cabarrocas, and Terukov, "Characterization of silicon heterojunction for solar cells", 2011 [93]

²Maslova, Alvarez, Gushina, Favre, Gueunier-Farret, Gudovskikh, Ankudinov, Terukov, and Kleider, "Observation by conductive-probe atomic force microscopy of strongly inverted surface layers at the hydrogenated amorphous silicon/crystalline silicon heterojunctions", 2010 [94]

³Schmidt, Korte, Laades, Stangl, Schubert, Angermann, Conrad, and Maydell, "Physical aspects of a-Si:H/c-Si hetero-junction solar cells", 2007 [95]

⁴Korte and Schmidt, "Doping type and thickness dependence of band offsets at the amorphous/crystalline silicon heterojunction", 2011 [96]

⁵Sebastiani, Di Gaspare, Capellini, Bittencourt, and Evangelisti, "Low-Energy Yield Spectroscopy as a Novel Technique for Determining Band Offsets: Application to the c-Si(100)/a-Si:H Heterostructure", 1995 [97]

⁶Brown, Bittencourt, Sebastiani, and Evangelisti, "Electronic states and band lineups in c-Si(100)/a-Si_{1-x}C_x:H heterojunctions", 1997 [98]

⁷Van de Walle and Yang, "Band discontinuities at heterojunctions between crystalline and amorphous silicon", 1995 [99]

pared to a simple heterojunction with no buffer layer, by two orders of magnitude.¹ Sanyo has been keeping on working on this topic and has improved the efficiencies of HIT cells to reach 23% on (n) c-Si wafers and could also thin down the wafer to 98 μm and still obtain an efficiency of 22.8%.²

The concept has also attracted a lot of research from public laboratories and institutes during the last decade. Some groups started to work without any intrinsic layer but only with doped layers directly on the c-Si substrate. The HZB (previously known as HMI) laboratory has worked on the optimization of doped layers for solar cells.³ By doing so and by optimizing their wet chemical cleaning of textured wafers,⁴ they could reach efficiencies up to 17.4% on (p) c-Si and 19.8% on (n) c-Si wafers.⁵ However, in those cases the high efficiency on (n) c-Si was mostly due to an extremely high current density higher than 39 $\text{mA}\cdot\text{cm}^{-2}$, a value extremely close to the one obtained by Sanyo in Ref. [101], whereas the V_{oc} remained rather low for it was of 640 mV even though their wet chemical cleaning allowed them to reach extremely low surface defect densities. Indeed, even if a high efficiency was obtained, such a low V_{oc} indicates that the interface is not good enough and suggests that an undoped layer is desirable.

Indeed, some researchers have also started to study the effects of such an (i) a-Si:H layer on the passivation properties of undoped/doped a-Si:H stacks on c-Si,⁶ and also its impact on completed solar cells.^{7,8,9,10} At the beginning, many groups experienced the epitaxial growth of this undoped layer on (100) Si wafers.^{11,12,13,14} Even if there was initially some contro-

¹Tanaka, Taguchi, Matsuyama, Sawada, Tsuda, Nakano, Hanafusa, and Kuwano, "Development of New a-Si/c-Si Heterojunction Solar Cells: ACJ-HIT (Artificially Constructed Junction-Heterojunction with Intrinsic Thin-Layer)", 1992 [100]

²Mishima, Taguchi, Sakata, and Maruyama, "Development status of high-efficiency HIT solar cells", 2011 [101]

³Maydell, Conrad, and Schmidt, "Efficient silicon heterojunction solar cells based on p- and n-type substrates processed at temperatures $\leq 220^\circ\text{C}$ ", 2006 [102]

⁴Angermann, Korte, Rappich, Conrad, Siebera, Schmidt, Hübener, and Hauschild, "Optimisation of electronic interface properties of a-Si:H/c-Si heterojunction solar cells by wet-chemical surface pre-treatment", 2008 [55]

⁵Schmidt, Korte, Laades, Stangl, Schubert, Angermann, Conrad, and Maydell, "Physical aspects of a-Si:H/c-Si heterojunction solar cells", 2007 [95]

⁶Olibet, Vallat-Sauvain, and Ballif, "Model for a-Si:H/c-Si interface recombination based on the amphoteric nature of silicon dangling bonds", 2007 [44]

⁷Jensen, Hausner, Bergmann, Werner, and Rau, "Optimization and characterization of amorphous/crystalline silicon heterojunction solar cells", 2002 [103]

⁸Fujiwara and Kondo, "Effects of a-Si:H layer thicknesses on the performance of a-Si:H/c-Si heterojunction solar cells", 2007 [104]

⁹Olibet, Monachon, Hessler-Wyser, Vallat-Sauvain, De Wolf, Fesquet, Damon-Lacoste, and Ballif, "Textured silicon heterojunction solar cells with over 700 mV open-circuit voltage studied by Transmission Electron Microscopy", 2008 [105]

¹⁰Schüttauf, Komatsu, Geerligs, Mai, Bink, Spee, and Schropp, "Emitter Optimization on a-Si:H/c-Si Heterojunction Solar Cells for Isotextured Wafers", 2008 [106]

¹¹De Wolf and Kondo, "Abruptness of a-Si:H/c-Si interface revealed by carrier lifetime measurements", 2007 [107]

¹²Fujiwara and Kondo, "Effects of a-Si:H layer thicknesses on the performance of a-Si:H/c-Si heterojunction solar cells", 2007 [104]

¹³Gielis, Hoex, van den Oever, van de Sanden, and Kessels, "Silicon surface passivation by hot-wire CVD Si thin films studied by in situ surface spectroscopy", 2009 [108]

¹⁴Olibet, Monachon, Hessler-Wyser, Vallat-Sauvain, De Wolf, Fesquet, Damon-Lacoste,

versy about its neutral or possibly positive effect on the passivation,^{1,2} it now seems confirmed that its effect is detrimental, as we will see in the next chapter.

2.3.4 Doped layers

Even though the intrinsic layer has a very important role in the reduction of the interface defect density, what is needed to achieve the separation of the photo-generated carriers is a doped a-Si:H layer. At the back side of the solar cell we also form an ohmic contact with a doped a-Si:H layer of the same type as the wafer. By doing so one will obtain a very efficient passivation of the back surface of the solar cell and a very efficient ohmic contact. On the emitter side, especially in the case of (n) c-Si wafers,^{3,4} the a-Si:H layer needs to be highly doped and not too thin,⁵ in order to behave like a (good) diode, as it will be confirmed in this manuscript.

However, a-Si:H layers, especially (p) a-Si:H, are very absorbing layers and can reduce the short current density. Indeed, from the experimental work of *Fujiwara and Kondo*,⁶ or from the simulations of *Rahmouni et al.*,⁷ we can deduce an estimation of the current losses with respect to the thickness increase of $\approx 0.1 \text{ mA.cm}^{-2}.\text{nm}^{-1}$. Thus, in order to decrease this parasitic absorption (doped a-Si:H is too defective to allow for the charge separation of the carriers generated in it) researchers started to work on many different materials, aiming reducing the absorption coefficient. Indeed, various kinds of layer have been developed, including for instance (p) $\mu\text{-Si:H}$ emitters,⁸ (n) $\mu\text{-SiC:H}$ emitters,⁹ (n) $\mu\text{-SiO:H}$ emitters,¹⁰ (n) $\text{a-SiC}_x\text{:H}$.¹¹

However, even if satisfactory, and potentially beneficial, optical and electrical properties of such layers have been confirmed, the best hetero-

and Ballif, "Textured silicon heterojunction solar cells with over 700 mV open-circuit voltage studied by Transmission Electron Microscopy", 2008 [105]

¹Centurioni, Iencinella, Rizzoli, and Zignani, "Silicon heterojunction solar cell: a new buffer Layer concept with low-temperature epitaxial silicon", 2004 [109]

²Damon-Lacoste and Roca i Cabarrocas, "Toward a better physical understanding of a-Si:H/c-Si heterojunction solar cells", 2009 [110]

³Kanevce and Metzger, "The role of amorphous silicon and tunneling in heterojunction with intrinsic thin layer (HIT) solar cells", 2009 [82]

⁴van Cleef, Rubinelli, Rath, Schropp, van der Weg, Rizzoli, Summonte, Pinghini, Centurioni, and Galloni, "Photocarrier collection in a-SiC:H/c-Si heterojunction solar cells", 1998 [84]

⁵Fujiwara and Kondo, "Effects of a-Si:H layer thicknesses on the performance of a-Si:H/c-Si heterojunction solar cells", 2007 [104]

⁶Fujiwara and Kondo, "Effects of a-Si:H layer thicknesses on the performance of a-Si:H/c-Si heterojunction solar cells", 2007 [104]

⁷Rahmouni, Datta, Chatterjee, Damon-Lacoste, Ballif, and Roca i Cabarrocas, "Carrier transport and sensitivity issues in heterojunction with intrinsic thin layer solar cells on N-type crystalline silicon: A computer simulation study", 2010 [89]

⁸Sritharathikhun, Jiang, Miyajima, Yamada, and Konagai, "Optimization of p-Type Hydrogenated Microcrystalline Silicon Oxide Window Layer for High-Efficiency Crystalline Silicon Heterojunction Solar Cells", 2009 [111]

⁹Miyajima, Irikawa, Yamada, and Konagai, "High-quality nanocrystalline cubic silicon carbide emitter for crystalline silicon heterojunction solar cells", 2010 [112]

¹⁰Banerjee, Sritharathikhun, Yamada, and Konagai, "Fabrication of heterojunction solar cells by using microcrystalline hydrogenated silicon oxide film as an emitter", 2008 [113]

¹¹Pysch, Bivour, Hermle, and Glunz, "Amorphous silicon carbide heterojunction solar cells on p-type substrates", 2011 [114]

junction solar cells were so far obtained using “standard” (p) a-Si:H layers.^{1,2,3}

2.3.5 ITO contact

Unlike crystalline silicon solar cells for which the conductivity of the emitter, made of highly doped crystalline silicon, allows for a sufficient lateral transport, here we use amorphous silicon which has poor conduction properties, and therefore needs the incorporation of a TCO layer. Initially, Sanyo started to use ITO since its resistivity is quite low and allow to reach small square resistances within thicknesses compatible with its use as an anti-reflective coating. However, the expected (depending notably on the PV market evolution) shortage of indium,⁴ is expected to increase the price of such a material.⁵ Therefore, improvements of the quality of aluminium- or boron-doped zinc oxide allowed some groups to replace ITO by doped-ZnO.^{6,7} However, the main problem remains the fact that the free carrier absorption in the ITO films leads to optical losses in the near IR part. A possible way to overcome such a limitation would be to increase the carriers mobility and thus the IR transmission of TCO films. Indeed, Sanyo has also claimed to get higher J_{sc} with a “new TCO”,⁸ on which nothing is said but at the same time, another Japanese group published some data about hydrogen-doped indium oxide which had a higher mobility so that for a constant resistivity the number of carriers, and their related absorption, can be reduced. They have shown a successful implementation of this TCO into heterojunction solar cells,⁹ or microcrystalline silicon solar cells.¹⁰

Apart from these intrinsic optical and electrical properties, TCO can also have an impact on the performance of solar cells, if they do not form a good contact with the (p) a-Si:H layer. This is the conclusion of several simulation works,^{11,12} based on the fact that ITO has a higher work func-

¹Mishima, Taguchi, Sakata, and Maruyama, “Development status of high-efficiency HIT solar cells”, 2011 [101]

²Muñoz et al., “Towards high efficiency on full wafer a-Si:H/c-Si heterojunction solar cells: 19.6% on 14 8cm²”, 2010 [115]

³De Wolf et al., “High-efficiency silicon heterojunction solar cells: From physics to production lines”, 2010 [116]

⁴National Renewable Energy Laboratory, *Does the world have enough materials for PV to help address climate change?*, 2005 [117]

⁵Green, “Estimates of Te and In prices from direct mining of known ores”, 2009 [118]

⁶Angermann, Conrad, Korte, Rappich, Schulze, and Schmidt, “Passivation of textured substrates for a-Si:H/c-Si hetero-junction solar cells: Effect of wet-chemical smoothing and intrinsic a-Si:H interlayer”, 2009 [119]

⁷Favier, Muñoz, Martín de Nicolás, and Ribeyron, “Boron-doped zinc oxide layers grown by metal-organic CVD for silicon heterojunction solar cells applications”, 2011 [120]

⁸Tsunomura, Yoshimine, Taguchi, Baba, Kinoshita, Kanno, Sakata, Maruyama, and Tanaka, “Twenty-two percent efficiency HIT solar cell”, 2009 [121]

⁹Koida, Fujiwara, and Kondo, “Reduction of Optical Loss in Hydrogenated Amorphous Silicon/Crystalline Silicon Heterojunction Solar Cells by High-Mobility Hydrogen-Doped In₂O₃ Transparent Conductive Oxide”, 2008 [122]

¹⁰Koida, Sai, and Kondo, “Application of hydrogen-doped In₂O₃ transparent conductive oxide to thin-film microcrystalline Si solar cells”, 2010 [123]

¹¹Centurioni and Iencinella, “Role of front contact work function on amorphous silicon/crystalline silicon heterojunction solar cell performance”, 2003 [124]

¹²Rached and Mostefaoui, “Influence of the front contact barrier height on the In-

tion than that of (p) a-Si:H and can induce a downward band bending of the (p) a-Si:H leading to a decrease of the built-in potential of the solar cell and reduce the carriers extraction. These results are also confirmed by the simulations on the entire solar cell structures.¹ However, no experimental studies have been carried out so far to confirm these results regarding the work function dependence of solar cells' parameters. Besides, all these studies have also shown that for sufficiently doped and sufficiently thick (p) a-Si:H, such an effect is suppressed.

2.4 Conclusions

This chapter introduced the structure of heterojunction solar cell in terms of process flow and detailed each step of its fabrication. This meant the description of the plasma enhanced chemical vapour deposition (PECVD), involved in the growth of a-Si:H, the physical vapour deposition (PVD) for ITO, as well as that of thermal evaporation of metals. The major characterization tools were also introduced, such as the spectroscopic ellipsometer used to determine the thickness and the dielectric function of the deposited films and the Sinton effective lifetime tester used to determine the effective lifetime of passivated wafers. In parallel, the band structure of the heterojunction solar cell was also introduced, highlighting its main features and pointing out the main differences with respect to the crystalline homojunction cell, mainly the unique a-Si:H based simultaneous passivation and junction formation. Passivation schemes were also introduced, presenting some of the most common films used in homojunction cells, as well as the major ones used in the frame of heterojunction cells.

dium Tin Oxide/hydrogenated p-doped amorphous silicon heterojunction solar cells", 2008 [125]

¹Kanevce and Metzger, "The role of amorphous silicon and tunneling in heterojunction with intrinsic thin layer (HIT) solar cells", 2009 [82]

REFERENCES

- [1] M. A. Green, K. Emery, Y. Hishikawa, and W. Warta. "Solar cell efficiency tables (version 36)". In: *Progress in photovoltaics: Research & applications* 18 (2010), p. 346. DOI: 10.1002/pip.1021 (cit. on p. 39).
- [2] C. Niikura, Y. Poissant, M.E. Gueunier, J.-P. Kleider, and J. E. Bourée. "Transport properties of hot-wire CVD μ -Si:H layers for solar cells". In: *Journal of Non-Crystalline Solids* 299-302 (2002), pp. 1179–1183. DOI: 10.1016/S0022-3093(01)01085-7 (cit. on p. 41).
- [3] A. Lacoste, T. Lagarde, S. Béchu, Y. Arnal, and J. Pelletier. "Multi-dipolar plasmas for uniform processing: physics, design and performance". In: *Plasma Sources Science and Technology* 11 (2002), p. 407. DOI: 10.1088/0963-0252/11/4/307 (cit. on p. 41).
- [4] D. Daineka, P. Bulkin, G. Girard, J.-E. Bourée, and B. Drévillon. "High density plasma enhanced chemical vapor deposition of optical thin films". In: *Eur. Phys. J. Appl. Phys.* 26 (2004), pp. 3–9. DOI: 10.1051/epjap:2004013 (cit. on p. 41).
- [5] R. Botha, B. Haj Ibrahim, P. Bulkin, and B. Drévillon. "Deposition of dielectrics using a matrix distributed electron cyclotron resonance plasma enhanced chemical vapor deposition system". In: *Thin Solid Films* 515 (2007), pp. 7594–7597. DOI: 10.1016/j.tsf.2006.11.184 (cit. on p. 41).
- [6] M.E. Gueunier-Farret, C. Bazin, J.-P. Kleider, C. Longeaud, P. Bulkin, D. Daineka, T.H. Dao, P. Roca i Cabarrocas, P. Descamps, T. Kervyn de Meerendre, P. Leempoel, M. Meaudre, and R. Meaudre. "Device quality a-Si:H deposited from electron cyclotron resonance at very high deposition rates". In: *Journal of Non-Crystalline Solids* 352 (2006), pp. 1913–1916. DOI: 10.1016/j.jnoncrysol.2006.01.080 (cit. on p. 41).
- [7] P. Roca i Cabarrocas, P. Bulkin, D. Daineka, T.H. Dao, P. Leempoel, P. Descamps, T. Kervyn de Meerendré, and J. Charliac. "Advances in the deposition of microcrystalline silicon at high rate by distributed electron cyclotron resonance". In: *Thin Solid Films* 516 (2008), pp. 6834–6838. DOI: 10.1016/j.tsf.2007.12.067 (cit. on p. 41).
- [8] Laurent Kroely. "Process and material challenges in the high rate deposition of microcrystalline silicon thin films and solar cells by Matrix Distributed Electron Cyclotron Resonance plasma". PhD thesis. École Polytechnique, 2010. URL: [http :](http://www.polytechnique.edu/theses/2010/01/01/laurent_kroely)

- //pastel.archives-ouvertes.fr/docs/00/55/02/41/PDF/PhD_thesis_Laurent_KROELY_final_version.pdf (cit. on p. 41).
- [9] S. K. Ram, L. Kroely, P. Bulkin, and P. Roca i Cabarrocas. "Effect of ion energy on structural and electrical properties of intrinsic microcrystalline silicon layer deposited in a matrix distributed electron cyclotron resonance plasma reactor". In: *physica status solidi (a)* 207 (2010), pp. 591–594. DOI: 10.1002/pssa.200982905 (cit. on p. 41).
- [10] P. Roca i Cabarrocas, J.-B. Chévrier, J. Huc, A. Lloret, J.-Y. Parey, and J.-P.-M. Schmitt. "A fully automated hot-wall multiplasma-monochamber reactor for thin film deposition". In: *J. Vac. Sci. Technol. A* 9 (1991), p. 2331. DOI: 10.1116/1.577318 (cit. on pp. 42, 43).
- [11] Pere Roca i Cabarrocas. "Science des matériaux et techniques du réacteur dans le dépôt par procédé plasma RF de photopiles et d'autres dispositifs en silicium amorphe hydrogéné". In: (1988) (cit. on pp. 42, 43).
- [12] Brian Chapman. *Glow Discharge Processes: Sputtering and Plasma Etching*. Wiley-Interscience, 1980 (cit. on p. 43).
- [13] Michael A. Lieberman and Allan J. Lichtenberg. *Principles of Plasma Discharges and Materials Processing, Second Edition*. John Wiley and Sons, Inc. (cit. on pp. 43, 44).
- [14] J.P.M. Schmitt. "Fundamental mechanisms in silane plasma decompositions and amorphous silicon deposition". In: *Journal of Non-Crystalline Solids* 59-60 (1983), pp. 649–657. DOI: 10.1016/0022-3093(83)90257-0 (cit. on p. 45).
- [15] J. Perrin. "Plasma and surface reactions during a-Si:H film growth". In: *Journal of Non-Crystalline Solids* 137-138 (1991), pp. 639–644. DOI: 10.1016/S0022-3093(05)80202-9 (cit. on pp. 45, 46).
- [16] M. J. Kushner. "A model for the discharge kinetics and plasma chemistry during plasma enhanced chemical vapor deposition of amorphous silicon". In: *Journal of Applied Physics* 63 (1988), pp. 2532–2551. DOI: 10.1063/1.340989 (cit. on p. 45).
- [17] A. Matsuda, K. Nomoto, Y. Takeuchi, A. Suzuki, A. Yuuki, and J. Perrin. "Temperature dependence of the sticking and loss probabilities of silyl radicals on hydrogenated amorphous silicon". In: *Surface Science* 227 (1990), pp. 50–56. DOI: 10.1016/0039-6028(90)90390-T (cit. on p. 46).
- [18] R.A. Street. *Hydrogenated Amorphous Silicon*. Ed. by Cambridge University Press. 1991 (cit. on p. 46).
- [19] W. M. M. Kessels, A. H. M. Smets, D. C. Marra, E. S. Aydil, D. C. Schram, and M. C. M. van de Sanden. "On the growth mechanism of a-Si:H". In: *Thin Solid Films* 383 (2001), pp. 154–160. DOI: 10.1016/S0040-6090(00)01594-7 (cit. on p. 46).

- [20] N. Itabashi, N. Nishiwaki, M. Magane, S. Naito, T. Goto, A. Matsuda, C. Yamada, and E. Hirota. "Spatial Distribution of SiH_3 Radicals in RF Silane Plasma". In: *Japanese Journal of Applied Physics* 29 (1990), pp. L505–L507. DOI: 10.1143/JJAP.29.L505 (cit. on p. 46).
- [21] A. Gallagher. "Neutral radical deposition from silane discharges". In: *Journal of Applied Physics* 63 (1988), pp. 2406–2413. DOI: 10.1063/1.341034 (cit. on p. 46).
- [22] T. Ohira, O. Ukai, T. Adachi, Y. Takeuchi, and M. Murata. "Molecular-dynamics simulations of SiH_3 radical deposition on hydrogen-terminated silicon (100) surfaces". In: *Phys. Rev. B* 52 (1995), pp. 8283–8287. DOI: 10.1103/PhysRevB.52.8283 (cit. on p. 47).
- [23] J. E. Gerbi and J. R. Abelson. "Deposition of microcrystalline silicon: Direct evidence for hydrogen-induced surface mobility of Si adspecies". In: *Journal of Applied Physics* 89 (2001), pp. 1463–1469. DOI: 10.1063/1.1334639 (cit. on p. 47).
- [24] S. Ramalingam, D. Maroudas, E. S. Aydil, and S. P. Walch. "Abstraction of hydrogen by SiH_3 from hydrogen-terminated $\text{Si}(001)-(2 \times 1)$ surfaces". In: *Surface Science* 418 (1998), pp. L8–L13. DOI: 10.1016/S0039-6028(98)00703-1 (cit. on p. 47).
- [25] S. Cereda, M. Ceriotti, F. Montalenti, M. Bernasconi, and Leo Miglio. "Quantitative estimate of H abstraction by thermal SiH_3 on hydrogenated $\text{Si}(001)(2 \times 1)$ ". In: *Phys. Rev. B* 75 (2007), p. 235311. DOI: 10.1103/PhysRevB.75.235311 (cit. on p. 47).
- [26] W. M. M. Kessels, A. H. M. Smets, and M. C. M. van de Sanden. "The a-Si:H growth mechanism and the role of H abstraction from the surface by SiH_3 radicals via an Eley-Rideal mechanism". In: *Journal of Non-Crystalline Solids* 338-340 (2004), pp. 27–31. DOI: 10.1016/j.jnoncrysol.2004.02.015 (cit. on p. 47).
- [27] C. Hollenstein. "The physics and chemistry of dusty plasmas". In: *Plasma Physics and Controlled Fusion* 42 (2000), R93. DOI: 10.1088/0741-3335/42/10/201 (cit. on p. 47).
- [28] P. Roca i Cabarrocas, Th. Nguyen-Tran, Y. Djeridane, A. Abramov, E. V. Johnson, and G. Patriarche. "Synthesis of silicon nanocrystals in silane plasmas for nanoelectronics and large area electronic devices". In: *Journal of Physics D: Applied Physics* 40 (2007), p. 2258. DOI: 10.1088/0022-3727/40/8/S04 (cit. on p. 47).
- [29] Th. Nguyen-Tran, P. Roca i Cabarrocas, and G. Patriarche. "Study of radial growth rate and size control of silicon nanocrystals in square-wave-modulated silane plasmas". In: *Applied Physics Letters* 91, 111501 (2007), p. 111501. DOI: 10.1063/1.2784294 (cit. on p. 47).
- [30] P. Roca i Cabarrocas, A. Fontcuberta i Morral, and Y. Poissant. "Growth and optoelectronic properties of polymorphous silicon thin films". In: *Thin Solid Films* 403-404 (2002), pp. 39–46. DOI: 10.1016/S0040-6090(01)01656-X (cit. on p. 47).

- [31] R. Dewarrat and J. Robertson. "Surface diffusion of SiH₃ radicals and growth mechanism of a-Si:H and microcrystalline Si". In: *Thin Solid Films* 427 (2003), pp. 11–15. DOI: 10.1016/S0040-6090(02)01173-2 (cit. on p. 47).
- [32] Mayur S. Valipa, Tamas Bakos, and Dimitrios Maroudas. "Surface smoothness of plasma-deposited amorphous silicon thin films: Surface diffusion of radical precursors and mechanism of Si incorporation". In: *Phys. Rev. B* 74 (2006), p. 205324. DOI: 10.1103/PhysRevB.74.205324 (cit. on p. 47).
- [33] A. Gupta, H. Yang, and G. N. Parsons. "Ab initio analysis of silyl precursor physisorption and hydrogen abstraction during low temperature silicon deposition". In: *Surface Science* 496 (2002), pp. 307–317. DOI: 10.1016/S0039-6028(01)01467-4 (cit. on p. 48).
- [34] Harland Tompkins and Eugene A Haber. *Handbook of ellipsometry*. Ed. by Springer. William Andrew, 2006 (cit. on pp. 50, 51).
- [35] G. E. Jr. Jellison, M. F. Chisholm, and S. M. Gorbalkin. "Optical functions of chemical vapor deposited thin-film silicon determined by spectroscopic ellipsometry". In: *Applied Physics Letters* 62 (1993), pp. 3348–3350. DOI: 10.1063/1.109067 (cit. on p. 50).
- [36] G.E. Jr. Jellison. "Optical functions of silicon determined by two-channel polarization modulation ellipsometry". In: *Optical Materials* 1 (1992), pp. 41–47. DOI: 10.1016/0925-3467(92)90015-F (cit. on p. 51).
- [37] D. E. Aspnes and A. A. Studna. "Dielectric functions and optical parameters of Si, Ge, GaP, GaAs, GaSb, InP, InAs, and InSb from 1.5 to 6.0 eV". In: *Phys. Rev. B* 27 (1983), p. 985. DOI: 10.1103/PhysRevB.27.985 (cit. on pp. 51, 52).
- [38] D.A.G. Bruggeman. "Berechnung verschiedener physikalischer Konstanten von heterogenen Substanzen. I. Dielektrizitätskonstanten und Leitfähigkeiten der Mischkörper aus isotropen Substanzen". In: *Annalen der Physik* 416 (1935), pp. 636–664. DOI: 10.1002/andp.19354160705 (cit. on p. 51).
- [39] G. E. Jellison, V. I. Merkulov, A. A. Puretzky, D. B. Geohegan, G. Eres, D. H. Lowndes, and J. B. Caughmans. "Characterization of thin-film amorphous semiconductors using spectroscopic ellipsometry". In: *Thin Solid Films* 377-378 (2000), pp. 68–73. DOI: 10.1016/S0040-6090(00)01384-5 (cit. on p. 52).
- [40] M. Moreno and P. Roca i Cabarrocas. "Ultra-thin crystalline silicon films produced by plasma assisted epitaxial growth on silicon wafers and their transfer to foreign substrates". In: *PV Direct* 1 (2010), p. 10301. DOI: 10.1051/pvd/2010001 (cit. on p. 54).
- [41] R. A. Sinton and A. Cuevas. "Contactless determination of current-voltage characteristics and minority-carrier lifetimes in semiconductors from quasi-steady-state photoconductance data". In: *Applied Physics Letters* 69 (1996), pp. 2510–2512. DOI: 10.1063/1.117723 (cit. on p. 54).

- [42] Isidro Garcia Martin. "Silicon surface passivation by Plasma Enhanced Chemical Vapor Deposited amorphous silicon carbide films". PhD thesis. Universitat Politecnica de Catalunya, 2001 (cit. on pp. 55, 56).
- [43] J. Schmidt and S. Dauwe. *Surface Passivation of Silicon Solar Cells using SiN_x:H : The Effect of Space Charge Recombination*. IMEC-Leuven. 2005. URL: <http://www.ipcrystalclear.info/data/pdf/Schmidt.pdf> (cit. on p. 57).
- [44] S. Olibet, E. Vallat-Sauvain, and C. Ballif. "Model for a-Si:H/c-Si interface recombination based on the amphoteric nature of silicon dangling bonds". In: *Physical Review B* 76, 035326 (2007), p. 035326. DOI: 10.1103/PhysRevB.76.035326 (cit. on pp. 57–59, 61, 65).
- [45] D.K. Biegelsen, N.M. Johnson, M. Stutzmann, E.H. Poindexter, and P.J. Caplan. "Native defects at the Si/SiO₂ interface-amorphous silicon revisited". In: *Applications of Surface Science* 22-23 (1985), pp. 879–890. DOI: 10.1016/0378-5963(85)90220-X (cit. on p. 58).
- [46] M. Garín, U. Rau, W. Brendle, I. Martín, and R. Alcubilla. "Characterization of a-Si:H/c-Si interfaces by effective-lifetime measurements". In: *Journal of Applied Physics* 98, 093711 (2005), p. 093711. DOI: 10.1063/1.2128047 (cit. on p. 58).
- [47] J. Hubin, A. V. Shah, and E. Sauvain. "Effects of dangling bonds on the recombination function in amorphous semiconductors". In: *Philosophical Magazine Letters* 66 (1992), pp. 115–125. DOI: 10.1080/09500839208229273 (cit. on p. 58).
- [48] B. Bahardoust, A. Chutinan, K. Leong, A. B. Gougam, D. Yeghikyan, T. Kosteski, N. P. Kherani, and S. Zukotynski. "Passivation study of the amorphous–crystalline silicon interface formed using DC saddle-field glow discharge". In: *physica status solidi (a)* 207 (2010), pp. 539–543. DOI: 10.1002/pssa.200982803 (cit. on p. 58).
- [49] T. T. A. Li, K. R. McIntosh, and A. Cuevas. "Limitations of a simplified dangling bond recombination model for a-Si:H". In: *Journal of Applied Physics* 104, 113718 (2008), p. 113718. DOI: 10.1063/1.3037235 (cit. on p. 58).
- [50] C. Leendertz, R. Stangl, T.F. Schulze, M. Schmidt, and L. Korte. "A recombination model for a-Si:H/c-Si heterostructures". In: *physica status solidi (c)* 7 (2010), pp. 1005–1010. DOI: 10.1002/pssc.200982698 (cit. on p. 58).
- [51] C.-T. Sah and W. Shockley. "Electron-Hole Recombination Statistics in Semiconductors through Flaws with Many Charge Conditions". In: *Phys. Rev.* 109 (1958), pp. 1103–1115. DOI: 10.1103/PhysRev.109.1103 (cit. on p. 58).

- [52] M. Mikolásek, J. Racko, L. Harmatha, P. Gaspierik, and P. Sutta. "Influence of the broken symmetry of defect state distribution at the a-Si:H/c-Si interface on the performance of hetero-junction solar cells". In: *Applied Surface Science* 256 (2010), pp. 5662–5666. DOI: 10.1016/j.apsusc.2010.03.023 (cit. on p. 58).
- [53] E. Yablonovitch, D. L. Allara, C. C. Chang, T. Gmitter, and T. B. Bright. "Unusually Low Surface-Recombination Velocity on Silicon and Germanium Surfaces". In: *Phys. Rev. Lett.* 57 (1986), pp. 249–252. DOI: 10.1103/PhysRevLett.57.249 (cit. on p. 58).
- [54] G. W. Trucks, Krishnan Raghavachari, G. S. Higashi, and Y. J. Chabal. "Mechanism of HF etching of silicon surfaces: A theoretical understanding of hydrogen passivation". In: *Phys. Rev. Lett.* 65 (1990), pp. 504–507. DOI: 10.1103/PhysRevLett.65.504 (cit. on p. 59).
- [55] H. Angermann, L. Korte, J. Rappich, E. Conrad, I. Siebera, M. Schmidt, K. Hübener, and J. Hauschild. "Optimisation of electronic interface properties of a-Si:H/c-Si hetero-junction solar cells by wet-chemical surface pre-treatment". In: *Thin Solid Films* 516 (2008), pp. 6775–6781. DOI: 10.1016/j.tsf.2007.12.033 (cit. on pp. 59, 65).
- [56] M.R. Page, E. Iwaniczko, Y. Xu, Q. Wang, Y. Yan, L. Roybal, H. M. Branz, and T.H. Wang. "Well-Passivated a-Si:H Back Contacts for Double-Heterojunction Solar cells". In: *IEEE 4th World Conference on Photovoltaic Energy Conversion, Waikoloa, Hawaii, May 7-12. 2006*. DOI: 10.1109/WCPEC.2006.279750 (cit. on p. 59).
- [57] A. G. Aberle. "Surface passivation of crystalline silicon solar cells: a review". In: *Progress in Pphotovoltaics: Research & applications* 8 (2000), pp. 473–487. DOI: 10.1002/1099-159X(200009/10)8:5<473::AID-PIP337>3.0.CO;2-D (cit. on pp. 59, 60).
- [58] A. G. Aberle. "Overview on SiN surface passivation of crystalline silicon solar cells". In: *Solar Energy Materials & Solar Cells* 65 (2001), pp. 239–248. DOI: 10.1016/S0927-0248(00)00099-4 (cit. on p. 59).
- [59] M. J. Kerr and A. Cuevas. "Recombination at the interface between silicon and stoichiometric plasma silicon nitride". In: *Semiconductor Science and Technology* 17 (2002), p. 166. DOI: 10.1088/0268-1242/17/2/314 (cit. on p. 59).
- [60] J.-F. Lelièvre, E. Fourmond, A. Kaminski, O. Palais, D. Ballutaud, and M. Lemi. "Study of the composition of hydrogenated silicon nitride SiN_x:H for efficient surface and bulk passivation of silicon". In: *Solar Energy Materials & Solar Cells* 93 (2009), pp. 1281–1289. DOI: 10.1016/j.solmat.2009.01.023 (cit. on p. 59).
- [61] H. F. W. Dekkers, L. Cernel, and G. Beaucarne. "Carrier trap passivation in multicrystalline Si solar cells by hydrogen from SiN_x:H layers". In: *Applied Physics Letters* 89, 013508 (2006), p. 013508. DOI: 10.1063/1.2219142 (cit. on p. 59).

- [62] Adolf Goetzberger, Joachim Knobloch, and Bernhard Voss. *Crystalline silicon solar cells*. Ed. by John Wiley & Sons. John Wiley & Sons, 1998 (cit. on p. 59).
- [63] J. Robertson, W.L. Warren, and J. Kanicki. "Nature of the Si and N dangling bonds in silicon nitride". In: *Journal of Non-Crystalline Solids* 187 (1995), pp. 297–300. DOI: 10.1016/0022-3093(95)00153-0 (cit. on p. 59).
- [64] H. Mäckel and R. Lüdemann. "Detailed study of the composition of hydrogenated SiN_x layers for high-quality silicon surface passivation". In: *Journal of Applied Physics* 92 (2002), pp. 2602–2609. DOI: 10.1063/1.1495529 (cit. on p. 59).
- [65] S. Dauwe, J. Schmidt, A. Metz, and R. Hezel. "Fixed charge density in silicon nitride films on crystalline silicon surfaces under illumination". In: *Photovoltaic Specialists Conference, 2002. Conference Record of the Twenty-Ninth IEEE*. May 2002, pp. 162–165. DOI: 10.1109/PVSC.2002.1190481 (cit. on p. 60).
- [66] J. Y. Lee and S.W. Glunz. "Investigation of various surface passivation schemes for silicon solar cells". In: *Solar Energy Materials & Solar Cells* 90 (2006), pp. 82–92. DOI: 10.1016/j.solmat.2005.02.007 (cit. on p. 60).
- [67] M. J. Kerr and A. Cuevas. "Very low bulk and surface recombination in oxidized silicon wafers". In: *Semiconductor Science and Technology* 17 (2002), p. 35. DOI: 10.1088/0268-1242/17/1/306 (cit. on p. 60).
- [68] J. Mizsei. "Silicon surface passivation by static charge". In: *Applied Surface Science* 252 (2006), pp. 7691–7699. DOI: 10.1016/j.apsusc.2006.03.075 (cit. on p. 60).
- [69] G. Agostinelli, A. Delabie, P. Vitanov, Z. Alexieva, H.F.W. Dekkers, S. De Wolf, and G. Beaucarne. "Very low surface recombination velocities on p-type silicon wafers passivated with a dielectric with fixed negative charge". In: *Solar Energy Materials & Solar Cells* 90 (2006), pp. 3438–3443. DOI: 10.1016/j.solmat.2006.04.014 (cit. on p. 60).
- [70] B. Hoex, J. J. H. Gielis, M. C. M. van de Sanden, and W. M. M. Kessels. "On the c-Si surface passivation mechanism by the negative-charge-dielectric Al₂O₃". In: *Journal of Applied Physics* 104, 113703 (2008), p. 113703. DOI: 10.1063/1.3021091 (cit. on p. 60).
- [71] G. Dingemans, W. Beyer, M. C. M. van de Sanden, and W. M. M. Kessels. "Hydrogen induced passivation of Si interfaces by Al₂O₃ films and SiO₂/Al₂O₃ stacks". In: *Applied Physics Letters* 97, 152106 (2010), p. 152106. DOI: 10.1063/1.3497014 (cit. on p. 60).
- [72] S. Dauwe, J. Schmidt, and R. Hezel. "Very low surface recombination velocities on p- and n-type silicon wafers passivated with hydrogenated amorphous silicon films". In: *Photovoltaic Specialists Conference, 2002. Conference Record of the Twenty-Ninth IEEE*. May 2002, pp. 1246–1249. DOI: 10.1109/PVSC.2002.1190834 (cit. on p. 60).

- [73] S. Dauwe, L. Mittelstadt, A. Metz, J. Schmidt, and R. Hezel. "Low-temperature rear surface passivation schemes for >20% efficient silicon solar cells". In: *Photovoltaic Energy Conversion, 2003. Proceedings of 3rd World Conference on*. Vol. 2. May 2003, 1395–1398 Vol.2 (cit. on p. 60).
- [74] D. Pysch, J. Ziegler, J.-P. Becker, D. Suwito, S. Janz, S. W. Glunz, and M. Hermle. "Stretched-exponential increase in the open-circuit voltage induced by thermal annealing of amorphous silicon-carbide heterojunction solar cells". In: *Applied Physics Letters* 94, 093510 (2009), p. 093510. DOI: 10.1063/1.3083552 (cit. on p. 60).
- [75] M. Vetter, I. Martín, R. Ferre, M. Garín, and R. Alcubilla. "Crystalline silicon surface passivation by amorphous silicon carbide films". In: *Solar Energy Materials & Solar Cells* 91 (2007), pp. 174–179. DOI: 10.1016/j.solmat.2006.08.004 (cit. on p. 60).
- [76] S.W. Glunz, S. Janz, M. Hofmann, T. Roth, and G. Willeke. "Surface passivation of silicon solar cells using amorphous silicon carbide layers". In: *IEEE 4th World Conference on Photovoltaic Energy Conversion, Waikoloa, HI, May 7-12*. 2006. DOI: 10.1109/WCPEC.2006.279291 (cit. on p. 60).
- [77] R. Ferre, A. Orpella, D. Munoz, I. Martín, F. Recart, C. Voz, J. Puigdollers, P Roca i Cabarrocas, and R Alcubilla. "Very low surface recombination velocity of crystalline silicon passivated by phosphorus-doped a-SiC_xN_y:H(n) alloys". In: *Progress in photovoltaics: Research and applications* 16 (2007), pp. 123–127. DOI: 10.1002/pip.802 (cit. on p. 60).
- [78] T. Mueller, S. Schwertheim, and W. R. Fahrner. "Crystalline silicon surface passivation by high-frequency plasma-enhanced chemical-vapor-deposited nanocomposite silicon suboxides for solar cell applications". In: *Journal of Applied Physics* 107, 014504 (2010), p. 014504. DOI: 10.1063/1.3264626 (cit. on p. 60).
- [79] J. J. H. Gielis, P. J. van den Oever, B. Hoex, M. C. M. van de Sanden, and W. M. M. Kessels. "Real-time study of a-Si:H/c-Si heterointerface formation and epitaxial Si growth by spectroscopic ellipsometry, infrared spectroscopy, and second-harmonic generation". In: *Phys. Rev. B* 77 (2008), p. 205329. DOI: 10.1103/PhysRevB.77.205329 (cit. on p. 61).
- [80] M. Taguchi, A. Terakawa, E. Maruyama, and M. Tanaka. "Obtaining a higher Voc in HIT cells". In: *Progress in Photovoltaics: Research & Applications* 13 (2005), pp. 481–488. DOI: 10.1002/pip.646 (cit. on p. 61).
- [81] W. Favre, M. Labrune, F. Dadouche, A. S. Gudovskikh, P. Roca i Cabarrocas, and J.-P. Kleider. "Study of the interfacial properties of amorphous silicon/n-type crystalline silicon heterojunction through static planar conductance measurements". In: *physica status solidi (c)* 7 (2010), pp. 1037–1040. DOI: 10.1002/pssc.200982800 (cit. on p. 62).

- [82] Ana Kanevce and Wyatt K. Metzger. "The role of amorphous silicon and tunneling in heterojunction with intrinsic thin layer (HIT) solar cells". In: *Journal of Applied Physics* 105, 094507 (2009), p. 094507. DOI: 10.1063/1.3106642 (cit. on pp. 62, 63, 66, 68).
- [83] T. H. Wang, M. R. Page, E. Iwaniczko, D. H. Levi, Y. Yan, H. M. Branz, V. Yelundur, A. Rohatgi, G. Bunea, A. Terao, and Q. Wang. "Toward Better Understanding and Improved Performance of Silicon Heterojunction Solar Cells". In: *14th Workshop on Crystalline Silicon Solar Cells and Materials, 8-11 August 2004, Winter Park, Colorado*. 2004 (cit. on p. 62).
- [84] M. W. M. van Cleef, F. A. Rubinelli, J. K. Rath, R. E. I. Schropp, W. F. van der Weg, R. Rizzoli, C. Summonte, R. Pinghini, E. Centurioni, and R. Galloni. "Photocarrier collection in a-SiC:H/c-Si heterojunction solar cells". In: *Journal of Non-Crystalline Solids* 227-230 (1998), pp. 1291-1294. DOI: 10.1016/S0022-3093(98)00210-5 (cit. on pp. 62, 63, 66).
- [85] A. Fantoni, Y. Vigranenko, M. Fernandes, R. Schwarz, and M. Vieira. "Influence of the band offset on the performance of photodevices based on the c-Si/a-Si:H heterostructure". In: *Thin Solid Films* 383 (2001), pp. 314-317. DOI: 10.1016/S0040-6090(00)01611-4 (cit. on pp. 62, 63).
- [86] M.R. Page, E. Iwaniczko, Y.-Q. Xu, L. Roybal, F. Hasoon, Q. Wang, and R.S. Crandall. "Amorphous/crystalline silicon heterojunction solar cells with varying i-layer thickness". In: *Thin Solid Films* In Press, Corrected Proof (2011), pp. -. ISSN: 0040-6090. DOI: 10.1016/j.tsf.2011.01.293 (cit. on p. 63).
- [87] A. Froitzheim, K. Brendel, L. Elstner, W. Fuhs, K. Kliefoth, and M. Schmidt. "Interface recombination in heterojunctions of amorphous and crystalline silicon". In: *Journal of Non-Crystalline Solids* 299-302 (2002), pp. 663-667. DOI: 10.1016/S0022-3093(01)01029-8 (cit. on p. 63).
- [88] K. Ghosh, C.J. Tracy, S. Herasimenka, C. Honsberg, and S. Bowden. "Explanation of the device operation principle of amorphous silicon/ crystalline silicon heterojunction solar cell and role of the inversion of crystalline silicon surface". In: *Photovoltaic Specialists Conference (PVSC), 2010 35th IEEE*. 2010, pp. 001383 -001386. DOI: 10.1109/PVSC.2010.5614387 (cit. on p. 63).
- [89] M. Rahmouni, A. Datta, P. Chatterjee, J. Damon-Lacoste, C. Ballif, and P. Roca i Cabarrocas. "Carrier transport and sensitivity issues in heterojunction with intrinsic thin layer solar cells on N-type crystalline silicon: A computer simulation study". In: *Journal of Applied Physics* 107, 054521 (2010), p. 054521. DOI: 10.1063/1.3326945 (cit. on pp. 63, 66).
- [90] M. W. M. van Cleef, R. E. I. Schropp, and F. A. Rubinelli. "Significance of tunneling in p⁺ amorphous silicon carbide n crystalline silicon heterojunction solar cells". In: *Applied Physics Letters* 73 (1998), pp. 2609-2611. DOI: 10.1063/1.122521 (cit. on p. 63).

- [91] M. Taguchi, E. Maruyama, and M. Tanaka. "Temperature Dependence of Amorphous/Crystalline Silicon Heterojunction Solar Cells". In: *Japanese Journal of Applied Physics* 47 (2008), pp. 814–818. DOI: 10.1143/JJAP.47.814 (cit. on p. 63).
- [92] J. P. Kleider, A.S. Gudovskikh, and P. Roca i Cabarrocas. "Determination of the conduction band offset between hydrogenated amorphous silicon and crystalline silicon from surface inversion layer conductance measurements". In: *Applied Physics Letters* 92, 162101 (2008), p. 162101. DOI: 10.1063/1.2907695 (cit. on p. 63).
- [93] J.-P. Kleider, J. Alvarez, A.V. Andkudinov, A.S. Gudovskikh, E.V. Gushina, M. Labrune, O. Maslova, W. Favre, M.-E. Gueunier-Farret, P. Roca i Cabarrocas, and E.I. Terukov. "Characterization of silicon heterojunction for solar cells". In: *Nanoscale Research Letters* 6 (2011), p. 152. DOI: 10.1186/1556-276X-6-152 (cit. on p. 64).
- [94] O. A. Maslova, J. Alvarez, E. V. Gushina, W. Favre, M. E. Gueunier-Farret, A. S. Gudovskikh, A. V. Ankudinov, E. I. Terukov, and J.-P. Kleider. "Observation by conductive-probe atomic force microscopy of strongly inverted surface layers at the hydrogenated amorphous silicon/crystalline silicon heterojunctions". In: *Applied Physics Letters* 97, 252110 (2010), p. 252110. DOI: 10.1063/1.3525166 (cit. on p. 64).
- [95] M. Schmidt, L. Korte, A. Laades, R. Stangl, Ch. Schubert, H. Angermann, E. Conrad, and K.v. Maydell. "Physical aspects of a-Si:H/c-Si hetero-junction solar cells". In: *Thin Solid Films* 515 (2007), pp. 7475–7480. DOI: 10.1016/j.tsf.2006.11.087 (cit. on pp. 64, 65).
- [96] L. Korte and M. Schmidt. "Doping type and thickness dependence of band offsets at the amorphous/crystalline silicon heterojunction". In: *Journal of Applied Physics* 109, 063714 (2011), p. 063714. DOI: 10.1063/1.3559296 (cit. on p. 64).
- [97] M. Sebastiani, L. Di Gaspare, G. Capellini, C. Bittencourt, and F. Evangelisti. "Low-Energy Yield Spectroscopy as a Novel Technique for Determining Band Offsets: Application to the c-Si(100)/a-Si:H Heterostructure". In: *Phys. Rev. Lett.* 75 (1995), pp. 3352–3355. DOI: 10.1103/PhysRevLett.75.3352 (cit. on p. 64).
- [98] T. M. Brown, C. Bittencourt, M. Sebastiani, and F. Evangelisti. "Electronic states and band lineups in c-Si(100)/a-Si_{1-x}C_x:H heterojunctions". In: *Phys. Rev. B* 55 (1997), pp. 9904–9909. DOI: 10.1103/PhysRevB.55.9904 (cit. on p. 64).
- [99] Chris G. Van de Walle and L. H. Yang. "Band discontinuities at heterojunctions between crystalline and amorphous silicon". In: *J. Vac. Sci. Technol. B* 13 (1995), pp. 1635–1638. DOI: 10.1116/1.587870 (cit. on p. 64).
- [100] M. Tanaka, M. Taguchi, T. Matsuyama, T. Sawada, S. Tsuda, S. Nakano, H. Hanafusa, and Y. Kuwano. "Development of New a-Si/c-Si Heterojunction Solar Cells: ACJ-HIT (Artificially Constructed Junction-Heterojunction with Intrinsic Thin-Layer)". In:

- Japanese Journal of Applied Physics* 31 (1992), pp. 3518–3522. DOI: 10.1143/JJAP.31.3518 (cit. on p. 65).
- [101] T. Mishima, M. Taguchi, H. Sakata, and E. Maruyama. “Development status of high-efficiency HIT solar cells”. In: *Solar Energy Materials & Solar Cells* 95 (2011), pp. 18–21. DOI: 10.1016/j.solmat.2010.04.030 (cit. on pp. 65, 67).
- [102] K. v. Maydell, E. Conrad, and M. Schmidt. “Efficient silicon heterojunction solar cells based on p- and n-type substrates processed at temperatures $\leq 220^\circ\text{C}$ ”. In: *Progress in Photovoltaics: Research & Applications* 14 (2006), pp. 289–295. DOI: 10.1002/pip.668 (cit. on p. 65).
- [103] N. Jensen, R. M. Hausner, R. B. Bergmann, J. H. Werner, and U. Rau. “Optimization and characterization of amorphous/crystalline silicon heterojunction solar cells”. In: *Progress in Photovoltaics: Research and Applications* 10 (2002), pp. 1–13. DOI: 10.1002/pip.398 (cit. on p. 65).
- [104] H. Fujiwara and M. Kondo. “Effects of a-Si:H layer thicknesses on the performance of a-Si:H/c-Si heterojunction solar cells”. In: *Journal of Applied Physics* 101, 054516 (2007), p. 054516. DOI: 10.1063/1.2559975 (cit. on pp. 65, 66).
- [105] S. Olibet, C. Monachon, A. Hessler-Wyser, E. Vallat-Sauvain, S. De Wolf, L. Fesquet, J. Damon-Lacoste, and C. Ballif. “Textured silicon heterojunction solar cells with over 700 mV open-circuit voltage studied by Transmission Electron Microscopy”. In: *23rd European Photovoltaic Solar Energy Conference, 1-5 September, Valencia, Spain. 2008* (cit. on pp. 65, 66).
- [106] J.W.A. Schüttauf, Y. Komatsu, L.J. Geerligs, Y. Mai, A. Bink, D.A. Spee, and R.E.I. Schropp. “Emitter Optimization on a-Si:H/c-Si Heterojunction Solar Cells for Isotextured Wafers”. In: *23rd EU PVSEC Valencia, Spain. 2008* (cit. on p. 65).
- [107] S. De Wolf and M. Kondo. “Abruptness of a-Si:H/c-Si interface revealed by carrier lifetime measurements”. In: *Applied Physics Letters* 90, 042111 (2007), p. 042111. DOI: 10.1063/1.2432297 (cit. on p. 65).
- [108] J.J.H. Gielis, B. Hoex, P.J. van den Oever, M.C.M. van de Sanden, and W.M.M. Kessels. “Silicon surface passivation by hot-wire CVD Si thin films studied by in situ surface spectroscopy”. In: *Thin Solid Films* 517 (2009), pp. 3456–3460. DOI: 10.1016/j.tsf.2009.01.076 (cit. on p. 65).
- [109] E. Centurioni, D. Iencinella, R. Rizzoli, and F. Zignani. “Silicon heterojunction solar cell: a new buffer Layer concept with low-temperature epitaxial silicon”. In: *IEEE TRANSACTIONS ON ELECTRON DEVICES, VOL. 51, NO. 11, NOVEMBER 2004*. Vol. 51. 2004, pp. 1818–1824. DOI: 10.1109/TED.2004.836801 (cit. on p. 66).

- [110] J. Damon-Lacoste and P. Roca i Cabarrocas. "Toward a better physical understanding of a-Si:H/c-Si heterojunction solar cells". In: *Journal of Applied Physics* 105, 063712 (2009), p. 063712. DOI: 10.1063/1.3091283 (cit. on p. 66).
- [111] J. Sritharathikhun, F. Jiang, S. Miyajima, A. Yamada, and M. Konagai. "Optimization of p-Type Hydrogenated Microcrystalline Silicon Oxide Window Layer for High-Efficiency Crystalline Silicon Heterojunction Solar Cells". In: *Japanese Journal of Applied Physics* 48 (2009), p. 101603. DOI: 10.1143/JJAP.48.101603 (cit. on p. 66).
- [112] S. Miyajima, J. Irikawa, A. Yamada, and M. Konagai. "High-quality nanocrystalline cubic silicon carbide emitter for crystalline silicon heterojunction solar cells". In: *Applied Physics Letters* 97, 023504 (2010), p. 023504. DOI: 10.1063/1.3460917 (cit. on p. 66).
- [113] C. Banerjee, J. Sritharathikhun, A. Yamada, and M. Konagai. "Fabrication of heterojunction solar cells by using microcrystalline hydrogenated silicon oxide film as an emitter". In: *Journal of Physics D: Applied Physics* 41 (2008), p. 185107. DOI: 10.1088/0022-3727/41/18/185107 (cit. on p. 66).
- [114] D. Pysch, M. Bivour, M. Hermle, and S. W. Glunz. "Amorphous silicon carbide heterojunction solar cells on p-type substrates". In: *Thin Solid Films* 519 (2011), pp. 2550–2554. DOI: 10.1016/j.tsf.2010.12.028 (cit. on p. 66).
- [115] D. Muñoz et al. "Towards high efficiency on full wafer a-Si:H/c-Si heterojunction solar cells: 19.6% on 14 8cm²". In: *Photovoltaic Specialists Conference (PVSC), 2010 35th IEEE*. 2010, pp. 000039–000043. DOI: 10.1109/PVSC.2010.5614179 (cit. on p. 67).
- [116] S. De Wolf et al. "High-efficiency silicon heterojunction solar cells: From physics to production lines". In: *Solid-State and Integrated Circuit Technology (ICSICT), 2010 10th IEEE International Conference on*. 2010, pp. 1986–1989. DOI: 10.1109/ICSICT.2010.5667849 (cit. on p. 67).
- [117] National Renewable Energy Laboratory. *Does the world have enough materials for PV to help address climate change?* U.S. Department of Energy Office of Energy Efficiency and Renewable Energy. 2005. URL: <http://www.nrel.gov/docs/fy05osti/37656.pdf> (cit. on p. 67).
- [118] M. A. Green. "Estimates of Te and In prices from direct mining of known ores". In: *Progress in Photovoltaics: Research & Applications* 17 (2009), pp. 347–359. DOI: 10.1002/pip.899 (cit. on p. 67).
- [119] H. Angermann, E. Conrad, L. Korte, J. Rappich, T.F. Schulze, and M. Schmidt. "Passivation of textured substrates for a-Si:H/c-Si heterojunction solar cells: Effect of wet-chemical smoothing and intrinsic a-Si:H interlayer". In: *Materials Science and Engineering: B* 159-160 (2009), pp. 219–223. DOI: 10.1016/j.mseb.2008.10.044 (cit. on p. 67).

- [120] A. Favier, D. Muñoz, S. Martín de Nicolás, and P.-J. Ribeyron. "Boron-doped zinc oxide layers grown by metal-organic CVD for silicon heterojunction solar cells applications". In: *Solar Energy Materials and Solar Cells* 95 (2011), pp. 1057–1061. DOI: 10.1016/j.solmat.2010.11.013 (cit. on p. 67).
- [121] Y. Tsunomura, Y. Yoshimine, M. Taguchi, T. Baba, T. Kinoshita, H. Kanno, H. Sakata, E. Maruyama, and M. Tanaka. "Twenty-two percent efficiency HIT solar cell". In: *Solar Energy Materials and Solar Cells* 93 (2009), pp. 670–673. DOI: 10.1016/j.solmat.2008.02.037 (cit. on p. 67).
- [122] T. Koida, H. Fujiwara, and M. Kondo. "Reduction of Optical Loss in Hydrogenated Amorphous Silicon/Crystalline Silicon Heterojunction Solar Cells by High-Mobility Hydrogen-Doped In₂O₃ Transparent Conductive Oxide". In: *Applied Physics Express* 1 (2008), p. 041501. DOI: 10.1143/APEX.1.041501 (cit. on p. 67).
- [123] T. Koida, H. Sai, and M. Kondo. "Application of hydrogen-doped In₂O₃ transparent conductive oxide to thin-film microcrystalline Si solar cells". In: *Thin Solid Films* 518 (2010), pp. 2930–2933. DOI: 10.1016/j.tsf.2009.08.060 (cit. on p. 67).
- [124] E. Centurioni and D. Iencinella. "Role of front contact work function on amorphous silicon/crystalline silicon heterojunction solar cell performance". In: *Electron Device Letters, IEEE* 24 (2003), pp. 177–179. DOI: 10.1109/LED.2003.811405 (cit. on p. 67).
- [125] D. Rached and R. Mostefaoui. "Influence of the front contact barrier height on the Indium Tin Oxide/hydrogenated p-doped amorphous silicon heterojunction solar cells". In: *Thin Solid Films* 516 (2008), pp. 5087–5092. DOI: 10.1016/j.tsf.2008.02.031 (cit. on pp. 67, 68).

AMORPHOUS/CRYSTALLINE HETEROJUNCTION SOLAR CELLS

3

Contents

3.1	Undoped layer : avoiding epitaxy	82
3.1.1	Low temperature approach	83
3.1.2	Plasma treatments	88
3.1.3	The alloy way	92
3.2	Doped layers	100
3.2.1	Passivation	100
3.2.2	Light soaking	107
3.2.3	Annealing	111
3.3	Heterojunction solar cells	114
3.3.1	Intrinsic layer	115
3.3.2	p-type layers	118
3.4	Inside and outside collaborations on heterojunctions	121
3.4.1	Multicrystalline silicon wafers	121
3.4.2	Plasma cleaning	125
3.4.3	Laser Fired Contacts (LFC)	129
3.5	Conclusions	134

THE goal of this chapter is to provide a comprehensive summary of the results of this doctoral work regarding the passivation of, mostly n -type, multi and mono-crystalline silicon surfaces, as well as to show how we have been able to implement them into photovoltaic devices.

3.1 Undoped layer : avoiding epitaxy

The heterojunction solar cell is a semiconductor device based on two materials with different bandgap energies to create the $p - n$ junction. However, researchers working on heterojunction solar cells have shown that it was quite common to grow epitaxial films on (100)-oriented c -Si wafers when they were trying to grow an undoped a -Si:H layer. Most of these groups have shown that such epitaxial growth was highly detrimental to the quality of the surface passivation.^{1,2,3,4} Indeed, even if *Damon-Lacoste and Roca i Cabarrocas*^{5,6} have claimed that the epitaxial growth was not harmful when the interface between the undoped epitaxial layer and the amorphous emitter layer was sharp *and* that the undoped layer did not exhibit mixed phase but was purely made of crystalline material, they could never reach very high open-circuit voltages, that is to say not above 680 mV.

Consequently, one should try to stay away from plasma conditions leading to epitaxial growth. We will present below the different routes we investigated to avoid such growth. Before that, we conducted some experiments to prove the negative effect of epitaxial growth. Indeed, on Fig. 3.1, we have plotted the carriers effective lifetime in symmetrically deposited (i) a -Si:H layers on (100) (n) c -Si wafers directly onto the wafer or in the presence of either a thin or thick epitaxial buffer layer between the c -Si wafer and the (i) a -Si:H. We have compared these lifetimes to the one of a symmetrical sample made on (111) c -Si on which we deposited a (i) a -Si:H layer in the conditions of an epitaxial layer on (100) c -Si so that this layer is really amorphous. The very thin a -SiC:H layer will be introduced later and has proved to impede epitaxial growth without damaging the surface passivation. The basic feature in this graph is that the thicker the epitaxial layer, the lower the passivation. A second point is also that the (i) a -Si:H grown on (111) in the conditions of epitaxial growth on (100) results in a very good passivation layer. Moreover, this graph also shows that the decrease of the lifetimes occurs in the entire excess carrier range meaning

¹De Wolf and Kondo, "Abruptness of a -Si:H/ c -Si interface revealed by carrier lifetime measurements", 2007 [1]

²Fujiwara and Kondo, "Effects of a -Si:H layer thicknesses on the performance of a -Si:H/ c -Si heterojunction solar cells", 2007 [2]

³Gielis, Hoex, van den Oever, van de Sanden, and Kessels, "Silicon surface passivation by hot-wire CVD Si thin films studied by in situ surface spectroscopy", 2009 [3]

⁴Olibet, Monachon, Hessler-Wyser, Vallat-Sauvain, De Wolf, Fesquet, Damon-Lacoste, and Ballif, "Textured silicon heterojunction solar cells with over 700 mV open-circuit voltage studied by Transmission Electron Microscopy", 2008 [4]

⁵Damon-Lacoste, "Vers une ingénierie de bandes des cellules solaires à hétérojonctions a -Si:H/ c -Si. Rôle prépondérant de l'hydrogène.", 2007 [5]

⁶Damon-Lacoste and Roca i Cabarrocas, "Toward a better physical understanding of a -Si:H/ c -Si heterojunction solar cells", 2009 [6]

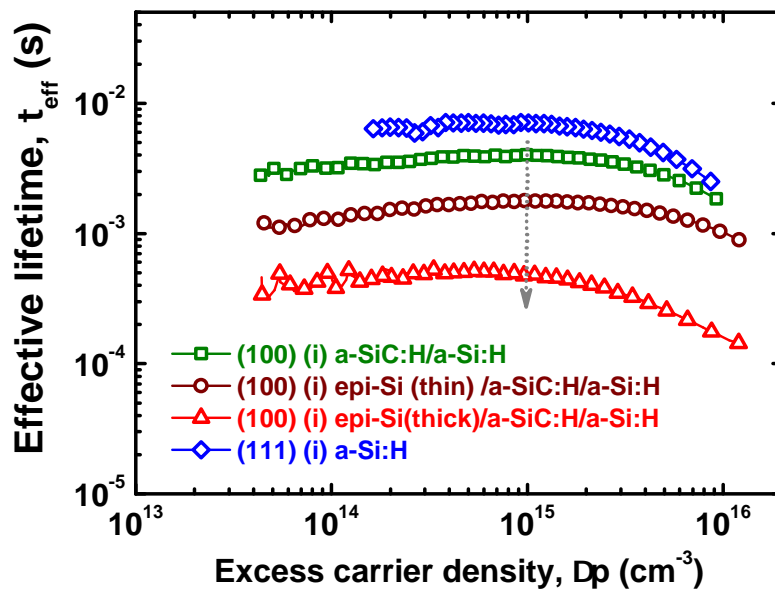


Figure 3.1 – Effective lifetimes in (n) c-Si wafers passivated by a (i) a-Si:H layer with buffer epitaxial layer of various thicknesses

that there is an increase of the surface defect density. Other experiments confirming these results will be discussed in §3.1.2.

In the following sections we will describe the different approaches we followed in order to hinder the initial epitaxial growth stages.

3.1.1 Low temperature approach

Some researchers working on heterojunction solar cells have shown that substrate temperature is an important parameter for the epitaxial growth and that reducing it could easily lead to a much more disordered material and therefore to an amorphous growth.^{1,2,3,4} However, it is well known that a-Si:H films deposited at low substrate temperatures have a high defect density, as it is shown on Fig. 3.2 extracted from *R.A. Street* textbook.⁵ This explains why all these authors have shown that the films deposited at low temperatures would always provide a very poor passivation of the crystalline silicon surface in their as-deposited state. Even though some researchers have been able to obtain device grade material at temperatures as low as 50°C,⁶ it was because they could decrease the plasma and sur-

¹De Wolf and Kondo, “Abruptness of a-Si:H/c-Si interface revealed by carrier lifetime measurements”, 2007 [1]

²Giellis, Hoex, van den Oever, van de Sanden, and Kessels, “Silicon surface passivation by hot-wire CVD Si thin films studied by in situ surface spectroscopy”, 2009 [3]

³Levi, Iwaniczko, Page, Wang, Branz, and Wang, “Silicon Heterojunction Solar Cell Characterization and Optimization using in Situ and Ex Situ Spectroscopic Ellipsometry”, 2006 [7]

⁴Fujiwara and Kondo, “Impact of epitaxial growth at the heterointerface of a-Si:H/c-Si solar cells”, 2007 [8]

⁵Street, *Hydrogenated Amorphous Silicon*, 1991 [9]

⁶Roca i Cabarrocas, “Deposition of intrinsic, phosphorus-doped, and boron-doped hydrogenated amorphous silicon films at 50°C”, 1994 [10]

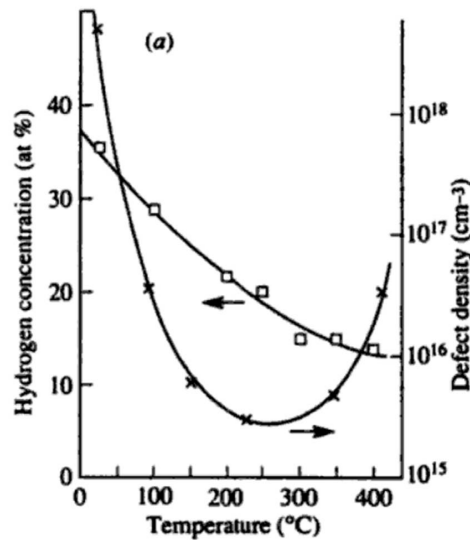


Figure 3.2 – Defect density and atomic hydrogen content of *a*-Si:H films as a function of the deposition temperature [9]

face polymerization reactions, known to lead to an *a*-Si:H material with poorer electronic properties, by using low pressure and very high dilution of silane in hydrogen. However, as it will be shown and discussed in the chapter 4 (Fig. 4.3 and 4.4), we wanted to avoid the high dilution regime since it is more prone to cause an initial epitaxial growth, even when the substrate temperature is decreased.

Films deposited at low temperature do not provide a good passivation in their as-deposited state but performing annealing at moderate temperatures ($T < 250^\circ\text{C}$) on symmetrical samples can eventually lead to a drastic (2 to 3 orders of magnitude) increase in the lifetime as demonstrated by the results from research groups like the ones from IMT,¹ and from HZB.² Also, similar results from Fraunhofer ISE demonstrated an increase in the V_{oc} of actual solar cells.³ The effective lifetime can be described as a stretched-exponential function of the cumulative annealing time where the lifetime increases until it reaches a saturation value, which depends on the deposition temperature. Even though full understanding of the mechanism remains under investigation, more studies have been carried out by the HZB group. It led them to publish additional data in *Schulze et al.*⁴ In this paper, they have shown that the interface between the *c*-Si wafer and the thin *a*-Si:H layer was not at equilibrium with the bulk *a*-Si:H film in the as-deposited state for films deposited at low temperatures. Furthermore, performing annealing on these samples lead to a

¹De Wolf, Olibet, and Ballif, “Stretched-exponential *a*-Si:H/*c*-Si interface recombination decay”, 2008 [11]

²Schulze, Beushausen, Hansmann, Korte, and Rech, “Accelerated interface defect removal in amorphous/crystalline silicon heterostructures using pulsed annealing and microwave heating”, 2009 [12]

³Pysch, Ziegler, Becker, Suwito, Janz, Glunz, and Hermle, “Stretched-exponential increase in the open-circuit voltage induced by thermal annealing of amorphous silicon-carbide heterojunction solar cells”, 2009 [13]

⁴Schulze, Beushausen, Leendertz, Dobrich, Rech, and Korte, “Interplay of amorphous silicon disorder and hydrogen content with interface defects in amorphous/crystalline silicon heterojunctions”, 2010 [14]

strong decrease of the interface defect density by allowing the interface to equilibrate with the bulk in terms of defect density. It has already been reported that a-Si:H films deposited at low substrate temperatures could lead to a gradient in the defect density towards the air/a-Si:H interface that could disappear upon annealing or by depositing films at a higher temperature.¹ However, the films here were extremely thin compared to the ones of Ref. [15], and *Schulze et al.* observed neither changes in the H bonding configuration (FTIR) nor changes in the Urbach energy value by the use of constant final state yield spectroscopy (CFSYS),^{2,3,4} suggesting that there is no significant (measurable) reconfiguration in the bulk a-Si:H network with respect to its measurable defect density. Its lower value is set by the Urbach energy value, following *Stutzmann's* model,⁵ for which there is a strong correlation between the bulk defect density of a-Si:H films and the Urbach energy value in this material. Therefore, *Schulze et al.* suggested that there was only short-range H diffusion and local reconfiguration at the interface. They argued that at low temperatures, the hydrogen content of a-Si:H films increases above a threshold value where it was possible that microscopic voids of up to a few nm existed, as also discussed in another paper,⁶ where a correlation between hydrogen content, mass density and vacancies to microvoids transition was also discussed. For them, such microvoids resulted in an as-deposited state with an incomplete film coverage of the surface and therefore to a poor surface passivation. Similar conclusions, regarding bulk versus surface mechanism, were drawn by *Mitchell et al.*,⁷ who calculated the activation energy of the time constants of the thermally activated decrease in defect density and found them to be incoherent with bulk a-Si:H diffusion of hydrogen, suggesting that such a process was a surface mechanism.

This material inhomogeneity between surface and bulk has already been pointed out by several authors such as *Antoine and Drévilion*,⁸ or *Fujiwara et al.*,^{9,10} whose papers have both shown, using ellipsometry, than on many substrates there was an initial growth step during which there was an incomplete nucleation thus resulting in a less dense material, with

¹Kleider, Longeaud, and Roca i Cabarrocas, "Experimental evidence for the annealing of surface defects in a-Si:H during deposition", 1992 [15]

²Sebastiani, Di Gaspare, Capellini, Bittencourt, and Evangelisti, "Low-Energy Yield Spectroscopy as a Novel Technique for Determining Band Offsets: Application to the c-Si(100)/a-Si:H Heterostructure", 1995 [16]

³Schmidt, Schoepke, Korte, Milch, and Fuhs, "Density distribution of gap states in extremely thin a-Si:H layers on crystalline silicon wafers", 2004 [17]

⁴Korte and Schmidt, "Investigation of gap states in phosphorous-doped ultra-thin a-Si:H by near-UV photoelectron spectroscopy", 2008 [18]

⁵Stutzmann, "The defect density in amorphous silicon", 1989 [19]

⁶Smets, Kessels, and van de Sanden, "Vacancies and voids in hydrogenated amorphous silicon", 2003 [20]

⁷Mitchell, Macdonald, and Cuevas, "Thermal activation energy for the passivation of the n-type crystalline silicon surface by hydrogenated amorphous silicon", 2009 [21]

⁸Antoine and Drévilion, "Influence of the substrate on the early stage of the growth of hydrogenated amorphous silicon evidenced by kinetic ellipsometry", 1988 [22]

⁹Fujiwara, Toyoshima, Kondo, and Matsuda, "Interface-layer formation mechanism in a-Si:H thin-film growth studied by real-time spectroscopic ellipsometry and infrared spectroscopy", 1999 [23]

¹⁰Fujiwara and Kondo, "Real-time monitoring and process control in amorphous/crystalline silicon heterojunction solar cells by spectroscopic ellipsometry and infrared spectroscopy", 2005 [24]

a larger amount of hydrogen than in the bulk material, and that such layers can be up to a few nm thick. This H-rich interface has been definitively highlighted for ultra thin a-Si:H layers.¹

Finally, the main result of these papers, especially the one by *Schulze et al.*, is that the quality of the a-Si:H/c-Si interface is determined by the quality of the bulk a-Si:H film, its defect density value. If this is correct, it is very tempting to use a low deposition temperature to avoid any epitaxial growth in a very straightforward fashion, while keeping the ability to reach high passivation levels by post-deposition annealing steps.

Therefore, we have produced a few samples in order to assess and if possible validate such an approach. The first samples were devoted to study the BSF structure. This series consisted of films deposited at 100°C. The BSF structure being a (n) a-Si:H layer with or without an undoped buffer layer. When present, the buffer layer was either deposited in the conditions of amorphous or polymorphous silicon. The films were isochronally annealed in ambient air during 30 min. at different temperatures. The effective lifetime measured at 1 sun is plotted on Fig. 3.3 against the annealing temperature for symmetrical BSF structures with stacks of (n) a-Si:H or with an amorphous or a polymorphous buffer layer. We have also added the result obtained with a thick undoped a-Si:H layer.

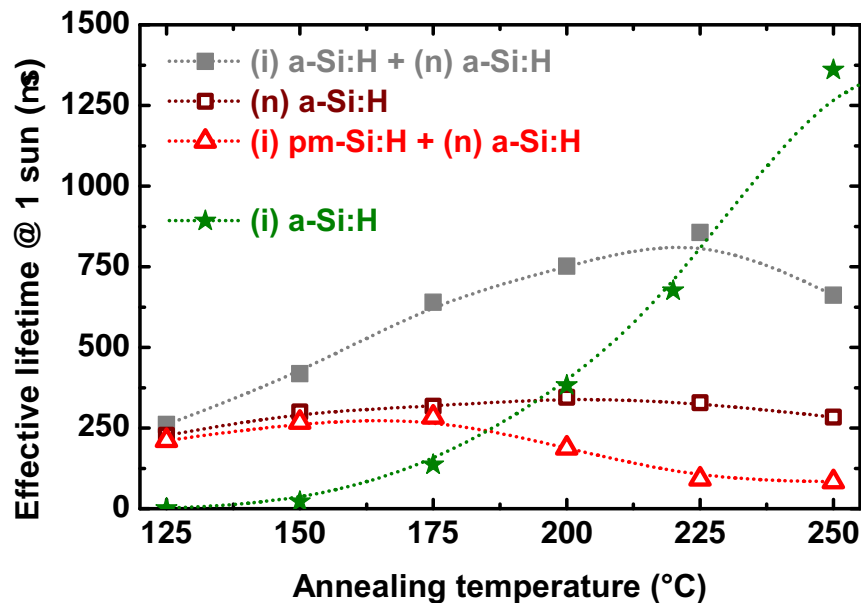


Figure 3.3 – Effective lifetime at 1 sun in symmetrical BSF structures on (n) c-Si with or without a buffer layer made of an amorphous or a polymorphous undoped layer. As a reference we also show the result obtained by a thick and symmetrical layer of 40 nm of (i) a-Si:H

As it will be presented in the next chapter, the polymorphous conditions led to epitaxial growth, even though at 100°C the film were more a mixed phase than a purely epitaxial film. Such a behaviour had al-

¹van den Oever, Gielis, van de Sanden, and Kessels, "Hot-wire deposition of a-Si:H thin films on wafer substrates studied by real-time spectroscopic ellipsometry and infrared spectroscopy", 2008 [25]

ready been observed by *De Wolf and Kondo*[1] who showed that no lifetime improvement upon annealing was observed when the growth was not purely amorphous. The results coming from the BSF with or without the undoped a-Si:H layer demonstrated a clear improvement upon annealing and showed that the undoped layer played a very crucial role. Indeed, after annealing at 225°C, we could reach an effective lifetime of more than 800 μs , implying an implicit V_{oc} of 685 mV. This is a decent open-circuit voltage value. However, the best passivation came from the 40 nm thick undoped a-Si:H layer. For all the BSF structures the lifetimes remained too low to hope for high V_{oc} in completed devices and indeed we could never observe a significant improvement upon annealing in our solar cells. This was mostly due to the fact that these improvements could never be obtained for emitter structures, as already observed by *De Wolf and Kondo*,¹ and shown in our case on Fig. 3.4. Indeed, on Fig. 3.4 we have plotted

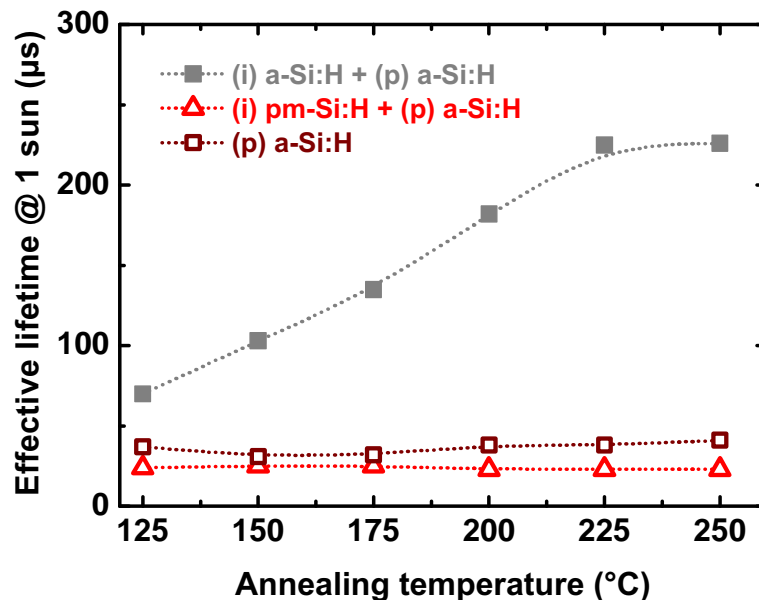


Figure 3.4 – Effective lifetime at 1 sun in symmetrical emitter structures on (n) c-Si with or without a buffer layer made of an amorphous or a polymorphous undoped layer.

the effective lifetime obtained at 1 sun against the annealing temperature for symmetrical emitter structures with stacks of (p) a-Si:H or with an amorphous or a polymorphous buffer layer. Again we obtained very similar results to those we obtained for BSF structure. Namely that there is definitely a beneficial effect of the (i) a-Si:H buffer layer regarding the passivation behaviour upon annealing and that a (p) a-Si:H layer by itself or coupled to a thin undoped epitaxial underlayer does not passivate well the surface and does not show any improvement upon annealing.

The result of these studies is that no solar cells with a high open-circuit voltage could be obtained from low temperature deposition in spite of the excellent passivation provided by intrinsic layers. Therefore, we took the decision to go back to “high” deposition temperatures, i.e. in the 200°C

¹De Wolf and Kondo, “Nature of doped a-Si:H/c-Si interface recombination”, 2009 [26]

range, looking for other and efficient ways to grow good, fully amorphous, a-Si:H material on any orientation as explained in §3.1.3 (p. 92).

3.1.2 Plasma treatments

In the previous section we have seen that low substrate temperature depositions can be used to avoid the epitaxial growth of silicon. Here, we will try to follow a different approach by using plasma treatments of the c-Si surface prior to the deposition of the silicon films. We can expect the ion bombardment from such plasma treatments to induce some defects or some amorphization at the surface of c-Si leading to a growth regime where epitaxy would not be feasible. We started by using NH_3 plasmas, following the example of *Wang et al.* who performed short ammonia treatments by HWCVD before the deposition of their emitters, claiming that this could hinder the epitaxial growth that they have always experienced above a substrate temperature of about 100°C .¹ Hence, we fabricated a series of samples consisting of an emitter structure deposited on both sides of a (n) c-Si wafer. On n-type c-Si, the emitter structure consists of a thin undoped layer capped by a (p) a-Si:H layer. Here we used two different undoped layers: (i) pm-Si:H and (i) a-Si:H. Prior to the deposition of the emitter structure we performed a short ammonia (NH_3) plasma treatment of the surface of the c-Si wafer. After that we deposited at three substrate temperatures (150 , 175 and 200°C) the emitter structure using both undoped layers. We measured the lifetime after the deposition and after successive annealing steps. On Fig. 3.5 we have plotted the results of such measurements. Irrespective of the deposition temperature, the effective lifetimes after the deposition were extremely low and of similar order of magnitude. However, they exhibited slightly different behaviours upon annealing in two ways:

1. the lower the deposition temperature, the higher the lifetime increase
2. the (i) pm-Si:H layer is more favourable than (i) a-Si:H

Interestingly we demonstrated here the need for the NH_3 plasma *and* for a low temperature deposition in the quest of a high effective lifetime. Indeed, in §3.1.1 we showed that in the case of (p) a-Si:H layers passivations, neither “high” nor “low” deposition temperatures would lead to high effective lifetimes in the as-deposited state or after annealing. The fact that the films deposited at 200°C did not show any improvement upon annealing might come from the fact that the film did not grow perfectly amorphous from the beginning and it has been shown that annealing of films showing epitaxial growth was much less prone to exhibit improvements upon annealing, as evidenced by *De Wolf and Kondo*.² This approach remained valid since we still had access to sharp and well-defined interfaces between the c-Si substrate and the amorphous film at 150 and 175°C , which had so far never been the case.

¹Wang, Wang, Iwaniczko, Page, Levi, Yan, Teplin, Xu, Wu, and Branz, “Heterojunction silicon solar cells with high open-circuit voltages by interface optimization”, 2004 [27]

²De Wolf and Kondo, “Abruptness of a-Si:H/c-Si interface revealed by carrier lifetime measurements”, 2007 [1]

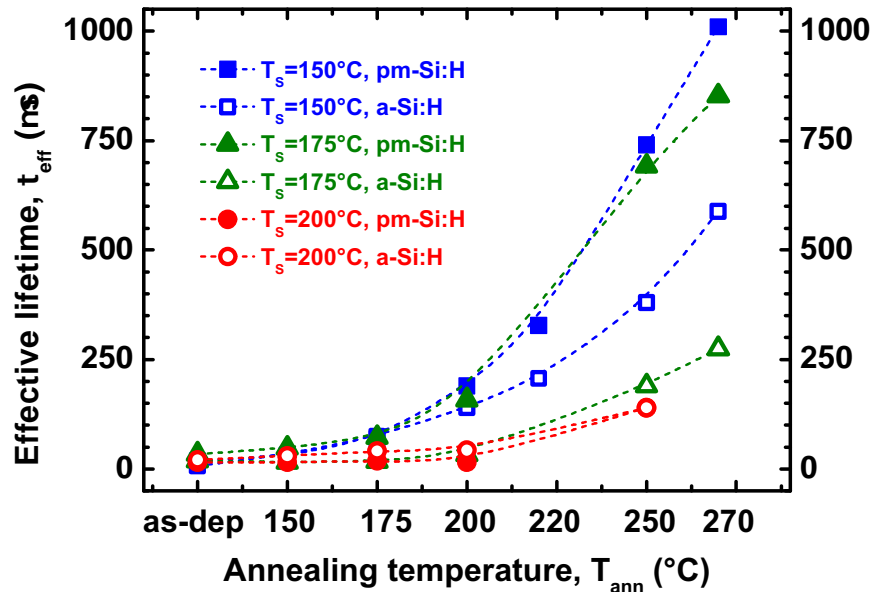


Figure 3.5 – Effective lifetimes at 1 sun illumination of symmetrical emitters deposited on (n) c-Si wafers at different substrate temperatures (150, 175 and 200°C) plotted against the annealing temperature

However, we do not only care about lifetimes but we care about solar cells. Hence we have used such a structure to make the emitter of (n) c-Si heterojunction solar cells. On Fig. 3.6, we have plotted the current-voltage characteristics of the solar cells fabricated on (n) c-Si using an emitter deposited at low temperature after a short ammonia plasma. The cells have been measured in the as-deposited state and also after successive annealing at different temperatures. We should first point out that these solar cells were made before we got the mechanical masks available so that we defined the cells by sputtering ITO through a shadow mask of 4 mm diameter. In this case, edge effects were tremendous so that the current density was overestimated even if regular current-voltage characteristics could be obtained on other cells, suggesting that there was no contact problem between ITO and the probe. Thus, only qualitative analysis could be made on these cells. For all the cells we obtained very pronounced S-shaped characteristics. Increasing the annealing temperature reduced the threshold voltage below which the solar cell allowed for current to flow and also decreased the series resistance in the positive current region. We could expect the annealing to activate the dopants, especially in the (p) a-Si:H layer, since they have been deposited at a rather low temperature. This could explain why the series resistance decreased with increasing the annealing temperature. However, even if there seemed to be an improvement with the annealing, the S-shaped characteristics did not disappear. The reason for such a behaviour could originate from the fact that the ammonia plasma, while being quite short, could still have a strong effect on the c-Si surface. The temperature we used for our ammonia plasma is too low for the NH_3 molecules to interact with the c-Si surface without

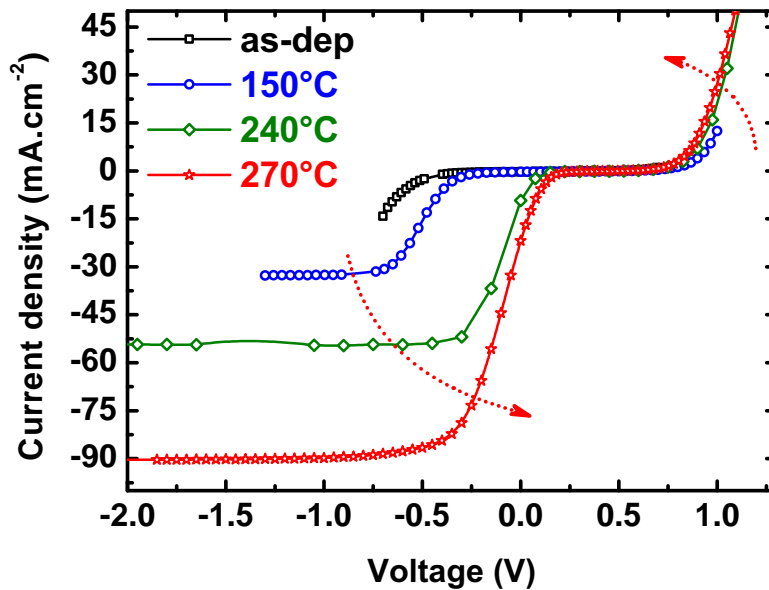


Figure 3.6 – Current-voltage characteristics of small solar cells on (n) c-Si using emitters deposited at low temperature after a short NH_3 plasma treatment, in the as deposited state and after successive annealings at different temperatures

the dissociation caused by plasma.¹ However, our plasma could lead to the incorporation of N atoms at the surface and created a thin a-SiN_x:H layer. Indeed, it has already been shown that nitridation of c-Si surfaces could be done by PECVD and could efficiently enhance the passivation obtained by subsequent deposition of a-SiN_x:H films which could exhibit smaller interface defect densities.² Indeed, it has been confirmed by SIMS measurements that we had a large amount of N atoms at the interface between a-Si:H and c-Si. This means that our ammonia plasma did not only have the effect of hindering epitaxial growth for temperatures below 200°C but also to “artificially” increase the passivation by creating a thin silicon nitride layer with good interface properties and fixed charges, increasing upon annealing. Hindering of the epitaxial growth could be explained by the creation of this thin a-SiN_x:H layer that would make the main requirement for the epitaxial growth disappear: a c-Si surface. However, this a-SiN_x:H layer would act as a resistive barrier for the carrier collection, explaining the strong S-shape obtained in our J-V characteristics. These S-shaped characteristics might also be explained by the fact that silicon nitride possesses bulk and interface positive charges,³ and by doing so can induce a downward band bending (accumulation layer) in the (n) c-Si, that will repel holes rather than attracting them, which is the

¹Dai, Wang, Kwon, Halls, and Chabal, “Nitrogen interaction with hydrogen-terminated silicon surfaces at the atomic scale”, 2009 [28]

²Bose, Basa, and Bose, “Effect of ammonia plasma pretreatment on the plasma enhanced chemical vapor deposited silicon nitride films”, 2001 [29]

³Aberle, “Overview on SiN surface passivation of crystalline silicon solar cells”, 2001 [30]

opposite of what we need to create the pn junction.¹ This is the reason why researchers, again from NREL, had developed a process in which after the ammonia treatment they etched back the surface of the wafer with hydrogen.² Even though we knew that such a nitridation was possible, we hoped that our low temperature approach coupled with a short treatment time would leave room for a suitable process window, which turned out not to be the case.

Another solution could be to repeat these experiments with a neutral gas, in our case a noble gas, namely argon. Like ammonia, argon was expected to modify the surface of the c-Si wafer but not to react in any way, and we expected the modified (amorphized) surface to hinder epitaxial growth.

Sample	Orientation	Film	τ_{eff} (ms)	Impl. V_{oc} (mV)
903022	111	(i) pm-Si:H + (n) a-Si:H	1.19	703
903023	111	(i) a-Si:H + (n) a-Si:H	1.25	707
903027	111	Ar + (i) pm-Si:H + (n) a-Si:H	1.61	723
903035	100	Ar + (i) pm-Si:H + (n) a-Si:H	1.42	709
903036	100	(i) pm-Si:H + (n) a-Si:H	0.465	665

Table 3.1 – Description and passivation results of various BSF stacks deposited on (111) and (100), with or without an argon plasma treatment

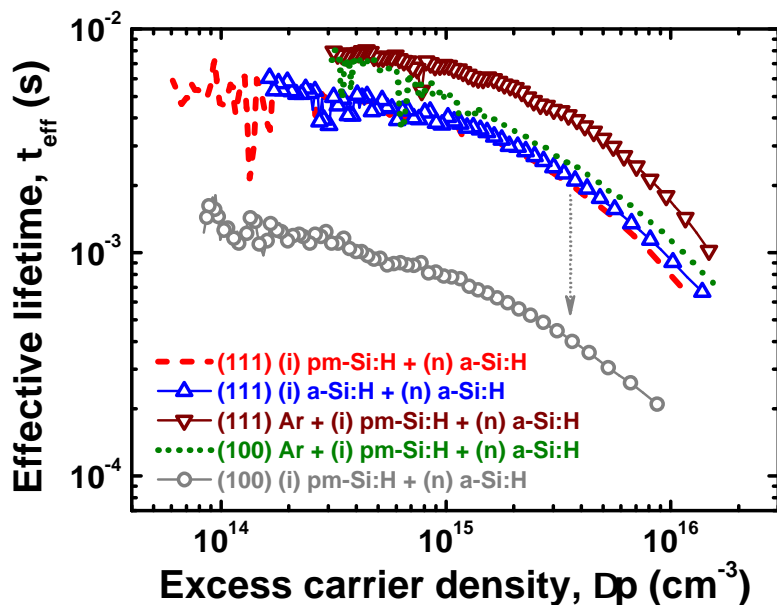


Figure 3.7 – Effective lifetimes various BSF stacks deposited on (111) or (100), with or without argon plasma treatment

In Tab. 3.1, we have presented the different BSF stacks that we wanted to test and indicated the passivation results obtained from such stacks.

¹Kunst, Abdallah, and Wunsch, "Passivation of silicon by silicon nitride films", 2002 [31]

²Yan, Page, Wang, Al-Jassim, Branz, and Wang, "Atomic structure and electronic properties of c-Si/a-Si:H heterointerfaces", 2006 [32]

The effective lifetimes against the excess carrier density have been plotted on Fig. 3.7. Even though there were a few differences in terms of passivation for the different BSF stacks, mainly due to the fact that at that time the thickness of the undoped layer was not really optimized yet, there is a clear behaviour showing that the initial epitaxial growth, only occurring on (100) wafers not submitted to the argon plasma, was able to decrease the effective lifetime values on the entire injection level range, meaning that there was a higher interface defect density compared to the others films. When exposed to an argon plasma, (100) wafers did not allow epitaxial growth to occur so that the (i) pm-Si:H deposition conditions did not produce an epitaxial growth and resulted in a much better passivation. Interestingly it seemed that the argon plasma was not so harmful and confirmed some of the results of *Damon-Lacoste and Roca i Cabarrocas*,¹ since the passivation obtained on (111) without Ar plasma was very similar to the one obtained on (100) and (111) after the Ar plasma. It is very likely, even though they have not mentioned it, that in the paper from *Damon-Lacoste and Roca i Cabarrocas*, on p-type, there was such a difference regarding the presence of the epitaxial layer. Nevertheless, the passivation quality, namely the V_{oc} value, was mostly determined by the quality of the passivation of the back side of the solar cell, so that the detrimental effect of the epitaxy on passivation quality was hidden by the higher back surface recombination velocity. Indeed, similar experiments were carried out on the same wafers as the ones used in Ref. [6], namely Cz (p) c-Si wafers of resistivity 18 Ω .cm, and we obtained the same results: the surface passivation was much better in the case of (i) pm-Si:H + (n) a-Si:H (emitter stack) when the wafer underwent an argon plasma, and SE spectra proved the pm-Si:H film to be amorphous.

As a conclusion, argon plasma treatment of the c-Si wafer resulted in a-Si:H films which were providing a much more efficient passivation than any stack involving an epitaxial layer. The conditions used for the argon plasma did not seem to create so many defects. However we repeated these experiments and obtained poorer passivation in some cases, which implied that a balance would have to be found between the very “soft” amorphization of the very first atomic layers and the creation of too many defects. Besides, no study of the reactor walls’ condition was performed so that no definitive conclusion could be drawn. Therefore we decided to go back to the studies of the growth itself rather than to the modification of the surface. This study is presented in the next section.

3.1.3 The alloy way

Even though the previous experiments have been successful in leading to an amorphous growth of the films, none of them has been successful in leading to high efficiency c-Si solar cells. Indeed, more experiments showed that the argon plasma was not so reproducible and could sometimes lead to a loss in passivation for similar treatment times. Besides, we believed that in an industrial frame the need for faster and more robust process parameters imposed us to look for simpler processes. Rather

¹Damon-Lacoste and Roca i Cabarrocas, “Toward a better physical understanding of a-Si:H/c-Si heterojunction solar cells”, 2009 [6]

than damaging the surface prior to any deposition it made more sense to look for a way to impose a more defective initial growth leading to an amorphous growth instead of an epitaxial (or mixed phase) growth. One possible way to do it was to introduce “impurities” to the gas mixture during the initial step of the growth. Here, by “impurities” we refer to atoms, often unwanted, that are not necessary to the growth of the a-Si:H layer, e.g. dopants or alloying elements. We chose to investigate a-SiC:H, a higher band gap material obtained by adding methane (CH_4) to the previous gas mixture. As presented earlier, this material has already been studied for passivation purposes by several groups (see §2.2, page 57). However, our approach was different here since we did not want to grow a full alloyed film but we only wanted to add some CH_4 to the gas mixture at the beginning of the deposition in order to impede epitaxy. This meant that even for the ultrathin, undoped, a-Si:H layer that we used as a buffer layer between the crystalline substrate and the doped a-Si:H layers in heterojunction solar cells, there would only be a very small fraction of this layer that would be made of a-SiC:H. On Fig. 3.8 we have plotted the effective lifetimes in symmetrically passivated c-Si samples for which we have varied the time during which CH_4 was incorporated to the gas mixture, varying from 15 seconds to 10 minutes. All these films were about 20 to 30 nm thick for the x a-SiC:H + $(10-x)$ a-Si:H stack with x being the time (in minutes) of CH_4 presence during the 10 minute deposition. This meant that in the 10 minutes case the entire film was made of a-SiC:H. The description of the samples is summarized in Tab. 3.2. We added on Fig. 3.8 the lifetime of sample 9061810 which is similar to sample 908202, to show that this process is very reproducible.

Sample	CH_4 time (s)	τ_{eff} (ms)	Impl. V_{oc} (mV)
908201	15	0.95	694
908202	30	1.9	730
908199	90	1.9	729
9081910	600	0.94	694

Table 3.2 – Description of different layers deposited at 200°C on (100) with different CH_4 gas presence time during the deposition

These results show that a “thick” a-SiC:H layer, at least grown in these conditions, did not provide a good enough passivation of our c-Si wafers. One explanation could be based on the work by Mahan *et al.*¹ that has shown that alloying silicon with carbon (and also germanium) induced an increase of the amount of microstructure which resulted in an increase of E_u , the Urbach energy. Another interesting paper, by Stutzmann,² has shown a strong correlation between the bulk defect density of a-Si:H films and their Urbach energy: when the Urbach energy rises from a value of ≈ 50 meV³ towards higher values, the bulk defect density of the films increases as well. Again, this particular result could be linked to the aforementioned paper from Schulze *et al.*⁴ in which a correlation seemed to be

¹Mahan, Menna, and Tsu, “Influence of microstructure on the Urbach edge of amorphous SiC:H and amorphous SiGe:H alloys”, 1987 [33]

²Stutzmann, “The defect density in amorphous silicon”, 1989 [19]

³Which is considered to be the value of state-of-the art, device grade, a-Si:H materials

⁴Schulze, Beushausen, Leendertz, Dobrich, Rech, and Korte, “Interplay of amorphous

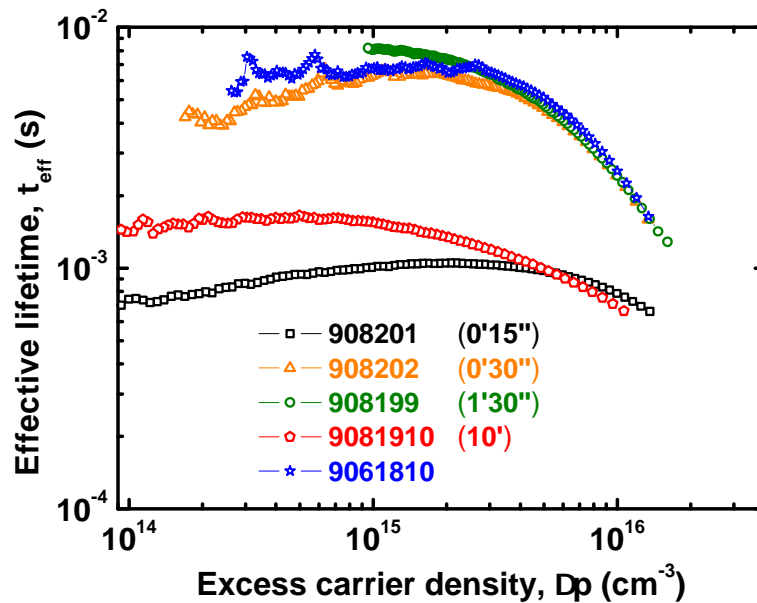


Figure 3.8 – Effective lifetimes in symmetrical samples deposited at 200°C on (100) with different CH₄ gas presence time during the deposition

established between interface defect density and bulk defect density that could explain our (slightly) poorer passivation results when a 20 nm (i) a-SiC_x:H layer replaces a 20 nm (i) a-Si:H layer.

However, these results also showed that the presence of CH₄ at the early stages of the deposition was not detrimental at all for the passivation and efficiently broke the epitaxial growth. Indeed, when the presence of CH₄ was too short (15 seconds case), there was a drastic decrease in the passivation quality. We can think that such duration was not enough to create a full coverage of the c-Si wafer by the a-SiC_x:H so that a sharp and fully epitaxial growth was disabled but not efficiently enough to make it grow fully amorphous. Instead we had a mixed phase growth, as it will be discussed on the ellipsometry measurements below. Interestingly, if we compared the passivation obtained in the presence of a mixed phased (908201) with the one obtained with an a-SiC_x:H layer (9081910), it appeared that they had similar behaviour at high injection, known to be dominated by the defect recombination whereas at lower injection levels, where the “field effect passivation” becomes more important, only the a-SiC_x:H layer allowed for a constant lifetime whereas the mixed phase’s lifetime kept on decreasing. As it will be confirmed by ellipsometry below, the mixed phase could be modelled by a bi-layer, the first one being a highly crystallized μc-Si:H layer and the second a much less crystallized μc-Si:H layer. The first layer did not reduce, if not increase, the interface defect density, whereas the second one was not thick enough and did not possess a wide bandgap value so that field-effect was rather inefficient and not able to shield the defect recombination at low injection levels.

To check the assertion that there was a mixed phase, we performed

silicon disorder and hydrogen content with interface defects in amorphous/crystalline silicon heterojunctions”, 2010 [14]

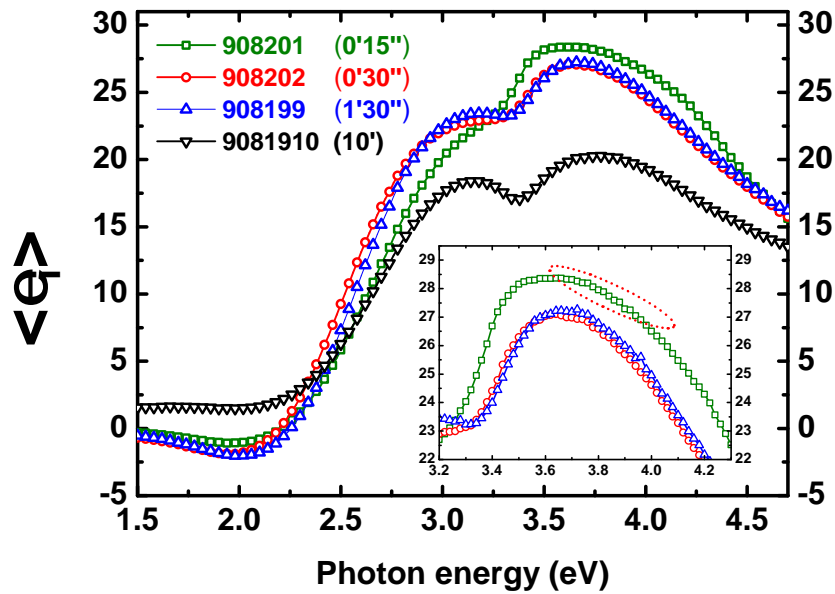


Figure 3.9 – Ellipsometric spectra of the samples deposited with the presence of CH_4 during the following times: 15'', 30'', 1'30'' and 10'

spectroscopic ellipsometry measurements on these samples. On Fig. 3.9, we have plotted the imaginary part of the pseudo-dielectric function of different stacks as they are described in Tab. 3.2. The samples processed with 30'' or 1'30'' of CH_4 showed very similar spectra since the actual a-SiC:H layers were extremely thin and contributed marginally to the signal which was dominated by the much thicker a-Si:H overlayer. However, when increasing the deposition time with CH_4 until depositing the entire stack with it or decreasing it to 15'' there were strong differences. Obviously, when the entire stack was made of a-SiC:H we had a different spectrum from the one obtained with an a-Si:H layer, for which we had a much higher amplitude of the signal of the imaginary part of the pseudo-dielectric function. However, when we used CH_4 for a very short time we had a very peculiar spectrum. Instead of having the usual symmetrical bump characteristic of amorphous material, we had an asymmetrical bump with a shoulder towards higher photon energies. This shoulder is the signature of a crystalline phase in the material. Indeed, in order to fit such a spectrum it was necessary to model it by describing the film by two layers of different crystallinity. The model we used is described in Tab. 3.3 where SG refers to "small grains" polysilicon material.

30% SG	64% a-Si:H	6% voids	↑↓ 13 nm
97% SG	2% a-Si:H	1% voids	↑↓ 10 nm
c-Si			↑ semi-infinite

Table 3.3 – SE model of the sample deposited with 15'' presence of CH_4

This model (3.3) can be interpreted as an initial mixed phase growth where both amorphous and crystalline regions existed, followed by a growth where the crystalline fraction over deposition time (or thickness) decreased. This is characteristic of a mixed phase growth regime in which

the quality of the epitaxial layer is poor and the amorphous part expands until covering the entire surface and leading to a fully amorphous growth regime. It is possible that there was not a full coverage of the surface with a-SiC:H at the beginning so that epitaxial sites still existed when CH₄ was removed from the gas phase. This was a confirmation that regimes leading to epitaxial or mixed phase growth should be avoided.¹ This was also an evidence that adding “impurities” was not detrimental to the passivation. However, we knew that the passivation was better in this case but we did not know yet if this passivation was the best passivation one could obtain on this wafers. One way to check that was to take advantage of this difference between (100) and (111) on the material growth. Indeed, on (111) all the films, deposited with or without CH₄, would result in perfectly amorphous materials, at least in our deposition temperature conditions. The idea was to compare the passivation obtained with different amorphous films on (111) wafers and to compare them to the passivation obtained on the samples we described before (Tab. 3.2). We have therefore symmetrically deposited on (111) c-Si substrates different layers as described in Tab. 3.4. Hence, we have deposited on (111) the following materials:

- a-Si:H from SiH₄
- a-Si:H from SiH₄ diluted in H₂
- pm-Si:H
- a-Si:H with a 30" CH₄ presence time

We also performed the last deposition on a (100) wafer, similarly to the deposition of Tab. 3.2. The description and results of this passivation study are summarized in Tab. 3.4 and the corresponding lifetimes are plotted on Fig. 3.10.

Sample	Si Orientation	Material	τ_{eff} (ms)	Impl. V_{oc} (mV)
906171	(111)	a-Si:H	1.9	729
906172	(111)	a-Si:H (H ₂ dilution)	1.97	731
906173	(111)	pm-Si:H	1.87	730
906183	(111)	a-SiC:H+a-Si:H	1.75	729
9061810	(100)	a-SiC:H+a-Si:H	1.96	730

Table 3.4 – Description of different layers deposited at 200°C on (111) and (100) orientations with different dilutions and in the presence or not of CH₄ gas

Based on these results it appeared that all the intrinsic layers that we had deposited possessed excellent passivation properties when grown on (111) wafer. However, we were not able to distinguish differences in the passivation properties when we changed the H₂ dilution of the SiH₄+H₂ gas mixture, even if the deposited materials were different. Indeed, on Tab. 3.5 we give the main optical parameters of the a-Si:H layers deposited on the (n) c-Si wafers, and recall the effective lifetime obtained at 1 sun illumination. We had a constant increase of the optical (T_{auc}, E_g) bandgap value with an increased hydrogen dilution at the same time as the material

¹De Wolf and Kondo, “Abruptness of a-Si:H/c-Si interface revealed by carrier lifetime measurements”, 2007 [1]

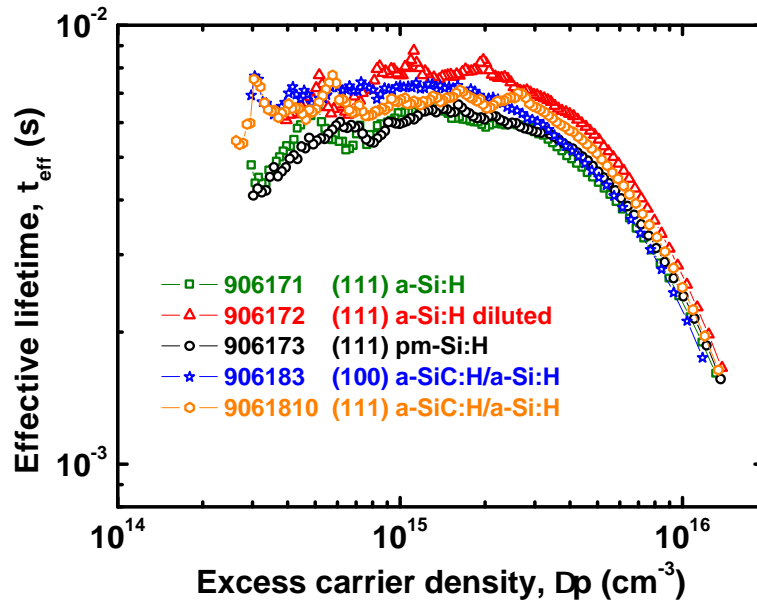


Figure 3.10 – Effective lifetimes of symmetrical samples deposited at 200°C on (111) and (100) orientations with different dilutions and in the presence or not of CH_4

$\frac{H_2}{H_2+SiH_4}$	Orientation	E_g (eV)	A (eV)	C (eV)	τ_{eff} (ms)
0	(111)	1.64	214	2.32	1.9
67	(111)	1.72	226	2.21	1.97
97	(111)	1.79	236	2.16	1.87
67	(111)	1.73	231	2.14	1.75
67	(100)	1.74	233	2.15	1.96

Table 3.5 – Optical parameters of the a-Si:H layers deposited in various hydrogen dilution on c-Si wafers from pure silane and hydrogen gas mixture (upper part) or with the presence of methane at the beginning of the deposition (lower part).

got denser and more ordered. However, there was almost no (significant) change on the passivation properties in this process window. Indeed all of these materials were device grade materials that were very likely to exhibit different properties in other devices such as a-Si:H pin solar cells but not on the passivation since in all cases the defect density was very low.^{1,2} Interestingly, it appeared that the use of the ultra thin a-SiC:H layer at the beginning of the deposition did not affect the material in terms of bandgap energy but seemed to result in a slightly denser material, which also showed a smaller roughness. These results are still to be confirmed, and nevertheless had no impact on the passivation itself but allowed to confirm that similar growth was definitively achievable on both (111) and (100) orientations.

¹Roca i Cabarrocas, "Plasma enhanced chemical vapor deposition of amorphous, polymorphous and microcrystalline silicon films", 2000 [34]

²Kleider, Longeaud, Gauthier, Meaudre, Meaudre, Butté, Vignoli, and Roca i Cabarrocas, "Very low densities of localized states at the Fermi level in hydrogenated polymorphous silicon from capacitance and space-charge-limited current measurements", 1999 [35]

*Das et al.*¹ and *Burrows et al.*² had already drawn a similar conclusion regarding the similar passivation quality on (111) and (100). In these papers they scanned a large range of (i) a-Si:H materials deposited from H₂ dilution in DC and RF plasmas. They showed that there was a sudden change in the passivation on (100) beyond a certain H₂ to SiH₄ ratio where the films started to grow epitaxial on (100) and remained amorphous on (111), which is very similar to our findings. Using FTIR measurements they detected some small variations in the monohydrate (Si-H) and dihydrate (Si-H₂) modes. They correlated the (small) increase, through vacuum annealing, in the interface monohydrate mode to the decrease in the defect density at the interface. Indeed, the monohydrate mode is usually associated with low defect density materials.³

We performed additional studies since we introduced depositions made from argon dilution of silane for the deposition of p-type layers (§3.2). Therefore, as we only wanted to change the dopant flow rate during the depositions, we needed to check that the argon introduced to deposit an undoped layer did not modify its passivation properties, at least without the (p) a-Si:H capping layer. The motivations for the argon addition were that the argon induced increase in ion bombardment was expected to densify the material during the deposition and argon was also expected to decrease the hydrogen content of the film,^{4,5} which was expected to be beneficial for the solar cell as it would decrease the potential barrier (the valence band offset ΔE_v) experienced by the holes willing to move from the c-Si substrate to the (p) a-Si:H layer.^{6,7} Hence, we have deposited (i) a-Si:H layers (> 20 nm) on (111)-oriented c-Si from gas mixtures made up of SiH₄, SiH₄+H₂ and SiH₄+Ar. The passivation results are summarized in Tab. 3.6 and we have plotted on Fig. 3.11 the lifetimes obtained from such passivation layers.

Once again, we had very similar quality regarding the passivation. Besides, from a reproducibility point of view, these results could be favourably compared to the ones from Tab. 3.4 when we deposited similar samples. Regarding the argon dilution, we should stress the fact that we have used a low dilution in the 50% range.⁸ It has been shown by *Knights*

¹Das, Burrows, Lu, Bowden, and Birkmire, "Surface passivation and heterojunction cells on Si (100) and (111) wafers using dc and rf plasma deposited Si:H thin films", 2008 [36]

²Burrows, Das, Opila, De Wolf, and Birkmire, "Role of hydrogen bonding environment in a-Si:H films for c-Si surface passivation", 2008 [37]

³Roca i Cabarrocas, Djebbour, Kleider, Longeaud, Mencaraglia, Sib, Bouizem, Thèye, Sardin, and Stoquert, "Hydrogen, microstructure and defect density in hydrogenated amorphous silicon", 1992 [38]

⁴Hamma and Roca i Cabarrocas, "Low temperature growth of highly crystallized silicon thin films using hydrogen and argon dilution", 1998 [39]

⁵Fukutani, Kanbe, Futako, Kaplan, Kamiya, Fortmann, and Shimizu, "Band gap tuning of a-Si:H from 1.55 eV to 2.10 eV by intentionally promoting structural relaxation", 1998 [40]

⁶Kanevce and Metzger, "The role of amorphous silicon and tunneling in heterojunction with intrinsic thin layer (HIT) solar cells", 2009 [41]

⁷Rahmouni, Datta, Chatterjee, Damon-Lacoste, Ballif, and Roca i Cabarrocas, "Carrier transport and sensitivity issues in heterojunction with intrinsic thin layer solar cells on N-type crystalline silicon: A computer simulation study", 2010 [42]

⁸The argon line had no MFC so that a comparison of pressure was made: adding argon to 50 sccm of SiH₄ doubled the pressure.

Sample	Material	τ_{eff} (ms)	Impl. V_{oc} (mV)
1006171	a-Si:H (H ₂ dilution)	1.98	730
1006172	a-Si:H (Ar dilution)	1.97	727
1006173	a-Si:H	1.94	730

Table 3.6 – Description of different layers deposited at 200°C on (111) and (100) orientation from SiH₄, SiH₄+H₂ and SiH₄+Ar

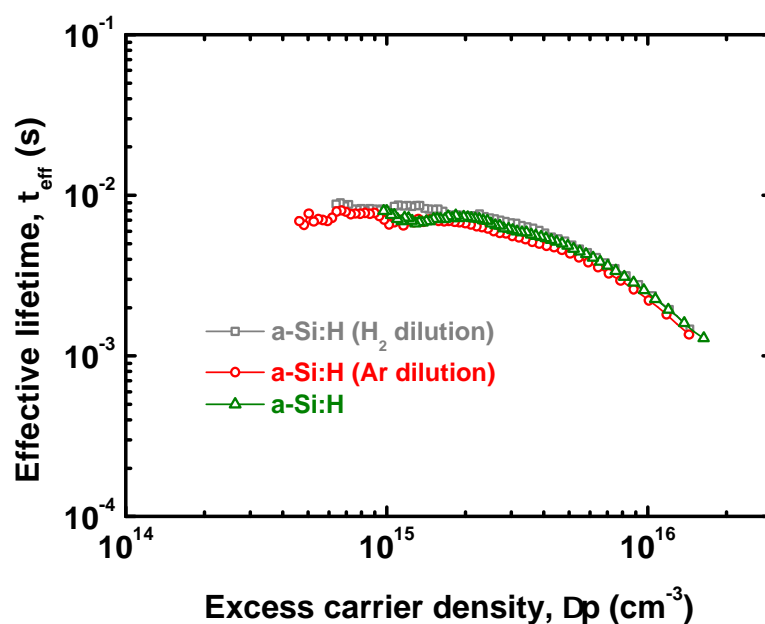


Figure 3.11 – Effective lifetimes of symmetrical samples deposited at 200°C on (111) orientation from SiH₄, SiH₄+H₂ and SiH₄+Ar

et al. that noble gases dilution increased the defect density of a-Si:H films and that this increase was strongly correlated with the increase in atomic weight.¹ Also, *Street et al.* have shown that an increased Ar dilution (and an increased power density) led to an increased ESR density signal.² Indeed, *Knights and Lujan* have shown that increasing the RF power density or the argon dilution resulted in an increased columnar morphology.³ This columnar morphology was due to a growth by islands and an imperfect coalescence. Such columnar growth has often been correlated with an increase in active defects by favouring H incorporation under the SiH₂ state over the incorporation under SiH, which was correlated to materials of lower quality [38]. On the other hand, a more recent paper has shown that in highly diluted ($\approx 90\%$) regimes one could expect to deposit a-Si:H films with defect densities comparable or even lower than the ones of state-of-the-art a-Si:H.⁴ They also showed that the increased defect density in our process window ($\approx 50\%$ dilution) reached values ($\approx 10^{16}$ cm⁻³) that may

¹Knights, Lujan, Rosenblum, Street, Biegelsen, and Reimer, "Effects of inert gas dilution of silane on plasma-deposited a-Si:H films", 1981 [43]

²Street, Knights, and Biegelsen, "Luminescence studies of plasma-deposited hydrogenated silicon", 1978 [44]

³Knights and Lujan, "Microstructure of plasma-deposited a-Si : H films", 1979 [45]

⁴Das, Middy, Rath, Longeaud, Williamson, and Chaudhuri, "Nanostructures and defects in silicon-hydrogen alloys prepared by argon dilution", 2000 [46]

still not be so harmful regarding the crystalline silicon passivation in the frame of the paper from HZB [14].

Last but not least, we have also deposited the intrinsic layer in the plasma box dedicated to the growth of doped layers. It appeared that in any of the three plasma box (i, n- or p-type) similar passivation with (i) a-Si:H layers could be obtained. This was a major result since it would allow us to make the entire stack in the same plasma box. From an industrial point of view it implies a much simpler process where only two chambers (i/n and i/p) are needed.

3.2 Doped layers

We have presented many convincing results on (i) a-Si:H layers but in order to obtain devices we need to bring into play doped layers as explained in Chapter 2. In this section we will present interesting experimental results on the passivation achievable with such doped layers, with or without an undoped buffer layer, and we will point out what the main difficulties are and how we have or could overcome them.

3.2.1 Passivation

3.2.1.1 n-type doping

The goal of the (n) a-Si:H layer in our devices based on a (n) c-Si absorber is to be used as a BSF. This layer should provide an efficient surface passivation of the solar cell and allow for a good electron extraction. On the contrary, holes should face a potential barrier to prevent their recombination in the n-layer. As seen in Chapter 2, the band diagram is quite favourable for such layers and it is possible for (n) a-Si:H layers to fulfil these conditions. Indeed, on the BSF side, the conduction band offset ΔE_c is rather small so that electrons do not have a very high barrier to overcome whereas the valence band offset ΔE_v will be rather high making it quite easy for holes to be repelled.

However, this needed to be experimentally confirmed in terms of passivation and solar cell characteristics. On Fig. 3.12, we have plotted the imaginary part of the pseudo-dielectric function of three films. We processed two samples with a (n) a-Si:H layer directly onto the c-Si wafer which was (111)-oriented for the 1001209 sample whereas it was (100)-oriented for the 1002177 sample. We also deposited a (i)+(n) a-Si:H stack. We usually obtained (n) a-Si:H layer from a gas mixture of 50 sccm of SiH_4 and 10 sccm of PH_3 diluted at 0.1% in H_2 . The pressure was 120 mTorr and the inter-electrode distance 28 mm for a power density of 6 mW.cm^{-2} . These process conditions gave a deposition rate of about 0.5 \AA.s^{-1} .

From Fig. 3.12 it appears that the films deposited in the conditions of (n) a-Si:H could lead to a material that was similar to $\mu\text{c-Si:H}$ or polysilicon on (100) c-Si whereas it was purely amorphous on (111) c-Si. This was a confirmation of the results obtained in the previous section showing that (100) surfaces favour epitaxial growth. Even though we used a fairly high amount of impurities (dopants) we still had an initial growth close to an

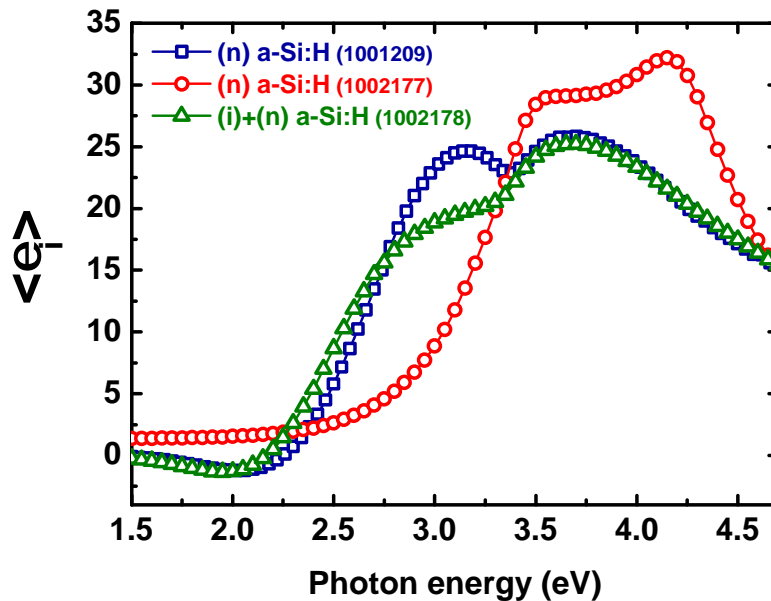


Figure 3.12 – Imaginary part of the pseudo-dielectric function of a (n) a-Si:H layer grown in the same conditions on (100) for sample 1001209 and on (111) for sample 1002177, and of a (i)+(n) a-Si:H stack.

epitaxial growth which confirmed the success of using methane at the early stages of the deposition as shown in the previous section.

It was also very interesting to look at the passivation properties provided by these layers. On Fig. 3.13, we have plotted the effective lifetime in these three symmetrical samples. We have also added the lifetimes obtained in symmetrical samples with an (i)+(n) a-Si:H stack where the (i) and the (n) layer were either deposited without stopping the plasma, in the same chamber, or by depositing the (i) and the (n) layer in different chambers, thus stopping the deposition between the (i) and the (n) layer. Interestingly enough, the striking differences observed by spectroscopic ellipsometry also appeared on this graph. The sample for which the growth was a mixed phase exhibited the smallest lifetimes whereas an amorphous growth resulted in a much higher lifetime. However, the highest lifetimes were achieved when a thin undoped amorphous layer was added. It is worth noting that we deposited two samples under the same conditions and deposition times but one in two different chambers and with a deposition interruption and the other in the same chamber without plasma interruption. These two samples, 10012517 and 10012518, exhibited very similar lifetimes. This was an evidence that depositing the so-called intrinsic layer and the doped layer in the same chamber was not a problem, confirming the results from the previous section where we had deposited intrinsic layers in chambers dedicated to the deposition of doped layers and therefore contaminated. Finally one should note that with an appropriate intrinsic thickness, sample 1002178, we could achieved the same passivation level as the one we obtained with intrinsic layers. Indeed, in this case we got an implicit V_{oc} of 730 mV.

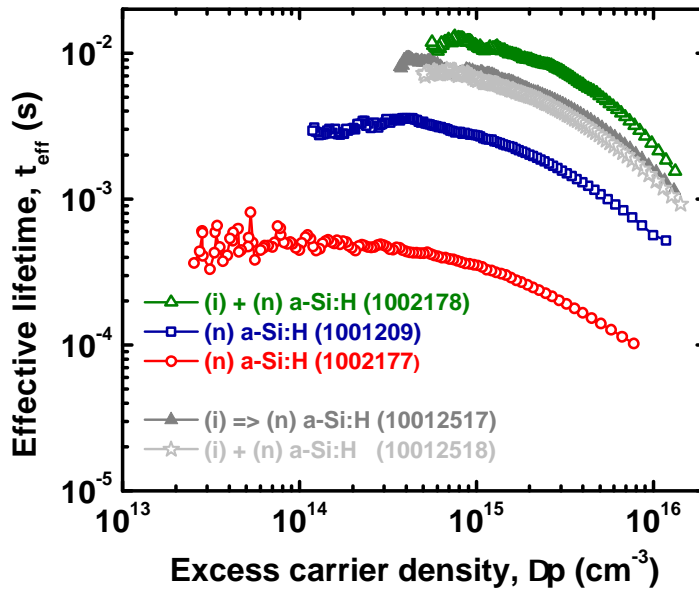


Figure 3.13 – Effective lifetime in symmetrical samples on (n) c-Si consisting of two (n) a-Si:H layers grown in the same conditions on (111) c-Si for sample 1001209 and on (111) for sample 1002177 and of a different (i)+(n) a-Si:H stacks

3.2.1.2 p-type doping

During this PhD thesis, a lot of work has been done on p-type layers. Indeed, obtaining a good passivation with such layers has always been more challenging than with their n-type counterparts, as experimentally observed by *Stefaan De Wolf* on (p) c-Si¹ as well as on (n) c-Si.²

3.2.1.2.1 (p) a-Si:H Let us first consider the case when the p-layer was amorphous. In Tab. 3.7, we have summarized most of the results obtained with (p) or (i)+(p) a-Si:H symmetrical stacks on (n) c-Si wafers regarding the passivation properties. The implicit V_{oc} and effective lifetime are taken at 1 sun equivalent injection level.

On Fig. 3.14 we have also plotted the effective lifetimes against the excess carrier density obtained from our different (p) and (i)+(p) a-Si:H passivation stacks.

Unlike (n) a-Si:H layers, the (p) a-Si:H layers studied during this work could never provide a decent passivation when deposited directly onto the c-Si wafer, which could be due to the fact that highly doped (p) a-Si:H layers are expected to be more defective than (n) a-Si:H layers.³ The second result to point out is that adding an undoped buffer layer did increase the passivation. Pushing the undoped buffer layer concept a bit further, one could think of using a doping gradient during the (p) a-Si:H

¹De Wolf and Beaucarne, “Surface passivation properties of boron-doped plasma-enhanced chemical vapor deposited hydrogenated amorphous silicon films on p-type crystalline Si substrates”, 2006 [47]

²De Wolf and Kondo, “Nature of doped a-Si:H/c-Si interface recombination”, 2009 [26]

³Stutzmann, Biegelsen, and Street, “Detailed investigation of doping in hydrogenated amorphous silicon and germanium”, 1987 [48]

Sample	Stack	Comment	Impl. V_{oc} (mV)	τ_{eff} (μ s)
1002171	(p) a-Si:H	-	624	175
1002172	(i/p) a-Si:H	-	672	576
10021713	(i/p) a-Si:H	Abrupt doping gradient	668	510
10021714	(i/p) a-Si:H	Smooth doping gradient	672	583
10021715	(i/p) a-Si:H	H ₂ during (i) deposition abrupt doping gradient	642	282
10021720	(p) a-Si:H	T _s = 180°C	629	197
10021721	(i/p) a-Si:H	T _s = 180°C	672	560
1002181	(p) a-Si:H	Argon dilution	604	94
1002191	(p) a-Si:H	Argon dilution, 2 Watts	602	89
1002182	(i/p) a-Si:H	Argon dilution	680	704
1002183	(i/p) a-Si:H	Argon dilution only for (p) a-Si:H	674	582
1002193	(i/p) a-Si:H	Argon dilution, 2 Watts	677	655
1002192	(i/p) a-Si:H	Argon dilution 2 Watts for (p) a-Si:H	697	990

Table 3.7 – Description of (p) and (i)+(p) a-Si:H stacks and their passivation properties at 1 sun. Unless stated the power of the plasma was 1 Watt, the substrate temperature set at 200°C and no H₂ was used for the deposition.

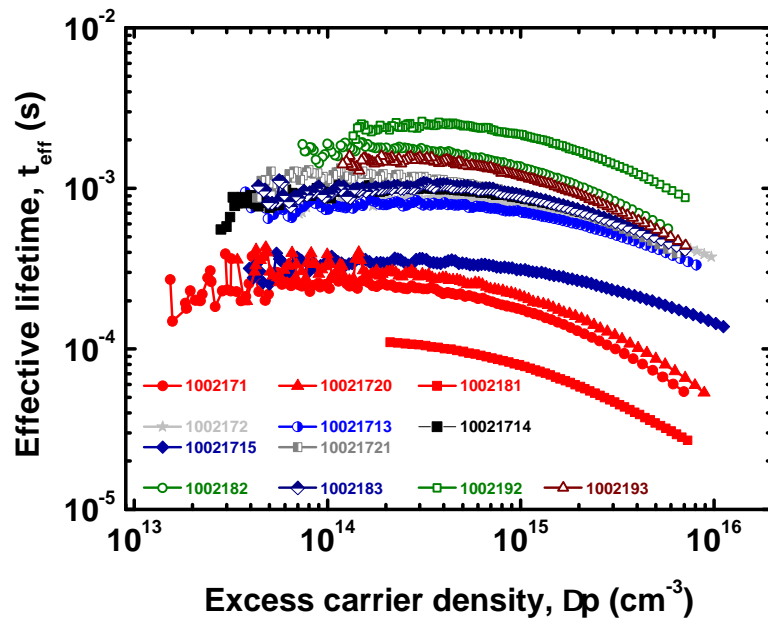


Figure 3.14 – Effective lifetime from (p) and (i)+(p) a-Si:H passivation stacks grown under various conditions detailed in the text and in Tab. 3.7

deposition. This idea had already been tested for n-layer on undoped epitaxial layer in *Damon-Lacoste* PhD thesis [5]. Here we have implemented this idea with two different gradients, one quite abrupt and another one smoother. “Smooth gradient” means that we have used more intermediate flow rates to go from 0 to 20 sccm of TMB, over a longer time, whereas “abrupt gradient” means that we used only one intermediate flow rate, only for a short time. 20 sccm being the flow rate generally used in our lab to grow (p) a-Si:H layers. However, it seemed that introducing a gradient did not improve noticeably the passivation, and this will be confirmed later on completed solar cells.

We also tried to decrease the substrate temperature, going from 200 to 180°C (10021720 and 10021721). Indeed, when H diffuses in c-Si, it creates defects, named platelets, that are harmful regarding the carrier recombination.^{1,2} Among the examples of this detrimental effect, *Damon-Lacoste and Roca i Cabarrocas* have shown that a hydrogen plasma was very detrimental to the passivation, a lot more than a longer argon plasma [6]. Similarly, using Hot Wire CVD, *Schüttauf et al.* have shown that a short hydrogen treatment of the c-Si surface was detrimental to the passivation obtained by the subsequent deposition of an (i) a-Si:H layer.³ In the case of HWCVD we expected to have atomic hydrogen impinging at the surface of the c-Si which would support *Damon-Lacoste and Roca i Cabarrocas'* results where the damage came from a “chemical” effect of the H rather than a “mechanical” effect due to ion bombardment, which is absent in HWCVD growth processes. Hydrogen comes from the deposition process and the deposited layers. The higher the temperature, the faster the diffusion. This became more critical in the case of (p) a-Si:H deposition since the hydrogen diffusion coefficient is much higher in (p) a-Si:H compared to n-type or intrinsic a-Si:H.^{4,5} It should be noted that these diffusion coefficients are increased in the presence of a plasma.⁶ However, it was impossible to change one parameter at a time, all things being equal, so that this 20°C decrease would also for instance increase the defect density of the deposited materials (cf. Fig. 3.2), and it was indeed observed that (i) a-Si:H layers deposited at a lower substrate temperature than 200°C exhibited a higher interface defect density. This meant that any potential gain on one side was already somehow lost on one other side before we could observe it. In addition to that, it should be remembered that the substrate deposition temperature had also an effect on the hydrogen content of a-Si:H layers. The lower the deposition, the higher the hydrogen content (Fig. 3.2). The conclusion was that it was not so easy to know what

¹Johnson, Ponce, Street, and Nemanich, “Defects in single-crystal silicon induced by hydrogenation”, 1987 [49]

²Ulyashin, Job, Fahrner, Richard, Bender, Claeys, Simoen, and Grambole, “Substrate orientation, doping and plasma frequency dependencies of structural defect formation in hydrogen plasma treated silicon”, 2002 [50]

³Schüttauf, van der Werf, van Sark, Rath, and Schropp, “Comparison of surface passivation of crystalline silicon by a-Si:H with and without atomic hydrogen treatment using hot-wire chemical vapor deposition”, 2011 [51]

⁴Beyer and Wagner, “Determination of the hydrogen diffusion coefficient in hydrogenated amorphous silicon from hydrogen effusion experiments”, 1982 [52]

⁵Street, Kakalios, Tsai, and Hayes, “Thermal-equilibrium processes in amorphous silicon”, 1987 [53]

⁶Santos and Jackson, “Trap-limited hydrogen diffusion in a-Si:H”, 1992 [54]

we could expect from the decrease of the substrate temperature and our experiments tended to say that the overall effect was mostly detrimental.

Another idea could be to grow our (p) a-Si:H films in argon dilution. Indeed, growing a film in an argon dilution can densify and reduce the hydrogen content of (i) a-Si:H films.^{1,2} By doing so we decreased the bandgap of the material and we decreased the valence band offset, which is determined by a thin layer close to the interface,³ which could possibly be favourable for the hole collection. Regarding the passivation properties, our work on undoped layer passivation has shown that growing layers from silane or silane and argon would lead to similar passivations. In Tab. 3.7, we have checked the passivation of different stacks. It appeared that the stacks deposited with argon dilution gave better passivation. Some fine optimisation was also performed to deposit the undoped layer at low power and the p layer at higher power. Indeed, we tried to use the lowest power for the undoped layer to avoid the creation of powders in the plasma that could be favoured by the presence of argon and the increase of pressure, whereas we increased the power for the (p) a-Si:H deposition, since boron is supposed to decrease the formation of powders, all things being equal.⁴ Unfortunately, spectroscopic ellipsometry measurements did not show very different optical properties for these layers.

- 3.2.1.2.2 (p) μ c-Si:H** μ c-Si:H is a material which shows a smaller absorption coefficient than the one of a-Si:H in the blue part.⁵ Therefore, it seemed to be a good idea to use a (p) μ c-Si:H layer as the emitter in order to decrease the absorption losses in the “blue” part of the spectrum (<650 nm). Besides, μ c-Si:H films are known to be more easily doped than a-Si:H films and could also be expected to form a better contact with ITO for it has a smaller bandgap energy, as it has been confirmed by the study of homojunction solar cells that were back contacted by a-Si:H/(p) μ c-Si:H.⁶ (p) μ c-Si:H has also been successfully implemented into heterojunction solar cells.⁷ It should be stressed that the structure would remain that of an heterojunction since there should always be an amorphous layer at the interface with the c-Si wafer. In order to test the passivation properties of such layers we fabricated a series of symmetrical samples of the following stack: (i) a-Si:H + (p) μ c-Si:H.

¹Fukutani, Kanbe, Futako, Kaplan, Kamiya, Fortmann, and Shimizu, “Band gap tuning of a-Si:H from 1.55 eV to 2.10 eV by intentionally promoting structural relaxation”, 1998 [40]

²Hamma and Roca i Cabarrocas, “Low temperature growth of highly crystallized silicon thin films using hydrogen and argon dilution”, 1998 [39]

³Van de Walle and Yang, “Band discontinuities at heterojunctions between crystalline and amorphous silicon”, 1995 [55]

⁴Suendo, Kharchenko, and Roca i Cabarrocas, “The effects of RF plasma excitation frequency and doping gas on the deposition of polymorphous silicon thin films”, 2004 [56]

⁵Meier, Dubail, Cuperus, Kroll, Platz, Torres, Anna Selvan, Pernet, Beck, Pellaton Vaucher, Hof, Fischer, Keppner, and Shah, “Recent progress in micromorph solar cells”, 1998 [57]

⁶Einsele, Rostan, Schubert, and Rau, “Recombination and resistive losses at ZnO/a-Si:H/c-Si interfaces in heterojunction back contacts for Si solar cells”, 2007 [58]

⁷Olibet, “Properties of interfaces in amorphous / crystalline silicon heterojunctions”, 2009 [59]

Before going into the details of the passivation that one could expect from such stacks, on Fig. 3.15 we have plotted the imaginary part of the pseudo-dielectric function of different stacks made up of a combination of 1 or 2 minutes of (i) a-Si:H coupled with 5 or 10 minutes of (p) μ c-Si:H. The

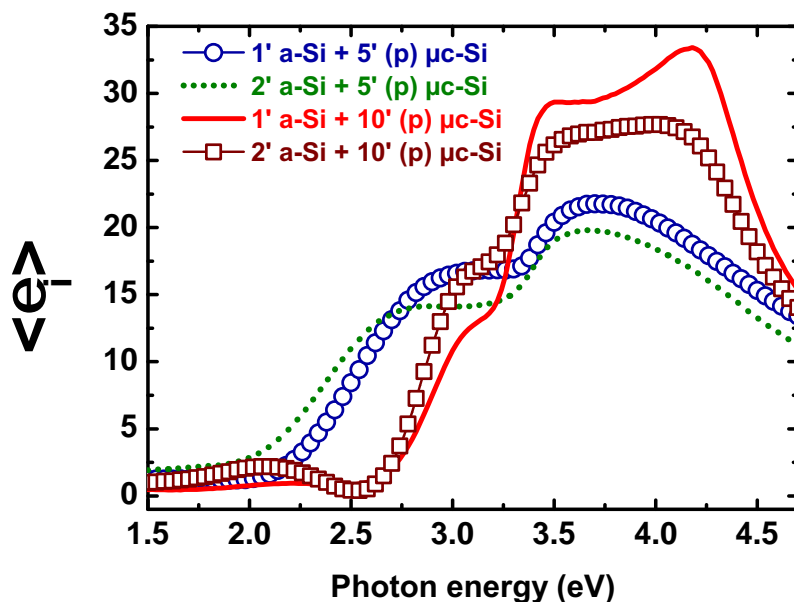


Figure 3.15 – Imaginary part of the pseudo-dielectric function of (i) a-Si:H + (p) μ c-Si:H stacks with different deposition times for both layers on (100) c-Si substrates.

very striking result that came from such spectra is that when the (p) μ c-Si:H deposition time remained too short, there was not enough time for the layer to crystallize so that it remained under the form of an hydrogen-rich amorphous layer called incubation layer.^{1,2,3} The passivation obtained with such films is high (see below) but as the doping efficiency of μ c-Si:H films is very high, a small flow rate of dopants was used, so that if the layer remained amorphous we did not expect it to be significantly doped and therefore unsuitable for solar cells applications. On the other hand, doubling the deposition time resulted in fully crystallized films. However, if the a-Si:H buffer layer was too thin, it could be etched and/or crystallized inducing the subsequent epitaxial growth of the (p) μ c-Si:H layer. This epitaxial growth would imply poor lifetimes.

To study the effect on the passivation we grew two series of symmetrical samples consisting of a first series with a (i) a-Si:H deposited at 200°C capped by a (p) μ c-Si:H layer deposited at 175°C, and of a second series where all the layers were grown at 175°C. The idea behind that was that it was easier to obtain μ c-Si:H at lower substrate temperatures but we also knew that (i) a-Si:H would be of better quality if deposited at higher tem-

¹Roca i Cabarrocas, "Plasma enhanced chemical vapor deposition of silicon thin films for large area electronics", 2002 [60]

²Roca i Cabarrocas, "Plasma enhanced chemical vapor deposition of amorphous, polymorphous and microcrystalline silicon films", 2000 [34]

³Fujiwara, Kondo, and Matsuda, "Real-time spectroscopic ellipsometry studies of the nucleation and grain growth processes in microcrystalline silicon thin films", 2001 [61]

perature. The p-layer was grown using 500 sccm of H_2 and 1.5 sccm of TMB with a varying SiH_4 flow rate. The imaginary part of the dielectric function of all the grown films is shown on Fig. 3.16.

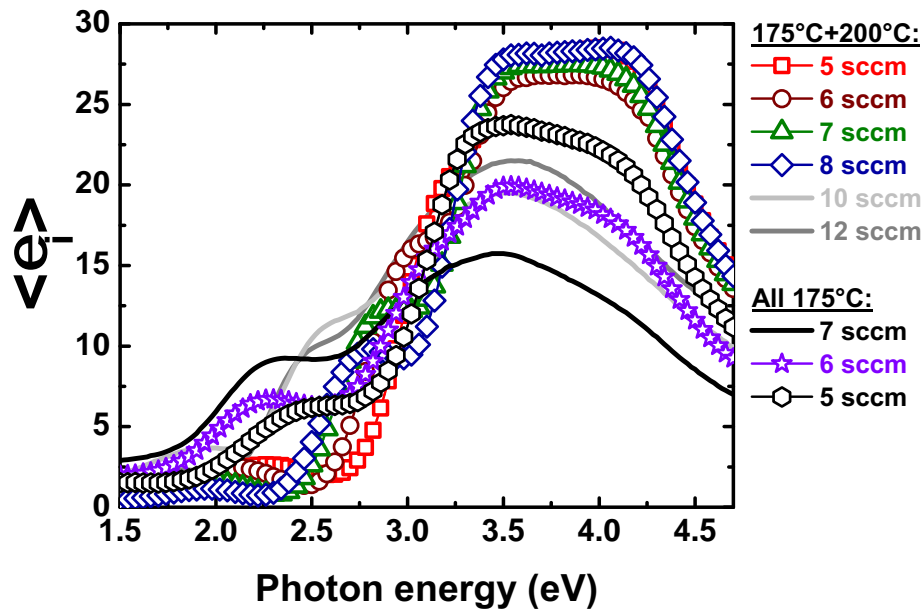


Figure 3.16 – Imaginary part of the pseudo-dielectric function of (i) a-Si:H + (p) μ c-Si:H stacks deposited entirely at 175°C, or with the i-layer at 200°C and the p-layer at 175°C. The SiH_4 flow rate is indicated in the legend.

This graphs showed that when the silane flow rate was too important, the process shifted from microcrystalline conditions to a regime of amorphous growth. However, when the silane flow rate was too low (or the hydrogen dilution too high), we went back to conditions where there was an epitaxial-like growth. Such strong difference in the ellipsometry spectra was also found in the effective lifetime measurements (Fig. 3.17) for which all the epitaxial-like films exhibited implicit V_{oc} below 600 mV and the two amorphous films resulted in implicit V_{oc} of 700 mV.

On Fig. 3.17, we have plotted the effective lifetimes of all the (p) μ c-Si:H samples. As already pointed out, the worst passivations were obtained when the films were epitaxial-like, and the best passivations were obtained when the films were amorphous. However, it seemed that we had a process window where we were able to grow neither epitaxial nor amorphous films but rather μ c-Si:H films while keeping a good passivation (implicit V_{oc} of 670 mV for 5 sccm and 680 mV for 6 sccm). Such films would be the basis of the solar cell tests that we will present in §3.3.

3.2.2 Light soaking

A major drawback of a-Si:H based solar cells is the *Staebler-Wronski effect*,¹ which decreases their efficiency upon light exposure. This decrease is related to an increase in the dangling bond density of undoped a-Si:H

¹Staebler and Wronski, "Reversible conductivity changes in discharge-produced amorphous Si", 1977 [62]

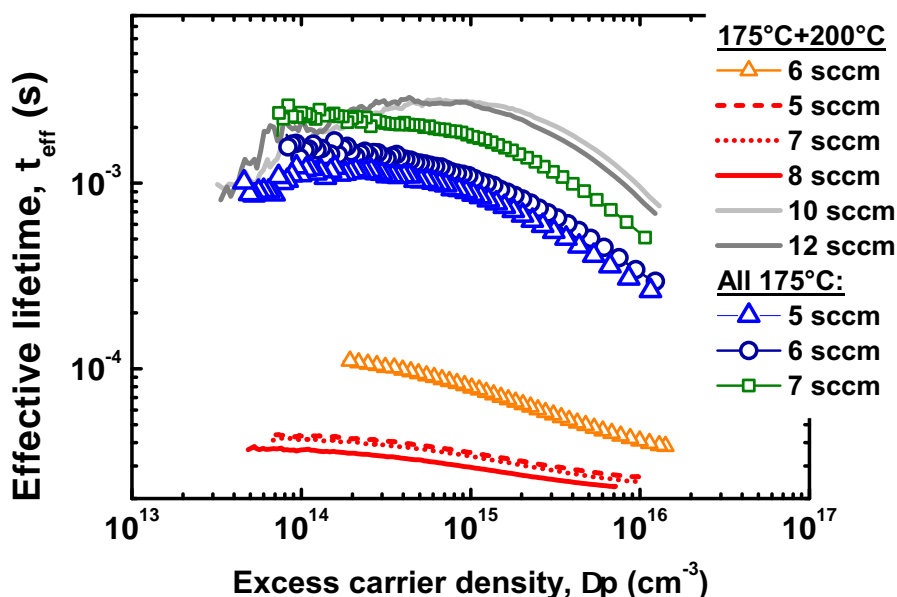


Figure 3.17 – Effective lifetimes in all the (i) *a*-Si:H + (p) μ c-Si:H stacks

films when exposed to light, increase that is recoverable by annealing, as described in the work by *Stutzmann et al.*¹ Crystalline silicon solar cells can also exhibit a light-induced degradation (LID) of their performance in the case of p-type oxygen-rich crystalline silicon. Indeed, light can activate the formation of boron-oxygen complexes that act as recombination centers.² Such complexes can be, temporarily, deactivated by annealing. Some studies have shown that it was possible to permanently deactivate these recombination centres to nearly get back to the original state.³ Even more interestingly, *Macdonald et al.* have recently published that the LID in n-type compensated (from boron doping) materials was in fact proportional to the net doping.⁴ Such finding was of great importance for crystalline silicon based solar cells on n-type for it opened the way to n-type solar-grade (highly or not) compensated material, since the total boron concentration did not determine the LID. However, *Schutz-Kuchly et al.* have shown that a degradation, ascribed to the additional boron, existed in n -type compensated silicon,⁵ thus questioning *Macdonald et al.*'s results. Finally, even more recently *Geilker et al.* have confirmed that there was indeed a LID in p- and n-type compensated materials and that the

¹Stutzmann, Jackson, and Tsai, "Light-induced metastable defects in hydrogenated amorphous silicon: A systematic study", 1985 [63]

²Schmidt and Bothe, "Structure and transformation of the metastable boron- and oxygen-related defect center in crystalline silicon", 2004 [64]

³Herguth, Schubert, Kaes, and Hahn, "Investigations on the long time behavior of the metastable boron-oxygen complex in crystalline silicon", 2008 [65]

⁴Macdonald, Rougieux, Cuevas, Lim, Schmidt, Di Sabatino, and Geerligs, "Light-induced boron-oxygen defect generation in compensated p-type Czochralski silicon", 2009 [66]

⁵Schutz-Kuchly, Veirman, Dubois, and Heslinga, "Light-Induced-Degradation effects in boron-phosphorus compensated n-type Czochralski silicon", 2010 [67]

amount of defects was in fact proportional to the “compensation ratio” $\frac{N_A+N_D}{N_A-N_D}$.¹

It appears that most solar cells based on silicon will experience LID, except for solar cells based on uncompensated (n) c-Si wafers. However, there were very few reports on such studies in the case of heterojunction solar cells. *Olibet et al.*² and *Bowden et al.*³ have reported that when the passivation was based on intrinsic a-Si:H layers a degradation of the passivation could be observed. *Olibet et al.* have shown that there was a thickness dependence of such degradation and that it was the opposite as it is for the SWE effect since increasing the thickness would lead to a much lower, if any, degradation. Both group of authors have noticed that there was a very similar degradation when the samples were merely stored in the dark and that they could recover upon annealing. Interestingly, *Bowden et al.* showed that when the intrinsic a-Si:H layer was capped by a silicon nitride (a-SiN_x:H) or a doped a-Si:H layer, no degradation would occur. For both group of authors, it is the water adsorption at the free surface of the (i) a-Si:H film rather than the a-Si:H/c-Si interface that is responsible for this degradation. Indeed, *Bowden et al.* used FTIR measurements to confirm that no change at the a-Si:H/c-Si interface occurred during the annealing step that allowed passivation to recover. *Olibet et al.* noticed that both annealing or HF-dip allowed their sample to recover their original lifetimes. They explained such behaviour thanks to their recombination model,⁴ acknowledging the fact that adsorption can cause a negative charge at the free surface of the (i) a-Si:H film that *is responsible for the increasing negative charge of the dangling bonds at the c-Si/a-Si:H interface, and corresponding increasing surface recombination rate* (quoting). Indeed their model assume higher charged than neutral capture cross section.

Our experiments were carried out on n-type, FZ, c-Si wafers for which the boron-oxygen complex could therefore be excluded. Light soaking was performed by putting the samples onto the surface of an overhead projector on which a fan was attached to cool the samples. They consisted of symmetrical stacks of the following materials:

- (i) a-Si:H (907228 and 9072214)
- (i) a-Si:H + (n) a-Si:H (908245)
- (i) a-Si:H + (p) a-Si:H (907227)

In all cases, the (i) a-Si:H was made with the first 30” of a-SiC_x:H. The lifetime was measured with our Sinton equipment.

The (i) a-Si:H symmetrical samples were obtained at two different substrate temperatures with 22-23 nm (200°C) and 24-27 nm (225°C) thick (i) a-Si:H films. On Fig. 3.18 we have plotted the effective lifetime at an injection level of 10¹⁵ cm⁻³ against the cumulated light soaking time until

¹Geilker, Kwapil, and Rein, “Light-induced degradation in compensated p- and n-type Czochralski silicon wafers”, 2011 [68]

²Olibet, Vallat-Sauvain, and Ballif, “Effect of light induced degradation on passivation properties of a-Si:H layers deposited on crystalline Si”, 2006 [69]

³Bowden, Das, Herasimenka, and Birkmire, “Stability of amorphous/crystalline silicon heterojunctions”, 2008 [70]

⁴Olibet, Vallat-Sauvain, and Ballif, “Model for a-Si:H/c-Si interface recombination based on the amphoteric nature of silicon dangling bonds”, 2007 [71]

18375 minutes, after what we performed a 45 minutes annealing in air at 150°C . Then we regularly measured the effective lifetime of the samples which were stored in ambient air but did not undergo any further light soaking, and were merely stored in the dark. We would like to highlight

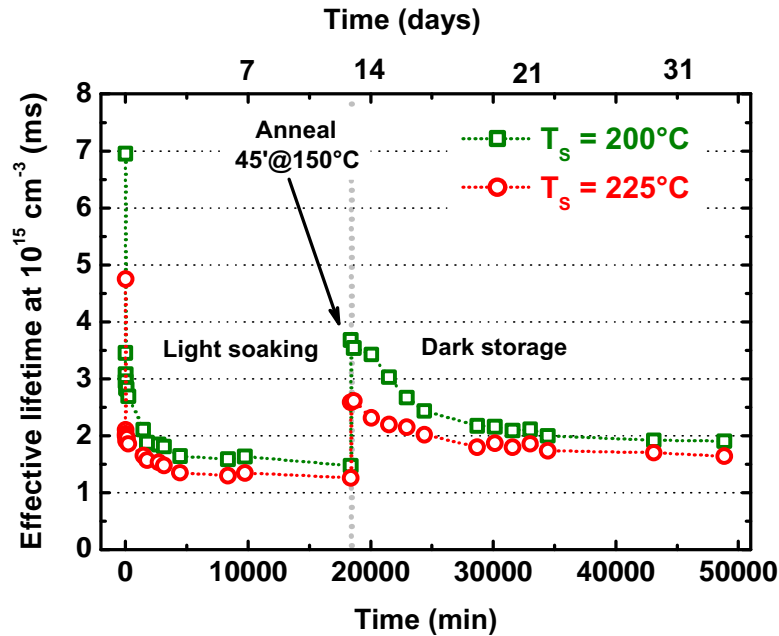


Figure 3.18 – Effective lifetime at 10^{15} cm^{-3} in a symmetrical sample passivated by a 22 nm (i) a-Si:H layer as a function of time

first the fact that the initial drop of the effective lifetime was not due to the light soaking but to the fact that we started our experiments some time after the deposition so that the lifetime had already degraded before we started the experiments. This graph brings up a few comments. The first is that the intrinsic layer did not seem to provide a very stable passivation. The second is that this degradation was not entirely related to the light soaking itself: even though the decrease may have appeared faster in the case of the light soaking phase, compared to dark storage, it did not affect so much the asymptotic limit of the lifetime itself. Indeed, the difference between the light soaking and dark storage implicit V_{oc} , that we did not plot for clarity, was of only 5 mV (710 versus 715 mV). Therefore we could not impute the degradation of the passivation to a light soaking effect. This would have been surprising anyway if we consider that the intrinsic layers we are talking about were about 15 times thinner than the ones used in p-i-n a-Si:H solar cells. Besides, we have shown earlier that good passivation could be obtained with (n) a-Si:H layers which are known to have a very high defect density, higher than the one of a light soaked (i) a-Si:H layer.

The (i)+(p) a-Si:H and (i)+(n) a-Si:H symmetrical samples were both obtained with a stack of 15 nm. On Fig. 3.19, which corresponded to the (i)+(p) a-Si:H case, we have plotted the effective lifetime at an injection level of 10^{15} cm^{-3} against the cumulated light soaking time until 18375 minutes when we performed a 45 minutes annealing in air at 150°C . Then we regularly measured the effective lifetime of the samples which was

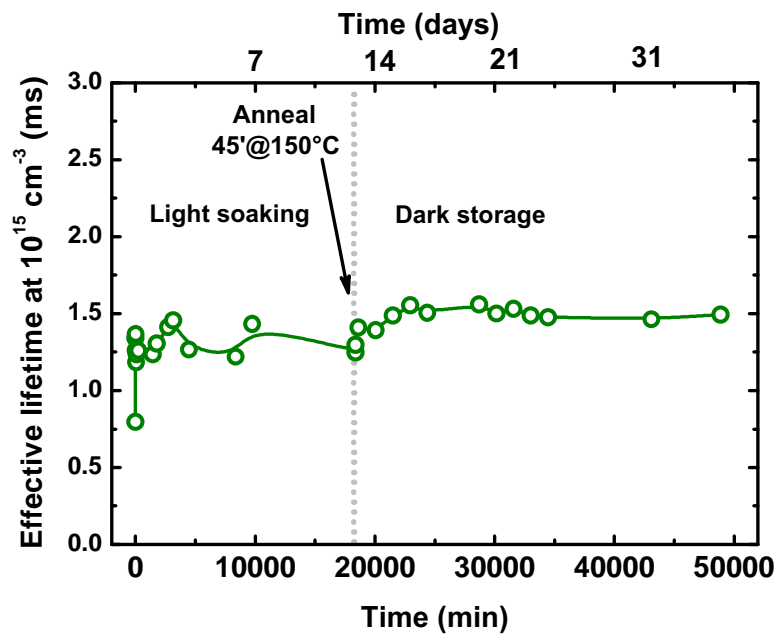


Figure 3.19 – Effective lifetime at 10^{15} cm^{-3} of a symmetrical sample passivated by a 15 nm (i)+(p) a-Si:H stack as a function of time

stored in ambient air but did not undergo any further light soaking, and were merely stored in the dark. On Fig. 3.20 we have plotted the effective lifetime at an injection level of 10^{15} cm^{-3} against the cumulated light soaking time for (i)+(n) a-Si:H sample.

Unlike the (i) a-Si:H samples, we did not see any degradation of the effective lifetimes, whether it underwent the light exposure or not, when the c-Si wafers were passivated by doped layers. These results were confirming the (few) results issued from the literature, namely that when a thin (i) a-Si:H layer was capped by a doped a-Si:H layer there was no degradation of the passivation, no matter whether it was stored in the dark or underwent light soaking, which was a very important for us since our heterojunctions only use doped layer and never (i) a-Si:H on their own. Therefore, we should expect our solar cells' efficiencies not to degrade under sun exposure.

3.2.3 Annealing

Until now we have mostly studied the effects of annealing steps on samples deposited at low temperature since we were expecting to get an increase in the passivation properties upon annealing and potential healing of the interface. In a different perspective it could have also been interesting to know how such layers could bear annealing up to higher temperatures. Here, instead of a usual hot-plate oven we have used a microwave annealing (900 W), following the approach of *Schulze et al.* who have claimed that such a method allows for much faster annealing steps.¹ It

¹Schulze, Beushausen, Hansmann, Korte, and Rech, "Accelerated interface defect removal in amorphous/crystalline silicon heterostructures using pulsed annealing and microwave heating", 2009 [72]

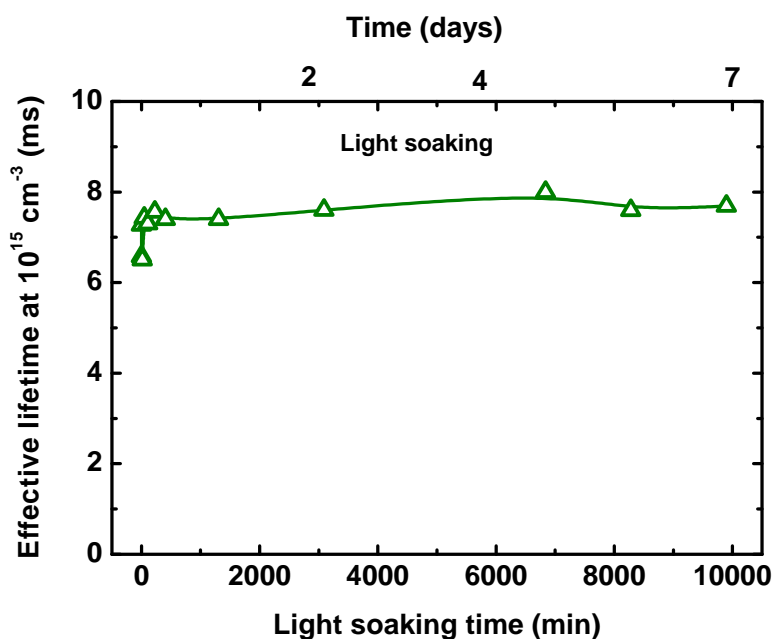


Figure 3.20 – Effective lifetime at 10^{15} cm^{-3} of a symmetrical sample passivated by a 15 nm (i)+(n) a-Si:H stack as a function of the light soaking time

should be noted that the trends observed here in terms of effective lifetimes were similar in the case of the hot-plate oven.

We have deposited two symmetrical samples, on (n) c-Si wafer, consisting of 20 nm stacks of (i/n) (1002178) or (i/p) (1002172) a-Si:H materials and checked the lifetime for successive annealing steps in the micro-wave oven. On Fig. 3.21, we have plotted the effective lifetimes of both samples for various successive annealing time steps: 10, 25, 60 and another 60 seconds.

Unfortunately, no quantitative measurement of the substrate temperature could be performed but we observed a very steep increase of the temperature leading to values higher than 200°C in less than 20 seconds. Interestingly enough, the (n) a-Si:H layer did not exhibit any change upon annealing. For short annealing times the (p) a-Si:H layer did not exhibit degradation either but for longer annealing times, there was a large decrease in the lifetime.

On Fig. 3.22, we have plotted the atomic concentration against the sputtering thickness for H, B, C, O, P elements, of the (i/n) a-Si:H and (i/p) a-Si:H stacks, in their as-deposited and final annealed state. The B and P concentrations and profiles remained unchanged upon annealing. This was rather reassuring since we were not expecting any change for such short treatments and confirmed the consistency of the SIMS measurement. There were very small changes in the O content which was slightly higher in the (i/p) stack. C was also much higher in the (i/p) stack, which was easily explained by our use of TMB gas which possesses three C atoms for one B atom and thus, was expected to induce a large incorporation of C atoms in the film. Finally, the H content showed interesting trends too. Indeed, it appeared that in the as-deposited state, there was more hydrogen in the (i/p) stacks. Upon annealing, no change occurred in the

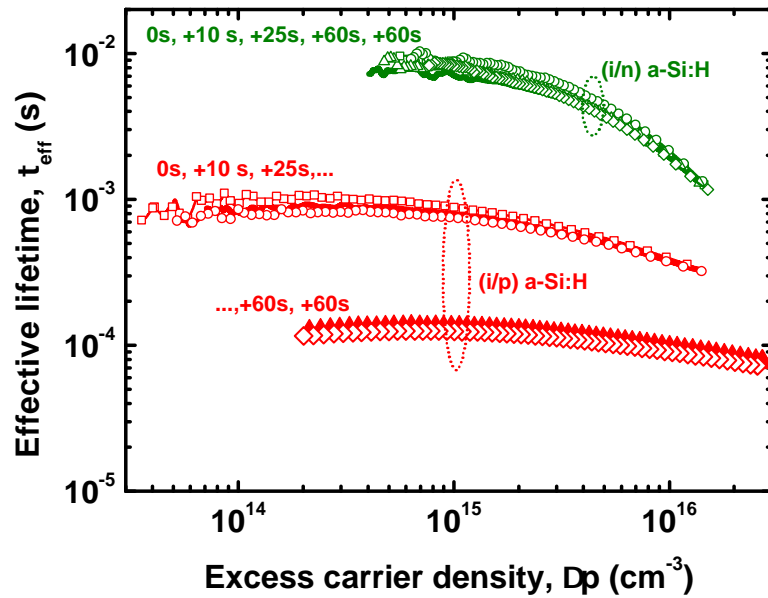


Figure 3.21 – Effective lifetimes in symmetrical (i/n) and (i/p) stacks for various consecutive micro-wave annealing times.

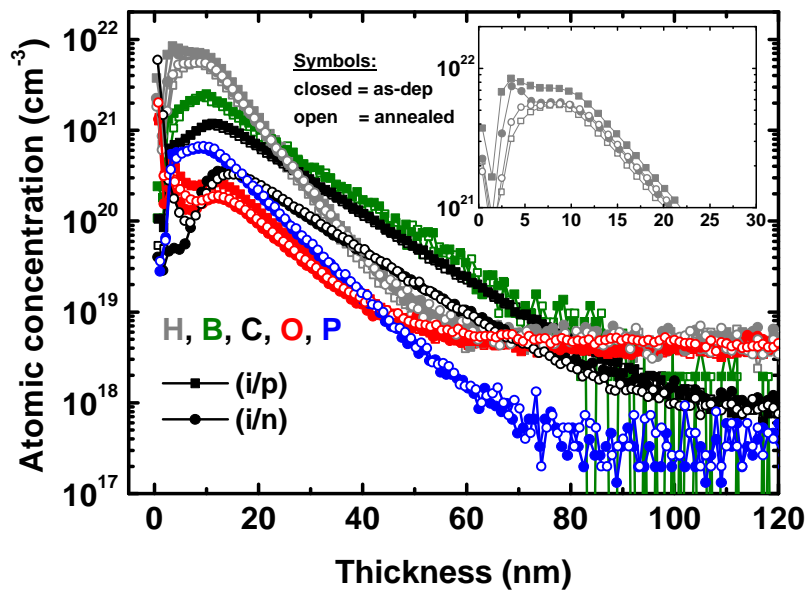


Figure 3.22 – Atomic concentrations in the (i/n) and (i/p) stacks, in their as-deposited or final annealed state as a function of depth as obtained by SIMS

(i/n) stack whereas there was a measurable drop of the hydrogen content of the (i/p) stack that brought its H content close to the one of a (i/n) stack. This meant that upon annealing hydrogen moved in the (p) a-Si:H layer, and possibly left it. This hydrogen redistribution may have created defects, and by moving from the a-Si:H/c-Si interface may have left unpassivated dangling bonds that would drastically reduce the passivation. Such a doping type selectivity may be explained by the hydrogen diffusion coefficients difference between n and p-type a-Si:H.^{1,2}

Such a result has led us to question ourselves about the impact, on the passivation quality, that the order of the i/n and i/p depositions could have. To answer this question we deposited solar cell structures starting either with the i/n or the i/p stack, and showed that when the (p) a-Si:H layer was deposited first, a loss of about 20-30 mV in the V_{oc} was to be expected.

3.3 Heterojunction solar cells

We have discussed so far mostly materials and deposition optimisation but not yet devices. This section will be devoted to presenting the results obtained on completed solar cells and discussing some issues. Before going into the details we would like first to remember that we have had two options during our thesis regarding the solar cell metallization. The first one was to screen-print the front grid and to laser cut the wafer to define 25 cm² square cells. By doing so, the measurement could be considered as accurate for no lateral effects could exist. The second one was to fabricate the entire cell at the LPICM laboratory. In that case, the area of the solar cells was defined by the ITO. However, we have always observed a huge increase in the short-circuit current density when decreasing the size of the cell. This increase could reach a factor of 2 or 3 as compared to the J_{sc} measured on the cells back-ended at INES, for very small areas. It is known that some lateral effects can exist in a-Si:H p-i-n, especially at low illumination levels, leading to an overestimation of J_{sc} and an underestimation of FF.³ However, in this Ref. [73], very small areas of a-Si:H p-i-n are referred to so that the results could not be applied directly to our case and could not provide an explanation for the discrepancies obtained on larger areas, typically 4 cm² in our case. Another possible explanation for that extra collection of carriers could originate from the fact that when the wafer was illuminated, carriers were generated in the entire wafer and not only under the ITO area. On the back side of the solar cell we have a metallization on the entire surface so that electrons, the majority carriers, can be easily collected. On the other side, as already pointed out in the second chapter, we have an inversion layer in the (n) c-Si wafer: this is a thin layer where holes become the majority carriers, and as the a-Si:H emitter is not etched, we still have this inversion layer outside the area defined by the ITO squares. Even if the conductivity of the (p) a-Si:H was

¹Beyer and Wagner, "Determination of the hydrogen diffusion coefficient in hydrogenated amorphous silicon from hydrogen effusion experiments", 1982 [52]

²Street, Kakalios, Tsai, and Hayes, "Thermal-equilibrium processes in amorphous silicon", 1987 [53]

³Martins and Fortunato, "Lateral effects in amorphous silicon photodiodes", 1996 [73]

too low to explain this additional current, this highly conductive inversion layer may provide an efficient channel for the photogenerated holes outside the ITO area. To support this hypothesis one can remember the concept of inverted layer emitters that stemmed from Erlangen University in the early 80's based on MIS structures and using a silicon nitride layer in most cases,^{1,2} that have gained interest recently.³

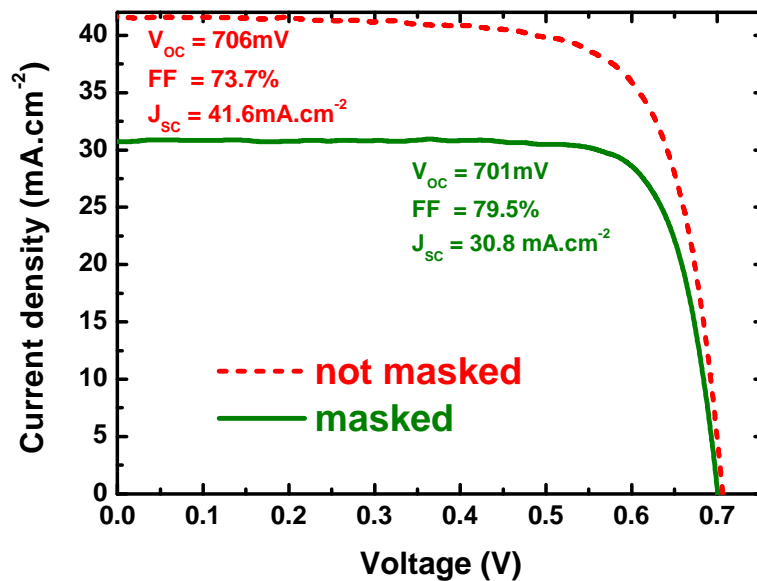


Figure 3.23 – Current-voltage characteristic of our best in-house 4 cm² solar cell measured with or without a shadow mask

On Fig. 3.23, we have plotted the current-voltage characteristic of our best, in-house, solar cell, measured directly or using an opaque mask (aperture area) at the dimensions of our 4 cm² cells. This graph confirmed that we had an overestimation of J_{sc} and an underestimation of FF.

3.3.1 Intrinsic layer

We have already shown in the previous section that epitaxial growth was to be avoided so that we mainly focused on (i) a-Si:H buffer layers. An example of tendency obtained by the incorporation of an (i) a-Si:H buffer layer is shown on Fig. 3.24 where we have plotted V_{oc} , implied V_{oc} and FF against the deposition time of the (i) a-Si:H layer for a constant deposition time for the (p) a-Si:H layer, all things equal especially regarding the (i)+(n) a-Si:H BSF stack. Detailed deposition times and solar cell parameters are given in Tab. 3.8. These cells were 4 cm² square cells, measured through a shadow mask as explained in the previous paragraph.

¹Hezel and Schörner, "Plasma Si nitride—A promising dielectric to achieve high-quality silicon MIS/IL solar cells", 1981 [74]

²Aberle, Kuhlmann, Meyer, Hübner, Hampe, and Hezel, "Comparison of p-n junction and inversion-layer silicon solar cells by means of experiment and simulation", 1996 [75]

³Martin, Lövbom, and Alcubilla, "High-efficiency solar cells based on inversion layer emitters", 2009 [76]

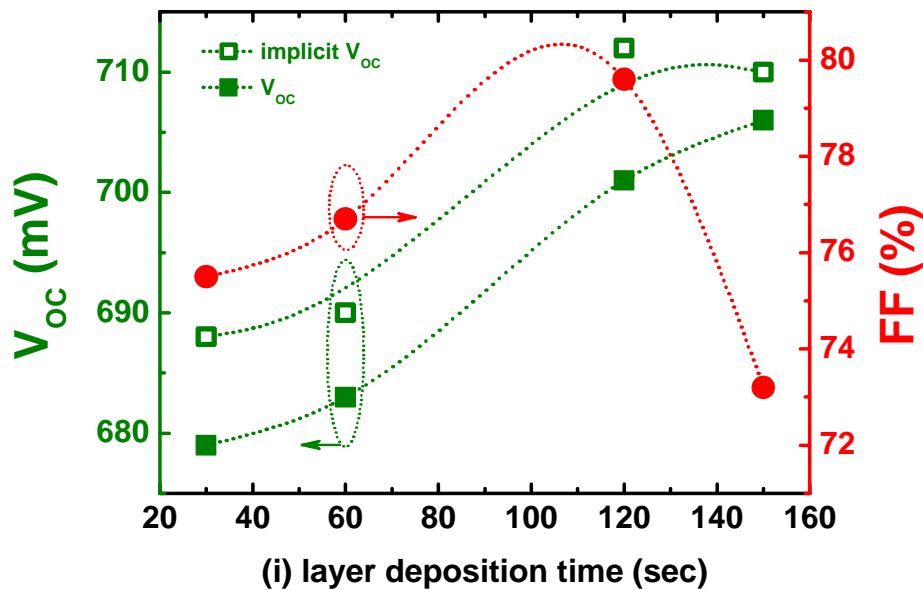


Figure 3.24 – Open-circuit voltage and short-circuit current density plotted against the deposition time for the (i) a-Si:H layer

This graph is very eloquent for it clearly evidences the beneficial role of the undoped layer. Indeed, when the (i) a-Si:H thickness was increased, both V_{oc} and FF increased as well. These results were similar to those of *Fujiwara and Kondo*,¹ or *Schüttauf et al.*,² who also showed that adding a thin a-Si:H buffer layer could increase both V_{oc} and FF. However, in both papers the increase in V_{oc} was not so dramatic and did not reach very high values. Strangely, for *Fujiwara and Kondo* the V_{oc} saturated at some value and the FF also remained at its maximum value after an initial increase and did not show any decrease with an increased intrinsic thickness even when the i layer thickness went up to 15 nm. One should note that the implicit V_{oc} values obtained from the Sinton lifetime tester measurement exhibited the same trend as the actual V_{oc} . The slight discrepancy between actual and implicit V_{oc} may have arisen from the additional steps such as ITO sputtering for instance which were likely to harm the interface.

Sample	(i) a-Si:H deposition time (min)	Impl. V_{oc} (mV)	V_{oc} (mV)	FF (%)	J_{sc} ($\text{mA}\cdot\text{cm}^{-2}$)	η (%)
10051713	0.5	688	679	75.5	30.3	15.5
10051714	1	690	683	76.7	30.8	16.1
10051715	2	712	701	79.6	30.8	17.2
10051719	2.5	710	706	73.2	30.6	15.8

Table 3.8 – Solar cell parameters of heterojunction solar cells with various (i) a-Si:H thicknesses indicated by their deposition time

¹Fujiwara and Kondo, "Effects of a-Si:H layer thicknesses on the performance of a-Si:H/c-Si heterojunction solar cells", 2007 [2]

²Schüttauf, Komatsu, Geerligs, Mai, Bink, Spee, and Schropp, "Emitter Optimization on a-Si:H/c-Si Heterojunction Solar Cells for Isotextured Wafers", 2008 [77]

The increase in the open-circuit voltage value could be explained by a reduced interface defect density as the thickness of the undoped buffer layer was increased resulting in a smaller recombination rate and thus in a higher V_{oc} . At the same time, this reduced defect density allowed for a better transport at the interface and thus we obtained higher FF. However, when the layer became thicker and thicker, the V_{oc} saturated or kept on slightly increasing while the FF value dropped because the (i) a-Si:H layer started to introduce resistive losses and one could have also expected that the tunnelling of holes from the c-Si inversion layer to the (p) a-Si:H had become more difficult.

We also performed dark J(V) characteristics of these solar cells with various (i) a-Si:H thicknesses and plotted them on Fig. 3.25. At high volt-

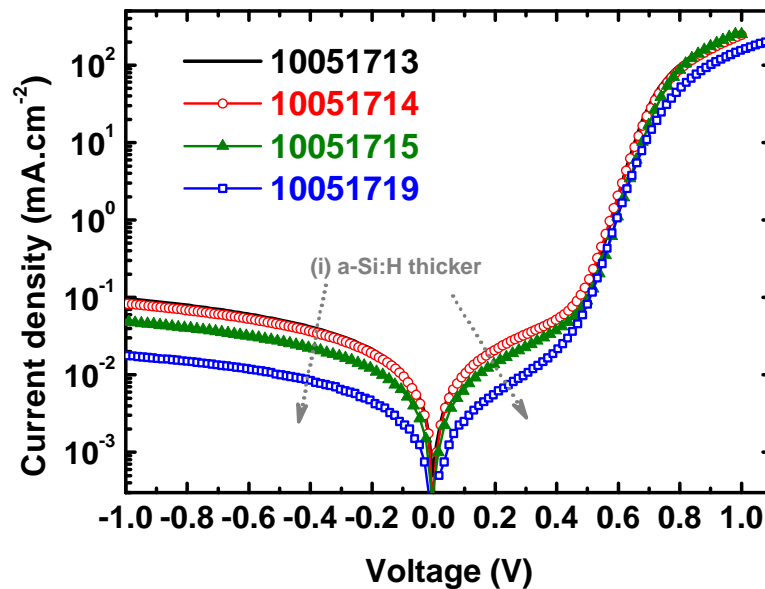


Figure 3.25 – Current-voltage characteristics in the dark of heterojunction solar cells with various (i) a-Si:H thicknesses

ages ($V > 0.8$ V), the slope of the current-voltage characteristic was mostly determined by the series resistance. When the thickness of the (i) a-Si:H layer was increased, the series resistance was also increased, as we saw for the extreme sample 10051719. However, the increased series resistance could not explain why we had an important decrease in the dark saturation current for the thick (i) a-Si:H film. In the 0.4-0.8 V range, where it is generally admitted that diffusion processes are dominant, there was almost no change whereas in the 0.1-0.4 V and reverse bias range there was an appreciable decrease of the current. However, we have already highlighted the fact that lateral effects existed in our solar cells, and were very likely to exist in the dark. In *Damon-Lacoste's* PhD thesis [5], such effects, on much smaller cells, were very important in the dark too in the low-bias region. However, in the high-forward bias region it was still possible to model the obtained curve using the Shockley's law:

$$J(V) = J_0 \times \left(\exp \left(\frac{eV}{nkT} \right) - 1 \right) + \frac{V}{R_p} \quad (3.1)$$

In Eq. 3.1, we did not incorporate the voltage drop arising from the series resistances as in the regions of fitting, the current density was too small compared. The shunt resistance was calculated by a linear fit in the -3 to -2 V range and removed from the J(V) characteristics then used for the fitting. The results of the fitting are shown in Tab. 3.9. We also indicated the calculated V_{oc} obtained using the following equation, with $J_{sc}=0.03 \text{ A.cm}^{-2}$:

$$V_{oc} = \frac{nkT}{e} \ln\left(\frac{J_{sc}}{J_0}\right) \quad (3.2)$$

Sample	(i) a-Si:H time (min)	J_0 (A.cm^{-2})	n	Calculated V_{oc} (mV)	Impl. V_{oc} (mV)
10051713	0.5	2.7×10^{-11}	1.29	690	688
10051714	1	1.6×10^{-10}	1.43	697	690
10051715	2	1.9×10^{-10}	1.49	720	712
10051719	2.5	5.9×10^{-11}	1.39	715	710

Table 3.9 – One diode model parameters of heterojunction solar cells with various (i) a-Si:H thicknesses indicated by their deposition time.

Alike the results of the HZB group,¹ we obtained calculated V_{oc} very close to those implied from effective lifetime measurements as well as those actually measured, from the fitting of the high-forward bias region. This simple and straightforward analysis allowed us to confirm the HZB results, for which the diode parameters calculated in the high-forward bias region allow one to estimate the V_{oc} of the actual cell.

3.3.2 p-type layers

It has been quite well established that there was a beneficial effect from the insertion of a thin undoped buffer layer but we have not seen much about the (p) a-Si:H layer so far. While studying the (i) a-Si:H layer, for the same series we also varied the (p) a-Si:H thickness. In Tab. 3.10, we presented the solar cell parameters of heterojunction solar cells with various p-layer thicknesses (one of them has a slightly thicker i layer). The (p) a-Si:H thicknesses were expected to be in the 15, 20 and 25 nm range.

Sample	(i) a-Si:H (min)	(p) a-Si:H (min)	V_{oc} (mV)	FF (%)	J_{sc} (mA.cm^{-2})	η (%)
10051720	1.75	2.5	690	77.9	30.5	16.4
10051715	2	3.25	701	79.6	30.8	17.2
10051721	1.75	4	691	79.9	30.5	16.8

Table 3.10 – Solar cell parameters of heterojunction solar cells with various (i) and (p) a-Si:H thicknesses indicated by their deposition time

From this table, it appeared that there is very little to gain by increasing the (p) a-Si:H thickness beyond a threshold value. Indeed, between 10051715 and 10051721, there were no change in V_{oc} , FF and J_{sc} . This was

¹Schulze, Korte, Conrad, Schmidt, and Rech, "Electrical transport mechanisms in a-Si:H/c-Si heterojunction solar cells", 2010 [78]

not very surprising and confirmed all the existing simulations.^{1,2} However, thinner (p) a-Si:H may have started to introduce problems. This has been confirmed by some other solar cells, for which no drop in V_{oc} was observed but a decrease of the FF appeared.

Also, we tried to implement (p) $\mu\text{-Si:H}$ in solar cells since the passivation results that we obtained were very promising. However, we have not been able yet to obtain a good diode with such layers. Indeed, it appeared that there was a compromise to be found between the thickness of the buffer layer, the process conditions of the (p) $\mu\text{-Si:H}$ layer and the passivation. Simply put, we could have only observed two extreme cases:

- the plasma conditions of the (p) $\mu\text{-Si:H}$ layer were too aggressive (too much etching) and/or the (i) a-Si:H buffer layer was too thin. This usually resulted in a stack where the (i) a-Si:H layer was either etched or crystallized by the large amount of atomic hydrogen resulting in the subsequent epitaxial growth of the p-type layer. By doing so the passivation was lost: epitaxial solar cells could be obtained (as it will be discussed in the next chapter) but with low V_{oc} .
- the (i) a-Si:H layer was too thick and/or the plasma conditions of the (p) $\mu\text{-Si:H}$ layer were too soft. This resulted in a large incubation layer, that acted as a very thick buffer layer and therefore we obtained S-shaped characteristics.

On Fig. 3.26, we have plotted the $J(V)$ characteristics of various heterojunction solar cells obtained during this work and that allowed us to highlight the main troubles and achievements observed during this period. All these 25 cm² cells were screen-printed, laser cut and measured at INES. The first thing to remark was that some solar cells exhibited a higher short-circuit current density. For these cells, a different ITO, deposited at Solems, was used and could account for the observed difference. Also, the solar cell with the lowest V_{oc} (810032) was deposited with a (p) $\mu\text{-Si:H}$ layer which turned out to be epitaxial. The poor passivation could explain why the V_{oc} was so low. When the thickness of the (i) a-Si:H layer was increased, in order to prevent such an epitaxial growth, it turned out that the passivation was excellent but that the (amorphous) incubation layer was quite thick resulting in such S-shaped characteristics (9032710). All the other characteristics were obtained using (p) a-Si:H layers. Earlier we talked about the low temperature approach. The sample 8111808 was obtained at low temperature. As already stressed out before, we could never obtain satisfying passivation upon annealing when (p) a-Si:H layers were involved. Upon annealing (not shown) all the solar cells parameters degraded. The sample 10062113 showed the beneficial role of growing our p-layers in argon dilution. It mostly increased the V_{oc} as expected from the improved effective lifetimes. However, when the p-layer was too thin (≈ 10 nm), as it was the case for the sample 1002231, we observed a large fall in the FF but without any drop in the V_{oc} .

¹Rahmouni, Datta, Chatterjee, Damon-Lacoste, Ballif, and Roca i Cabarrocas, "Carrier transport and sensitivity issues in heterojunction with intrinsic thin layer solar cells on N-type crystalline silicon: A computer simulation study", 2010 [42]

²Kanevce and Metzger, "The role of amorphous silicon and tunneling in heterojunction with intrinsic thin layer (HIT) solar cells", 2009 [41]

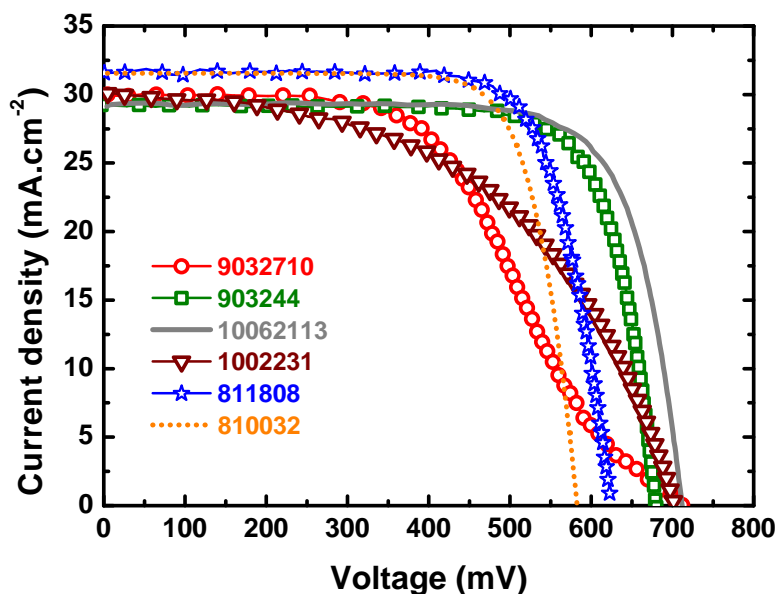


Figure 3.26 – Current-voltage characteristics of silicon heterojunction solar cells obtained during this doctoral work.

In conclusion, many depositions have been done to confirm these trends. From these results, including passivation and buffer layer studies, it appeared that a few guidelines could be drawn. To us, the most clear and definitive trends were that we absolutely needed to have an undoped, amorphous, buffer layer in order to greatly reduce the interface defect density and by doing so increase the open-circuit voltage. The first nanometres of this layer could have even led to an increase in the FF. The second thing was that, unlike (n) a-Si:H layers that are highly doped we needed to have thicker (p) a-Si:H films in order to get the best possible diode. Increasing its thickness proved to have no interest. A combination of ≈ 4 nm of (i) a-Si:H with ≈ 15 nm of (p) a-Si:H has resulted in the best solar cells, shown in Tab. 3.11. The smaller FF obtained on larger areas

	V_{oc} (mV)	FF (%)	J_{sc} (mA.cm ⁻²)	η (%)
(n) c-Si				
2×2 cm ²	701	79.6	30.8	17.2
5×5 cm ² (3 cell average)	710	76.3	29.4	15.9
(p) c-Si				
5×5 cm ²	704	77.4	30.3	16.3

Table 3.11 – Best solar cells obtained on flat c-Si wafers, of p and n-type

were due to the fact that we were using a dense, silver grid on smaller cells, hence a lower series resistance and a higher FF. However, V_{oc} were generally slightly larger for the larger cells. The smaller current for the cells on 25 cm² was due to an incorrect ITO thickness which decreased the anti-reflection action of this layer. Interestingly enough, when using the symmetrical structure on (p) c-Si wafers, nice solar cells could be obtained.

However, we had no time to test other possibilities. Pursuing the work

on (p) $\mu\text{-Si:H}$ layers could be an interesting option, for emitters on (n) c-Si as well as for BSF on (p) c-Si wafers. Some more work would be needed since it is known that growing $\mu\text{-Si:H}$ on a-Si:H is more difficult than on glass or on c-Si.^{1,2,3} Indeed, we need to obtain a crystallized film with no incubation layer. One possible way to do so could be to use SiF_4 which has demonstrated to result in a more crystallized material,⁴ with excellent electrical properties when incorporated in a $\mu\text{-Si:H}$ p-i-n.⁵ It has also been shown that such a material could be easily doped, p- or n-type, with little impact with respect to the undoped material.⁶ Also, it could be interesting to work on higher bandgap materials such as (p) a-SiC:H layers for instance, used in a-Si:H p-i-n devices to increase the blue response.

3.4 Inside and outside collaborations on heterojunctions

So far, we have dealt with heterojunction solar cells made in a “traditional” way, where the cleaning was done by HF, where the silicon was monocrystalline and where we only used doped a-Si:H materials. In this section we will present the results we obtained from “alternative” routes we tried to follow. Indeed, we will present a few results obtained on multicrystalline silicon wafers, as well as the results obtained from plasma etching of the native oxide and finally we will introduce the heterojunction solar cells made using laser doping.

3.4.1 Multicrystalline silicon wafers

During this doctoral work, the LPICM was involved in two research projects that implied to study the viability of the use of multicrystalline silicon wafers to fabricate silicon heterojunction solar cells. The first one, MULTIXEN, was a French ANR contract whose main goal was to work on the development of solar grade n-type mc-Si. The fabrication of homojunction and heterojunction solar cells was part of this project. The second one, HETSI, was an European project targeting to the development of heterojunction solar cells on n-type material with industrial scale techniques. Also, some tasks of this project were devoted to mc-Si. For both of these projects, the mc-Si material was provided by the French photovoltaic company *Photowatt* that grew ingots especially for that pur-

¹Schüttauf, Komatsu, Geerligs, Mai, Bink, Spee, and Schropp, “Emitter Optimization on a-Si:H/c-Si Heterojunction Solar Cells for Isotextured Wafers”, 2008 [77]

²Olibet, “Properties of interfaces in amorphous / crystalline silicon heterojunctions”, 2009 [59]

³van Cleef, Rath, Rubinelli, van der Werf, Schropp, and van der Weg, “Performance of heterojunction p^{++} microcrystalline silicon n crystalline silicon solar cells”, 1997 [79]

⁴Djeridane, Abramov, and Roca i Cabarrocas, “Silane versus silicon tetrafluoride in the growth of microcrystalline silicon films by standard radio frequency glow discharge”, 2007 [80]

⁵Zhang, Johnson, Djeridane, Abramov, and Roca i Cabarrocas, “Decoupling crystalline volume fraction and V_{OC} in microcrystalline silicon pin solar cells by using a $\mu\text{-Si:F:H}$ intrinsic layer”, 2008 [81]

⁶Abramov, Djeridane, Vanderhaghen, and Roca i Cabarrocas, “Large grain $\mu\text{-Si:H}$ films deposited at low temperature: Growth process and electronic properties”, 2006 [82]

pose (instead of the usual p-type material).¹ Therefore, unlike the high quality Float-Zone monocrystalline silicon wafers of constant quality we regularly purchased from Topsil, we have been provided with wafers of various qualities and of various surface states. Indeed, on Fig. 3.27 we have plotted the effective lifetimes in solar cell structures deposited onto various silicon substrates having undergone different cleanings. Only the substrates from the HETSI project, the ones with very low lifetimes, had a thick (i) a-Si:H layer on both sides since we did not consider them as suitable for heterojunction solar cells. The lifetimes obtained in the passivated

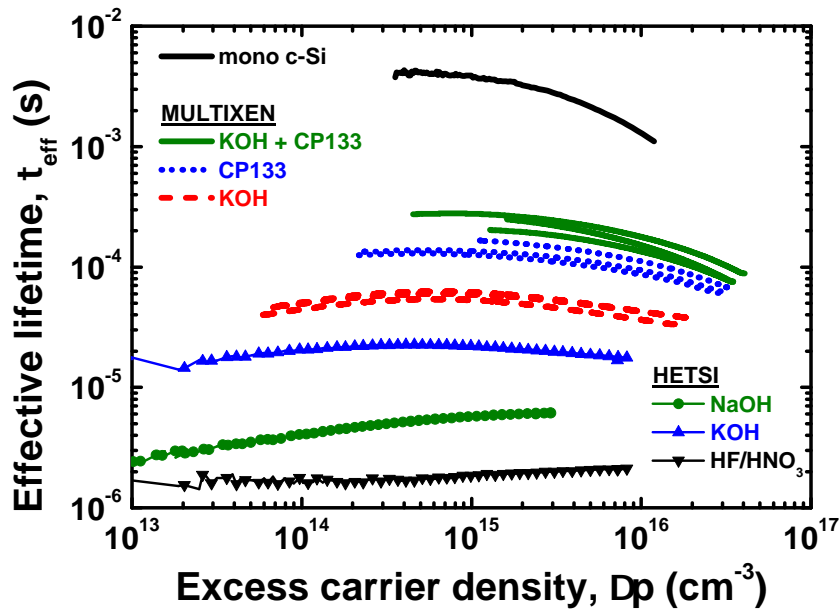


Figure 3.27 – Effective lifetimes in solar cell structures deposited on various mono and multicrystalline wafers

monocrystalline substrates were of course much higher than on any mc-Si substrates. However, the results obtained on the different mc-Si substrates were all extremely different. Unlike the monocrystalline c-Si wafers that were all polished on both sides and carefully cleaned, the mc-Si wafers were obtained by sawing ingots into wafers and then by chemically removing the saw damage. After that, the wafers underwent a chemical treatment of the surface. We did not have much details about the chemical treatments but they were designated on the graph of Fig. 3.27 by the chemical solutions: KOH; HF; HNO₃; NaOH; CP₁₃₃.² All the wafers had very similar resistivity, in the 1–5 Ω.cm range, for thicknesses of 220 μm, so that doping could not account for the difference observed in the effective lifetimes between the HETSI and MULTIXEN samples. Indeed, such a difference was more likely to originate from different surface states, since the MULTIXEN samples had been cleaned at the INES institute during the project, whereas the HETSI samples had been cleaned at Photowatt. Besides, it seemed that NaOH and HF/HNO₃ were not able to provide a

¹<http://www.photowatt.com/en/>

²CP₁₃₃ stands for Chemical Polishing 133 which consists of a solution of HF (50%), CH₃COOH, and HNO₃ in the ratio 1:3:3

nice surface state, as they were, in the HETSI samples, the ones with the lowest lifetimes suggesting that KOH would be preferable. And from the MULTIXEN samples it also seemed that KOH was not as good as a CP133 cleaning, or better than KOH+CP133 cleaning. Therefore it sounded reasonable to fabricate heterojunction solar cells on the MULTIXEN samples.

In Tab. 3.12 and 3.13 we present the solar cell parameters of two series of heterojunction solar cells on (n) mc-Si substrates with different surface treatments. The main difference between these two series was the thickness of the (i) a-Si:H layer, which was increased for the second series.

Surface treatment	V_{oc} (mV)	J_{sc} (mA.cm ⁻²)	FF (%)	η (%)
KOH + CP133	622	26.6	72.9	12.1
KOH + CP133	630	26.2	73.8	12.2
KOH	582	25.9	70.8	10.7
KOH	586	27.2	70.5	11.2
KOH	582	26.4	70.6	10.9
CP133	615	26.2	71.3	11.5
CP133	620	27.8	71.7	12.4
CP133	612	27.2	72.6	12.1

Table 3.12 – Solar cell parameters on (n) mc-Si substrates of different surface states on 25 cm², thin (i) a-Si:H series

Surface treatment	V_{oc} (mV)	J_{sc} (mA.cm ⁻²)	FF (%)	η (%)
KOH + CP133	639	29.2	68.8	12.8
KOH + CP133	637	29.2	69	12.8
KOH	577	28.3	57.8	9.4
KOH	575	28.5	68.1	11.2
KOH	578	28.4	64.8	10.6

Table 3.13 – Solar cell parameters on (n) mc-Si substrates of different surface states on 25 cm², thick (i) a-Si:H series

As one can see, there were several differences. The two most remarkable ones were the increase in V_{oc} and fall in FF for the cells with a thicker (i) a-Si:H buffer layer (Tab. 3.13) on the KOH+CP133 samples. This increase in V_{oc} was due to the thicker (i) a-Si:H layer which resulted in a decreased defect density, as confirmed by the lifetime measurements. The fall in FF was due to an increased series resistance due to this thicker undoped layer as it had already been observed on flat monocrystalline silicon wafers. However, the V_{oc} did not seem to change for the KOH samples. One possible explanation for this behaviour was that the surface after the HF dip still contained a lot of defects, due to the KOH texturing, that could not be all passivated. So there was a lower limit for the interface defect density, with our layers, imposed by the wafer. Such a limit was increased when a CP133 cleaning step was applied to the wafer after the KOH texturing.

Also one can see a difference in the J_{sc} values between the first and second series, and also a much bigger scattering of the J_{sc} values for the first series that could be explained by the fact that for these cells the multi print steps were not perfectly aligned, so that a bigger shadowing coupled

to some aluminium paste droplets left by an aged screen on the ITO surface led to a poorer J_{sc} . All this meant that it was more a technological issue than a physical difference in the solar cells themselves.

As already pointed out, the thickness of the undoped layer was not so easy to adjust. On mc-Si substrates it became even more critical since we have used here KOH, hence anisotropic etchings: the (100)-oriented grains would be etched, revealing (111) pyramid-like facets,^{1,2} whereas (111)-oriented grains would develop step structures.³ More generally we had different etching rates depending on the crystalline orientations. Fig.3.28 shows a SEM picture obtained on one of our mc-Si substrates.

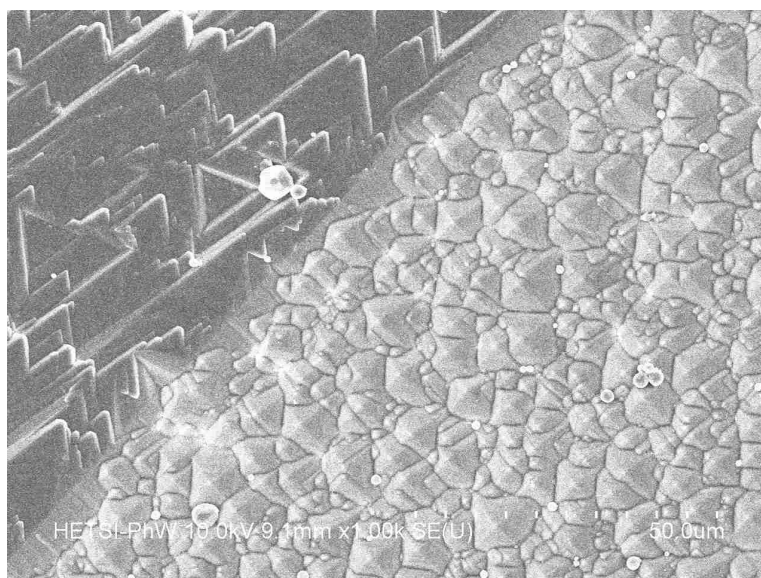


Figure 3.28 – SEM picture of a HETSI mc-Si sample

On this picture, we can see two distinct areas on the surface: one with pyramids (right) and one without (left). In that case we could expect to encounter one major issue on such substrates, due to the fact that a-Si:H films deposited by PECVD, in our conditions, were conformal.⁴ Hence we would have different deposition rates in the direction perpendicular to the local surface, as it has already been confirmed on thin a-Si:H films grown on textured silicon wafers by TEM.^{5,6} Therefore, we would have different passivation properties and diode quality depending on the grains, making the optimization of the cells extremely difficult. Additionally, one should note that this issue also applied for the ITO sputtering, having made it harder to obtain an efficient anti-reflection coating everywhere.

¹Barycka and Zubel, "Silicon anisotropic etching in KOH-isopropanol etchant", 1995 [83]

²Lee, "Anisotropic Etching of Silicon", 1969 [84]

³Shikida, Tokoro, Uchikawa, and Sato, "Surface morphology of anisotropically etched single-crystal silicon", 2000 [85]

⁴Tsai, Knights, Chang, and Wacker, "Film formation mechanisms in the plasma deposition of hydrogenated amorphous silicon", 1986 [86]

⁵Olibet, Monachon, Hessler-Wyser, Vallat-Sauvain, De Wolf, Fesquet, Damon-Lacoste, and Ballif, "Textured silicon heterojunction solar cells with over 700 mV open-circuit voltage studied by Transmission Electron Microscopy", 2008 [4]

⁶Wang, Page, Iwaniczko, Xu, Roybal, Bauer, To, Yuan, Duda, and Yan, "Crystal silicon heterojunction solar cells by hot-wire CVD", 2008 [87]

As a confirmation we have shown on Fig. 3.29, a mapping of the lifetime on a quarter of 4 in. c-Si wafer (left) and on a truncated $5 \times 5 \text{ cm}^2$ mc-Si substrate (right), both passivated by a thick (i) a-Si:H film on both sides.

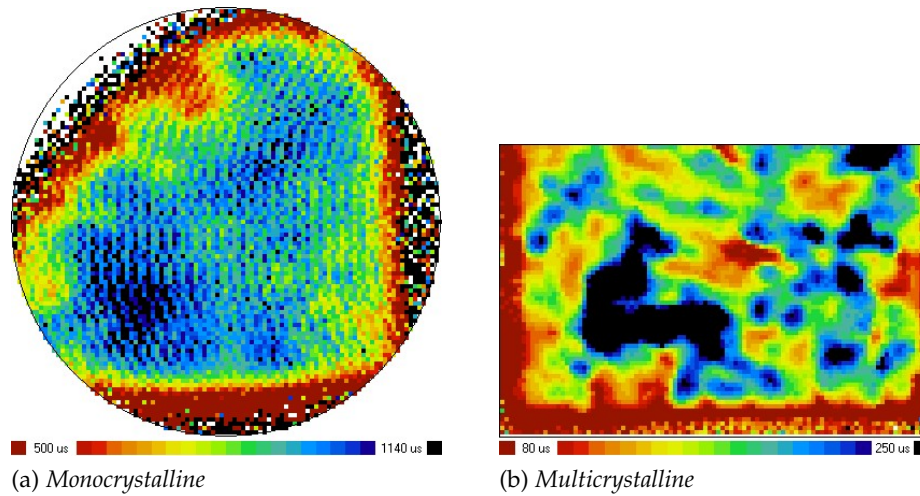


Figure 3.29 – $\mu\text{W-PCD}$ mapping of the effective lifetime in monocrystalline (left) and multicrystalline (right) silicon substrates capped by a thick (i) a-Si:H layer. Note the difference in the colour scales

These mappings have been obtained at INES, using a $\mu\text{W-PCD}$ equipment from Semilab.¹ This set-up measured the effective lifetime, like the Sinton lifetime tester, but allowed for a mapping instead of averaging it. It measured the reflection coefficient of micro-waves, which depends on the conductivity (carrier concentration), as a function of time, after the carriers have been photogenerated by a pulsed laser operating at a wavelength of 904 nm and a power density of 1320 W.cm^{-2} . This technique did not allow for an injection level dependent measurement but allowed for a mapping since the micro-wave can be extremely localized. On these two images, we could see that the mc-Si sample exhibited much higher variations in lifetime that we could not find on the c-Si substrate. The lower lifetimes on the edges on both images were due to the absence of a-Si:H deposition, because of our substrate holders.

3.4.2 Plasma cleaning

The hydrofluoric acid (HF) we use to remove the native oxide is extremely dangerous. Besides being an acid, the presence of fluorine can lead to extremely severe injuries if not death. When handling such a product one has to be very careful and use all the protective equipments² designed for that purpose. However, replacing such a wet cleaning step, which means huge amounts of HF at the industrial level, could be very interesting in the perspective of reducing costs and safety issues and allowing for a one pump down process (no vacuum break during the process from the wafer to the cell). Some work was also carried out on plasma texturing by Reactive Ion Etching with processes involving $\text{SF}_6 + \text{O}_2$ mixtures by *Moreno*

¹<http://www.semilab.com/technologies/si/%C2%B5-pcd-lifetime>

²Nitrile gloves, goggles, safety cloth, Teflon flat beaker, dedicated containers for used solutions collection

*et al.*¹ Here we focused on what could be effectively implemented in a RF PECVD reactor.

Plasma etching is a very important field of plasma physics since it has many applications in the semiconductor industry and has been studied by many research groups. A lot of material has already been published on this topic and a reference textbook has been written by *M.A. Lieberman*.² CF_4 is one of the most common halogen based gases used for etching purposes. Another one is silicon tetrafluoride (SiF_4). In our laboratory, under some conditions SiF_4 could be used for depositions, as it was for instance the case for $\mu\text{c-Si:H}$.³ Fortunately, it is known that both Si and SiO_2 can be etched by plasma. SiO_2 can for instance be etched by CF_4 or CHF_3 ,⁴ but also XeF_2 , F_2 and Cl_2 .^{5,6} Etching mechanism of Si ⁷ and SiO_2 [90] by fluor have been proposed. All the studies agree on the fact that SiF_4 is the main etch product. Also, in the presence of silicon oxide, and using no carbon containing gas, O_2 is an other major reaction product in the case of SiO_2 etching [92].

A few plasma cleaning trials had already been carried out a few years ago in our laboratory using SiF_4 ,⁸ or in other laboratories using CF_4 based gas mixtures,⁹ in order to remove the native oxide from c-Si wafers before a-Si:H depositions. However, in both cases the results were not very satisfactory, and since then not much has been published on this topic, i.e. for heterojunction purposes.

Recently, some work was carried out in our laboratory by *Mario Moreno*.¹⁰ A standard RF PECVD reactor mounted with an in-situ ellipsometer was used. As we know, the imaginary part of the dielectric function of c-Si possesses two sharp peaks at 3.4 and 4.2 eV. As being at a higher energy, and based on the fact that the absorption coefficient of c-Si increases with the photon energy, it is the second peak (4.2 eV) which is of interest for us with our SE set-up since the presence of a thin oxide layer is extremely easily noticeable, as one can see in *Moreno et al.*'s paper [95]. In the case of native oxide the thickness is about 12 Å.

We knew that we could optically monitor the state of the surface, then we had to find the optimal conditions to etch the native oxide. The study

¹Moreno, Daineka, and Roca i Cabarrocas, "Plasmas for texturing, cleaning, and deposition: towards a one pump down process for heterojunction solar cells", 2010 [88]

²Lieberman and Lichtenberg, *Principles of Plasma Discharges and Materials Processing, Second Edition*, [89]

³Djeridane, Abramov, and Roca i Cabarrocas, "Silane versus silicon tetrafluoride in the growth of microcrystalline silicon films by standard radio frequency glow discharge", 2007 [80]

⁴Steinbrüchel, Lehmann, and Frick, "Mechanism of Dry Etching of Silicon Dioxide", 1985 [90]

⁵Coburn and Winters, "Ion- and electron-assisted gas-surface chemistry—An important effect in plasma etching", 1979 [91]

⁶Winters, "Etch products from the reaction of XeF_2 with SiO_2 , Si_3N_4 , SiC , and Si in the presence of ion bombardment", 1983 [92]

⁷Flamm, Donnelly, and Mucha, "The reaction of fluorine atoms with silicon", 1981 [93]

⁸Damon-Lacoste, "Vers une ingénierie de bandes des cellules solaires à hétérojonctions a-Si:H/c-Si. Rôle prépondérant de l'hydrogène.", 2007 [5]

⁹Tucci, Salurso, Roca, and Palma, "Dry cleaning process of crystalline silicon surface in a-Si:H/c-Si heterojunction for photovoltaic applications", 2002 [94]

¹⁰Moreno, Labrune, and Roca i Cabarrocas, "Dry fabrication process for heterojunction solar cells through in-situ plasma cleaning and passivation", 2010 [95]

was summarized below and emphasis has been put on the tests carried out to transfer the ARCAM plasma reactor, more suitable to fabricate devices and able to handle 4 in. wafers. When the c-Si wafer with its native oxide was placed on the substrate holder of the reactor, the ellipsometer was set to measure in real-time the value of the imaginary part of the pseudo-dielectric function of our wafer at 4.2 eV. Several gas mixtures composed of H₂ and SiF₄ were tried. It was found that the maximum achievable ϵ_i value at 4.2 eV was when only SiF₄ was present. The initial goal was to use this cleaning approach for passivation so that a subsequent (i) a-Si:H deposition was used to assess the quality of the passivation. After the SiF₄ cleaning, and without any additional treatment, the passivation was much lower than the one we could get from the same a-Si:H layer deposited on a wafer cleaned by HF. Among various plasma treatments, it was shown that a very short hydrogen plasma on the surface of the wafer could drastically (roughly one order of magnitude) increase the passivation obtained from the subsequent a-Si:H deposition. A plausible explanation could be the fact that when SiF₄ is used, only F and Si atoms are present, whereas we know that the best state for passivation and subsequent a-Si:H growth of the Si surface is to be H-terminated. We could expect a very short hydrogen treatment to remove some of the left F atoms and leave an H-terminated surface, similarly to what happens with wet HF-dips.¹

Based on these experiments we tried to apply these results to the ARCAM reactor. One of the main advantages of such CCP RF PECVD reactors is that we have the ability to transfer processes from one reactor to another quite easily. However, in our case, the main drawback was that the PECVD reactor used for the initial studies (of Ref. [95]) had an in-situ ellipsometer, which was not the case of the ARCAM reactor.² Thus we had not the possibility to monitor the ϵ_i value at 4.2 eV in real-time and we had to perform passivation studies afterwards.

A few samples, including solar cells, were fabricated in order to check the validity of such a cleaning. For these experiments, we used inter-electrode distance of 28 mm, with a SiF₄ flow rate of 30 sccm, and the pressure was adjusted to be of 40 mTorr. The power and exposure time were varied. On Fig. 3.30, we have plotted the effective lifetimes obtained by the deposition of a 20 nm a-Si:H film. In all cases, after SiF₄ etching, a hydrogen plasma treatment of 10 seconds was applied under a pressure of 1 Torr and a power of 30 mW.cm⁻². On Fig. 3.30, we have also indicated the plasma power and duration.³ As an indication we have also measured the effective lifetime in a silicon wafer on which we had deposited 20 nm of a-Si:H without removing the native oxide, in order to highlight the fact that native silicon oxide did not provide a good passivation, even if capped by a passivation layer. A bare wafer (with oxide) exhibits lifetimes of a few μ s.

From this graph it appeared that when a too low power (2W) was used, the etching was incomplete and the lifetimes remained too low. Lifetimes could indeed increase but saturated for the longest plasma dura-

¹Trucks, Raghavachari, Higashi, and Chabal, "Mechanism of HF etching of silicon surfaces: A theoretical understanding of hydrogen passivation", 1990 [96]

²For safety and usability reasons.

³In our configuration, a power of 2 Watts translates into a power density of 12 mW.cm⁻².

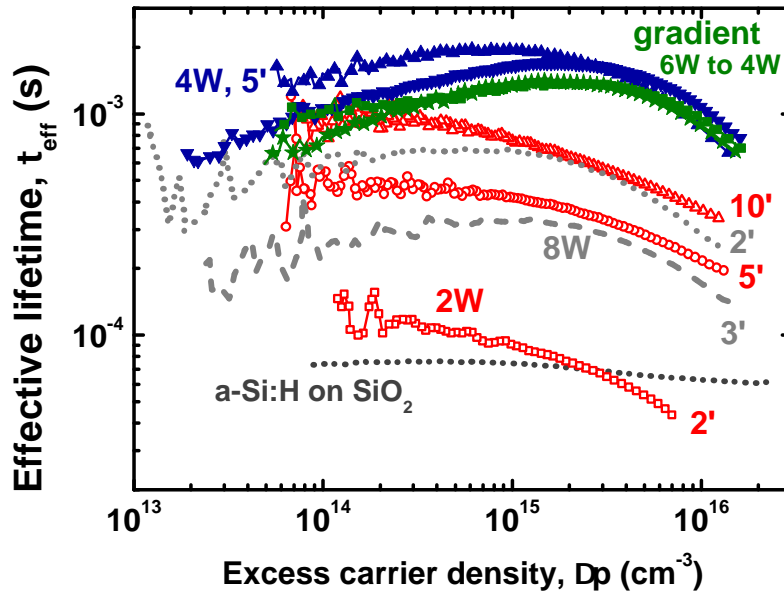


Figure 3.30 – Effective lifetimes in symmetrical samples with 20 nm of a-Si:H for various powers and durations of SiF₄ etching plasma.

tions. Contrariwise, when a too high power (8 W) was used, the lifetimes remained even lower and decreased with longer plasma times. Therefore, some optimum process conditions must exist between these two extreme cases. Using a gradient of power, starting from very aggressive conditions to promote SiO₂ etching and then decreasing the power in order to avoid c-Si surface damage by ion bombardment may seem reasonable. Similarly, using moderate (4 W) powers should also lead to trade off between the defect creation and the efficient etching. On the graph, it can be seen that the best lifetimes were obtained using either a moderate power or a power gradient. So far these effective lifetimes remained lower than those obtained with a HF cleaning but for symmetrical (i) a-Si:H layers, implicit V_{oc} of 700-710 mV could be obtained. However, it also appeared to us that such depositions were not so easy to reproduce and that an extremely careful control of the conditions would be needed.

In this way, we have been able to fabricate solar cells for which the native oxide of both side was removed using this approach. For this cells we used a 4 Watts SiF₄ plasma. The solar cell parameters of two cells are shown in Tab. 3.14. These cells were back-ended at INES and measured there. These results were obtained after a 10 minutes annealing at 170°C. Even if these solar cell parameters remained slightly inferior to those obtained with a HF dip these results were a successful proof of concept of the dry plasma cleaning method.

Sample name	V _{oc} (mV)	J _{sc} (mA.cm ⁻²)	FF (%)	η (%)
9091413	685	29.5	72.4	14,6
9041415	698	29.9	72.2	15.1

Table 3.14 – Solar cell parameters of two cells whose native oxide was removed by a SiF₄ plasma etching.

3.4.3 Laser Fired Contacts (LFC)

As we have seen, obtaining a good passivation with p-type layers has always been more challenging than for n-type layers, and unfortunately we cannot fabricate heterojunction devices without such a layer, whatever the doping type of the wafer is. However, it is possible not to deposit a p-type layer but rather to deposit an intrinsic layer that will be used as a passivation layer and fire, with a laser, p-type dopants through this dielectric barrier.¹ This is what we call Laser Fired Contacts (LFC) solar cells. This was a collaboration with *Dr. Isidro Martín García* from the *Universitat Politècnica de Catalunya* (UPC). We will first describe more specifically how such a cell works and then the encouraging results obtained with it.

3.4.3.1 Laser firing

During our study, we only worked on (p) c-Si wafers, but this could also be applied to (n) c-Si wafers to realize structures like inverted emitters for instance or maybe inter-digitated back contacted solar cells (patent filed). For the configuration on (p) c-Si wafer, we realized an emitter by using a stack made of a thin (i) a-Si:H layer capped by a (n) a-Si:H layer, like we would have done for a full heterojunction solar cell. At the back side of the solar cell we needed a highly passivating layer to ensure a high V_{oc} but we did not need it to be doped since the electrical transport would not occur through this layer but rather through the fired contacts. This layer could be made of a-Si:H, a-SiC:H, a-SiN:H, etc. On top of this layer we grew a thick aluminium layer. Then a pulsed laser fired regularly to create $\approx 100 \mu\text{m}$ wide contacts, the distance between two spots is called the pitch. The strong local heating made the aluminium and the silicon melt. The aluminium and the silicon inter-diffused and upon solidification some aluminium remained in the dielectric layer and in the wafer itself where it created locally a highly doped p-type material that we would use as a base contact. The firing step was performed at the UPC laboratory and the process parameters were described elsewhere.² Quickly we can say that it used a 100 ns pulsed Nd:YAG LASER (1064 nm) operating at a frequency of 8 kHz. The solar cell fabrication has been summarized on Fig. 3.31 and 3.32. On Fig. 3.31, we have shown the solar cell precursor before the laser firing step. The pulsed laser firing was performed at the back side of the solar cell, the spots creating a regular pattern of squares whose 4 corners are occupied by a spot and whose side length is called the pitch and was varied between 0.4 and 1.5 mm.

On Fig. 3.32 we have shown the schematic view of the LFC solar cell after the firing step. For all the work on LFC, we sputtered ITO on top of the emitter and sent the wafers to UPC where ITO squares of $2 \times 2 \text{ cm}^2$ or $1 \times 1 \text{ in.}^2$ were defined by lithography, a front contact silver grid was evaporated and a $2 \mu\text{m}$ thick aluminium layer was evaporated at the back before the laser was fired to create the p+ contacts.

¹Preu, Schneiderlochner, Grohe, Glunz, and Willeke, "Laser-fired contacts - transfer of a simple high efficiency process scheme to industrial production", 2002 [97]

²Muñoz, Voz, Blanque, Ibarz, Bertomeu, and Alcubilla, "Development of laser-fired contacts for amorphous silicon layers obtained by Hot-Wire CVD", 2009 [98]

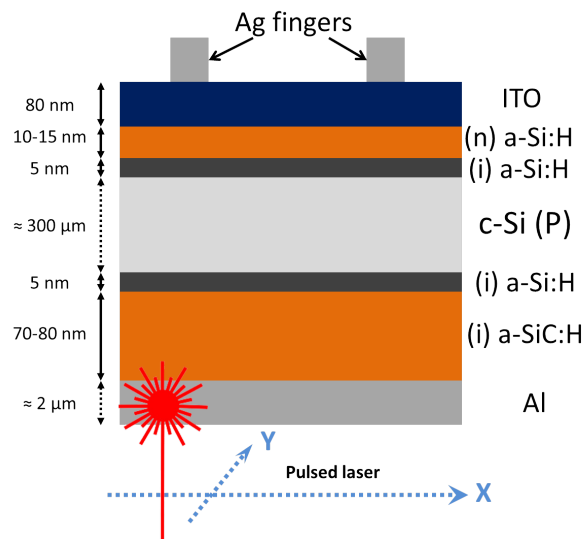


Figure 3.31 – Schematic view of the future Laser Fired Contacts solar cell structure before the laser firing of the thick dielectric back surface passivation layer

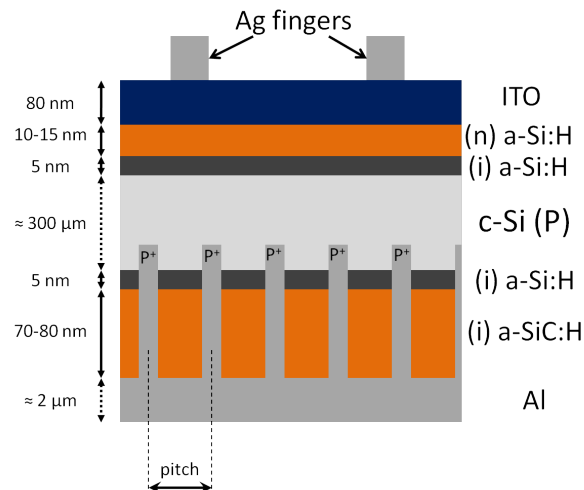


Figure 3.32 – Schematic view of the Laser Fired Contacts solar cell structure after the laser firing of the thick dielectric back surface passivation layer

3.4.3.2 LFC and full heterojunction cells

Unlike full heterojunction cells, the back contact of LFC cells was not made on the entire surface but rather on very localized point contacts. The consequence of this is that both the wafer resistivity and the pitch value were of great importance. We will present the results we obtained on two different (p) c-Si wafers:

- $\rho = 1.5 \text{ } \Omega \cdot \text{cm}$, thickness = 280 μm , (100)-oriented, Float-Zone
- $\rho = 0.8 \text{ } \Omega \cdot \text{cm}$, thickness = 390 μm , (100)-oriented, Float-Zone

The front emitter consisted of a 14 nm thick (i)+(n) a-Si:H stack capped by a 80 nm thick ITO layer in all the samples. On the back side, we deposited either 25 nm of a (i)+(p) a-Si:H stack (full heterojunction) or 80 nm of a-Si_x:H (LFC solar cell). The effective lifetimes in these samples have been plotted on Fig. 3.33. These lifetimes were measured just after

deposition. Neither the ITO sputtering nor the laser firing had already occurred. The bulk lifetime of the 0.8 $\Omega\cdot\text{cm}$ wafer was expected to be lower than the one of the 3 $\Omega\cdot\text{cm}$ wafer so that any comparison between effective lifetimes should be done for the same wafer resistivity. However, in order to compare the four samples one to each other, we extracted the value of the implicit V_{oc} of these samples and indicated them in Tab. 3.15

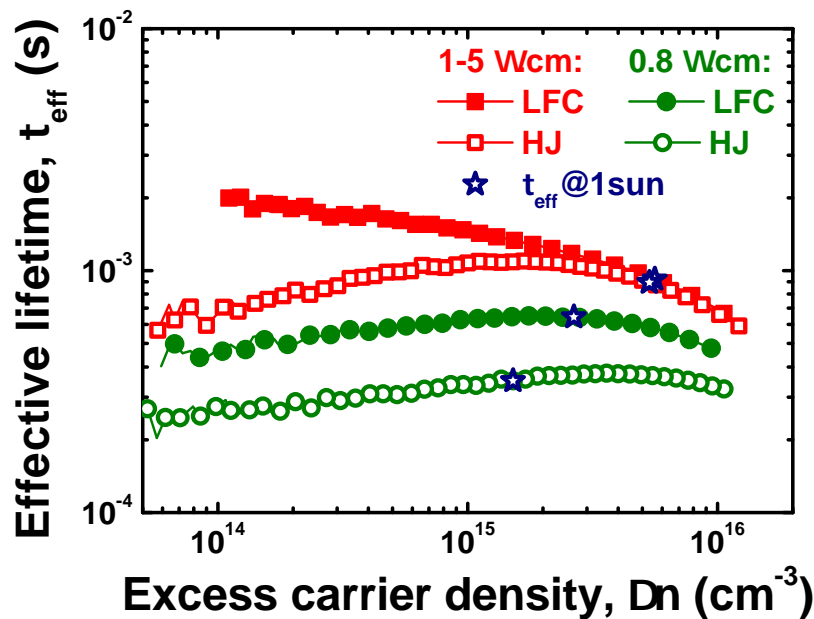


Figure 3.33 – Effective lifetimes in the heterojunction and LFC samples measured in the as-deposited state, before any ITO deposition or laser firing

Sample	c-Si resistivity ($\Omega\cdot\text{cm}$)	Structure	Impl. V_{oc} (mV)
1003178	0.8	Heterojunction	688
1003177	0.8	LFC	704
10031615	1–5	Heterojunction	702
10031612	1–5	LFC	702

Table 3.15 – Implicit V_{oc} of the heterojunction and LFC samples measured in the as-deposited state, before any ITO deposition or laser firing step

These results showed that in both cases the passivation was similar or superior when the solar cell was in the LFC configuration as we expected. It should also be noted that the passivation of the more doped substrates was more difficult to achieve in the HJ case since it was more difficult to obtain the so-called high–low junction on such highly doped substrates. Also, the passivation was better at low injection for the LFC samples but it was not expected to affect the performance of the solar cells.

The laser firing was performed on the LFC samples with four different pitch values: 0.4, 0.7, 1 and 1.5 mm. We measured the current-voltage characteristics of the solar cells under AM1.5 and plotted the values of the open-circuit voltage (V_{oc}) and the fill factor (FF) as a function of the pitch value (HJ refers to the heterojunction sample) on Fig. 3.34. On this graph it appeared first that the actual V_{oc} value remained close to that of the im-

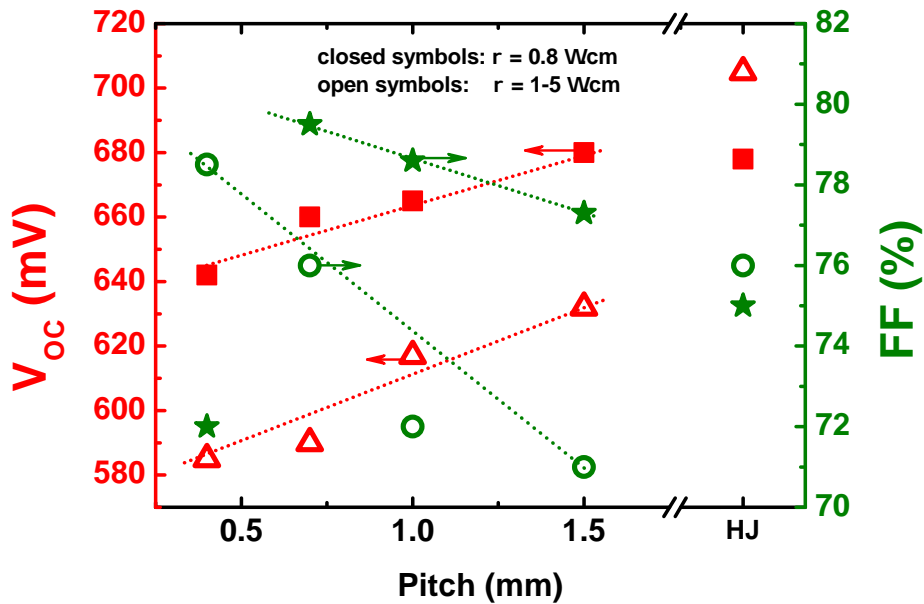


Figure 3.34 – V_{oc} and FF of the solar cells as a function of the pitch value for the 0.8 $\Omega\cdot\text{cm}$ wafers (closed symbols) and for the 1–5 $\Omega\cdot\text{cm}$ (open symbols). HJ refers to the full heterojunction sample

implicit V_{oc} in the case of the full heterojunction samples. This makes sense if we keep in mind that these samples did not undergo any laser firing after the deposition of the a-Si:H layers. However, when the contacts were made by laser firing the V_{oc} was much smaller than the implicit V_{oc} value and was quite proportional to the pitch value. We expected the laser firing to greatly increase the back surface recombination velocity and by doing so to decrease the V_{oc} of the solar cell. Also, the more doped the substrate, the less sensitive to surface recombination velocity, so that the fall in V_{oc} was much more dramatic with the 1–5 $\Omega\cdot\text{cm}$ samples. This could be confirmed by numerical simulations done in collaboration with UPC, where the V_{oc} could be fitted to a model that allowed to determine the rear surface passivation, and could also be confirmed by EQE measurements. Indeed, we have shown on Fig. 3.35 the external quantum efficiency measured on different samples made on 0.8 $\Omega\cdot\text{cm}$ wafers: a full heterojunction and LFC samples of different pitch values (0.4, 0.7, 1 and 1.5 mm). It is known that an increase in the back surface recombination results in a poorer collection in the long wavelength part of the absorbed spectrum, which is what we observed on Fig. 3.35 where the heterojunction had a higher quantum efficiency than the LFC samples in the 900–1100 nm range due to a lower back surface recombination. And this decrease in the quantum efficiency got more pronounced as the pitch value was decreased, which was consistent with the fact that the mean back surface recombination velocity was expected to increase. Some electro-luminescence monitoring could also be performed on these samples resulting in the picture shown on Fig. 3.36 (top view of the cell), where we measured the EL signal on a LFC solar cell with a pitch of 1.5 mm. We did not use the EL set-up but as a quantitative tool as a qualitative observation of the enhancement (darkening of

the picture) of the recombination at the localized contacts. The spots have a radius of about $200\ \mu\text{m}$, wider than the dimension determined by optical microscopy. The dark lines correspond to the silver grid on top of the cell which is blocking the light.

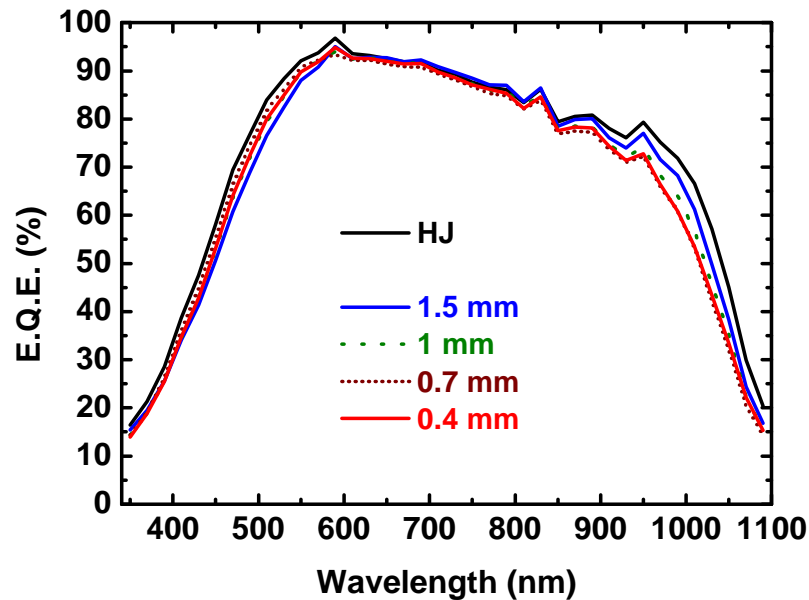


Figure 3.35 – External quantum efficiency of the samples made on $0.8\ \Omega\cdot\text{cm}$ wafer for a full heterojunction and for LFC samples with pitches of 0.4, 0.7, 1 and 1.5 mm.

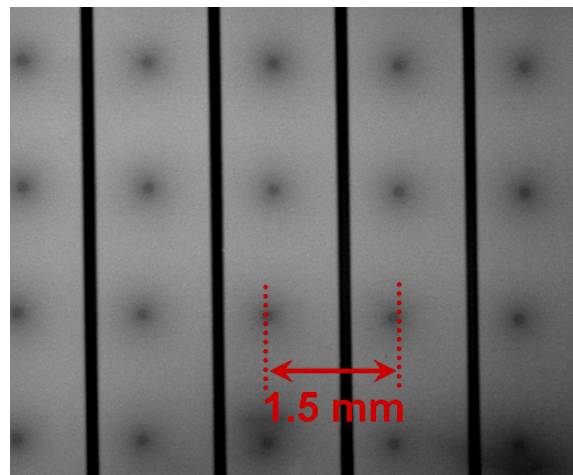


Figure 3.36 – Electro-luminescence of a LFC solar cell on a $0.8\ \Omega\cdot\text{cm}$ wafer

In the meantime, decreasing the pitch value should result in a much higher contact density that should lead to an enhanced carrier collection and thus in a higher fill factor, which was indeed observed on Fig. 3.34. Given that the efficiency is proportional to the product of V_{oc} , FF and J_{sc} , and that V_{oc} and FF follow opposite trends, we expect to have an optimum for the efficiency in the case of LFC solar cells. Indeed, on Tab. 3.16 we have shown the solar cell parameters of the full heterojunction and the best LFC solar cell among those made on $0.8\ \Omega\cdot\text{cm}$ wafers. These results

Sample	V_{oc} (mV)	FF (%)	J_{sc} (mA.cm ⁻²)	η (%)
Heterojunction	678	75	31	15.8
LFC 1 mm	665	78.6	30.6	16

Table 3.16 – Efficiencies comparison between the full heterojunction and the best LFC solar cell made on 0.8 Ω .cm wafers

indicated that LFC solar cells compared favourably with full heterojunction solar cells in terms of efficiency. Unfortunately, as this was mostly a side project, we did not work more on this topic but we could expect that working on the laser firing optimization and developing new dielectric layers, more robust to the firing step, could lead to an increase in the efficiency. Indeed, the choice of the back side passivation layer can have an important impact on the device: the first tests we did on 1–5 Ω .cm were done by using a thick (i) a-Si:H (not alloyed), that gave an excellent passivation, before firing, similar to those we would obtain by using the a-SiC_x:H layer we used afterwards, but that could not resist to the firing and resulted in V_{oc} 10 to 20 mV smaller than with the a-SiC_x:H layer.

3.5 Conclusions

In this chapter we have demonstrated the very negative impact that epitaxial growth, easily occurring on (100) surfaces, could have on surface passivation, no matter the film deposited on top of the epitaxial layer. We therefore investigated three ways to avoid epitaxy. The first one consisted in lowering the substrate temperature to obtain a purely amorphous, and quite defective growth, resulting in low lifetimes which would be increased by 2 to 3 orders of magnitude by post-deposition annealing. However, it turned out that even if i and i/n stacks could greatly be improved upon annealing, the effect was always very limited for i/p stacks, making the entire process unsuitable. The second one consisted in exposing the crystalline silicon surface to an argon bombardment resulting in a subsequent amorphous growth. Even if it demonstrated to hinder epitaxial growth and showed promising results, it appeared to be not so reproducible, in addition to not being an industrial solution. The third way, the successful one, was to introduce some methane at the beginning of the deposition in order to promote an amorphous growth. After 30 seconds, methane could be removed from the gas mixture and the deposition can go on. By doing so we could prevent the epitaxial growth on any crystalline orientation and such layers proved to have similar passivation properties to device grade a-Si:H films without methane. This procedure was extremely simple, reproducible, scalable, and hardly altered the process.

The following step was to optimise the p and n-type layers in order to get the highest passivation and the best solar cell parameters. The (p) a-Si:H layer was found to be much more difficult to optimize than the (n) a-Si:H. However, depositing in argon dilution proved to lead to slightly higher lifetimes, and consecutively higher V_{oc} . Also, we demonstrated the prominent role of the insertion of a thin, undoped, amorphous layer between the substrate and the doped a-Si:H layer in increasing the V_{oc} . That

was of much lesser importance in the (n) a-Si:H case. These optimisations led to solar cells with stable V_{oc} above 710 mV and an efficiency of 17.2% on 4 cm² on flat wafers.

Some work was also carried out on multicrystalline silicon substrates. This work highlighted the fact that the optimisation on anisotropic textured wafers was difficult due to the very different surface morphologies depending on the initial grain orientation and the fact that the surface state determined by the chemical cleaning imposed the upper limit of the surface recombination velocity, for wafers from the same brick and with similar bulk lifetimes. Best cells had a 12.8% efficiency for a V_{oc} of 638 mV.

We also implemented the removal of the native oxide of our wafers by a SiF₄ plasma etching which resulted, after a first optimization round, in solar cells with a best V_{oc} of 698 mV, very close to the ones obtained with a standard HF-dip.

Finally, we also did some research on (p) c-Si, in collaboration with the UPC of Barcelona, in which the emitter was formed by a (n) a-Si:H whereas on the back side a thick a-SiC_x:H layer was deposited. A thick aluminium film was evaporated before being laser fired to create contacts in the (p) c-Si base by the melting induced diffusion of aluminium and silicon. A comparison with (p) a-Si:H back side was performed for different c-Si resistivities. The potential of such a structure was demonstrated on the more doped wafers.

REFERENCES

- [1] S. De Wolf and M. Kondo. "Abruptness of a-Si:H/c-Si interface revealed by carrier lifetime measurements". In: *Applied Physics Letters* 90, 042111 (2007), p. 042111. DOI: 10.1063/1.2432297 (cit. on pp. 82, 83, 87, 88, 96).
- [2] H. Fujiwara and M. Kondo. "Effects of a-Si:H layer thicknesses on the performance of a-Si:H/c-Si heterojunction solar cells". In: *Journal of Applied Physics* 101, 054516 (2007), p. 054516. DOI: 10.1063/1.2559975 (cit. on pp. 82, 116).
- [3] J.J.H. Gielis, B. Hoex, P.J. van den Oever, M.C.M. van de Sanden, and W.M.M. Kessels. "Silicon surface passivation by hot-wire CVD Si thin films studied by in situ surface spectroscopy". In: *Thin Solid Films* 517 (2009), pp. 3456–3460. DOI: 10.1016/j.tsf.2009.01.076 (cit. on pp. 82, 83).
- [4] S. Olibet, C. Monachon, A. Hessler-Wyser, E. Vallat-Sauvain, S. De Wolf, L. Fesquet, J. Damon-Lacoste, and C. Ballif. "Textured silicon heterojunction solar cells with over 700 mV open-circuit voltage studied by Transmission Electron Microscopy". In: *23rd European Photovoltaic Solar Energy Conference, 1-5 September, Valencia, Spain. 2008* (cit. on pp. 82, 124).
- [5] Jérôme Damon-Lacoste. "Vers une ingénierie de bandes des cellules solaires à hétérojonctions a-Si:H/c-Si. Rôle prépondérant de l'hydrogène." PhD thesis. École Polytechnique, 2007. URL: http://tel.archives-ouvertes.fr/docs/00/25/95/75/PDF/Damon-Lacoste_These_protege.pdf (cit. on pp. 82, 104, 117, 126).
- [6] J. Damon-Lacoste and P. Roca i Cabarrocas. "Toward a better physical understanding of a-Si:H/c-Si heterojunction solar cells". In: *Journal of Applied Physics* 105, 063712 (2009), p. 063712. DOI: 10.1063/1.3091283 (cit. on pp. 82, 92, 104).
- [7] D. Levi, E. Iwaniczko, M. Page, Q. Wang, H. Branz, and T. Wang. "Silicon Heterojunction Solar Cell Characterization and Optimization using in Situ and Ex Situ Spectroscopic Ellipsometry". In: *Photovoltaic Energy Conversion, Conference Record of the 2006 IEEE 4th World Conference on*. Vol. 2. May 2006, pp. 1740–1743. DOI: 10.1109/WCPEC.2006.279828 (cit. on p. 83).
- [8] H. Fujiwara and M. Kondo. "Impact of epitaxial growth at the heterointerface of a-Si:H/c-Si solar cells". In: *Applied Physics Letters* 90, 013503 (2007), p. 013503. DOI: 10.1063/1.2426900 (cit. on p. 83).
- [9] R.A. Street. *Hydrogenated Amorphous Silicon*. Ed. by Cambridge University Press. 1991 (cit. on pp. 83, 84).

- [10] Pere Roca i Cabarrocas. "Deposition of intrinsic, phosphorus-doped, and boron-doped hydrogenated amorphous silicon films at 50°C". In: *Applied Physics Letters* 65 (1994), pp. 1674–1676. DOI: 10.1063/1.112882 (cit. on p. 83).
- [11] S. De Wolf, S. Olibet, and C. Ballif. "Stretched-exponential a-Si:H/c-Si interface recombination decay". In: *Applied Physics Letters* 93, 032101 (2008), p. 032101. DOI: 10.1063/1.2956668 (cit. on p. 84).
- [12] T. F. Schulze, H. N. Beushausen, T. Hansmann, L. Korte, and B. Rech. "Accelerated interface defect removal in amorphous/crystalline silicon heterostructures using pulsed annealing and microwave heating". In: *Applied Physics Letters* 95, 182108 (2009), p. 182108. DOI: 10.1063/1.3255018 (cit. on p. 84).
- [13] D. Pysch, J. Ziegler, J.-P. Becker, D. Suwito, S. Janz, S. W. Glunz, and M. Hermle. "Stretched-exponential increase in the open-circuit voltage induced by thermal annealing of amorphous silicon-carbide heterojunction solar cells". In: *Applied Physics Letters* 94, 093510 (2009), p. 093510. DOI: 10.1063/1.3083552 (cit. on p. 84).
- [14] T. F. Schulze, H. N. Beushausen, C. Leendertz, A. Dobrich, B. Rech, and L. Korte. "Interplay of amorphous silicon disorder and hydrogen content with interface defects in amorphous/crystalline silicon heterojunctions". In: *Applied Physics Letters* 96, 252102 (2010), p. 252102. DOI: 10.1063/1.3455900 (cit. on pp. 84, 93, 94, 100).
- [15] J. P. Kleider, C. Longeaud, and P. Roca i Cabarrocas. "Experimental evidence for the annealing of surface defects in a-Si:H during deposition". In: *Journal of Applied Physics* 72 (1992), pp. 4727–4731. DOI: 10.1063/1.352079 (cit. on p. 85).
- [16] M. Sebastiani, L. Di Gaspare, G. Capellini, C. Bittencourt, and F. Evangelisti. "Low-Energy Yield Spectroscopy as a Novel Technique for Determining Band Offsets: Application to the c-Si(100)/a-Si:H Heterostructure". In: *Phys. Rev. Lett.* 75 (1995), pp. 3352–3355. DOI: 10.1103/PhysRevLett.75.3352 (cit. on p. 85).
- [17] M. Schmidt, A. Schoepke, L. Korte, O. Milch, and W. Fuhs. "Density distribution of gap states in extremely thin a-Si:H layers on crystalline silicon wafers". In: *Journal of Non-Crystalline Solids* 338-340 (2004), pp. 211–214. DOI: 10.1016/j.jnoncrysol.2004.02.055 (cit. on p. 85).
- [18] L. Korte and M. Schmidt. "Investigation of gap states in phosphorous-doped ultra-thin a-Si:H by near-UV photoelectron spectroscopy". In: *Journal of Non-Crystalline Solids* 354 (2008), pp. 2138–2143. DOI: DOI : 10.1016/j.jnoncrysol.2007.09.010 (cit. on p. 85).
- [19] M. Stutzmann. "The defect density in amorphous silicon". In: *Philosophical Magazine Part B* 60 (1989), pp. 531–546. DOI: 10.1080/13642818908205926 (cit. on pp. 85, 93).

- [20] A. H. M. Smets, W. M. M. Kessels, and M. C. M. van de Sanden. "Vacancies and voids in hydrogenated amorphous silicon". In: *Applied Physics Letters* 82 (2003), pp. 1547–1549. DOI: 10.1063/1.1559657 (cit. on p. 85).
- [21] J. Mitchell, D. Macdonald, and A. Cuevas. "Thermal activation energy for the passivation of the n-type crystalline silicon surface by hydrogenated amorphous silicon". In: *Applied Physics Letters* 94, 162102 (2009), p. 162102. DOI: 10.1063/1.3120765 (cit. on p. 85).
- [22] A. M. Antoine and B. Drévilon. "Influence of the substrate on the early stage of the growth of hydrogenated amorphous silicon evidenced by kinetic ellipsometry". In: *Journal of Applied Physics* 63 (1988), pp. 360–367. DOI: 10.1063/1.340247 (cit. on p. 85).
- [23] H. Fujiwara, Y. Toyoshima, M. Kondo, and A. Matsuda. "Interface-layer formation mechanism in a-Si:H thin-film growth studied by real-time spectroscopic ellipsometry and infrared spectroscopy". In: *Phys. Rev. B* 60 (1999), pp. 13598–13604. DOI: 10.1103/PhysRevB.60.13598 (cit. on p. 85).
- [24] H. Fujiwara and M. Kondo. "Real-time monitoring and process control in amorphous/crystalline silicon heterojunction solar cells by spectroscopic ellipsometry and infrared spectroscopy". In: *Applied Physics Letters* 86, 032112 (2005), p. 032112. DOI: 10.1063/1.1850612 (cit. on p. 85).
- [25] P.J. van den Oever, J.J.H. Gielis, M.C.M. van de Sanden, and W.M.M. Kessels. "Hot-wire deposition of a-Si:H thin films on wafer substrates studied by real-time spectroscopic ellipsometry and infrared spectroscopy". In: *Thin Solid Films* 516 (2008), pp. 511–516. DOI: 10.1016/j.tsf.2007.06.092 (cit. on p. 86).
- [26] S. De Wolf and M. Kondo. "Nature of doped a-Si:H/c-Si interface recombination". In: *Journal of Applied Physics* 105, 103707 (2009), p. 103707. DOI: 10.1063/1.3129578 (cit. on pp. 87, 102).
- [27] T.H. Wang, Q. Wang, E. Iwaniczko, M.R. Page, D.H. Levi, Y. Yan, C.W. Teplin, Y. Xu, X.Z. Wu, and H.M. Branz. "Heterojunction silicon solar cells with high open-circuit voltages by interface optimization". In: *19th EUPVSEC, 7-11 June, Paris, France. 2004* (cit. on p. 88).
- [28] M. Dai, Y. Wang, J. Kwon, M. D. Halls, and Y. J. Chabal. "Nitrogen interaction with hydrogen-terminated silicon surfaces at the atomic scale". In: *Nature Materials* 8 (2009), pp. 825–830. DOI: 10.1038/nmat2514 (cit. on p. 90).
- [29] M. Bose, D. K. Basa, and D. N. Bose. "Effect of ammonia plasma pretreatment on the plasma enhanced chemical vapor deposited silicon nitride films". In: *Materials Letters* 48 (2001), pp. 336–341. DOI: 10.1016/S0167-577X(00)00323-2 (cit. on p. 90).
- [30] A. G. Aberle. "Overview on SiN surface passivation of crystalline silicon solar cells". In: *Solar Energy Materials & Solar Cells* 65 (2001), pp. 239–248. DOI: 10.1016/S0927-0248(00)00099-4 (cit. on p. 90).

- [31] M. Kunst, O. Abdallah, and F. Wünsch. "Passivation of silicon by silicon nitride films". In: *Solar Energy Materials and Solar Cells* 72 (2002), pp. 335–341. DOI: 10.1016/S0927-0248(01)00181-7 (cit. on p. 91).
- [32] Y. Yan, M. Page, T. H. Wang, M. M. Al-Jassim, H. M. Branz, and Q. Wang. "Atomic structure and electronic properties of c-Si/a-Si:H heterointerfaces". In: *Applied Physics Letters* 88, 121925 (2006), p. 121925. DOI: 10.1063/1.2189670 (cit. on p. 91).
- [33] A. H. Mahan, P. Menna, and R. Tsu. "Influence of microstructure on the Urbach edge of amorphous SiC:H and amorphous SiGe:H alloys". In: *Applied Physics Letters* 51 (1987), pp. 1167–1169. DOI: 10.1063/1.98721 (cit. on p. 93).
- [34] P. Roca i Cabarrocas. "Plasma enhanced chemical vapor deposition of amorphous, polymorphous and microcrystalline silicon films". In: *Journal of Non-Crystalline Solids* 266-269 (2000), pp. 31–37. DOI: 10.1016/S0022-3093(99)00714-0 (cit. on pp. 97, 106).
- [35] J. P. Kleider, C. Longeaud, M. Gauthier, M. Meaudre, R. Meaudre, R. Butté, S. Vignoli, and P. Roca i Cabarrocas. "Very low densities of localized states at the Fermi level in hydrogenated polymorphous silicon from capacitance and space-charge-limited current measurements". In: *Applied Physics Letters* 75 (1999), pp. 3351–3353. DOI: 10.1063/1.125348 (cit. on p. 97).
- [36] U.K. Das, M. Z. Burrows, M. Lu, S. Bowden, and R. W. Birkmire. "Surface passivation and heterojunction cells on Si (100) and (111) wafers using dc and rf plasma deposited Si:H thin films". In: *Applied Physics Letters* 92, 063504 (2008), p. 063504. DOI: 10.1063/1.2857465 (cit. on p. 98).
- [37] M. Z. Burrows, U. K. Das, R. L. Opila, S. De Wolf, and R. W. Birkmire. "Role of hydrogen bonding environment in a-Si:H films for c-Si surface passivation". In: *Journal of Vacuum Science & Technology A* 26 (2008), pp. 683–687. DOI: 10.1116/1.2897929 (cit. on p. 98).
- [38] P. Roca i Cabarrocas, Z. Djebbour, J. P. Kleider, C. Longeaud, D. Mencaraglia, J. Sib, Y. Bouizem, M. L. Thèye, G. Sardin, and J. P. Stoquert. "Hydrogen, microstructure and defect density in hydrogenated amorphous silicon". In: *J. Phys. I France* 2 (1992), pp. 1979–1998. DOI: 10.1051/jp1:1992260 (cit. on pp. 98, 99).
- [39] S. Hama and P. Roca i Cabarrocas. "Low temperature growth of highly crystallized silicon thin films using hydrogen and argon dilution". In: *Journal of Non-Crystalline Solids* 227-230 (1998), pp. 852–856. ISSN: 0022-3093. DOI: 10.1016/S0022-3093(98)00342-1 (cit. on pp. 98, 105).
- [40] K. Fukutani, M. Kanbe, W. Futako, B. Kaplan, T. Kamiya, C.M. Fortmann, and I. Shimizu. "Band gap tuning of a-Si:H from 1.55 eV to 2.10 eV by intentionally promoting structural relaxation". In: *Journal of Non-Crystalline Solids* 227-230 (1998), pp. 63–67. DOI: 10.1016/S0022-3093(98)00022-2 (cit. on pp. 98, 105).

- [41] Ana Kanevce and Wyatt K. Metzger. "The role of amorphous silicon and tunneling in heterojunction with intrinsic thin layer (HIT) solar cells". In: *Journal of Applied Physics* 105, 094507 (2009), p. 094507. DOI: 10.1063/1.3106642 (cit. on pp. 98, 119).
- [42] M. Rahmouni, A. Datta, P. Chatterjee, J. Damon-Lacoste, C. Ballif, and P. Roca i Cabarrocas. "Carrier transport and sensitivity issues in heterojunction with intrinsic thin layer solar cells on N-type crystalline silicon: A computer simulation study". In: *Journal of Applied Physics* 107, 054521 (2010), p. 054521. DOI: 10.1063/1.3326945 (cit. on pp. 98, 119).
- [43] J. C. Knights, R. A. Lujan, M. P. Rosenblum, R. A. Street, D. K. Biegelsen, and J. A. Reimer. "Effects of inert gas dilution of silane on plasma-deposited a-Si:H films". In: *Applied Physics Letters* 38 (1981), pp. 331–333. DOI: 10.1063/1.92359 (cit. on p. 99).
- [44] R. A. Street, J. C. Knights, and D. K. Biegelsen. "Luminescence studies of plasma-deposited hydrogenated silicon". In: *Phys. Rev. B* 18 (1978), pp. 1880–1891. DOI: 10.1103/PhysRevB.18.1880 (cit. on p. 99).
- [45] J. C. Knights and R. A. Lujan. "Microstructure of plasma-deposited a-Si : H films". In: *Applied Physics Letters* 35 (1979), pp. 244–246. DOI: 10.1063/1.91086 (cit. on p. 99).
- [46] U. K. Das, A. R. Middya, J. K. Rath, C. Longeaud, D. L. Williamson, and P. Chaudhuri. "Nanostructures and defects in silicon-hydrogen alloys prepared by argon dilution". In: *Journal of Non-Crystalline Solids* 276 (2000), pp. 46–55. DOI: 10.1016/S0022-3093(00)00279-9 (cit. on p. 99).
- [47] S. De Wolf and G. Beaucarne. "Surface passivation properties of boron-doped plasma-enhanced chemical vapor deposited hydrogenated amorphous silicon films on p-type crystalline Si substrates". In: *Applied Physics Letters* 88, 022104 (2006), p. 022104. DOI: 10.1063/1.2164902 (cit. on p. 102).
- [48] M. Stutzmann, D. K. Biegelsen, and R. A. Street. "Detailed investigation of doping in hydrogenated amorphous silicon and germanium". In: *Phys. Rev. B* 35 (1987), pp. 5666–5701. DOI: 10.1103/PhysRevB.35.5666 (cit. on p. 102).
- [49] N. M. Johnson, F. A. Ponce, R. A. Street, and R. J. Nemanich. "Defects in single-crystal silicon induced by hydrogenation". In: *Phys. Rev. B* 35 (1987), pp. 4166–4169. DOI: 10.1103/PhysRevB.35.4166 (cit. on p. 104).
- [50] A. G. Ulyashin, R. Job, W. R. Fahrner, O. Richard, H. Bender, C. Claeys, E. Simoen, and D. Grambole. "Substrate orientation, doping and plasma frequency dependencies of structural defect formation in hydrogen plasma treated silicon". In: *Journal of Physics: Condensed Matter* 14 (2002), p. 13037. DOI: 10.1088/0953-8984/14/48/349 (cit. on p. 104).

- [51] J.W.A. Schüttauf, C.H.M. van der Werf, W.G.J.H.M. van Sark, J.K. Rath, and R.E.I. Schropp. "Comparison of surface passivation of crystalline silicon by a-Si:H with and without atomic hydrogen treatment using hot-wire chemical vapor deposition". In: *Thin Solid Films* In Press, Corrected Proof (2011), pp. -. DOI: 10.1016/j.tsf.2011.01.319 (cit. on p. 104).
- [52] W. Beyer and H. Wagner. "Determination of the hydrogen diffusion coefficient in hydrogenated amorphous silicon from hydrogen effusion experiments". In: *Journal of Applied Physics* 53 (1982), pp. 8745–8750. DOI: 10.1063/1.330474 (cit. on pp. 104, 114).
- [53] R. A. Street, J. Kakalios, C. C. Tsai, and T. M. Hayes. "Thermal-equilibrium processes in amorphous silicon". In: *Phys. Rev. B* 35 (1987), pp. 1316–1333. DOI: 10.1103/PhysRevB.35.1316 (cit. on pp. 104, 114).
- [54] P. V. Santos and W. B. Jackson. "Trap-limited hydrogen diffusion in a-Si:H". In: *Phys. Rev. B* 46 (1992), pp. 4595–4606. DOI: 10.1103/PhysRevB.46.4595 (cit. on p. 104).
- [55] Chris G. Van de Walle and L. H. Yang. "Band discontinuities at heterojunctions between crystalline and amorphous silicon". In: *J. Vac. Sci. Technol. B* 13 (1995), pp. 1635–1638. DOI: 10.1116/1.587870 (cit. on p. 105).
- [56] V. Suendo, A. V. Kharchenko, and P. Roca i Cabarrocas. "The effects of RF plasma excitation frequency and doping gas on the deposition of polymorphous silicon thin films". In: *Thin Solid Films* 451-452 (2004), pp. 259–263. DOI: 10.1016/j.tsf.2003.11.019 (cit. on p. 105).
- [57] J. Meier, S. Dubail, J. Cuperus, U. Kroll, R. Platz, P. Torres, J. A. Anna Selvan, P. Pernet, N. Beck, N. Pellaton Vaucher, Ch. Hof, D. Fischer, H. Keppner, and A. Shah. "Recent progress in micromorph solar cells". In: *Journal of Non-Crystalline Solids* 227-230 (1998), pp. 1250–1256. DOI: 10.1016/S0022-3093(98)00352-4 (cit. on p. 105).
- [58] F. Einsele, P. J. Rostan, M. B. Schubert, and U. Rau. "Recombination and resistive losses at ZnO/a-Si:H/c-Si interfaces in heterojunction back contacts for Si solar cells". In: *Journal of Applied Physics* 102, 094507 (2007), p. 094507. DOI: 10.1063/1.2803749 (cit. on p. 105).
- [59] S. Olibet. "Properties of interfaces in amorphous / crystalline silicon heterojunctions". PhD thesis. Université de Neuchâtel, 2009. URL: http://doc.rero.ch/lm.php?url=1000,40,4,20090325123849-OX/Th_OlibetS.pdf (cit. on pp. 105, 121).
- [60] P. Roca i Cabarrocas. "Plasma enhanced chemical vapor deposition of silicon thin films for large area electronics". In: *Current Opinion in Solid State and Materials Science* 6 (2002), pp. 439–444. DOI: 10.1016/S1359-0286(02)00112-2 (cit. on p. 106).

- [61] H. Fujiwara, M. Kondo, and A. Matsuda. "Real-time spectroscopic ellipsometry studies of the nucleation and grain growth processes in microcrystalline silicon thin films". In: *Phys. Rev. B* 63 (2001), p. 115306. DOI: 10.1103/PhysRevB.63.115306 (cit. on p. 106).
- [62] D. L. Staebler and C. R. Wronski. "Reversible conductivity changes in discharge-produced amorphous Si". In: *Applied Physics Letters* 31 (1977), pp. 292–294. DOI: 10.1063/1.89674 (cit. on p. 107).
- [63] M. Stutzmann, W. B. Jackson, and C. C. Tsai. "Light-induced metastable defects in hydrogenated amorphous silicon: A systematic study". In: *Phys. Rev. B* 32 (1985), pp. 23–47. DOI: 10.1103/PhysRevB.32.23 (cit. on p. 108).
- [64] J. Schmidt and K. Bothe. "Structure and transformation of the metastable boron- and oxygen-related defect center in crystalline silicon". In: *Phys. Rev. B* 69 (2004), p. 024107. DOI: 10.1103/PhysRevB.69.024107 (cit. on p. 108).
- [65] A. Herguth, G. Schubert, M. Kaes, and G. Hahn. "Investigations on the long time behavior of the metastable boron-oxygen complex in crystalline silicon". In: *Progress in Photovoltaics: Research & Applications* 16 (2008), pp. 135–140. DOI: 10.1002/pip.779 (cit. on p. 108).
- [66] D. Macdonald, F. Rougieux, A. Cuevas, B. Lim, J. Schmidt, M. Di Sabatino, and L. J. Geerligs. "Light-induced boron-oxygen defect generation in compensated p-type Czochralski silicon". In: *Journal of Applied Physics* 105, 093704 (2009), p. 093704. DOI: 10.1063/1.3121208 (cit. on p. 108).
- [67] T. Schutz-Kuchly, J. Veirman, S. Dubois, and D. R. Heslinga. "Light-Induced-Degradation effects in boron-phosphorus compensated n-type Czochralski silicon". In: *Applied Physics Letters* 96, 093505 (2010), p. 093505. DOI: 10.1063/1.3334724 (cit. on p. 108).
- [68] J. Geilker, W. Kwapil, and S. Rein. "Light-induced degradation in compensated p- and n-type Czochralski silicon wafers". In: *Journal of Applied Physics* 109, 053718 (2011), p. 053718. DOI: 10.1063/1.3552302 (cit. on p. 109).
- [69] S. Olibet, E. Vallat-Sauvain, and C. Ballif. "Effect of light induced degradation on passivation properties of a-Si:H layers deposited on crystalline Si". In: *21st EU-PV Conference, Dresden, Germany, September, 2006*. 2006 (cit. on p. 109).
- [70] S. Bowden, U. Das, S. Herasimenka, and R. Birkmire. "Stability of amorphous/crystalline silicon heterojunctions". In: *Photovoltaic Specialists Conference, 2008. PVSC '08. 33rd IEEE*. May 2008, pp. 1–4. DOI: 10.1109/PVSC.2008.4922850 (cit. on p. 109).
- [71] S. Olibet, E. Vallat-Sauvain, and C. Ballif. "Model for a-Si:H/c-Si interface recombination based on the amphoteric nature of silicon dangling bonds". In: *Physical Review B* 76, 035326 (2007), p. 035326. DOI: 10.1103/PhysRevB.76.035326 (cit. on p. 109).

- [72] T. F. Schulze, H. N. Beushausen, T. Hansmann, L. Korte, and B. Rech. "Accelerated interface defect removal in amorphous/crystalline silicon heterostructures using pulsed annealing and microwave heating". In: *Applied Physics Letters* 95, 182108 (2009), p. 182108. DOI: 10.1063/1.3255018 (cit. on p. 111).
- [73] R. Martins and E. Fortunato. "Lateral effects in amorphous silicon photodiodes". In: *Optical Materials* 5 (1996), pp. 137–144. DOI: 10.1016/0925-3467(95)00043-7 (cit. on p. 114).
- [74] R. Hezel and R. Schörner. "Plasma Si nitride—A promising dielectric to achieve high-quality silicon MIS/IL solar cells". In: *Journal of Applied Physics* 52 (1981), pp. 3076–3079. DOI: 10.1063/1.329058 (cit. on p. 115).
- [75] A. G. Aberle, B. Kuhlmann, R. Meyer, A. Hübner, C. Hampe, and R. Hezel. "Comparison of p-n junction and inversion-layer silicon solar cells by means of experiment and simulation". In: *Progress in Photovoltaics: Research & Applications* 4 (1996), pp. 193–204. DOI: 10.1002/(SICI)1099-159X(199605/06)4:3<193::AID-PIP118>3.0.CO;2-S (cit. on p. 115).
- [76] I. Martin, R. Lövblom, and R. Alcubilla. "High-efficiency solar cells based on inversion layer emitters". In: *24th European Photovoltaic Solar Energy Conference, Hamburg*. 2009 (cit. on p. 115).
- [77] J.W.A. Schüttauf, Y. Komatsu, L.J. Geerligs, Y. Mai, A. Bink, D.A. Spee, and R.E.I. Schropp. "Emitter Optimization on a-Si:H/c-Si Heterojunction Solar Cells for Isotextured Wafers". In: *23rd EU PVSEC Valencia, Spain*. 2008 (cit. on pp. 116, 121).
- [78] T. F. Schulze, L. Korte, E. Conrad, M. Schmidt, and B. Rech. "Electrical transport mechanisms in a-Si:H/c-Si heterojunction solar cells". In: *Journal of Applied Physics* 107, 023711 (2010), p. 023711. DOI: 10.1063/1.3267316 (cit. on p. 118).
- [79] M. W. M. van Cleef, J. K. Rath, F. A. Rubinelli, C. H. M. van der Werf, R. E. I. Schropp, and W. F. van der Weg. "Performance of heterojunction p⁺⁺ microcrystalline silicon n crystalline silicon solar cells". In: *Journal of Applied Physics* 82 (1997), pp. 6089–6095. DOI: 10.1063/1.366479 (cit. on p. 121).
- [80] Y. Djeridane, A. Abramov, and P. Roca i Cabarrocas. "Silane versus silicon tetrafluoride in the growth of microcrystalline silicon films by standard radio frequency glow discharge". In: *Thin Solid Films* 515 (2007), pp. 7451–7454. DOI: 10.1016/j.tsf.2006.11.112 (cit. on pp. 121, 126).
- [81] Q. Zhang, E. V. Johnson, Y. Djeridane, A. Abramov, and P. Roca i Cabarrocas. "Decoupling crystalline volume fraction and V_{OC} in microcrystalline silicon pin solar cells by using a μ c-Si:F:H intrinsic layer". In: *physica status solidi (RRL)* 2 (2008), pp. 154–156. DOI: 10.1002/pssr.200802106 (cit. on p. 121).

- [82] A. Abramov, Y. Djeridane, R. Vanderhaghen, and P. Roca i Cabarrocas. "Large grain $\mu\text{-Si:H}$ films deposited at low temperature: Growth process and electronic properties". In: *Journal of Non-Crystalline Solids* 352 (2006), pp. 964–967. DOI: 10.1016/j.jnoncrysol.2005.10.060 (cit. on p. 121).
- [83] I. Barycka and I. Zubeł. "Silicon anisotropic etching in KOH-isopropanol etchant". In: *Sensors and Actuators A: Physical* 48 (1995), pp. 229–238. DOI: 10.1016/0924-4247(95)00992-2 (cit. on p. 124).
- [84] D. B. Lee. "Anisotropic Etching of Silicon". In: *Journal of Applied Physics* 40 (1969), pp. 4569–4574. DOI: 10.1063/1.1657233 (cit. on p. 124).
- [85] M. Shikida, K. Tokoro, D. Uchikawa, and K. Sato. "Surface morphology of anisotropically etched single-crystal silicon". In: *Journal of Micromechanics and Microengineering* 10 (2000), p. 522. DOI: 10.1088/0960-1317/10/4/306 (cit. on p. 124).
- [86] C. C. Tsai, J. C. Knights, G. Chang, and B. Wacker. "Film formation mechanisms in the plasma deposition of hydrogenated amorphous silicon". In: *Journal of Applied Physics* 59 (1986), pp. 2998–3001. DOI: 10.1063/1.336920 (cit. on p. 124).
- [87] Q. Wang, M.R. Page, E. Iwaniczko, Y.Q. Xu, L. Roybal, R. Bauer, B. To, H.C. Yuan, A. Duda, and Y.F. Yan. "Crystal silicon heterojunction solar cells by hot-wire CVD". In: *Photovoltaic Specialists Conference, 2008. PVSC '08. 33rd IEEE*. May 2008, pp. 1–5. DOI: 10.1109/PVSC.2008.4922448 (cit. on p. 124).
- [88] M. Moreno, D. Daineka, and P. Roca i Cabarrocas. "Plasmas for texturing, cleaning, and deposition: towards a one pump down process for heterojunction solar cells". In: *physica status solidi (c)* 7 (2010), pp. 1112–1115. DOI: 10.1002/pssc.200982704 (cit. on p. 126).
- [89] Michael A. Lieberman and Allan J. Lichtenberg. *Principles of Plasma Discharges and Materials Processing, Second Edition*. John Wiley and Sons, Inc. (cit. on p. 126).
- [90] Ch. Steinbrüchel, H. W. Lehmann, and K. Frick. "Mechanism of Dry Etching of Silicon Dioxide". In: *Journal of The Electrochemical Society* 132 (1985), pp. 180–186. DOI: 10.1149/1.2113757 (cit. on p. 126).
- [91] J. W. Coburn and H. F. Winters. "Ion- and electron-assisted gas-surface chemistry—An important effect in plasma etching". In: *Journal of Applied Physics* 50 (1979), pp. 3189–3196. DOI: 10.1063/1.326355 (cit. on p. 126).
- [92] Harold H. F. Winters. "Etch products from the reaction of XeF_2 with SiO_2 , Si_3N_4 , SiC , and Si in the presence of ion bombardment". In: *Journal of Vacuum Science & Technology B: Microelectronics and Nanometer Structures* 1 (1983), pp. 927–931. DOI: 10.1116/1.582713 (cit. on p. 126).

- [93] D. L. Flamm, V. M. Donnelly, and J. A. Mucha. "The reaction of fluorine atoms with silicon". In: *Journal of Applied Physics* 52 (1981), pp. 3633–3639. DOI: 10.1063/1.329098 (cit. on p. 126).
- [94] M. Tucci, E. Salurso, F. Roca, and F. Palma. "Dry cleaning process of crystalline silicon surface in a-Si:H/c-Si heterojunction for photovoltaic applications". In: *Thin Solid Films* 403-404 (2002), pp. 307–311. DOI: 10.1016/S0040-6090(01)01645-5 (cit. on p. 126).
- [95] M. Moreno, M. Labruno, and P. Roca i Cabarrocas. "Dry fabrication process for heterojunction solar cells through in-situ plasma cleaning and passivation". In: *Solar Energy Materials & Solar Cells* 94 (2010), pp. 402–405. DOI: 10.1016/j.solmat.2009.10.016 (cit. on pp. 126, 127).
- [96] G. W. Trucks, Krishnan Raghavachari, G. S. Higashi, and Y. J. Chabal. "Mechanism of HF etching of silicon surfaces: A theoretical understanding of hydrogen passivation". In: *Phys. Rev. Lett.* 65 (1990), pp. 504–507. DOI: 10.1103/PhysRevLett.65.504 (cit. on p. 127).
- [97] R. Preu, E. Schneiderlochner, A. Grohe, S.W. Glunz, and G. Willeke. "Laser-fired contacts - transfer of a simple high efficiency process scheme to industrial production". In: *Photovoltaic Specialists Conference, 2002. Conference Record of the Twenty-Ninth IEEE*. May 2002, pp. 130–133. DOI: 10.1109/PVSC.2002.1190473 (cit. on p. 129).
- [98] D. Muñoz, C. Voz, S. Blanque, D. Ibarz, J. Bertomeu, and R. Alcubilla. "Development of laser-fired contacts for amorphous silicon layers obtained by Hot-Wire CVD". In: *Materials Science and Engineering: B* 159-160 (2009), pp. 23–26. DOI: 10.1016/j.mseb.2008.10.049 (cit. on p. 129).

EPITAXY

4

Contents

4.1	Undoped and doped silicon thin films	148
4.1.1	Precedents in RF PECVD	149
4.1.2	Early results	150
4.1.3	Does someone know what happens ?	157
4.1.4	Intrinsic epitaxy: towards a wafer equivalent approach	162
4.1.5	Epitaxial growth of doped layers	168
4.2	Germanium films	176
4.2.1	Precedents	177
4.2.2	Preliminary studies	178
4.2.3	Multilayer samples	179
4.3	Conclusions	188

THE films that we deposit by PECVD have properties (electrical, structural, optical, etc) which depend on the plasma conditions used for their deposition, such as pressure, gas ratios or power, but also on some substrate properties: whether it is conductive or not, biased or grounded or at floating potential, amorphous or with a preferential crystalline orientation, etc. One effect for instance, comes from the bias voltage of the substrate. Indeed, putting the sample on the cathode (the RF electrode) or on the anode (in our case the grounded substrate holder), or changing the DC bias voltage applied to our substrate can modify the deposition rate and the structure of the films as it has been shown when changing the bias applied to the substrate for $\mu\text{c-Si:H}$ deposition by *Kalache et al.*¹ or *Chaâbane et al.*² Another effect is of course the nature of the substrate itself, whether it is crystalline or not. Indeed, many research groups,^{3,4,5} including the LPICM,^{6,7} mostly working on a-Si:H/c-Si heterojunctions, have found that when they were applying plasma conditions used to grow a-Si:H materials (or $\mu\text{c-Si:H}$ materials) they would eventually obtain crystalline films, on (100) Si substrates. These films are called epitaxial films since they adopt the crystalline nature of their underlying substrate.

In addition, some researchers also pointed out the fact that the epitaxial growth occurred only⁸ on (100)-oriented c-Si wafers in comparison to (111)-oriented c-Si wafers,⁹ or similarly that epitaxial growth could occur in the flat valleys of textured c-Si wafers which are (100)-oriented leading to a degradation of the solar cells' performances.¹⁰

4.1 Undoped and doped silicon thin films

Even though this doctoral work consisted in focusing on heterojunction solar cells, it seemed that such an epitaxial growth occurring at such a low temperature as 200°C could also be interesting to study. Indeed, it

¹Kalache, Kosarev, Vanderhaghen, and Roca i Cabarrocas, "Ion bombardment effects on microcrystalline silicon growth mechanisms and on the film properties", 2003 [1]

²Chaâbane, Suendo, Vach, and Roca i Cabarrocas, "Soft landing of silicon nanocrystals in plasma enhanced chemical vapor deposition", 2006 [2]

³Gielis, van den Oever, Hoex, van de Sanden, and Kessels, "Real-time study of a-Si:H/c-Si heterointerface formation and epitaxial Si growth by spectroscopic ellipsometry, infrared spectroscopy, and second-harmonic generation", 2008 [3]

⁴Wang, Teplin, Stradins, To, Jones, and Branz, "Significant improvement in silicon chemical vapor deposition epitaxy above the surface dehydrogenation temperature", 2006 [4]

⁵De Wolf and Kondo, "Abruptness of a-Si:H/c-Si interface revealed by carrier lifetime measurements", 2007 [5]

⁶Veschetti, Muller, Damon-Lacoste, Cabarrocas, Gudovskikh, Kleider, Ribeyron, and Rolland, "Optimisation of amorphous and polymorphous thin silicon layers for the formation of the front-side of heterojunction solar cells on p-type crystalline silicon substrates", 2006 [6]

⁷Damon-Lacoste and Roca i Cabarrocas, "Toward a better physical understanding of a-Si:H/c-Si heterojunction solar cells", 2009 [7]

⁸At least in the "low" temperature range ($T < 250^\circ\text{C}$)

⁹Das, Burrows, Lu, Bowden, and Birkmire, "Surface passivation and heterojunction cells on Si (100) and (111) wafers using dc and rf plasma deposited Si:H thin films", 2008 [8]

¹⁰Olibet, Monachon, Hessler-Wyser, Vallat-Sauvain, De Wolf, Fesquet, Damon-Lacoste, and Ballif, "Textured silicon heterojunction solar cells with over 700 mV open-circuit voltage studied by Transmission Electron Microscopy", 2008 [9]

can have many potential applications. For instance, undoped layers can be used as the absorber of photovoltaic devices, including multi-junction solar cells. Doped layers can be used to form emitters or BSF of crystalline homojunction solar cells, or used in microelectronics where there is a crucial need to have shallow junctions with very well-defined thicknesses and doping concentrations.

There are already quite a broad range of techniques available for this purpose and they are described in very comprehensive reviews made by *Beaucarne*,¹ or *McCann* on native substrates,² or by *Catchpole* on foreign substrates.³ All the mentioned processes are based on high temperature steps.

More recently, epitaxial growth of silicon films on silicon substrates has been demonstrated using several alternative techniques such as Atmospheric Pressure CVD,⁴ Hot-Wire CVD,⁵ Mesoplasma CVD,⁶ Electron Cyclotron Resonance PECVD.⁷ Chapter 3 dealt with some of the possible ways to avoid such a growth, detrimental for heterojunction solar cells, but it can also be wondered how we can understand and control such an epitaxial growth and how to take benefit of an epitaxial growth at such low temperatures.

4.1.1 Precedents in RF PECVD

The epitaxial growth on (100) Si has recently gained a lot of interest with the direct and frequent observation of such growths by researchers of the a-Si:H/c-Si heterojunction community [3, 4, 5, 6]. However, such epitaxial growths by RF PECVD at very low substrate temperatures had already been observed two decades earlier. In those days, research on a-Si:H materials (growth, properties, devices) was already very active and people had already observed, for various conditions, such growths. For instance, using silane and hydrogen gas mixtures, and for substrates temperatures in the 175-300°C range, the Xerox group,^{8,9} and others,¹⁰ had observed epitaxial growth on (100) Si. Other researchers had also used fluorine con-

¹Beaucarne, Duerinckx, Kuzma, Van Nieuwenhuysen, Kim, and Poortmans, "Epitaxial thin-film Si solar cells", 2006 [10]

²McCann, Catchpole, Weber, and Blakers, "A review of thin-film crystalline silicon for solar cell applications. Part 1: Native substrates", 2001 [11]

³Catchpole, McCann, Weber, and Blakers, "A review of thin-film crystalline silicon for solar cell applications. Part 2: Foreign substrates", 2001 [12]

⁴Schmich, Schillinger, and Reber, "Silicon CVD deposition for low cost applications in photovoltaics", 2007 [13]

⁵Teplin, Wang, Iwaniczko, Jones, Al-Jassim, Reedy, and Branz, "Low-temperature silicon homoepitaxy by hot-wire chemical vapor deposition with a Ta filament", 2006 [14]

⁶Kambara, Yagi, Sawayanagi, and Yoshida, "High rate epitaxy of silicon thick films by medium pressure plasma chemical vapor deposition", 2006 [15]

⁷Varhue, Rogers, Andry, and Adams, "Epitaxial film thickness in the low-temperature growth of Si(100) by plasma enhanced chemical vapor deposition", 1996 [16]

⁸Tsai, Anderson, and Thompson, "Low temperature growth of epitaxial and amorphous silicon in a hydrogen-diluted silane plasma", 1991 [17]

⁹Tsai, Anderson, Thompson, and Wacker, "Control of silicon network structure in plasma deposition", 1989 [18]

¹⁰Chen and Yew, "Silicon epitaxial growth by plasma enhanced chemical vapor deposition from SiH₄/H₂ at 165-350°C", 1995 [19]

taining gases or combined them with silane.¹ One can also note the work of one group from MIT that also uses PECVD but at higher substrate temperatures, over 700°C.² However, after these early publications, very few papers were published on the topic of low temperature epitaxy by PECVD. Indeed, some researchers claimed in the early 2000's that they could grow p-type heterojunction and homojunction emitters on n-type silicon.^{3,4} More recently, some other researchers claimed that they obtained epitaxial growth of phosphorous-doped silicon emitters on p-type multicrystalline silicon wafer using PECVD at 250°C,⁵ and also a group from *AIST* published about phosphorous-doped emitter on monocrystalline silicon by PECVD for temperatures ranging from 200°C to room temperature!⁶

4.1.2 Early results

Our work had basically two motivations: to seek for a better knowledge of this epitaxial growth and for a way to avoid such an epitaxial growth. Our work on amorphous growth is comprehensively presented in Chapter 3 (§3, p. 81). Thus, this section will be devoted to non amorphous growths. As mentioned earlier, epitaxial growth is prone to occur on (100)-oriented substrates and not on (111)-oriented substrates. A very straightforward way to look at it is to have a look at the pictures of two samples shown on Fig. 4.1.

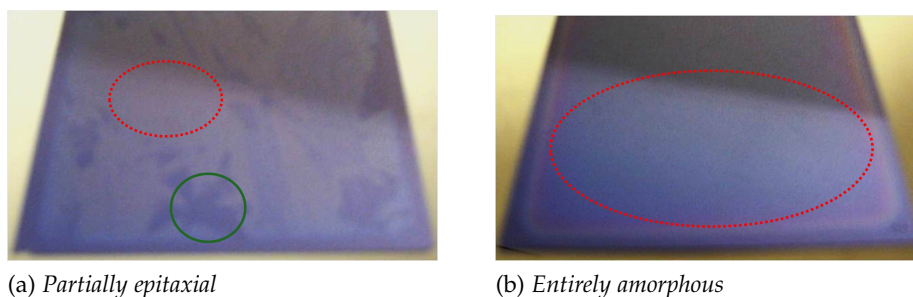


Figure 4.1 – *Optically polished multicrystalline silicon samples on which we used two different plasma conditions known to lead to amorphous silicon*

The samples were deposited under conditions leading to epitaxial growth (4.1a) or amorphous growth (4.1b) silicon films on multicrystalline silicon wafers, kindly provided by Photowatt, that had been previously

¹Nagamine, Yamada, Konagai, and Takahashi, "Epitaxial Growth of Silicon by Plasma Chemical Vapor Deposition at a Very Low Temperature of 250°C", 1987 [20]

²Ohi, Burger, and Reif, "Enhanced electrical quality of low-temperature ($T < 800^{\circ}\text{C}$) epitaxial silicon deposited by plasma-enhanced chemical vapor deposition", 1988 [21]

³Plá, Centurioni, Summonte, Rizzoli, Migliori, Desalvo, and Zignani, "Homojunction and heterojunction silicon solar cells deposited by low temperature-high frequency plasma enhanced chemical vapour deposition", 2002 [22]

⁴Rizzoli, Centurioni, Plá, Summonte, Migliori, Desalvo, and Zignani, "Open circuit voltage in homojunction and heterojunction silicon solar cells grown by VHF-PECVD", 2002 [23]

⁵Farrokh-Baroughi and Sivoththaman, "A Novel Silicon Photovoltaic Cell Using a Low-Temperature Quasi-Epitaxial Silicon Emitter", 2007 [24]

⁶Shimokawa, Yamanaka, and Sakata, "Very Low Temperature Epitaxial Growth of Silicon Films for Solar Cells", 2007 [25]

polished for optical purposes.¹ Unlike monocrystalline, multicrystalline is a material made of several crystals therefore exhibiting different crystal orientations at its surface. One can “easily” distinguish on Fig. 4.1a different areas at the surface. Interestingly, the areas were large enough to allow us to perform spectroscopic ellipsometry on different spots of the surface showing different natures of the growth, epitaxial in some areas, amorphous in other areas, as it was further confirmed by other depositions on (111) and (100), as shown on Fig. 4.2. The ellipsometry spectra confirmed that the grown materials could be either amorphous or crystalline depending on the grain orientation. This was a fast and visually straightforward evidence of the substrate orientation dependence but it did not tell us much about epitaxy itself.

A confirmation of this substrate orientation dependence could be obtained very easily. For this purpose we have co-deposited a silicon film onto various substrates. The films (1001084) were grown at a pressure of 2100 mTorr and flow rates of hydrogen of 500 sccm and of silane of 35 sccm for 21 min 30 sec. The SE spectra of these films are shown on Fig. 4.2 on which we have plotted the imaginary part of the pseudo-dielectric function of the films grown on (111) c-Si, (100) c-Si and Corning glass. We also added the dielectric function of crystalline silicon.

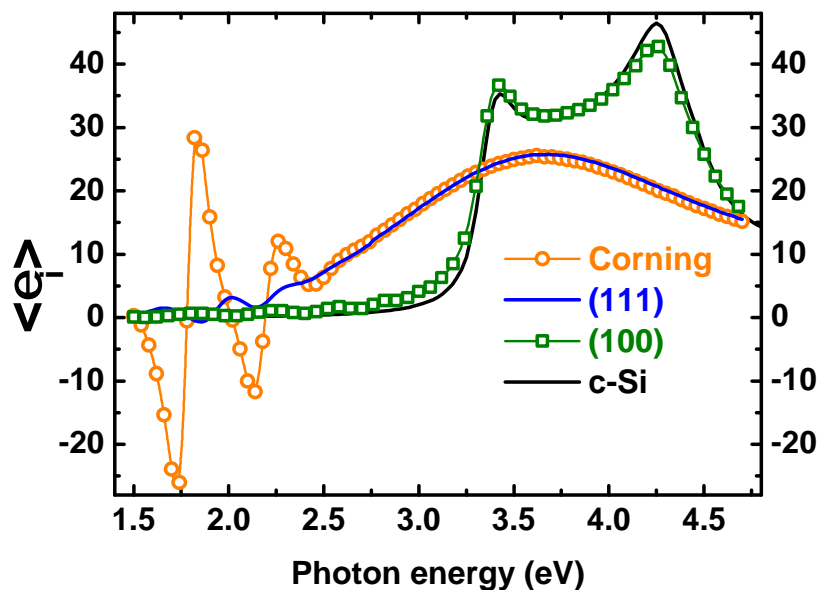


Figure 4.2 – Imaginary part of the pseudo-dielectric function of silicon thin films co-deposited on various substrates (111) Si, (100) Si and Corning glass

On Fig. 4.2, it appeared very clearly that the films deposited on glass and on (111) Si were very similar and showed typical a-Si:H spectra, whereas the film deposited on (100) exhibited a typical crystalline spectrum, with a very little difference compared to the c-Si spectrum. Such dif-

¹Multicrystalline wafers are normally not polished and the roughness of such samples make it very difficult to obtain a signal in the high photon energy part (> 3 eV) of spectroscopic ellipsometry measurements where it is precisely extremely relevant to determine the crystalline nature of a silicon film.

ferences have been detailed earlier in the paragraph introducing spectroscopic ellipsometry (§2.1.4, p. 49). Interestingly enough, deposition rates were found to be similar for epitaxial and amorphous growth. The crystalline orientation sensitivity has been now quite well established, based on our own results and those from the aforementioned references [3, 4, 5]. However, such a difference, if ever mentioned, was scarcely commented or discussed. Some of the published results suggested that hydrogen dilution^{1,2} and substrate temperature^{3,4} were two key parameters.

In order to collect more data on the role of hydrogen dilution, we performed two more depositions, at 200°C, where we co-deposited on (111) and (100) c-Si wafers two different stacks made of a bi-layer:

1. a 5' (i) pm-Si:H layer in the conditions: $H_2 = 200$; $SiH_4 = 12$; $p = 1200$ mTorr
2. a 7' (i) a-Si:H made with or without hydrogen dilution:
 - $H_2 = 100$; $SiH_4 = 50$; $p = 230$ mTorr
 - $H_2 = 0$; $SiH_4 = 50$; $p = 60$ mTorr

The pm-Si:H conditions are known to lead to an epitaxial growth on (100) and to an amorphous growth on (111). The SE spectra are shown on Fig. 4.3 where we have plotted the pseudo-dielectric function of the stacks deposited with a hydrogen dilution on (100) and (111) Si, as well as the stacks deposited from pure SiH_4 on (100) and (111) Si. The dielectric function of c-Si was also added for reference.

On this graph (Fig. 4.3), we could observe very similar spectra, irrespectively of the hydrogen dilution. These results show that the epitaxial (re)growth can occur on a previously epitaxially grown Si film, in conditions where silane was diluted in hydrogen or was the only gas used.

In order, now, to collect more data on the effect of the substrate temperature, known from the previous chapter to promote a more disordered (amorphous) growth, it was tempting to see if these two variables (hydrogen and temperature) were “independent”, or if we could “compensate” a factor with the other. In other words, was it still possible to sustain an epitaxial growth at lower temperatures when the gas mixture included a larger amount of hydrogen. This was why we have produced films at 100°C and even at room temperature (RT), from pure silane or from silane diluted in hydrogen. The conditions of these films are summarized in Tab. 4.1 and the SE spectra are plotted on Fig. 4.4.

On Fig. 4.4, we showed the SE spectra of films grown on (100) c-Si deposited at 100°C from pure SiH_4 or from a SiH_4+H_2 gas mixture, as well as

¹Tsai, Anderson, and Thompson, “Low temperature growth of epitaxial and amorphous silicon in a hydrogen-diluted silane plasma”, 1991 [17]

²Das, Burrows, Lu, Bowden, and Birkmire, “Surface passivation and heterojunction cells on Si (100) and (111) wafers using dc and rf plasma deposited Si:H thin films”, 2008 [8]

³De Wolf and Kondo, “Abruptness of a-Si:H/c-Si interface revealed by carrier lifetime measurements”, 2007 [5]

⁴Levi, Iwaniczko, Page, Wang, Branz, and Wang, “Silicon Heterojunction Solar Cell Characterization and Optimization using in Situ and Ex Situ Spectroscopic Ellipsometry”, 2006 [26]

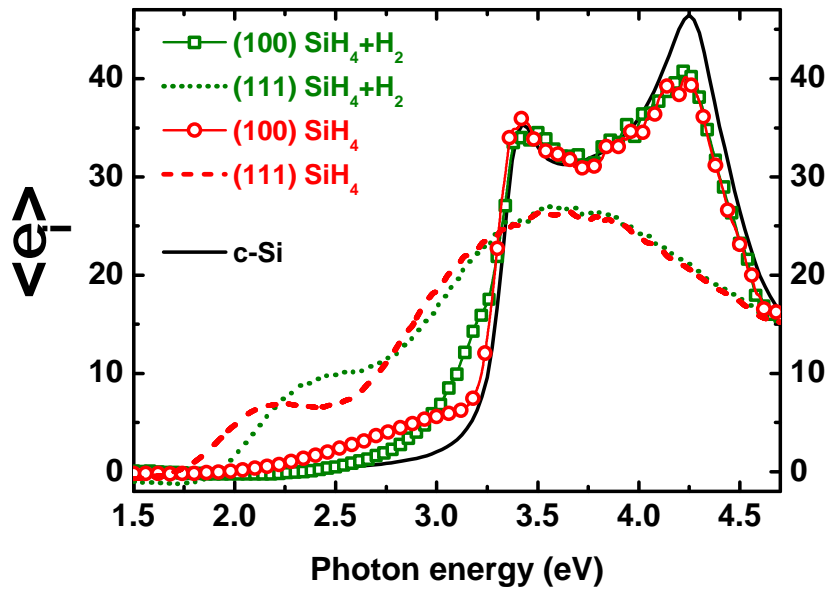


Figure 4.3 – Imaginary part of the pseudo-dielectric functions of Si stacks deposited at 200°C on (111) and (100) wafers, consisting of a first layer deposited in the conditions of *pm*-Si:H and of a second layer deposited in the condition of *a*-Si:H from pure silane (red) or from a silane+hydrogen gas mixture. We also plotted the dielectric function of a crystalline silicon wafer (black line)

Sample name	Substrate temperature (°C)	H ₂ (sccm)	SiH ₄ (sccm)	Pressure (mTorr)
804026	100	200	50	230
804027	100	0	50	60
805051	25	200	50	230

Table 4.1 – Deposition conditions of Si films deposited at low substrate temperatures

at room temperature from a SiH_4+H_2 gas mixture. We added the dielectric function of c-Si for reference. It should be stressed that on the surface of the room temperature sample (805051) several areas were distinguishable, ones exhibiting purely amorphous spectra (not shown here but very similar to the one of the film deposited from SiH_4 at 100°C), the others exhibiting spectra as the one shown on Fig. 4.4. This meant that at this temperature and in these conditions, the depositions may not have been so stable or reproducible. Also we could suspect, from our experience and based on the literature,¹ that powders were more easily produced at lower temperatures resulting in an inhomogeneous plasma that could lead to these different growth regimes on the same substrate.

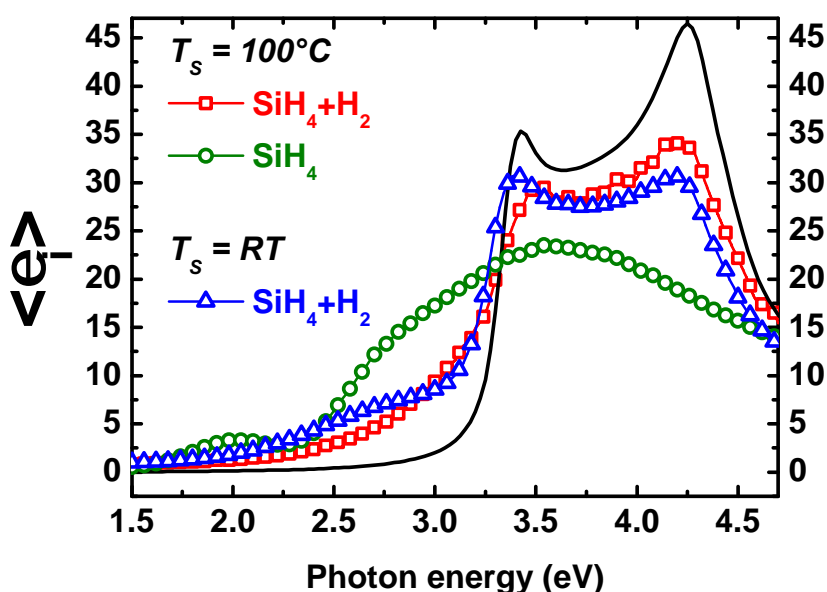


Figure 4.4 – Imaginary part of the pseudo-dielectric functions of films deposited in H_2 dilution at 100°C (red squares) and at room temperature (RT) (blue triangles), or in pure SiH_4 at 100°C (green circles), and a crystalline silicon wafer (black line)

This graph (4.4) shows us that at 100°C or even at RT, ordered growth was still achievable, provided that we used a certain amount of hydrogen in the gas mixture. Indeed, at 100°C the film deposited from pure SiH_4 was purely amorphous whereas the film deposited from the SiH_4+H_2 mixture showed a high degree of crystallinity. Keeping the same conditions but decreasing even further the temperature to room temperature allowed us to keep a high degree of crystallinity. These results did not demonstrate a 100% crystalline growth at very low temperatures but they allowed to rule out the decrease of the temperature as the unique mean of preventing any crystallized growth.

Finally, from all the studies on hydrogen in a-Si:H it is known that a “regular” (not extreme) hydrogen content in an a-Si:H film is in the 8-25% range.² However, it is hard to conceive an epitaxial film with such an

¹Boufendi and Bouchoule, “Particle nucleation and growth in a low-pressure argon-silane discharge”, 1994 [27]

²Street, *Hydrogenated Amorphous Silicon*, 1991 [28]

hydrogen content. Indeed, on Fig. 4.5 we have plotted the hydrogen counts profile of silicon thin films deposited on (100) and (111) Si substrates, with or without a H₂ plasma treatment. Spectroscopic ellipsometry showed that the films were amorphous on (111) and epitaxial on (100). This graph allowed us to check that there was indeed a much lower hydrogen content in epitaxial films. Such a difference in hydrogen content for a-Si:H or epitaxial films deposited at the same temperature had already been noted by Tsai *et al.*,¹ and Teplin *et al.*² This ratio was found, by Tsai *et al.*, to increase with an increase of the temperature: the H content decreases much faster in the epitaxial film. Interestingly enough, one can see that a rather short (2 min.) H₂ plasma treatment prior to the depositions resulted in a significant diffusion of H into (100) Si and not in (111) Si, that could not be ascribed to the SIMS technique itself.

On Fig. 4.6, we have plotted the H content against the thickness of a silicon film co-deposited on (100) and (111) Si and for which the $\frac{H_2}{SiH_4+H_2}$ ratio was unintentionally varied from 80% to 0% during the deposition. This allowed us to confirm that there was one order of magnitude difference in H content in a-Si:H and epitaxial films. Besides, the H content did not exhibit an abrupt, but rather a smooth change along the growth direction, indicating that the transition from crystalline to amorphous growth was also not abrupt. Indeed, SE measurements indicated a purely amorphous growth on (111) whereas no easy modelling was achievable for the film on (100) for which we could only fit the experimental spectrum to an optical model consisting of a thin a-Si:H layer with a smaller bandgap than standard a-Si:H (≈ 1.5 eV). The thickness of this amorphous layer compared well with the one deduced from the length of the high hydrogen content part on the SIMS measurement. This H concentration gradient with the increase of the a-Si:H content has also been reported by Teplin *et al.* [14].

These SIMS data were very valuable since they indicated that hydrogen content was definitively lower in epitaxial films as compared to a-Si:H ones, and also indicated the possibility that H could diffuse much more easily in (100) Si than in (111) Si. Indeed, if one wanted to grow an epitaxial film, one would expect to get rid of hydrogen in the growing film, and hydrogen, if not incorporated, has only two options: going back to the gas phase or diffuse into c-Si. It would require a much finer resolution to investigate the H diffusion into c-Si during the deposition since the only significant change occurred upon a H₂ plasma treatment rather than upon the deposition itself but it has still enabled us to discriminate a different diffusion coefficient of H, *under plasma exposure* at least, depending on the c-Si orientation. So far, these measurements did not allow to check if there were more hydrogen in the crystalline silicon when the film was epitaxial or not. However, it should be noted that Tsai *et al.* [17] had performed deposition with D₂ dilution that led them to conclude that in both a-Si:H and epitaxial film there was about the same 17 ratio between hydrogen coming from SiH₄ and from H₂. We are still lacking of data regarding the possibility of hydrogen being sent back to the gas phase and questions

¹Tsai, Anderson, and Thompson, "Low temperature growth of epitaxial and amorphous silicon in a hydrogen-diluted silane plasma", 1991 [17]

²Teplin, Wang, Iwaniczko, Jones, Al-Jassim, Reedy, and Branz, "Low-temperature silicon homoepitaxy by hot-wire chemical vapor deposition with a Ta filament", 2006 [14]

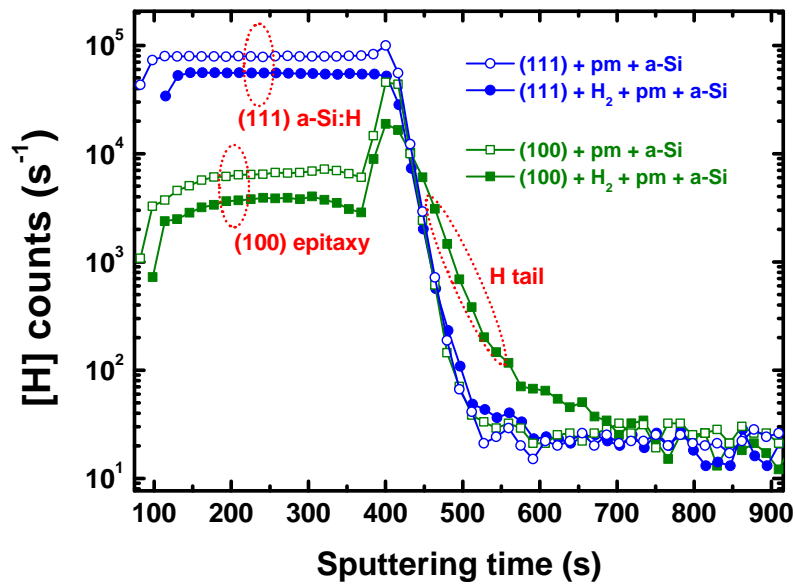


Figure 4.5 – SIMS profiles of H atoms along silicon thin films grown on (111) and (100), with or without a 2' H₂ plasma treatment. Films on (100) are epitaxial in both cases, films on (111) are amorphous.

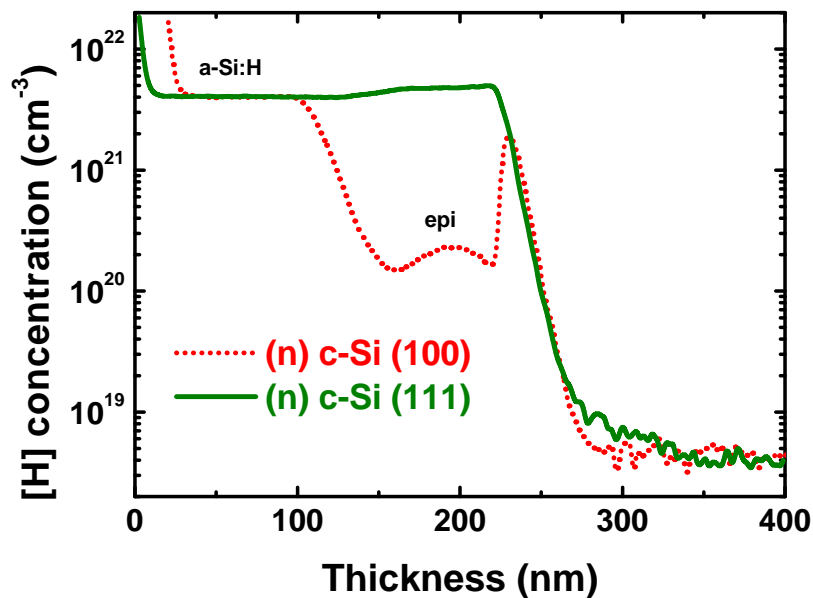


Figure 4.6 – H concentration from SIMS along silicon thin films grown on (111) and (100) for which the $\frac{H_2}{SiH_4+H_2}$ ratio varied (unintentionally) during the deposition from 80% to 0%.

about possible growth models are numerous. The next section will try to give an overview of what could be said about them.

4.1.3 Does someone know what happens ?

A detailed discussion of the growth mechanisms leading to an epitaxial growth at such low temperature in a standard RF PECVD system was beyond the scope of this thesis. This work would have involved many plasma characterizations coupled to some in-situ surface investigations. It would have also included some numerical calculations of molecular dynamics. Nevertheless, it could be interesting to discuss our experimental results with respect to experimental and simulated results obtained by different research groups.

4.1.3.1 The facts

Epitaxial growth by low temperature plasma processes has not been in itself an active subject of research over the last three decades by researchers working in the field of amorphous and microcrystalline silicon. However, many papers reported the occurrence of such an epitaxial growth, but hardly provided a detailed discussion on the growth mechanisms.

Over the last decade, our group has been more and more focused on the generation of Si atoms clusters in the plasma, called nanoparticles. These particles, generated in the gas phase, depending on the plasma conditions, can exist under an amorphous or a crystallized form in the plasma: quantum molecular dynamics studies by *Brulin et al.* have shown that when exposed to atomic hydrogen, these nanoparticles could crystallize in the gas phase.¹ A nice review article on this experimental work has been published by *Roca i Cabarrocas et al.*,² and more general information on the physics and chemistry of dusty plasmas can be found in a review paper by *Hollenstein*.³ Additionally, these nanocrystals have been shown to play a very important role during the deposition of our films on glass. This was the case of polymorphous silicon, which is a material made up of small nanocrystals embedded in an amorphous silicon matrix.⁴ This was also the case of microcrystalline silicon.^{5,6} Indeed, in the work of *Kasouit et al.* [33], the nanoparticles, whose main driving force in such plasma reactor conditions was thermophoresis were more likely to deposit on the cold parts of the reactor (a cold finger in the paper) which was consistent with very crystallized $\mu\text{c-Si:H}$ films, instead of less crystallized or amorphous

¹Brulin, Ning, and Vach, "Hydrogen-induced crystallization of amorphous silicon clusters in a plasma reactor", 2006 [29]

²Roca i Cabarrocas, Nguyen-Tran, Djeridane, Abramov, Johnson, and Patriarche, "Synthesis of silicon nanocrystals in silane plasmas for nanoelectronics and large area electronic devices", 2007 [30]

³Hollenstein, "The physics and chemistry of dusty plasmas", 2000 [31]

⁴Roca i Cabarrocas, Fontcuberta i Morral, and Poissant, "Growth and optoelectronic properties of polymorphous silicon thin films", 2002 [32]

⁵Kasouit, Damon-Lacoste, Vanderhaghen, and Roca i Cabarrocas, "Contribution of plasma generated nanocrystals to the growth of microcrystalline silicon thin films", 2004 [33]

⁶Chaâbane, Suendo, Vach, and Roca i Cabarrocas, "Soft landing of silicon nanocrystals in plasma enhanced chemical vapor deposition", 2006 [2]

films. In the paper from *Chaâbane et al.* [2], it was also shown that as such small nanocrystals are not large enough to be systematically negatively charged, so that they can experience charge fluctuations and be positively charged, as it could be experimentally observed by *Abolmasov et al.*¹. Depending on the value of the DC bias applied to the cooled substrate holder they could get 100% a-Si:H or 100% $\mu\text{c-Si:H}$ films.

Interestingly enough, we have found that such deposition conditions, polymorphous or microcrystalline silicon, when applied to (100) oriented crystalline silicon substrates, would lead to an epitaxial growth.^{2,3} Moreover, similar process conditions applied to germane (GeH_4) plasmas have been shown to produce epitaxial growth on (100) GaAs wafers. These conditions were again correlated to the formation of Ge nanocrystals in the plasma that could be collected on a TEM grid.⁴ Similarly, *Diaz et al.* have also published about the detection of nanoclusters in their mesoplasma and have correlated this appearance with epitaxial growth regimes.⁵ However in this case the substrate temperatures were usually much higher, in the 500-700°C range, so that it cannot be directly compared to our results.

4.1.3.2 Questioning

Based on this set of experiments, one can reasonably wonder if such nanocrystals are absolutely necessary to the epitaxial growth and if so, how such a growth occurs. In order to address this question, as we lack of clear experimental results, we need the assistance of researchers working on numerical calculations for molecular dynamics studies. Luckily enough, the LPICM possesses a small team dedicated to molecular dynamics studies. Indeed *Ning et al.* have published two papers about the interactions of silicon nanoclusters (Si_nH_m) with Si surfaces.^{6,7} Very roughly we could say that they have studied different sizes of clusters impinging with different impact energies on (100) Si surfaces at different temperatures. The authors suggested that epitaxial-like growth could occur when the impact energy is high enough to destroy the initial structure of the nanocluster and allows its atoms to greatly diffuse at the surface and be incorporated to the network, accompanied by H evaporation. The impact energy should also be low enough for the cluster not to penetrate the substrate, so that no damage of the c-Si surface is created. According

¹Abolmasov, Kroely, and Roca i Cabarrocas, "Negative corona discharge: application to nanoparticle detection in rf reactors", 2009 [34]

²Veschetti, Muller, Damon-Lacoste, Cabarrocas, Gudovskikh, Kleider, Ribeyron, and Rolland, "Optimisation of amorphous and polymorphous thin silicon layers for the formation of the front-side of heterojunction solar cells on p-type crystalline silicon substrates", 2006 [6]

³Labrune, Moreno, and Cabarrocas, "Ultra-shallow junctions formed by quasi-epitaxial growth of boron and phosphorous-doped silicon films at 175°C by rf-PECVD", 2010 [35]

⁴Johnson, Patriarche, and Roca i Cabarrocas, "Directional growth of Ge on GaAs at 175°C using plasma-generated nanocrystals", 2008 [36]

⁵Diaz, Kambara, and Yoshida, "Detection of Si nanoclusters by x-ray scattering during silicon film deposition by mesoplasma chemical vapor deposition", 2008 [37]

⁶Ning, Rinaldi, and Vach, "An atomic-scale study of hydrogenated silicon cluster deposition on a crystalline silicon surface", 2009 [38]

⁷Ning and Vach, "Deposition Dynamics of Hydrogenated Silicon Clusters on a Crystalline Silicon Substrate under Typical Plasma Conditions", 2010 [39]

to them these conditions could be easily fulfilled by loosely bonded clusters, as it is the case for amorphous ones. They even suggested that H concentration in the plasma should be decreased and that neutral carrier gases (Ar, He) could be used to cool down the structures, favouring an amorphous final state. To support this, they cited the work of *Biswas et al.* who also studied, by molecular dynamics simulations, the deposition of nanoclusters on (111) Si,¹ and who observed that epitaxial growth of silicon thin films could be achieved if there were a large spreading of the cluster's atoms at the surface upon impinging to allow for a larger surface diffusion and a rearrangement in a crystalline way.

Such results suggest that nanocluster assisted deposition could be the explanation for epitaxial growth. Indeed, NREL researchers have reported epitaxial growth on (100) Si with HWCVD process at temperatures as low as 200°C,² but believed such a growth to depend on SiH₃ radicals and H chemistry. Nevertheless, it has also been shown that HWCVD process could lead to the generation of crystalline nanoparticles in the gas phase.³

On the other hand, such explanations did not provide a clear answer to the crystalline orientation selectivity of the epitaxial growth no more did they provide a clear view on the role of hydrogen, which seemed experimentally to be necessary. We may also consider that not all of the people who experienced epitaxial growth were working in plasma conditions favourable to important gas phase reactions leading to the creation of nanocrystals. Indeed, we observed an epitaxial over-growth on a first epitaxial layer (Fig. 4.3) by using a silane plasma at 60 mTorr, a pressure commonly considered to be sufficiently low to avoid powders formation, if not any nucleation. Additionally, some ab initio calculations performed by *Cereda et al.*⁴ have evidenced the role, already experimentally perceived, of hydrogen in the promotion of epitaxial growth of silicon by PECVD on (100) Si. The paper by *Tsai et al.*⁵ was used by them as the experimental base of their work. Their calculations showed that thermal H can etch weakly adsorbed species (not epitaxial sites) and promote the incorporation of adsorbed -SiH₃ into epitaxial sites: if an H atom from a Si-H bond is removed from a neighbouring site of an adsorbed SiH₃ radical, it will very easily allow its incorporation into an epitaxial site. These calculations could also explain the etching selectivity of H, also introduced by *Tsai et al.*, which consisted in a much faster etching of the amorphous areas compared to the crystalline areas. Similarly, other kinetic Monte-Carlo calculations were performed by *Tan and Yang*,⁶ leading to some sim-

¹Biswas, Grest, and Soukoulis, "Molecular-dynamics simulation of cluster and atom deposition on silicon (111)", 1988 [40]

²Thiesen, Iwaniczko, Jones, Mahan, and Crandall, "Growth of epitaxial silicon at low temperatures using hot-wire chemical vapor deposition", 1999 [41]

³Lee, Kim, and Hwang, "Gas phase nucleation of crystalline silicon and their role in low-temperature deposition of microcrystalline films during hot-wire chemical vapor deposition", 2008 [42]

⁴Cereda, Zipoli, Bernasconi, Miglio, and Montalenti, "Thermal-Hydrogen Promoted Selective Desorption and Enhanced Mobility of Adsorbed Radicals in Silicon Film Growth", 2008 [43]

⁵Tsai, Anderson, Thompson, and Wacker, "Control of silicon network structure in plasma deposition", 1989 [18]

⁶Tan and Yang, "Physical mechanisms of hydrogen-enhanced onset of epitaxial growth of silicon by plasma-enhanced chemical vapor deposition", 2008 [44]

ilar conclusions as *Cereda et al.* This paper added some information on the temperature dependence of such processes but their calculations were directly based on the transition probabilities extracted from the work of *Cereda et al.* In *Tan and Yang* case, surface diffusion was even ignored for it was said to have no significant impact on the onset of epitaxial growth, whereas in the case of *Cereda et al.*, it was proved to be significant for temperatures higher than 300°C. These results [43, 44] did not assume, in fact did not need, the presence of nanoclusters, but assumed that H atoms could etch some bound H and thus create DB at the surface. Such a mechanism has been proposed to be even more likely than the direct H abstraction by a SiH_3 radical,¹ proposed by several authors.^{2,3} Regarding the crystalline orientation dependence, there were some experimental evidences and geometrical explanations for the strong orientation dependence of the epitaxial regrowth, i.e. recrystallization of an a-Si layer on top of a c-Si substrate, which favoured (100) over (111), as it has been observed experimentally by *Csepregi et al.*⁴ On Fig. 4.7, we have shown two figures,

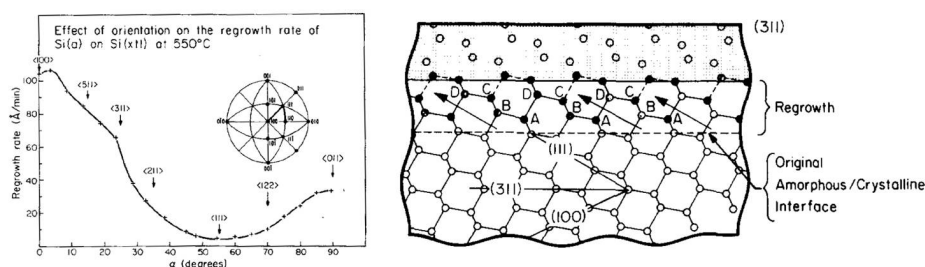


Figure 4.7 – On the left, regrowth rate of an amorphous silicon on crystalline silicon at 550°C as a function of the crystalline orientation of the a-Si/c-Si interface. On the right, section looking down the $[01\bar{1}]$ axis in Si. Indices denote intersections of the named plane with the $[01\bar{1}]$ plane. Assuming atoms can be transferred from the amorphous to crystalline phase at positions where at least two nearest-neighboring atoms are already in crystalline positions, the atoms marked A will occupy the crystalline position first, then B, C, etc. Images and legends from Ref. [48]

extracted from Ref. [48], which shows on the left, the regrowth rate of the a-Si/c-Si interface where the a-Si layer is obtained by the amorphization of c-Si. The regrowth rate was maximum for (100) planes and minimum for (111) planes. In their article, the authors predicted a zero regrowth rate, non observed, for (111) planes. On the right, the intersection lines of the named planes with the $[01\bar{1}]$ plane are shown. Their assumption was that one silicon atom needed two silicon atoms in lattice positions to bond in a crystalline lattice site, which was much easier perpendicular to (100) planes or (311) planes compared to (111). Note that this was a 2D representation of a 3D network so that some bonds are to be considered even if not drawn. On Fig. 4.8 we have represented the unit cell of the Si (dia-

¹Gupta, Yang, and Parsons, "Ab initio analysis of silyl precursor physisorption and hydrogen abstraction during low temperature silicon deposition", 2002 [45]

²Ramalingam, Maroudas, Aydil, and Walch, "Abstraction of hydrogen by SiH_3 from hydrogen-terminated $\text{Si}(001)-(2 \times 1)$ surfaces", 1998 [46]

³Cereda, Ceriotti, Montalenti, Bernasconi, and Miglio, "Quantitative estimate of H abstraction by thermal SiH_3 on hydrogenated $\text{Si}(001)(2 \times 1)$ ", 2007 [47]

⁴Csepregi, Kennedy, Mayer, and Sigmon, "Substrate-orientation dependence of the epitaxial regrowth rate from Si-implanted amorphous Si", 1978 [48]

mond) lattice. On both figure we have represented in red the atoms of the

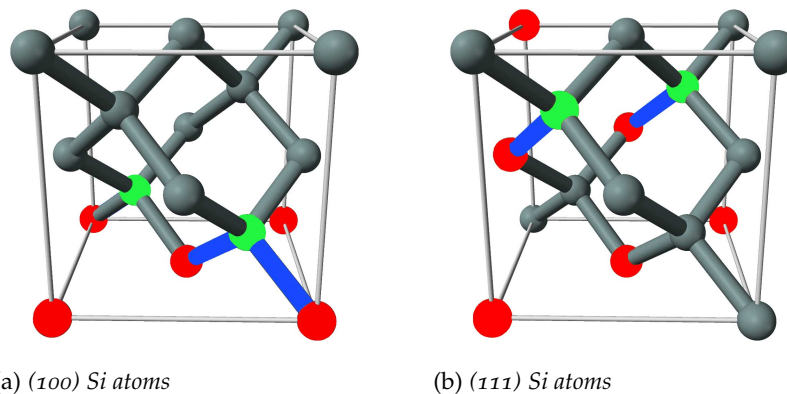


Figure 4.8 – Si atoms in the unit cell of the diamond lattice in (100), left, or (111) positions for two alternate planes and the possible bonds perpendicular to these planes.

first plane, in green the atoms of the next plane and in blue the possible bonds between these two planes for (100) planes on Fig. 4.8a and for (111) planes on Fig. 4.8b. It appears that in the case of (100) planes, each Si atom in the next plane has two bonds that allow for it to be incorporated in a lattice position whereas in the case of (111) it has only one bond, which may not be sufficient to favour an epitaxial growth. According to the authors regrowth on (111) planes would favour stacking faults and they also speculated on the fact that regrowth may require nucleation on (111) to grow epitaxially.

Similarly, *Weir et al.*¹ have shown that both (111) and (100) orientations possessed transition temperature below which there was no epitaxy but an amorphous growth on (100) and a great increase in defects leading to an amorphous growth on (111). They observed that such growth transition was relatively sharp regarding the temperature dependence in both cases ($\approx 30^\circ\text{C}$). They also showed, experimentally and by molecular dynamics simulations that the temperature needed to achieve a good quality epitaxy on (111) Si was a few hundreds degrees higher than on (100) which could occur close to room temperature, as also observed using MBE on (100) Si by *Eaglesham et al.*,² who obtained similar results as they confirmed that no temperature cut-off existed but there was an exponential decrease of the epitaxial thickness which led to thicknesses of 10-30 Å at room temperature. Interestingly enough, *Weir et al.* obtained from their calculations a surface diffusion rate, generally acknowledged as a requirement for good epitaxial quality, one order of magnitude higher on (111) than on (100) despite the fact that there was a $\approx 300^\circ\text{C}$ difference in their transition temperature. Citing the already mentioned work of *Csepregi et al.* [48], they finally ascribed such a difference to the different bonding geometries and the propensity of growing stacking faults on (111) Si.

Regarding the epitaxy breakdown phenomenon, it appeared to be rather abrupt, as seen from TEM in Ref. [50] for MBE process and has

¹Weir, Freer, Headrick, Eaglesham, Gilmer, Bevk, and Feldman, "Low-temperature homoepitaxy on Si(111)", 1991 [49]

²Eaglesham, Gossmann, and Cerullo, "Limiting thickness h_{epi} for epitaxial growth and room-temperature Si growth on Si(100)", 1990 [50]

been ascribed by the authors to a roughening of the interface causing an amorphous nucleation growth. We have no data at LPICM on epitaxy breakdown but interestingly enough, *Teplin et al.*^{1,2} reported TEM analysis on Si epitaxial films grown by HWCVD where the transition from crystalline to amorphous was much less abrupt and where existed cone-shaped areas of amorphous in the crystalline layer. Thus, crystalline and amorphous growth existed at the same time on the surface, with an increasing amorphous to crystalline ratio, until all the amorphous areas were big enough to cover the entire surface of the film and resulting in a subsequent 100% amorphous growth. Their TEM images showed cone-shaped structures, with an increasing amorphous fraction. Additionally, they performed SIMS analysis and showed an increasing H concentration as the a-Si:H/c-Si area ratio increased. This is similar to our results of Fig. 4.6, which showed that epitaxial layers had an hydrogen content about one order of magnitude lower than that of a-Si:H layers.

4.1.3.3 Lessons

Finally it appeared that no definitive conclusions could be drawn from our experimental results and from the literature. Even though nanocrystal assisted depositions could lead to increased deposition rates, there was no clear evidence, both from simulations and experiments, that their presence was a mandatory requirement for epitaxial growth. However, it seemed that the presence of hydrogen played a major role, suggesting that we are facing a growth in very different conditions from what is known from MBE for instance, where hydrogen is known to disrupt the epitaxial growth.^{3,4} It also appeared that surface diffusion at such low temperatures (<175°C) was not dominant. Therefore we should take into account the specificities of PECVD processes, which can include ion bombardment, atomic H and nanoclusters impingements, by nature significantly different from MBE processes, for which the surface mobility of evaporated atoms is very low at such temperatures,⁵ that could result in an enhanced mobility of the species at the surface, favouring the incorporation into epitaxial sites, and allowing for much higher epitaxial thicknesses, e.g. up to 2.4 μm at 165°C, as we will show in the next section, that what could be expected from MBE at higher temperatures.

4.1.4 Intrinsic epitaxy: towards a wafer equivalent approach

Crystalline silicon solar cells use for their contacts (emitter and BSF) heavily doped silicon layers. In this case, one of the main requirement is to

¹Teplin, Wang, Iwaniczko, Jones, Al-Jassim, Reedy, and Branz, "Low-temperature silicon homoepitaxy by hot-wire chemical vapor deposition with a Ta filament", 2006 [14]

²Teplin, Levi, Iwaniczko, Jones, Perkins, and Branz, "Monitoring and modeling silicon homoepitaxy breakdown with real-time spectroscopic ellipsometry", 2005 [51]

³Wolff, Wagner, Bean, Hull, and Gibson, "Hydrogen surface coverage: Raising the silicon epitaxial growth temperature", 1989 [52]

⁴Eaglesham, Unterwald, Luftman, Adams, and Yalisove, "Effect of H on Si molecular-beam epitaxy", 1993 [53]

⁵Nützel, Brichzin, and Abstreiter, "RHEED investigations of surface diffusion on Si(001)", 1996 [54]

have a low resistivity film to collect efficiently the carriers and the unavoidable defects in such layers are of lesser importance compared to the material used to make the absorber of the solar cell itself. In the next section we will see that our experimental set-up does not allow us to grow lowly doped Si films¹ that could be desirable for such thick p-i-n structures, possibly thicker than the length on which the depletion zone extends. Such a long distance collection cannot happen in very doped layers where carriers would recombine. However we can grow undoped layers, where the “undoped” has to be understood in the meaning of “non intentionally doped”. Indeed, one way to take advantage of the ability to deposit undoped epitaxial layers could be to use them in a so-called wafer equivalent approach. The usual acceptance of this denomination is to grow a relatively thick epitaxial layer (2–50 μm), on a highly doped seed substrate, by epitaxial growth or by recrystallization processes. Indeed, recent results for various thicknesses have demonstrated efficiencies of 7% for 2 μm ,² a 15% efficiency for 20 μm ,³ and a 17% efficiency for 50 μm .⁴

We have already shown that the conditions leading to $\mu\text{c-Si:H}$ or pm-Si:H or a-Si:H in hydrogen dilution all led to epitaxial growth on (100)-oriented substrates. However, even though the growth mechanisms in the case of the epitaxial growth were not well described in the literature, as seen in the previous section, we still have had to find, experimentally, what were the “best” conditions to grow undoped epitaxial films. The fact is that this was not an easy task since our laboratory is not specialized in epitaxy and its associated characterization techniques. Our approach was to study, as a first order approximation, the grown films by spectroscopic ellipsometry. Indeed, spectroscopic ellipsometry is a very powerful tool to characterize thin films, regarding their thicknesses and composition, but only provides macroscopic information on optical properties. Still, such optical studies have already been carried out on epitaxial films, showing that it was possible, not only to detect the presence of an epitaxial growth instead of an amorphous growth,^{5,6} but also to model the epitaxial films like *Teplin et al.*⁷ or even in our laboratory with *Moreno et al.*⁸

The spectroscopic ellipsometry technique and the way to design a sim-

¹Mass Flow Controller not adapted, dopant cylinders not diluted enough

²Alberi, Martin, Shub, Teplin, Romero, Reedy, Iwaniczko, Duda, Stradins, Branz, and Young, “Material quality requirements for efficient epitaxial film silicon solar cells”, 2010 [55]

³Kuzma-Filipek, Nieuwenhuysen, Hoeymissen, Payo, Kerschaver, Poortmans, Mertens, Beaucarne, Schmich, Lindekugel, and Reber, “Efficiency (>15%) for thin-film epitaxial silicon solar cells on 70 cm² area offspec silicon substrate using porous silicon segmented mirrors”, 2010 [56]

⁴Reuter, Brendle, Tobail, and Werner, “50 μm thin solar cells with 17.0% efficiency”, 2009 [57]

⁵Gielis, van den Oever, Hoex, van de Sanden, and Kessels, “Real-time study of a-Si:H/c-Si heterointerface formation and epitaxial Si growth by spectroscopic ellipsometry, infrared spectroscopy, and second-harmonic generation”, 2008 [3]

⁶Wang, Teplin, Stradins, To, Jones, and Branz, “Significant improvement in silicon chemical vapor deposition epitaxy above the surface dehydrogenation temperature”, 2006 [4]

⁷Teplin, Levi, Iwaniczko, Jones, Perkins, and Branz, “Monitoring and modeling silicon homoepitaxy breakdown with real-time spectroscopic ellipsometry”, 2005 [51]

⁸Moreno and Roca i Cabarrocas, “Ultra-thin crystalline silicon films produced by

ple model and fit it to the experimental data has been presented in chapter 2 (§2.1.4, p. 49). Based on that, spectroscopic ellipsometry allowed us to distinguish between amorphous, epitaxial and mixed phase materials. Thus, it was reasonable to start a rough optimization of the epitaxial growth conditions based on this technique. Hence, we made a series of depositions on (100)-oriented c-Si substrates where we varied the SiH_4 flow rate while keeping all the other parameters constant. All the depositions were made at 175°C , with a 17 mm inter-electrode distance, at a pressure of 2.2 Torr and a power density of $58 \text{ mW}\cdot\text{cm}^{-2}$. The H_2 flow rate was set at 500 sccm and we varied the SiH_4 flow rate in the range from 8 to 50 sccm. The lowest SiH_4 flow rate, namely 8 sccm, corresponded to conditions known to lead to $\mu\text{c-Si:H}$ on glass. As soon as the SiH_4 flow rate was increased, the plasma conditions moved towards pm-Si:H conditions.

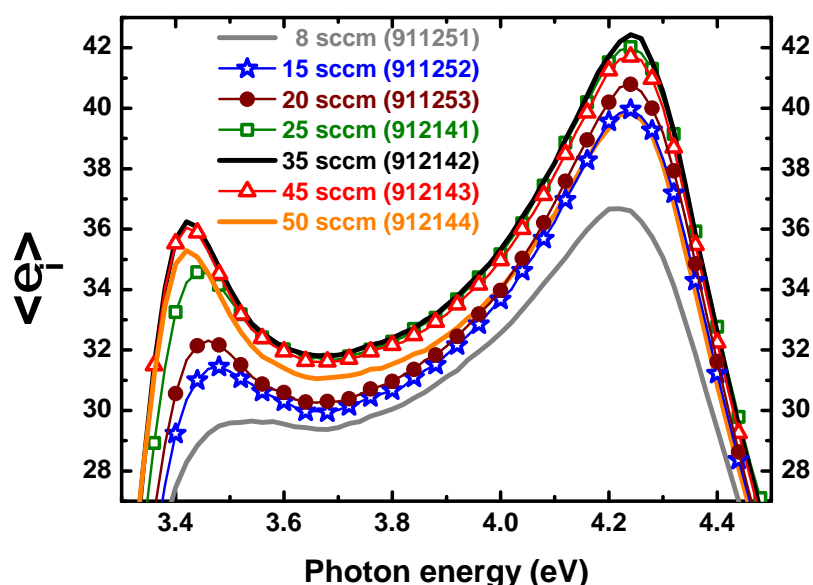


Figure 4.9 – Imaginary part of the pseudo-dielectric function of epitaxial films grown with different SiH_4 flow rates, close-up view in the photon energy range of interest for crystalline films

On Fig. 4.9, we have plotted the imaginary part of the pseudo-dielectric function of these films deposited on c-Si. This graph has been zoomed in order to get a close-up picture of what happened in the range of interest when dealing with crystalline Si materials, i.e. around the 3.4 and 4.2 eV peaks. On this graph, one could observe an increase in the value of the pseudo-dielectric function until a certain SiH_4 flow rate before it started to decrease. At 50 sccm of SiH_4 , the surface of the sample exhibited inhomogeneous properties in a similar way of that of Fig. 4.1a and performing SE measurements on other spots on the same sample showed amorphous spectra. This meant that the surface of the sample was divided into areas with epitaxial growth and amorphous growth. This amorphous growth could be the result of an initial amorphous growth starting from the sub-

plasma assisted epitaxial growth on silicon wafers and their transfer to foreign substrates”, 2010 [58]

strate or of an epitaxial breakdown, which has been studied by *Teplin et al.*^{1,2} In these papers, they performed TEM measurements on epitaxially grown films showing amorphous silicon cones extending towards the surface, embedded in a crystalline matrix.

On Fig. 4.10, we plotted the maximum of the pseudo-dielectric function measured by SE and the deposition rate against the SiH₄ flow rate. We also plotted on Fig. 4.11 the maximum of the pseudo-dielectric function and the percentage of monocrystalline silicon used to model the bulk layer of the epitaxial film.

Here, we need to make two short comments on these two graphs (4.10 and 4.11). Indeed, these samples were made in two different series:

1. SiH₄ flow rates of 8, 15, 20 and 25 sccm (November 2009)
2. SiH₄ flow rates of 25, 35, 45 and 50 sccm (December 2009)

The first remark is that these experiments were quite reproducible regarding the deposition rate since these two series have an overlapping point at 25 sccm. One can also note that the deposition rate was in our conditions proportional to the SiH₄ flow rate. The second one is that even if there was clear, concave, trend regarding the maximum of the pseudo-dielectric function of the films, there was a small discontinuity between the two series. This gap may have originated from a difference in the calibration of the ellipsometer and from a difference in the air exposure time resulting in slightly different surface oxides. However, this did not impede us from showing that a maximum exists. It was even more pronounced on Fig. 4.11 where we showed the fraction of monocrystalline silicon material used to model the bulk layer of our epitaxial films. The variations looked important but one should remember that in the case of highly crystallized films, the bulk layer was modelled by a mixture of monocrystalline, large grains and small grains polysilicon so that even though the ratio between these materials have changed the sum of the monocrystalline silicon and large grains polysilicon fractions was always extremely high so that the discontinuity at 25 sccm between the November and December series was not so drastic in terms of overall crystallinity.

As we said at the beginning of this paragraph, we were interested in using such undoped layers as the absorber of solar cells. This work received some great assistance from a summer student, Romain Cariou.³ The solar cell structure we used for this work is described in Fig. 4.12. It consisted of a (100)-oriented, p-type c-Si, highly doped ($\rho=0.01-0.02 \Omega\cdot\text{cm}$) that we used as a substrate for the epitaxial growth as well as an electrical contact to make a solar cell. On this wafer, we grew undoped epitaxial Si films of various thicknesses that we capped by a (n) a-Si:H layer in order to produce an heterojunction solar cell aiming at reducing the front surface recombination. The solar cells were finally defined by sputtering

¹Teplin, Levi, Iwaniczko, Jones, Perkins, and Branz, "Monitoring and modeling silicon homoepitaxy breakdown with real-time spectroscopic ellipsometry", 2005 [51]

²Teplin, Wang, Iwaniczko, Jones, Al-Jassim, Reedy, and Branz, "Low-temperature silicon homoepitaxy by hot-wire chemical vapor deposition with a Ta filament", 2006 [14]

³Cariou, Labrune, and Roca i Cabarrocas, "Thin crystalline silicon solar cells based on epitaxial films grown at 165°C by RF PECVD", 2011 [59]

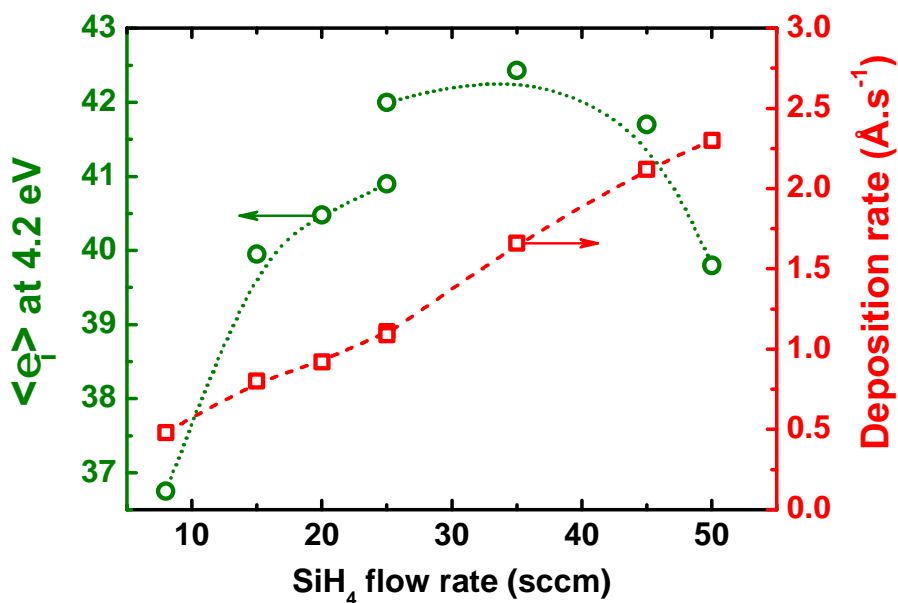


Figure 4.10 – Maximum of the pseudo-dielectric function and deposition rate plotted against the SiH_4 flow rate

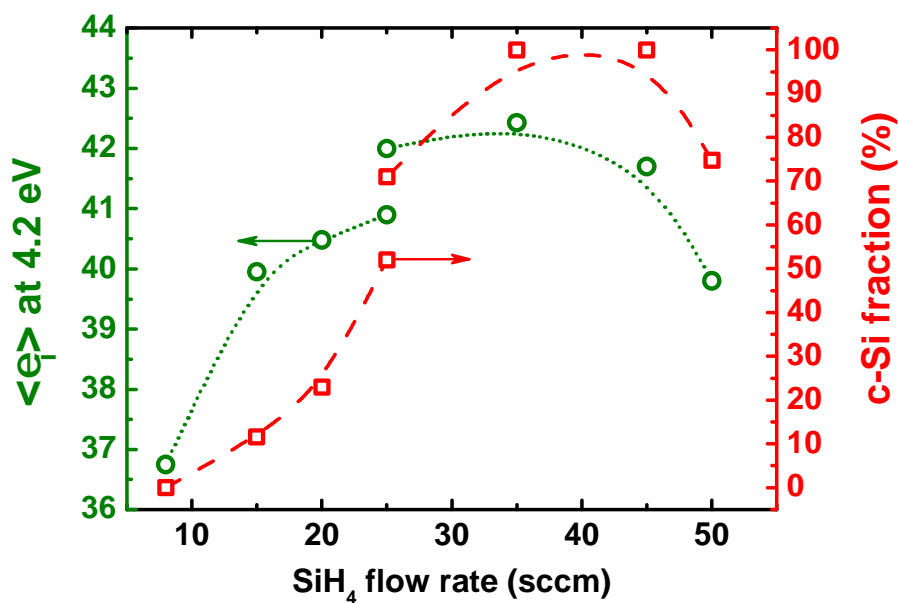


Figure 4.11 – Maximum of the pseudo-dielectric function and percentage of monocrystalline silicon in the model of the bulk layer plotted against the SiH_4 flow rate

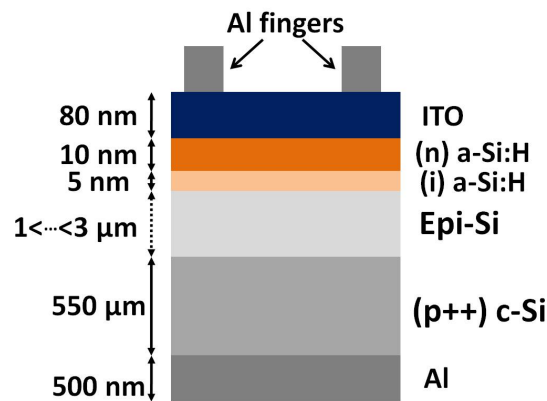


Figure 4.12 – Schematic view of the structure of the epitaxial cells we used

ITO squares through a shadow mask on top of which we evaporated aluminium grids. To ensure a better back contact we evaporated aluminium on the rear side of the solar cell.

The results of the current-voltage characteristics are shown on Fig. 4.13.

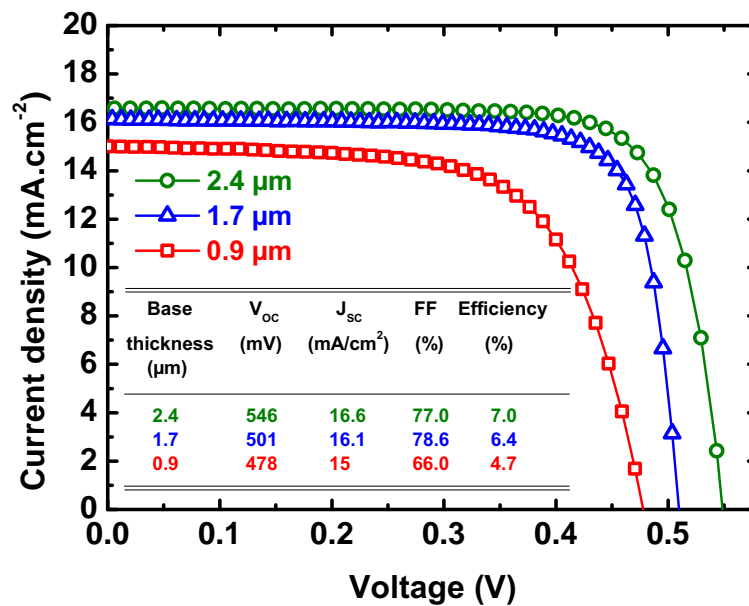


Figure 4.13 – Current-voltage characteristics of epitaxial solar cells deposited at 165°C with different base thicknesses

These results showed a clear increase of the short-circuit current density as the thickness of the absorber was increased. This trend was expected from the fact that the light that went through the device could be absorbed everywhere in the device but the carriers that could be collected only originated from the creation of electron-hole pairs in the epitaxial absorber layer and there was no (significant) contribution from the (n) a-Si:H emitter or the very doped substrate template. Such an assertion has been checked by a comparison between the experimental and modelled¹ exter-

¹Using the PC1D software

nal quantum efficiency. More details on the simulations can be found in the Ref. [59].

Interestingly we had a constant increase in the V_{oc} with increasing the thickness of the absorber layer, and also an increase in FF for thicker absorbers. One could argue that our depositions were done at 165°C , a rather low substrate temperature, and that increasing the deposition time (thickness) would have allowed for better material properties since it was annealed during the deposition, the deposition time increasing with the base thickness. At the same time that the bulk properties may improved, by increasing the thickness of the base, it became less sensitive to the interface and thus the bulk quality started to show a more pronounced role, as long as we stayed in a thickness range smaller than a few diffusion length [55].

We believe that these results are extremely important for they showed that epitaxial growth of high quality material, at least for PV applications, was feasible at very low substrate temperatures. The growth rate of $\approx 1.5 \text{ \AA}\cdot\text{s}^{-1}$ was not very impressive but remained of the same order of magnitude as the ones we obtained for a-Si:H or $\mu\text{-Si:H}$ depositions for similar substrate temperatures. To our knowledge, most people involved in this so-called wafer-equivalent approach used growth techniques that involved fairly high substrate temperatures, and thus higher deposition rates, but have claimed to be unable to decrease the temperature without a great loss in the material properties (or diode characteristics) if not a loss of the epitaxial regime itself [55].

4.1.5 Epitaxial growth of doped layers

Undoped epitaxial layers are of great interest but we are also very interested in getting doped semiconducting layers. Hence we have tried, with the same available PECVD tool to grow doped epitaxial films by adding phosphine for n-type doping or diborane or TMB for p-type doping. Both TMB and diborane were 2%-diluted in H_2 whereas phosphine was 0.1%-diluted in H_2 .

4.1.5.1 Boron-doped epitaxy

At the early stages of the optimisation of the intrinsic series we made a few tests on boron doping by incorporating some diborane to the gas mixture. That was the first series. We used the conditions that gave the best epitaxy at that time¹ and incorporated diborane to the gas mixture at various flow rates. We grew the film at 175°C , with a 17 mm inter-electrode distance and a pressure of 2200 mTorr for a power density of $62 \text{ mW}\cdot\text{cm}^{-2}$. The description of the samples is given in Tab. 4.2.

Sample name	911255	911256	911257	911258	911259	9112510
B_2H_6 (sccm)	0.5	1	1.5	2	3	5

Table 4.2 – Sample name and corresponding flow rate of the B_2H_6 series

¹We used 25 sccm instead of 35 sccm for the SiH_4 flow rate, which resulted in a very similar material, optically (SE) speaking, but at a smaller deposition rate and did not allow for minimum $\frac{\text{B}_2\text{H}_6}{\text{SiH}_4}$ ratio.

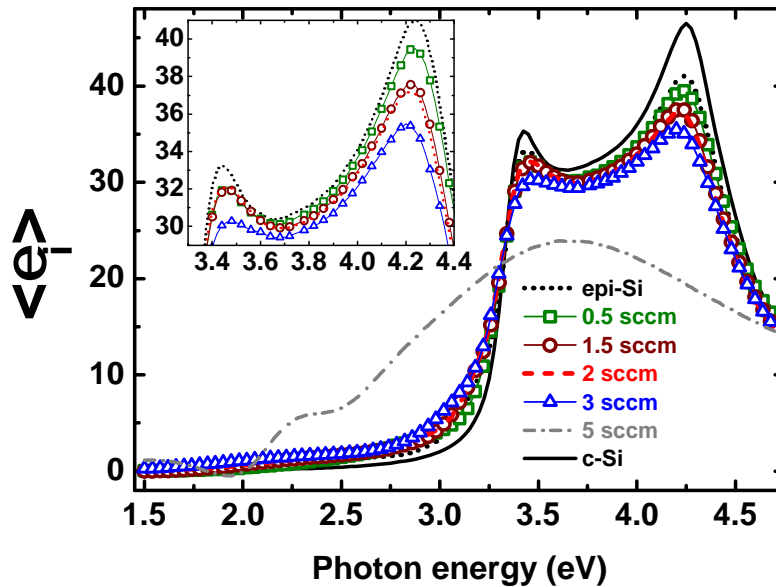


Figure 4.14 – Imaginary part of the pseudo-dielectric function of silicon thin films grown on (100) Si substrates for various flow rates for B_2H_6 . We added the pseudo-dielectric function of the film grown without dopant (undoped) and the dielectric function of silicon for comparison

On Fig. 4.14, we have plotted the imaginary part of the pseudo-dielectric function of the boron-doped silicon thin films. We also added the pseudo-dielectric function of the film grown without the diborane gas and the one from c-Si. On this graph, it appeared very clearly that increasing the diborane flow rate degraded the SE spectrum in terms of crystallinity until we reached an amorphous growth. However, we had the ability to increase the flow rate of diborane until a value of 3 sccm while maintaining the crystalline nature of the film and even at 2 sccm there was almost no loss in the crystallinity, with respect to the undoped sample, but rather in the roughness, which was slightly increased, as it appeared from the height of the peak at 4.2 eV. These results were very interesting but did not tell much about the electronic properties of such layers. Indeed, additional data would be needed in order to assess the quality of such layers in terms of carrier transport and electrical conductivity.

One possible way to investigate the quality of doped layers is to fabricate a device based on such layers. The best example being a photovoltaic cell. This has been done and will be discussed below but this will not give straightforward information. For that purpose we could use a Hall effect measurement set-up that allowed for temperature dependent measurements. In that case, the epitaxial films were grown on highly resistive (100) c-Si wafers that were purchased from PBT Silicon and were 500 μm thick for a resistivity higher than 10000 $\Omega\cdot\text{cm}$.

We grew a second series of samples. The goal of this series was to perform Hall effect measurements and in that case to have a closer look to the influence of the substrate temperature on the growth of our epitaxial films. These samples are described in Tab. 4.3 and the SE measurements

are plotted on Fig. 4.15. Basically we chose two flow rates for both diborane and TMB gases. We used 3 sccm for diborane which is known to be a relatively high flow rate (based on Fig. 4.14) but that belongs to a range where the mass flow controller worked quite accurately whereas we chose 0.8 sccm for TMB which is the flow rate used to grow (p) $\mu\text{c-Si:H}$ layers.

Dopant	Flow rate (sccm)	175°C	200°C	225°C
diborane	3	1001073	1001074	1001075
TMB	0.8	1001083	1001082	1001081

Table 4.3 – Sample name and corresponding growth temperature of the Boron-doping series

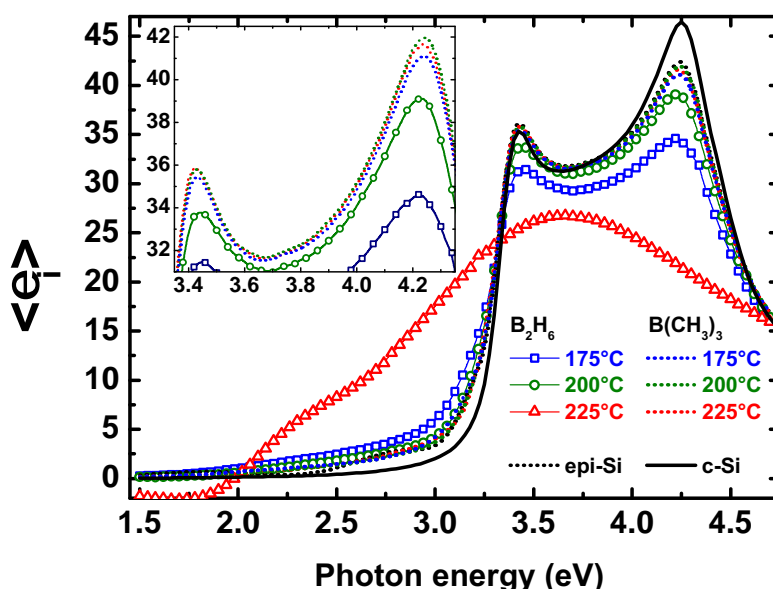


Figure 4.15 – Imaginary part of the pseudo-dielectric function of silicon thin films grown on (100) Si substrates for various substrate temperatures at fixed flow rates for B_2H_6 and TMB ($\text{B}(\text{CH}_3)_3$). We added the pseudo-dielectric function of the film grown without dopant (undoped) and the dielectric function of silicon for comparison

On Fig. 4.15, we have plotted the pseudo-dielectric function of our boron-doped silicon thin films for the three substrate temperatures and the two doping gases. From this graph it appeared that the temperature had no significant effect on the samples for which the dopant was TMB, whereas there were drastic changes in the spectra of the films grown with diborane. The sample grown at 200°C showed a better crystallinity that the one grown at 175°C but the one at 225°C was amorphous (at least on most of the growth area). This epitaxial to amorphous transition could be explained by the fact that diborane is a gas known to be able to dissociate thermally, even at 175°C. It is known that such a dissociation can lead to a CVD-like growth of boron-silicon alloys when a surface is exposed to a

$\text{SiH}_4 + \text{B}_2\text{H}_6$ gas mixture.^{1,2} In our case this meant that the “effective” flow rate of impinging boron reactive compounds at the surface was fixed not only by the diborane flow rate but also by the reactor temperature. At 225°C, we incorporated more boron to the film and it became much easier to get an epitaxial breakdown than at lower temperatures.

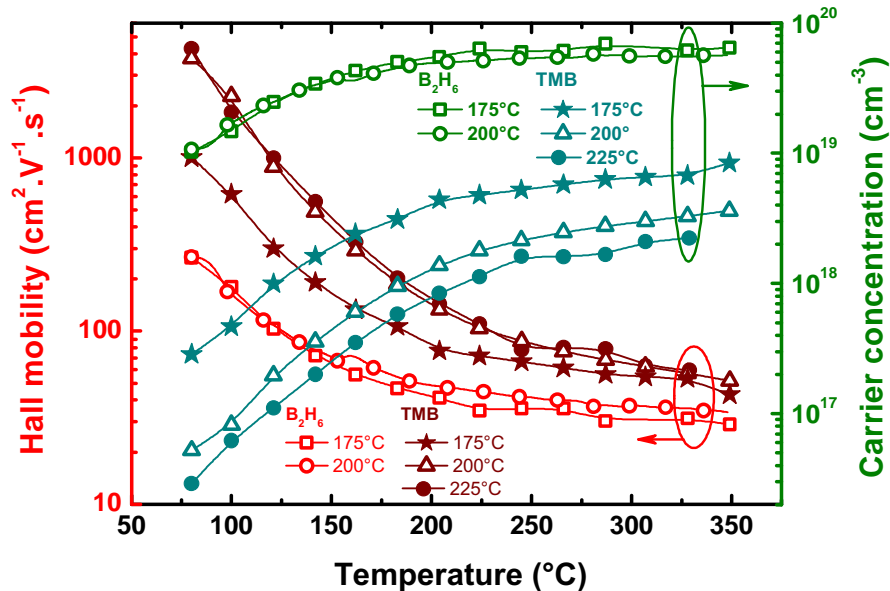


Figure 4.16 – Carrier concentration and mobilities as a function of the sample temperature as deduced from Hall effect measurements for epitaxial films grown at various substrate temperatures and at fixed flow rates for B_2H_6 and TMB ($\text{B}(\text{CH}_3)_3$).

On Fig. 4.16 we have plotted both carrier concentration and Hall mobility as a function of the sample temperature for all the boron-doped films of this series, except for the amorphous one (diborane at 225°C). These measurements were carried out after a 30 minutes anneal at 270°C. Indeed, it was not possible to obtain a good ohmic contact on any of the films in their as-deposited state. After this short annealing step, Hall effect measurements were much easier, with or without the help of small silver paste dots in the corners of the square samples.

The two series of films followed a similar behaviour regarding the mobility and the carrier (hole) concentration, no matter whether diborane or TMB was used. The main difference came from the fact that the films doped with diborane showed a carrier concentration of about one order of magnitude higher than those doped with TMB. This was probably due to the fact that diborane flow rate was set at a rather high value and the TMB flow rate to a rather low value. Moreover, TMB is a molecule ($\text{B}(\text{CH}_3)_3$) that possesses three carbon atoms for one boron atom. We could expect the TMB to introduce more defects into the crystalline network and by do-

¹Roca i Cabarrocas, Kumar, and Drévilion, “In situ study of the thermal decomposition of B_2H_6 by combining spectroscopic ellipsometry and Kelvin probe measurements”, 1989 [60]

²Collins, “In situ study of p-type amorphous silicon growth from $\text{B}_6\text{H}_6:\text{SiH}_4$ mixtures: Surface reactivity and interface effects”, 1988 [61]

ing so decrease the doping efficiency and the transport properties of such doped films. Anyway, these data could give us a rather good idea of the available doping densities achievable in our PECVD set-up.

Finally, one should note that both TMB and diborane gases were 2%-diluted in H₂ so that it would require even more diluted cylinders to achieve lower carrier concentrations in our films. A more diluted diborane cylinder has been purchased but not yet used.

We have a set of experimental data but we needed to compare these results to what we could expect. *Masetti et al.*¹ have published a paper in which they give an analytical formula to describe the mobility of silicon films doped with boron and phosphorous as a function of the temperature and the doping concentration over a very wide range of doping concentration. This formula has been checked against a very large number of experimental data already published. From this paper we can express, in the case of boron-doping in the 10¹⁴ to 10²¹ cm⁻³ range, the mobility at 300 K as follows:

$$\mu_h = \mu_0 e^{\frac{-pc}{p}} + \frac{\mu_{max}}{1 + (\frac{p}{C_r})^\alpha} - \frac{\mu_1}{1 + (\frac{C_s}{p})^\beta}$$

The values of each of the constant parameters can be found in Ref. [62]. Based on this formula we could obtain the mobility at 300 K for our two sets of films. We obtained $\mu = 52 \text{ cm}^2 \cdot \text{V}^{-1} \cdot \text{s}^{-1}$ at a carrier concentration of $6 \times 10^{19} \text{ cm}^{-3}$ and $\mu = 100 \text{ cm}^2 \cdot \text{V}^{-1} \cdot \text{s}^{-1}$ at a carrier concentration of $3 \times 10^{18} \text{ cm}^{-3}$. Even though these values remained higher by a factor of about two than the experimental values, they remained fairly high for such a high doping, in the near-degenerated range. Thus, despite of the low temperature growth process our layers exhibited electrical properties close to those of c-Si.

As said earlier, another interesting way to look at doped epitaxial layers is to use them in a photovoltaic cell. That was what we did at the early stages of our studies. We fabricated heterojunction solar cells on (n) c-Si wafers where we grew a p-type epitaxial layer instead of a (p) a-Si:H layer to form the emitter, whereas the BSF was still made up of a (i/n) a-Si:H stack. Lifetime measurements showed that almost no passivation was achieved on such cells leading to low implied V_{oc} . The fact is that in such structure there was no passivation scheme on the front side, such as an a-SiN_x:H layer. Instead, we sputtered an ITO film onto the front side, as for the heterojunction solar cells. The results are shown on Fig. 4.17 where we plotted the current-voltage characteristics of a homojunction (810032) and of a heterojunction solar cell where the only two differences were at the front side where the (p) a-Si:H layer was replaced by a p-type epitaxial layer and the ITO was DC-sputtered at Solems in the case of the homojunction and RF-sputtered at LPICM in the case of the heterojunction solar cell. In both cases the metal contacts were screen-printed, and the cells were laser cut to define a square cell with an area of 25 cm², and measured at INES. The above mentioned absence of passivation scheme showed on the values of the V_{oc} of the two cells. In the absence of passivation, homojunction, cell, the V_{oc} was more than 100 mV smaller. There

¹Masetti, Severi, and Solmi, "Modeling of carrier mobility against carrier concentration in arsenic-, phosphorus-, and boron-doped silicon", 1983 [62]

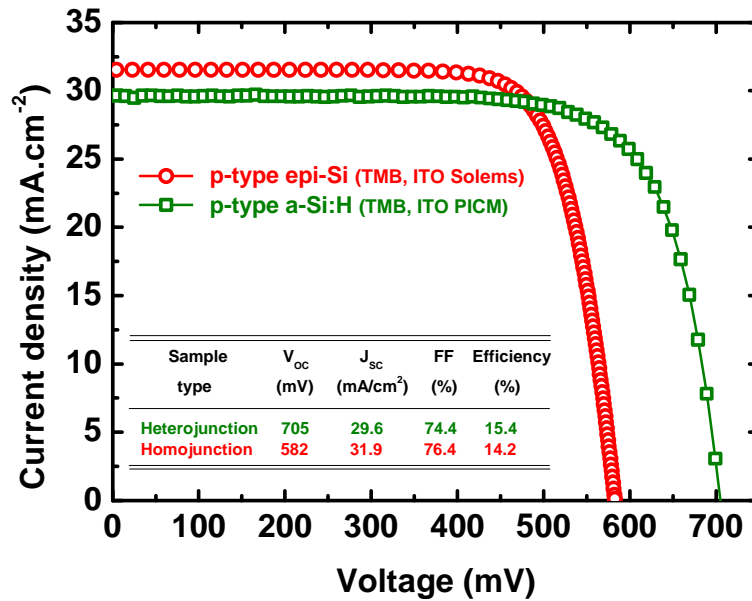


Figure 4.17 – Current-voltage of our homojunction and heterojunction solar cell

was also a difference between these two cells regarding the short-circuit current density. This difference could be explained by a higher absorption in the (p) a-Si:H layer compared to the p-type epitaxial layer but it mostly arose from the fact that the ITO from SOLEMS had always demonstrated higher short-circuit current density.

4.1.5.2 Phosphorous-doped epitaxy

In this series of experiments we grew silicon films using the same optimised conditions as the one used to grow undoped epitaxial Si films.¹ The difference here came from the fact that we added some phosphine (PH_3) to the gas mixture. The deposition was made at 200°C on c-Si substrates whose native oxide was removed by a HF-dip. We grew a few samples with various PH_3 flow rates. The samples have been described in Tab. 4.4 and we have plotted the imaginary part of the pseudo-dielectric function of these films on Fig. 4.18.

Sample name	1002251	1002255	1002252	1002253	1002254
PH_3 (sccm)	0.1	0.3	0.5	1	5

Table 4.4 – Sample name and corresponding flow rate of the PH_3 series

On Fig. 4.18, it appeared that the film grown with only 0.1 sccm of phosphine had a spectrum quite close to the one of the undoped layer. Indeed, the modelling of this stack showed a 100% c-Si layer. The only difference originated from the smaller peak at 4.2 eV which could be explained by a change in the roughness of the film which was higher for

¹These conditions were a pressure of 2200 mTorr for an inter-electrode distance of 17 mm and a plasma power density of $62 \text{ mW}\cdot\text{cm}^{-2}$. The flow rates were set at 500 sccm for H_2 and 35 sccm for SiH_4 .

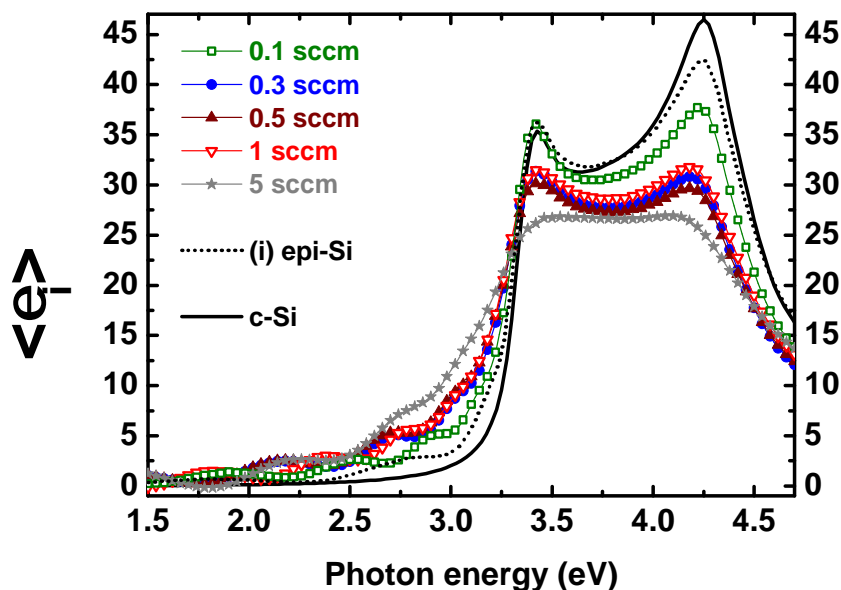


Figure 4.18 – Imaginary part of the pseudo-dielectric function of silicon thin films grown on (100) Si substrates with various PH_3 flow rates. We added the pseudo-dielectric function of the film grown without dopant (undoped) and the dielectric function of silicon for comparison

the phosphorous-doped film. The other films showed, even though scattered, quite similar spectra for the 0.3, 0.5 and 1 sccm, and had a lower amplitude for both peaks meaning that we had less crystallized films. Indeed, we needed to use the large grains and small grain polysilicon material to model the bulk layer. Here it must be remembered that we used our mass flow controller in the very small flow rate range. Therefore it was very difficult to obtain a repeatable and reliable flow rate at such values. This could explain why we did not “see” much difference between these three flow rates. The last sample, at 5 sccm, showed an even more degraded spectrum, meaning that we had an even less crystallized film, getting closer to the spectra obtained for highly crystallized $\mu\text{-Si:H}^1$ or polysilicon films, for which we could expect a different transport mechanism where grain barriers could play an important role, not to say determine, the electrical transport as explicated by *John Seto*.²

Based on these results, we could already conclude that even though it was possible to maintain a crystallized film, phosphorous was very efficient in decreasing the epitaxial quality. More studies would be needed to fully investigate the impact of phosphine on the growth of epitaxial Si thin films and an even more diluted cylinder (below the current 0.1% in H_2 dilution) would also be most desirable. Also, one could speculate on the fact that in plasma conditions close to those of polymorphous silicon, adding TMB has a tendency to slow down the creation of powders,

¹Djeridane, “Synthèse de nanocristaux par plasma froid et leur rôle dans la croissance de couches minces de silicium microcristallin: Application aux transistors”, 2008 [63]

²Seto, “The electrical properties of polycrystalline silicon films”, 1975 [64]

whereas phosphine has little effect, if not the opposite,¹ resulting in a different growth depending on the dopant type and possibly explaining the less crystallized materials when using phosphine even though this gas is 20 times more diluted.

Similarly, as we had planned to investigate the electrical properties of such films, we took care of co-depositing the samples on several (100) c-Si substrates, including an intrinsic wafer to allow for temperature dependent Hall effect measurements. The results of these measurements has been shown on Fig. 4.19 where we have plotted the mobility and the carrier concentration for various PH_3 flow rates. These measurements were performed after a 30 minutes annealing at 275°C but did not show noticeable difference with the measurements performed on samples in the as-deposited state (in fact in the annealed state it was much easier to obtain ohmic contacts for the Hall effect set-up). The measurement of the

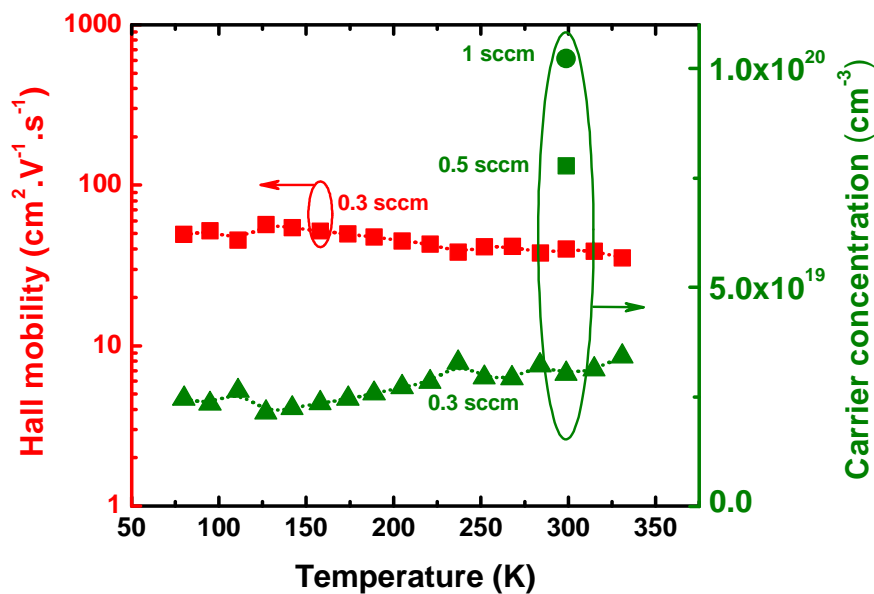


Figure 4.19 – Carrier concentration and mobilities as a function of the sample temperature as deduced from Hall effect measurements from several PH_3 flow rates

0.1 sccm sample would have been interesting but it was difficult to obtain reliable measurements on it. The measurements showed an increase of the carrier concentration upon the increase of the PH_3 flow rate. However, the Hall mobility and the carrier concentration showed almost no change when varying the substrate temperature. Indeed, this seemed to be a confirmation that for doping levels comparable to those of p-type epitaxial films we had a different transport mechanism. If we refer to the Seto's model [64], originally developed for p-type polysilicon films but also applicable to n-type films, for high doping values ($> 1.10^{19} \text{ cm}^{-3}$) the Hall mobility was pinned at some value and showed little change with the temperature, and that the activation energy of the resistivity as a function of the (inverse) temperature reached almost zero, resulting in a very

¹Suendo, Kharchenko, and Roca i Cabarrocas, "The effects of RF plasma excitation frequency and doping gas on the deposition of polymorphous silicon thin films", 2004 [65]

small change of the carrier concentration with the temperature. It seemed that ellipsometry and Hall effect measurements agreed on the fact that the films were not single crystal but highly crystallized polysilicon, thus possessing different properties than those of a single crystal.

Nevertheless, the mobility could be compared to the one obtained from the model developed by *Masetti et al.* in Ref. [62] whose analytical formula was expressed as follows:

$$\mu_e = \mu_0 + \frac{\mu_{max} - \mu_0}{1 + \left(\frac{n}{C_r}\right)^\alpha} - \frac{\mu_1}{1 + \left(\frac{C_s}{n}\right)^\beta}$$

The constant coefficients were described in the paper and this formula could be used over the 10^{13} to 5×10^{21} cm^{-3} range of carrier concentration. Based on that formula we calculated $\mu \approx 85 \text{ cm}^2 \cdot \text{V}^{-1} \cdot \text{s}^{-1}$ at a carrier concentration of $4 \cdot 10^{19} \text{ cm}^{-3}$. Once again, we obtained mobilities lower than expected from *Masetti's* model but in the same order of magnitude and thus potentially interesting. So far we did not use these n-doped layers into devices but they remain as promising as their p-type counterparts.

4.2 Germanium films

The epitaxial growth of silicon is very interesting and very promising but silicon is not the only material that should be looked at in photovoltaics. Indeed, the efficiency of a solar cell, beyond the technological limits, is based on how much light it can absorb. This is why industrials and researchers have been looking for multi-junction solar cells made up of materials with different bandgap energies. This can be made by using only silicon to make tandem cells where the top cell's absorber is made of a-Si:H and the bottom cell's absorber is made of $\mu\text{c-Si:H}$. Such solar cells can absorb the sunlight on a much wider absorption range and therefore generate more power.^{1,2} Some research has also been carried out on triple junction solar cells including two nc-Si:H (very similar to $\mu\text{c-Si:H}$) instead of one bottom cell of different crystallinity.³ Following this approach, three-junction solar cells have also been developed using silicon-germanium alloys (a-SiGe:H) with increasing the Ge fraction between the second and third (last) junction to gradually decrease the absorption bandgap.⁴ Of course we could also mention the multi-junctions designed for spatial energy applications. Efficiencies, under concentrated

¹Yoshimi, Sasaki, Sawada, Suezaki, Meguro, Matsuda, Santo, Wadano, Nakajima, and Yamamoto, "High efficiency thin film silicon hybrid solar cell module on 1 m²-class large area substrate", 2003 [66]

²Parascandolo, Bugnon, Feltrin, and Ballif, "High-rate deposition of microcrystalline silicon in a large-area PECVD reactor and integration in tandem solar cells", 2010 [67]

³Xu, Su, Beglau, Ehlert, Pietka, Bobela, Li, Lord, Yue, Zhang, Yan, Worrel, Beernink, DeMaggio, Banerjee, Yang, and Guha, "High efficiency large area multi-junction solar cells incorporating a-SiGe:H and nc-Si:H using MVHF technology", 2009 [68]

⁴Guha, Yang, Glatfelter, Hoffman, and Xu, "Progress in multijunction amorphous silicon alloy-based solar cells and modules", 1994 [69]

light, above 40% have already been obtained.^{1,2} They are involving many junctions and are based on elaboration techniques quite different from ours, which rely on ultra high vacuum systems, to obtain extremely high quality materials. All these approaches show that the path towards higher efficiencies can only be followed if we include different materials. If we remember that obtaining a good a-SiGe_x:H,³ or a-Ge:H material,⁴ is not easy, and that such materials (Si, Ge) exhibit much better properties when they are crystalline, it makes a lot of sense to look at the epitaxy of Ge, in a similar fashion as we looked at the epitaxy of Si. However, unlike silicon epitaxy which was a homoepitaxial growth, here we will try to grow a material on a different substrate, with a different lattice parameter: Ge has a 4% higher lattice parameter, compared to silicon, which is considerable for epitaxy.

4.2.1 Precedents

Unlike silicon, germanium has not attracted as much attention over the last decades. Even if the first transistor was made in germanium,⁵ and even if germanium exhibits higher mobilities than silicon,⁶ it remains more expensive and has been, so far, much less used than silicon in microelectronics (and photovoltaics) since silicon forms an “ideal couple” with its thermal oxide (SiO₂) which can passivate very well its surface down to surface state densities of 10⁹ cm⁻².eV⁻¹,⁷ which is the main reason for its success in the microelectronics industry. Alike silicon, the most common way to grow epitaxial Ge films is to use MBE and has proven to be successful to grow Ge on (100)-oriented GaAs substrates.⁸ However, a very early paper had already demonstrated the growth of Ge films by PECVD on (100)-oriented NaCl, that allows the film to be easily detached, at a substrate temperature of 450°C.⁹ More recently, at LPICM, *Johnson et al.*¹⁰ have been able to produce Ge epitaxial films on (100)-oriented GaAs wafers, as demonstrated by Raman spectroscopy and TEM analysis.

¹Guter, Schöne, Philipps, Steiner, Siefer, Wekkeli, Welser, Oliva, Bett, and Dimroth, “Current-matched triple-junction solar cell reaching 41.1% conversion efficiency under concentrated sunlight”, 2009 [70]

²Geisz, Friedman, Ward, Duda, Olavarria, Moriarty, Kiehl, Romero, Norman, and Jones, “40.8% efficient inverted triple-junction solar cell with two independently metamorphic junctions”, 2008 [71]

³Wickboldt, Pang, Paul, Chen, Zhong, Cohen, Chen, and Williamson, “Improved a-Si_{1-x}Ge_x:H of large x deposited by PECVD”, 1996 [72]

⁴Turner, Jones, Pang, Bateman, Chen, Li, Marques, Wetsel, Wickboldt, Paul, Bodart, Norberg, El Zawawi, and Theye, “Structural, optical, and electrical characterization of improved amorphous hydrogenated germanium”, 1990 [73]

⁵Shockley, Sparks, and Teal, “*p - n* Junction Transistors”, 1951 [74]

⁶Kittel, *Introduction to Solid State Physics, 7th edition*, 1995 [75]

⁷Aberle, “Surface passivation of crystalline silicon solar cells: a review”, 2000 [76]

⁸Jenichen, Kaganer, Shayduk, Braun, and Trampert, “Heteroepitaxial growth of lattice matched films on GaAs(001)”, 2009 [77]

⁹Outlaw and Hopson Jr. “Free-standing thin Ge single crystals grown by plasma-enhanced chemical vapor deposition”, 1984 [78]

¹⁰Johnson, Patriarche, and Roca i Cabarrocas, “Directional growth of Ge on GaAs at 175°C using plasma-generated nanocrystals”, 2008 [36]

4.2.2 Preliminary studies

The first tests were dedicated to find process conditions suitable to obtain epitaxial growth on (100) Si, since such a growth had previously been obtained only on (100) GaAs [36], for which there is very small lattice mismatch. In Tab. 4.5, we have given the process conditions used to grow Ge films at 175°C, for an inter-electrode distance of 22 mm.

Sample	H ₂ (sccm)	GeH ₄ (sccm)	Pressure (mTorr)	Time (min)
905061	200	5	1570	30
905062	200	10	1620	30
905066	0	100	520	30
905067	200	5	1440	37
905068	200	6	1480	35

Table 4.5 – Process parameters for different Ge films grown on (100) Si, (111) Si and Glass

On Fig. 4.20, we have plotted the Raman intensity around the 300 cm⁻¹ peak of the Ge films deposited at 5 and 6 sccm (905067 and 905068). On

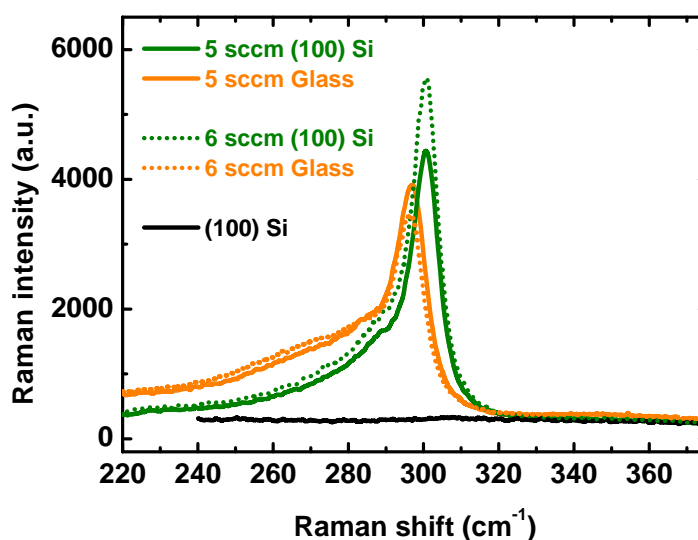


Figure 4.20 – Raman spectra around the 300 cm⁻¹ of Ge films deposited at two different GeH₄ flow rate on (100) Si and Corning Glass.

(100) Si, these films showed a narrow peak at 300 cm⁻¹, known to be due to crystalline Ge.^{1,2} However, a paper pointed out the fact that Si could also exhibit a peak at 300 cm⁻¹ so that people should be careful while examining Ge nanostructures on Si,³ but such peak appeared to be insignificant. On glass and on Si (111) (not shown for clarity) we found very similar spectra, suggesting that the Ge film was similar on glass and Si (111). Ge

¹Parker, Feldman, and Ashkin, "Raman Scattering by Silicon and Germanium", 1967 [79]

²Bermejo and Cardona, "Raman scattering in pure and hydrogenated amorphous germanium and silicon", 1979 [80]

³Kolobov, "Raman scattering from Ge nanostructures grown on Si substrates: Power and limitations", 2000 [81]

also has a TO mode at 278 cm^{-1} that corresponds to its amorphous phase.¹ The combination of these two peaks suggested that both phases coexisted in our Ge films. By analogy with what we know from silicon we can name such a material microcrystalline germanium ($\mu\text{c-Ge:H}$).²

On Fig. 4.21, we have plotted the imaginary part of the pseudo-dielectric function of the films grown under the process conditions listed in Tab. 4.5. We have also added the dielectric function c-Ge for reference. To model these films was not very easy since the layers are quite thin ($\leq 30\text{ nm}$). The film obtained from undiluted germane, which is still 2%-diluted in H_2 , were amorphous. In the lower part of the photon energy range SE was more sensitive to the substrate and the thickness of the film but the 3.5-4.5 eV part allowed us to acknowledge an epitaxial growth at 5, 6 and 10 sccm of germane. However, at 10 sccm the film appeared to be rougher. The deposition rate of films grown with 5 sccm of germane was

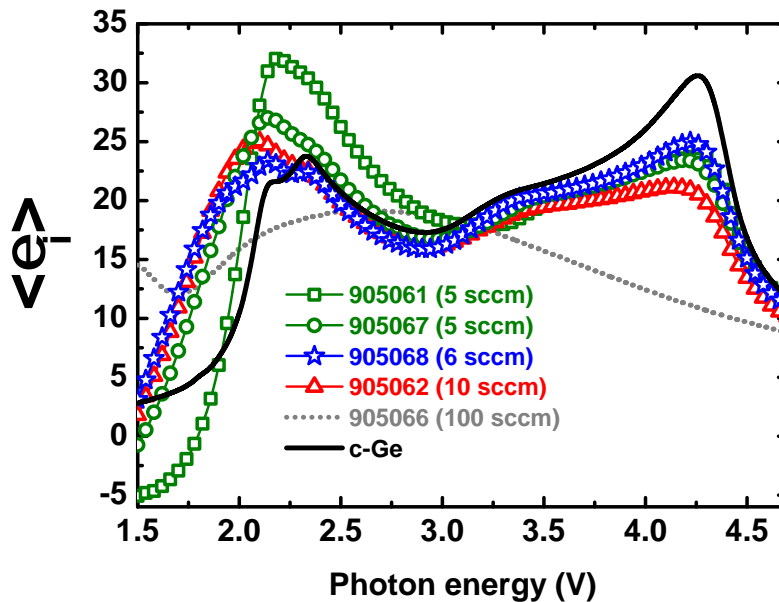


Figure 4.21 – Imaginary part of the pseudo-dielectric function of Ge films grown on (100) Si substrates under different process conditions.

$\approx 0.2\text{ \AA}\cdot\text{s}^{-1}$.

4.2.3 Multilayer samples

In the previous section (§4.2.2), we studied the growth of Ge epitaxial films on Si substrates. Here we go further and make more elaborated structures, such as multiple quantum-well-like structures. Indeed, we will show that multilayer samples, alternating layers of Si and Ge, are feasible, while keeping the crystalline phase on the entire structure. We demonstrated the growth of Ge films on Si, to reach this goal the next step is to

¹Bermejo and Cardona, "Raman scattering in pure and hydrogenated amorphous germanium and silicon", 1979 [80]

²Drévilion and Godet, "In situ investigation of the microcrystalline germanium nucleation and growth processes", 1988 [82]

combine process conditions leading to epi-Ge on c-Si with those leading to epi-Si on c-Ge. Therefore we deposited an epitaxial Ge film on c-Si and deposited consecutively an epitaxial Si film on the epitaxially grown Ge film: this was done for the sample 905065 whose deposition conditions are summarized in Tab. 4.6. For the Ge layer we used condition from §4.2.2

H ₂ (sccm)	SiH ₄ (sccm)	GeH ₄ (sccm)	Pressure (Torr)	Power density (mW.cm ⁻²)	Deposition time (min)
200	12	-	1.2	25	15
200	-	5	1.6	31	28

Table 4.6 – Plasma conditions used to grow Ge and Si epitaxial film, at 175°C

which led to an epitaxial growth on (100) Si and to a μ c-Ge:H material on (111) Si. For the Si layer we used conditions of pm-Si:H, known to lead to an epitaxial growth on (100) Si and to an amorphous (polymorphous) material on (111) Si.

As we did in our previous experiments we performed Raman spectroscopy and Spectroscopic Ellispometry on this sample. On Fig. 4.22,

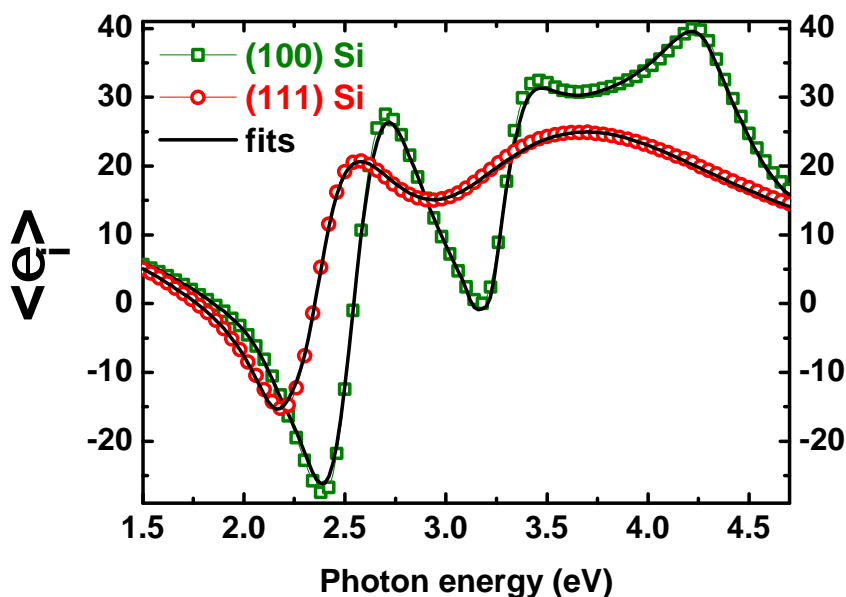


Figure 4.22 – Imaginary part of the pseudo-dielectric function of the Ge/Si stack co-deposited onto various substrates as deduced from SE measurements, the black line corresponds to the fits obtained by modelling the stack deposited on the (100) Si and (111) Si substrates using the optical model described in Tab. 4.7 on (100) Si or in Tab. 4.8 for (111) Si

73% LG Si	27% SiO ₂	↑ 0.5 nm
LG Si		↑ 43.3 nm
95% c-Ge	5% GeO ₂	↑ 29.8 nm
(100) c-Si		↑ semi-infinite

Table 4.7 – SE model of the Ge/Si stack deposited on the (100) Si wafer

we have plotted the imaginary part of the pseudo-dielectric function of

38% a-Si:H	62% voids		↑↓ 2 nm
a-Si:H			↑↓ 42.6 nm
88% c-Ge	8% a-Ge	4% GeO ₂	↑↓ 31.8 nm
(111) c-Si			↑ semi-infinite

Table 4.8 – SE model of the Ge/Si stack deposited on the (111) Si wafer

the stack, obtained by SE measurements, co-deposited on various substrates: on (100) Si and on (111) Si. The two black lines correspond to the fit obtained by modelling the stacks using the optical models described in Tab. 4.7 for the (100) Si substrate or in Tab. 4.8 for the (111) Si substrate. Once again, these models were based on the results of the previous sections (§4.1.4, p. 162 and §4.2.2, p. 178). Indeed, on (100) Si (model of Tab. 4.7) the Ge layer was modelled by a mixture of 95% of c-Ge and 5% of GeO₂, whereas the Si layer was modelled by a large grain polysilicon material, including a surface roughness. Even though a fit based on crystalline silicon and germanium materials provided a reasonable match with the experimental data, we could improve the fit by using the dielectric function of large grains polysilicon material in the reference file obtained by *Jellison et al.*¹ for the silicon layers and a mixture of crystalline germanium and a small fraction of germanium oxide (1-5%), as obtained by *Aspnes et al.*² for the germanium layers. The fact that the model could not reproduce the experimental data with using just c-Si and c-Ge materials can nevertheless be explained and clarified. Indeed, there were at least two reasons that may have explain that. The first one was that we cannot expect to have films with no roughness so that among our four interfaces, none was perfectly flat (as shown by the presence of a surface roughness of about 2 nm in the model of Fig. 4.22). Introducing a rough interface between each layer could even reduce further χ^2 but this was at the cost of drastically increasing the number of parameters of the model. The second one was that these films were produced at 175°C in a standard RF PECVD reactor without load-lock nor special precaution concerning gas purity (no gas purifiers) so that we could expect our films to contain carbon and oxygen impurities (see SIMS results below) as well as a significant amount of hydrogen, so that the film can have a different density from the theoretical one and thus a different refractive index. On the (111) Si substrate, the model we used (Tab. 4.8) consisted of a first Ge layer that we described as a mixture of c-Ge, a-Ge and GeO₂. The results showed that we had a very crystallized material. The Si layer grown on top was fitted by a a-Si:H layer, including a roughness layer. It is interesting to note that the films showed similar thicknesses in their amorphous or crystallized phase.

On Fig. 4.23, we have plotted the Raman scattering intensity against the Raman shift for the samples on the (100) Si and (111) Si substrates. This graph showed that the films had sharp peaks at 300 cm⁻¹ and 520 cm⁻¹ for the (100) Si substrate. This meant that the Ge layer was crystallized. Crys-

¹Jellison, Chisholm, and Gorbatkin, "Optical functions of chemical vapor deposited thin-film silicon determined by spectroscopic ellipsometry", 1993 [83]

²Aspnes and Studna, "Dielectric functions and optical parameters of Si, Ge, GaP, GaAs, GaSb, InP, InAs, and InSb from 1.5 to 6.0 eV", 1983 [84]

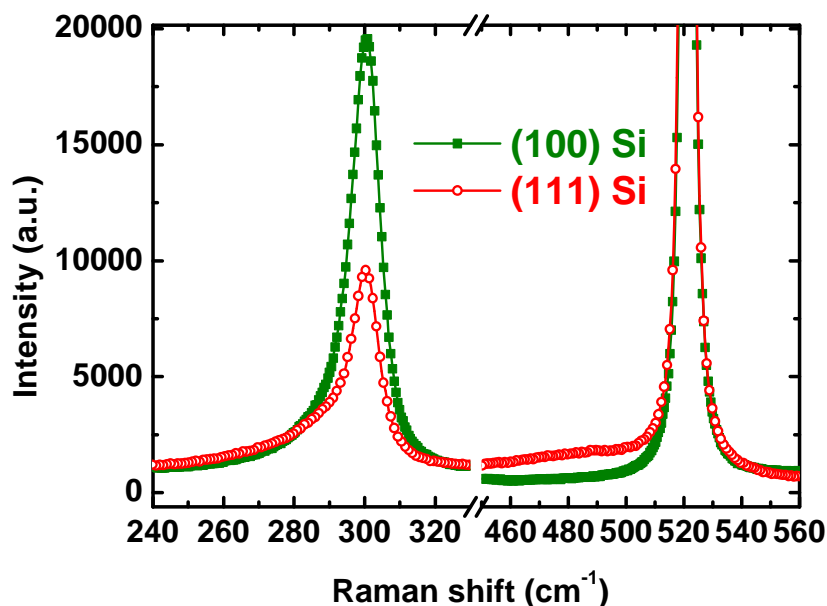


Figure 4.23 – Raman scattering intensity of the Ge/Si stack co-deposited on (100) Si and (111) Si

talline silicon has a peak at 520 cm^{-1} .¹ For the Si peak it was less obvious since the Si substrate was responsible for the most part of the peak at 520 cm^{-1} . However, we could compare with the spectrum obtained on the (111) Si substrate, which possessed a small bump around 480 cm^{-1} as expected from the thin pm-Si:H layer and which is absent from the (100) Si substrate. Interestingly enough, spectroscopic ellipsometry showed a much higher sensitivity, compared to Raman spectroscopy, to demonstrate the crystalline nature of the Si top layer. Finally, on the (111) Si substrate we had a peak at 300 cm^{-1} with a small shoulder towards lower wavenumbers which implied the necessity to fit this peak with both the 300 (c-Ge) and 280 (a-Ge) cm^{-1} peaks. However, the Ge layer, was very crystallized when grown on (111) Si, thus confirming the SE fit of Tab. 4.8.

The second incremental step was to repeat this deposition in order to get the following stack: Ge/Si/Ge/Si. As we were planning to investigate this multilayer sample by TEM we were interested in getting a different substrate from the films we were to deposit so that we co-deposited our stack on various substrates: glass, Si (111), Si (100) and GaAs (100). We used the same plasma conditions as the ones used in Tab. 4.6 to grow our Si and Ge films. In that case, the deposition times were 10 minutes for the Si films and 20 minutes for the Ge film. The sample was first characterized by Spectroscopic Ellipsometry. On Fig. 4.24 we have plotted the pseudo-dielectric function obtained from SE measurements of the multi layer stack co-deposited onto various substrates: (100) Si, (111) Si, (100) GaAs, and Corning glass. The black line corresponds to the fit obtained by modelling the stack deposited on the (100) Si substrate using the optical model described in Tab. 4.9. In our case, on Fig. 4.24, we

¹Parker, Feldman, and Ashkin, "Raman Scattering by Silicon and Germanium", 1967 [79]

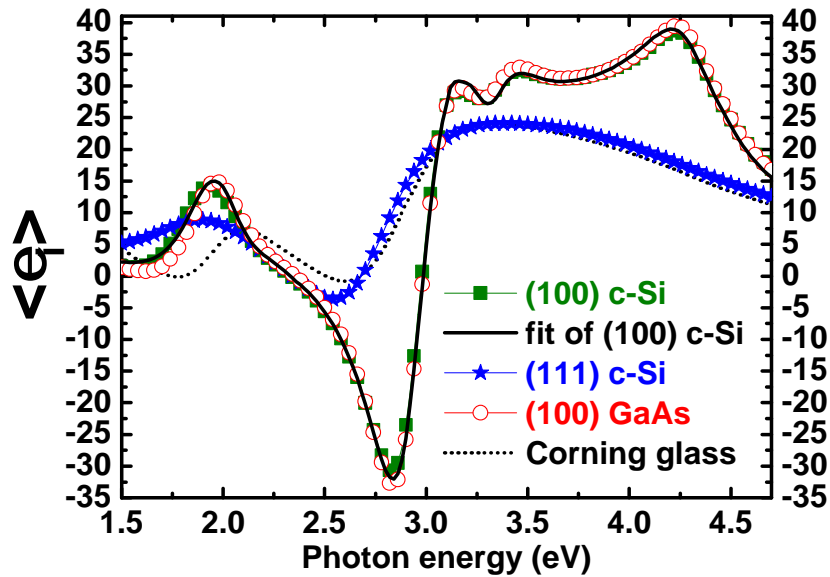


Figure 4.24 – Imaginary part of the pseudo-dielectric function of the multi layer stack co-deposited onto various substrates as deduced from SE measurements, the black line corresponds to the fit obtained by modelling the stack deposited on the (100) Si substrate using the optical model described in Tab. 4.9

32% LG Si	68% SiO ₂	↑ ↓ < 1 nm
LG Si		↑ ↓ 27 nm
95% c-Ge	5% GeO ₂	↑ ↓ 20 nm
LG Si		↑ ↓ 35 nm
99% c-Ge	1% GeO ₂	↑ ↓ 13 nm
(100) Si or GaAs		↑ semi-infinite

Table 4.9 – SE model of the multilayer stack deposited on the (100) Si and GaAs wafers

could see the characteristic spectrum of c-Si on both GaAs and Si (100)-oriented substrates, whereas on (111) c-Si substrate and Corning glass, the silicon films were amorphous, and the germanium films microcrystalline, as observed earlier (§4.2.2). Interestingly, the measurement performed on the film grown on the (100) GaAs substrate, could be fitted using the same model as the one used to model the measurement performed on the (100) Si. This meant that we obtained the same stack on both (100) substrates.

This sample was also characterized by Raman spectroscopy. The Raman scattering intensity has been plotted against the Raman shift for the co-deposited samples on Fig. 4.25 : (100) Si, (111) c-Si, and (100) GaAs. In the inset of Fig. 4.25 we have zoomed the spectrum of the stack deposited on (100) GaAs around 520 cm^{-1} in order to magnify the signal coming from the Si layers. The Raman spectra of the films deposited on (100) GaAs and

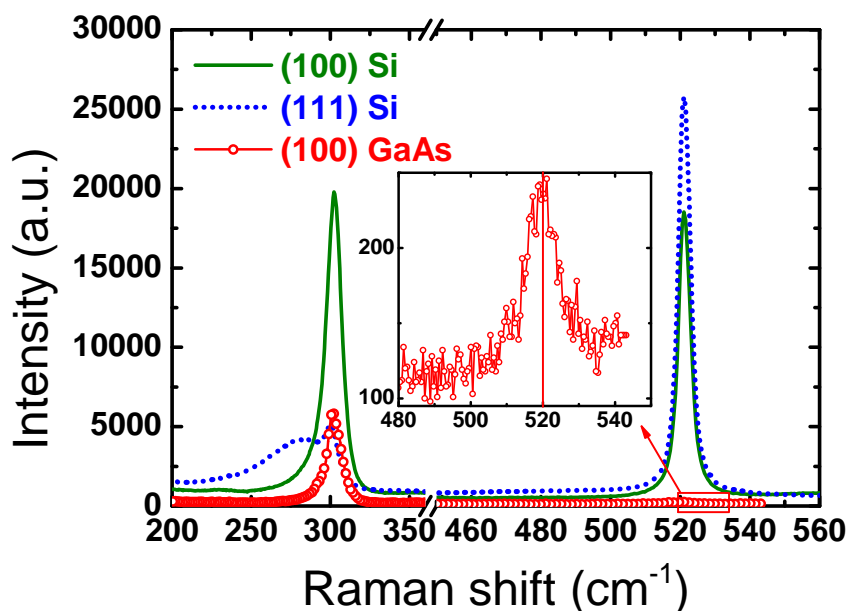


Figure 4.25 – Raman scattering intensity as a function of the Raman shift for the multi layer samples (905071) co-deposited on various substrates ((100) GaAs, (100) Si and (111) Si)

(100) Si showed a sharp peak around 300 cm^{-1} , which was consistent with fully crystallized Ge layers. On the other hand, the film deposited on (111) c-Si substrate displayed a shoulder towards lower wavenumbers, indicating that the film was partially crystallized and contained an amorphous phase, since the hydrogenated amorphous Ge has a TO mode at 278 cm^{-1} . The peak at 520 cm^{-1} could be assigned to crystalline silicon. However, it was very difficult to distinguish between the spectra for (111) and (100) Si substrates around this peak because the signal due to the substrate was so strong that it masked the contribution of the amorphous film (at 480 cm^{-1}) to the Raman spectrum. However, on the GaAs substrate, we could detect the signal from the c-Si film despite of its small thickness (see inset in Fig. 4.25). Moreover, one could see that the film was fully crystallized as there was no shoulder at 480 cm^{-1} , as it would have been the case if

there had been an amorphous silicon phase, but only a peak centred at about 520 cm^{-1} .

The sample deposited on (100) GaAs was also used for (HR)TEM and STEM studies that were performed at the LPN laboratory by *Dr. Gilles Patriarche*. On Fig. 4.26, there is a TEM image of the entire stack (four layers) on the (100) GaAs substrate. On Fig. 4.27a and Fig. 4.27b we show two HRTEM images of the different interfaces as described by the red squares in the Fig. 4.26. These zoomed in images allowed us to check that all the layers were crystalline. As we went further away from the GaAs surface, dislocations and other defects started to appear. Nevertheless, a major feature of these HRTEM images was that the layers remained single crystalline, and that their thicknesses were very similar to the ones deduced from the SE measurements, except for the first Ge layer whose thickness was more difficult to obtain from SE since we were not going far enough in the IR part of the spectrum. We could also operate the TEM in the STEM mode, more precisely in the HAADF STEM mode (High Angle Annular Dark Field), where we scanned the electrons that had been deviated the most and by doing we were extremely sensitive to the Z value of the elements. So, rather than the structure, Fig. 4.28 showed the chemical composition of the stack. This image showed that even if we kept a crystalline structure for all the layers there was chemical roughness or mixing at the interface. One should remember that both Si and Ge layers were grown in the same plasma chamber so that a cross-contamination was unavoidable.

We also performed SIMS measurements on another sample which was a replica of the multi layer sample studied before, but capped with a hydrogenated amorphous silicon layer to protect it from oxidation in air (910193). We were able to obtain the profiles of Si and Ge along the samples as well as the profiles of impurities that we could also quantify (graph not shown here). On Fig. 4.29, we have plotted the profiles of silicon, germanium, carbon and oxygen as functions of the sputtering time. The sputtering of our sample was done using a Cs⁺ ion beam and we measured the positive ions in the case of Si and Ge (namely $^{28}\text{Si}^+$ and $^{74}\text{Ge}^+$) while for the signal C and O we used the molecular ions formed with Cs (namely $^{12}\text{C}^{133}\text{Cs}^+$ and $^{16}\text{O}^{133}\text{Cs}^+$). We did so in order to improve the signals and obtain well-defined interfaces for each element. The carbon spike at the a-Si:H/c-Si interface was due to a thin hydrogenated amorphous silicon carbide layer (a-Si:C:H) introduced to prevent any epitaxial growth, as discussed in Chapter 3. It appeared that we had a much higher oxygen and carbon content in the Ge layers. Even if in the a-Si:H protective layer the oxygen content remained below $3 \times 10^{19}\text{ cm}^{-3}$, in the Si epitaxial layer it went up to $7 \times 10^{19}\text{ cm}^{-3}$ and in the Ge layer we can estimate it to be of $4 \times 10^{20}\text{ cm}^{-3}$. While the multilayer presented here had a high oxygen concentration, which could be an issue for devices, recent improvements in the vacuum system and gas purity have led to oxygen concentrations lower than 10^{19} cm^{-3} .

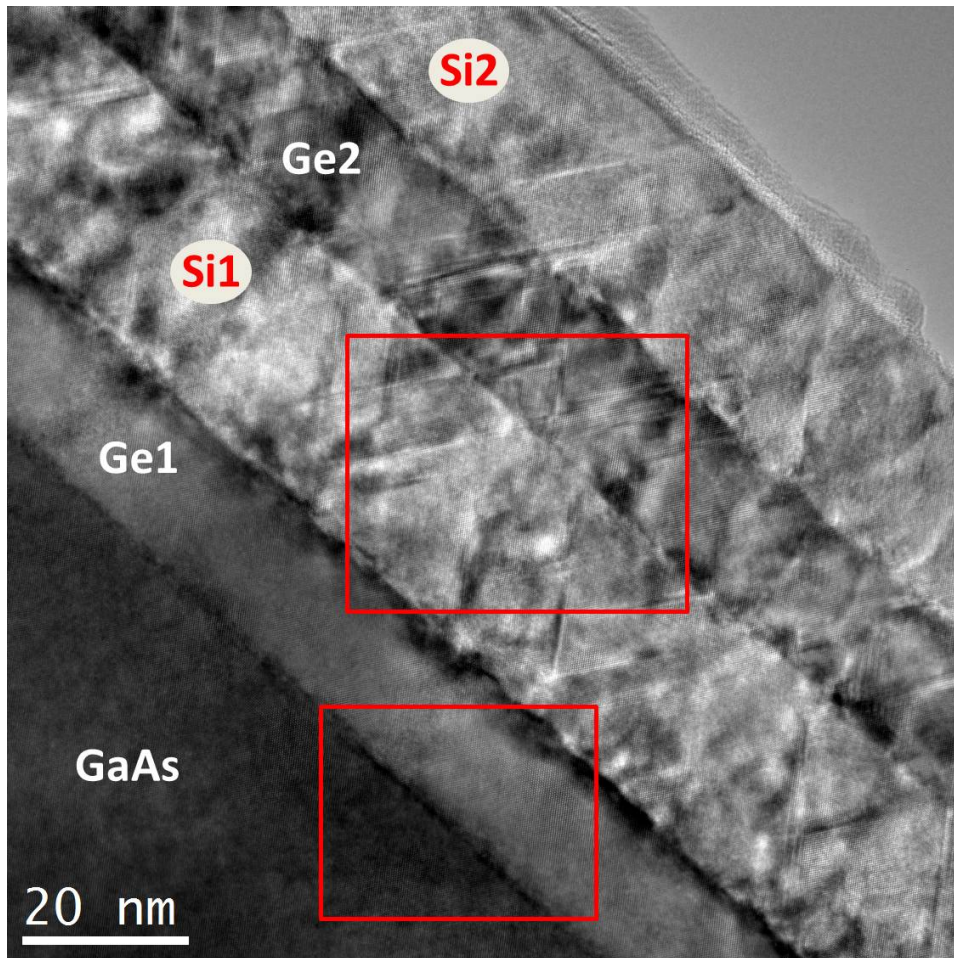
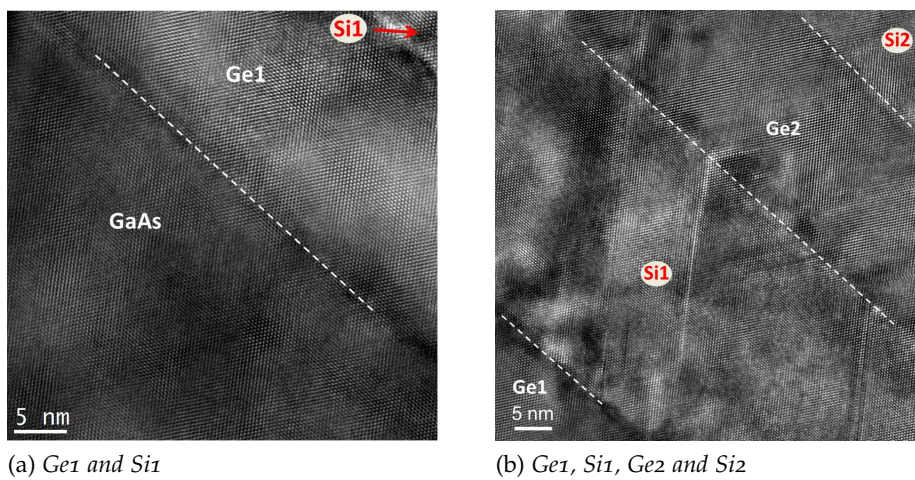


Figure 4.26 – TEM image of the Ge/Si/Ge/Si stack grown on (100) GaAs



(a) Ge₁ and Si₁

(b) Ge₁, Si₁, Ge₂ and Si₂

Figure 4.27 – HRTEM images of the Ge₁/Si₂/Ge₂/Si₂ stack on (100) GaAs at different interfaces

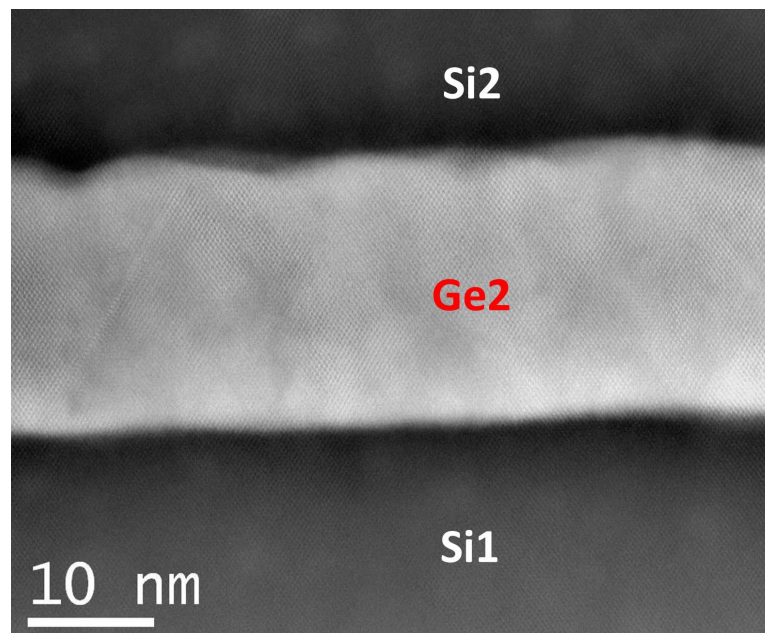


Figure 4.28 – HAADF STEM image of the Si₁/Ge₂/Si₂ interfaces

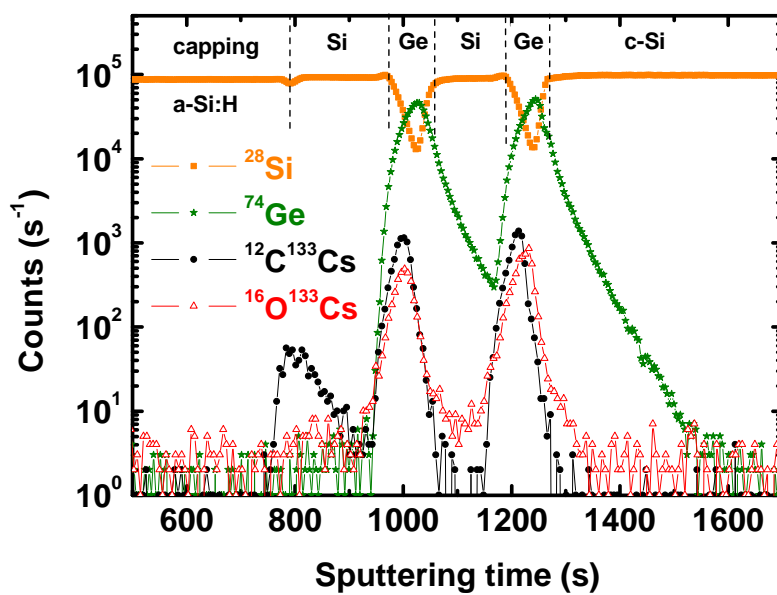


Figure 4.29 – SIMS profiles of Si, Ge, C and O against the sputtering time

4.3 Conclusions

In this chapter, we demonstrated and discussed the epitaxial growth of silicon and germanium films on (100) Si substrates. The process conditions for the epitaxial growth of silicon thin films were optimized by spectroscopic ellipsometry. When undoped (not intentionally doped), these epitaxial silicon films could be used as the absorbers of wafer-equivalent solar cells grown on highly-doped (100) Si wafers, resulting in efficiencies of 4.7% to 7% for epitaxial layers with thicknesses ranging from 0.9 μm to 2.4 μm . Such films could also be doped by the addition of small flow rates of dopants. While p-type doping was found to be achievable with moderate flow rates of both TMB and diborane gases (2% in H_2), n-type doping resulted in films of lower crystallinity. Temperature dependent Hall effect measurements were performed on these films grown on intrinsic wafers. P-type epitaxial films were found to have a crystalline silicon behaviour with Hall mobilities close to that of (p) c-Si, with carriers concentration ranging from $3.10^{18} \text{ cm}^{-3}$ to $6.10^{19} \text{ cm}^{-3}$. N-type epitaxial films were found to be less crystallized, closer to polycrystalline films, from both ellipsometry and Hall effect measurements. P-type films could be grown on (n) c-Si wafers to form the emitter of an homojunction solar cell resulting in an efficiency of 14.2%.

Similarly, Ge epitaxial films could be obtained on (100) Si films, as deduced from spectroscopic ellipsometry and Raman spectroscopy. Besides, multilayer samples could be produced by the alternation of epitaxial films of Si and Ge. Ellipsometry, Raman and HRTEM characterisations were found to be in good agreement and all supported the conservation of the single crystalline nature of all the films. At the time of writing no devices were produced but several ongoing projects of the laboratory would be devoted to the implementation of such Ge layers in solar cells.

REFERENCES

- [1] B. Kalache, A. I. Kosarev, R. Vanderhaghen, and P. Roca i Cabarrocas. "Ion bombardment effects on microcrystalline silicon growth mechanisms and on the film properties". In: *Journal of Applied Physics* 93 (2003), pp. 1262–1273. DOI: 10.1063/1.1524707 (cit. on p. 148).
- [2] N. Chaâbane, V. Suendo, H. Vach, and P. Roca i Cabarrocas. "Soft landing of silicon nanocrystals in plasma enhanced chemical vapor deposition". In: *Applied Physics Letters* 88, 203111 (2006), p. 203111. DOI: 10.1063/1.2204439 (cit. on pp. 148, 157, 158).
- [3] J. J. H. Gielis, P. J. van den Oever, B. Hoex, M. C. M. van de Sanden, and W. M. M. Kessels. "Real-time study of a-Si:H/c-Si heterointerface formation and epitaxial Si growth by spectroscopic ellipsometry, infrared spectroscopy, and second-harmonic generation". In: *Phys. Rev. B* 77 (2008), p. 205329. DOI: 10.1103/PhysRevB.77.205329 (cit. on pp. 148, 149, 152, 163).
- [4] Q. Wang, C. W. Teplin, P. Stradins, B. To, K. M. Jones, and H. M. Branz. "Significant improvement in silicon chemical vapor deposition epitaxy above the surface dehydrogenation temperature". In: *Journal of Applied Physics* 100, 093520 (2006), p. 093520. DOI: 10.1063/1.2363766 (cit. on pp. 148, 149, 152, 163).
- [5] S. De Wolf and M. Kondo. "Abruptness of a-Si:H/c-Si interface revealed by carrier lifetime measurements". In: *Applied Physics Letters* 90, 042111 (2007), p. 042111. DOI: 10.1063/1.2432297 (cit. on pp. 148, 149, 152).
- [6] Y. Veschetti, J.-C. Muller, J. Damon-Lacoste, P. Roca i Cabarrocas, A.S. Gudovskikh, J.-P. Kleider, P.-J. Ribeyron, and E. Rolland. "Optimisation of amorphous and polymorphous thin silicon layers for the formation of the front-side of heterojunction solar cells on p-type crystalline silicon substrates". In: *Thin Solid Films* 511-512 (2006), pp. 543–547. DOI: 10.1016/j.tsf.2005.12.166 (cit. on pp. 148, 149, 158).
- [7] J. Damon-Lacoste and P. Roca i Cabarrocas. "Toward a better physical understanding of a-Si:H/c-Si heterojunction solar cells". In: *Journal of Applied Physics* 105, 063712 (2009), p. 063712. DOI: 10.1063/1.3091283 (cit. on p. 148).
- [8] U.K. Das, M. Z. Burrows, M. Lu, S. Bowden, and R. W. Birkmire. "Surface passivation and heterojunction cells on Si (100) and (111) wafers using dc and rf plasma deposited Si:H thin films". In: *Applied Physics Letters* 92, 063504 (2008), p. 063504. DOI: 10.1063/1.2857465 (cit. on pp. 148, 152).

- [9] S. Olibet, C. Monachon, A. Hessler-Wyser, E. Vallat-Sauvain, S. De Wolf, L. Fesquet, J. Damon-Lacoste, and C. Ballif. "Textured silicon heterojunction solar cells with over 700 mV open-circuit voltage studied by Transmission Electron Microscopy". In: *23rd European Photovoltaic Solar Energy Conference, 1-5 September, Valencia, Spain*. 2008 (cit. on p. 148).
- [10] G. Beaucarne, F. Duerinckx, I. Kuzma, K. Van Nieuwenhuysen, H.J. Kim, and J. Poortmans. "Epitaxial thin-film Si solar cells". In: *Thin Solid Films* 511-512 (2006), pp. 533-542. DOI: 10.1016/j.tsf.2005.12.003 (cit. on p. 149).
- [11] M. J. McCann, K. R. Catchpole, K. J. Weber, and A. W. Blakers. "A review of thin-film crystalline silicon for solar cell applications. Part 1: Native substrates". In: *Solar Energy Materials and Solar Cells* 68 (2001), pp. 135-171. DOI: 10.1016/S0927-0248(00)00242-7 (cit. on p. 149).
- [12] Kylie R. Catchpole, Michelle J. McCann, Klaus J. Weber, and Andrew W. Blakers. "A review of thin-film crystalline silicon for solar cell applications. Part 2: Foreign substrates". In: *Solar Energy Materials & Solar Cells* 68 (2001), pp. 173-215. DOI: 10.1016/S0927-0248(00)00246-4 (cit. on p. 149).
- [13] E. Schmich, N. Schillinger, and S. Reber. "Silicon CVD deposition for low cost applications in photovoltaics". In: *Surface and Coatings Technology* 201 (2007), pp. 9325-9329. DOI: 10.1016/j.surfcoat.2007.04.089 (cit. on p. 149).
- [14] C. W. Teplin, Q; Wang, E. Iwaniczko, K. M. Jones, M. Al-Jassim, R. C. Reedy, and H. M. Branz. "Low-temperature silicon homoepitaxy by hot-wire chemical vapor deposition with a Ta filament". In: *Journal of Crystal Growth* 287 (2006), pp. 414-418. DOI: 10.1016/j.jcrysgro.2005.11.055 (cit. on pp. 149, 155, 162, 165).
- [15] M. Kambara, H. Yagi, M. Sawayanagi, and T. Yoshida. "High rate epitaxy of silicon thick films by medium pressure plasma chemical vapor deposition". In: *Journal of Applied Physics* 99, 074901 (2006), p. 074901. DOI: 10.1063/1.2181279 (cit. on p. 149).
- [16] W. J. Varhue, J. L. Rogers, P. S. Andry, and E. Adams. "Epitaxial film thickness in the low-temperature growth of Si(100) by plasma enhanced chemical vapor deposition". In: *Applied Physics Letters* 68 (1996), pp. 349-351. DOI: 10.1063/1.116712 (cit. on p. 149).
- [17] C.C. Tsai, G.B. Anderson, and R. Thompson. "Low temperature growth of epitaxial and amorphous silicon in a hydrogen-diluted silane plasma". In: *Journal of Non-Crystalline Solids* 137-138 (1991), pp. 673-676. DOI: 10.1016/S0022-3093(05)80210-8 (cit. on pp. 149, 152, 155).
- [18] C.C. Tsai, G.B. Anderson, R. Thompson, and B. Wacker. "Control of silicon network structure in plasma deposition". In: *Journal of Non-Crystalline Solids* 114 (1989), pp. 151-153. DOI: 10.1016/0022-3093(89)90096-3 (cit. on pp. 149, 159).

- [19] C.-H. Chen and T.-R. Yew. "Silicon epitaxial growth by plasma enhanced chemical vapor deposition from SiH₄/H₂ at 165-350°C". In: *Journal of Crystal Growth* 147 (1995), pp. 305-312. DOI: 10.1016/0022-0248(95)80011-5 (cit. on p. 149).
- [20] K. Nagamine, A. Yamada, M. Konagai, and K. Takahashi. "Epitaxial Growth of Silicon by Plasma Chemical Vapor Deposition at a Very Low Temperature of 250°C". In: *Japanese Journal of Applied Physics* 26 (1987), pp. L951-L953. DOI: 10.1143/JJAP.26.L951 (cit. on p. 150).
- [21] S. Ohi, W. R. Burger, and R. Reif. "Enhanced electrical quality of low-temperature (T < 800°C) epitaxial silicon deposited by plasma-enhanced chemical vapor deposition". In: *Applied Physics Letters* 53 (1988), pp. 891-893. DOI: 10.1063/1.100106 (cit. on p. 150).
- [22] J. Plá, E. Centurioni, C. Summonte, R. Rizzoli, A. Migliori, A. Desalvo, and F. Zignani. "Homojunction and heterojunction silicon solar cells deposited by low temperature-high frequency plasma enhanced chemical vapour deposition". In: *Thin Solid Films* 405 (2002). DOI: 10.1016/S0040-6090(01)01709-6 (cit. on p. 150).
- [23] R. Rizzoli, E. Centurioni, J. Plá, C. Summonte, A. Migliori, A. Desalvo, and F. Zignani. "Open circuit voltage in homojunction and heterojunction silicon solar cells grown by VHF-PECVD". In: *Journal of Non-Crystalline Solids* 299-302 (2002), p. 120-1207. DOI: 10.1016/S0022-3093(01)01088-2 (cit. on p. 150).
- [24] M. Farrokh-Baroughi and S. Sivoththaman. "A Novel Silicon Photovoltaic Cell Using a Low-Temperature Quasi-Epitaxial Silicon Emitter". In: *Electron Device Letters, IEEE* 28 (2007), pp. 575-577. DOI: 10.1109/LED.2007.897873 (cit. on p. 150).
- [25] R. Shimokawa, M. Yamanaka, and I. Sakata. "Very Low Temperature Epitaxial Growth of Silicon Films for Solar Cells". In: *Japanese Journal of Applied Physics* 46 (2007), pp. 7612-7618. DOI: 10.1143/JJAP.46.7612 (cit. on p. 150).
- [26] D. Levi, E. Iwaniczko, M. Page, Q. Wang, H. Branz, and T. Wang. "Silicon Heterojunction Solar Cell Characterization and Optimization using in Situ and Ex Situ Spectroscopic Ellipsometry". In: *Photovoltaic Energy Conversion, Conference Record of the 2006 IEEE 4th World Conference on*. Vol. 2. May 2006, pp. 1740-1743. DOI: 10.1109/WCPEC.2006.279828 (cit. on p. 152).
- [27] L. Boufendi and A. Bouchoule. "Particle nucleation and growth in a low-pressure argon-silane discharge". In: *Plasma Sources Science and Technology* 3 (1994), p. 262. DOI: 10.1088/0963-0252/3/3/004 (cit. on p. 154).
- [28] R.A. Street. *Hydrogenated Amorphous Silicon*. Ed. by Cambridge University Press. 1991 (cit. on p. 154).
- [29] Q. Brulin, N. Ning, and H. Vach. "Hydrogen-induced crystallization of amorphous silicon clusters in a plasma reactor". In: *Journal of Non-Crystalline Solids* 352 (2006), pp. 1055-1058. DOI: 10.1016/j.jnoncrysol.2006.01.049 (cit. on p. 157).

- [30] P. Roca i Cabarrocas, Th. Nguyen-Tran, Y. Djeridane, A. Abramov, E. V. Johnson, and G. Patriarche. "Synthesis of silicon nanocrystals in silane plasmas for nanoelectronics and large area electronic devices". In: *Journal of Physics D: Applied Physics* 40 (2007), p. 2258. doi: 10.1088/0022-3727/40/8/S04 (cit. on p. 157).
- [31] C. Hollenstein. "The physics and chemistry of dusty plasmas". In: *Plasma Physics and Controlled Fusion* 42 (2000), R93. doi: 10.1088/0741-3335/42/10/201 (cit. on p. 157).
- [32] P. Roca i Cabarrocas, A. Fontcuberta i Morral, and Y. Poissant. "Growth and optoelectronic properties of polymorphous silicon thin films". In: *Thin Solid Films* 403-404 (2002), pp. 39-46. doi: 10.1016/S0040-6090(01)01656-X (cit. on p. 157).
- [33] S. Kasouit, J. Damon-Lacoste, R. Vanderhaghen, and P. Roca i Cabarrocas. "Contribution of plasma generated nanocrystals to the growth of microcrystalline silicon thin films". In: *Journal of Non-Crystalline Solids* 338-340 (2004), pp. 86-90. doi: 10.1016/j.jnoncrysol.2004.02.027 (cit. on p. 157).
- [34] S N Abolmasov, L Kroely, and P Roca i Cabarrocas. "Negative corona discharge: application to nanoparticle detection in rf reactors". In: *Plasma Sources Science and Technology* 18 (2009), p. 015005. doi: 10.1088/0963-0252/18/1/015005 (cit. on p. 158).
- [35] M. Labrune, M. Moreno, and P. Roca i Cabarrocas. "Ultra-shallow junctions formed by quasi-epitaxial growth of boron and phosphorous-doped silicon films at 175°C by rf-PECVD". In: *Thin Solid Films* 518 (2010), pp. 2528-2530 (cit. on p. 158).
- [36] E. V. Johnson, G. Patriarche, and P. Roca i Cabarrocas. "Directional growth of Ge on GaAs at 175°C using plasma-generated nanocrystals". In: *Applied Physics Letters* 92 (2008), p. 103108. doi: 10.1063/1.2895636 (cit. on pp. 158, 177, 178).
- [37] J. M. A. Diaz, M. Kambara, and T. Yoshida. "Detection of Si nanoclusters by x-ray scattering during silicon film deposition by mesoplasma chemical vapor deposition". In: *Journal of Applied Physics* 104, 013536 (2008), p. 013536. doi: 10.1063/1.2956692 (cit. on p. 158).
- [38] N. Ning, S. M. Rinaldi, and H. Vach. "An atomic-scale study of hydrogenated silicon cluster deposition on a crystalline silicon surface". In: *Thin Solid Films* 517 (2009), pp. 6234-6238. doi: 10.1016/j.tsf.2009.02.086 (cit. on p. 158).
- [39] N. Ning and H. Vach. "Deposition Dynamics of Hydrogenated Silicon Clusters on a Crystalline Silicon Substrate under Typical Plasma Conditions". In: *The Journal of Physical Chemistry A* 114 (2010), pp. 3297-3305. doi: 10.1021/jp909446c. eprint: <http://pubs.acs.org/doi/pdf/10.1021/jp909446c> (cit. on p. 158).

- [40] R. Biswas, Gary S. Grest, and C. M. Soukoulis. "Molecular-dynamics simulation of cluster and atom deposition on silicon (111)". In: *Phys. Rev. B* 38 (1988), pp. 8154–8162. DOI: 10.1103/PhysRevB.38.8154 (cit. on p. 159).
- [41] J. Thiesen, E. Iwaniczko, K. M. Jones, A. Mahan, and R. Crandall. "Growth of epitaxial silicon at low temperatures using hot-wire chemical vapor deposition". In: *Applied Physics Letters* 75 (1999), pp. 992–994. DOI: 10.1063/1.124576 (cit. on p. 159).
- [42] M.-S. Lee S.-S. and Ko, C.-S. Kim, and N.-M. Hwang. "Gas phase nucleation of crystalline silicon and their role in low-temperature deposition of microcrystalline films during hot-wire chemical vapor deposition". In: *Journal of Crystal Growth* 310 (2008), pp. 3659–3662. DOI: 10.1016/j.jcrysgro.2008.05.009 (cit. on p. 159).
- [43] S. Cereda, F. Zipoli, M. Bernasconi, Leo Miglio, and F. Montalenti. "Thermal-Hydrogen Promoted Selective Desorption and Enhanced Mobility of Adsorbed Radicals in Silicon Film Growth". In: *Phys. Rev. Lett.* 100 (2008), p. 046105. DOI: 10.1103/PhysRevLett.100.046105 (cit. on pp. 159, 160).
- [44] X. Tan and G. W. Yang. "Physical mechanisms of hydrogen-enhanced onset of epitaxial growth of silicon by plasma-enhanced chemical vapor deposition". In: *Applied Physics Letters* 93, 061902 (2008), p. 061902. DOI: 10.1063/1.2957674 (cit. on pp. 159, 160).
- [45] A. Gupta, H. Yang, and G. N. Parsons. "Ab initio analysis of silyl precursor physisorption and hydrogen abstraction during low temperature silicon deposition". In: *Surface Science* 496 (2002), pp. 307–317. DOI: 10.1016/S0039-6028(01)01467-4 (cit. on p. 160).
- [46] S. Ramalingam, D. Maroudas, E. S. Aydil, and S. P. Walch. "Abstraction of hydrogen by SiH₃ from hydrogen-terminated Si(001)-(2×1) surfaces". In: *Surface Science* 418 (1998), pp. L8–L13. DOI: 10.1016/S0039-6028(98)00703-1 (cit. on p. 160).
- [47] S. Cereda, M. Ceriotti, F. Montalenti, M. Bernasconi, and Leo Miglio. "Quantitative estimate of H abstraction by thermal SiH₃ on hydrogenated Si(001)(2×1)". In: *Phys. Rev. B* 75 (2007), p. 235311. DOI: 10.1103/PhysRevB.75.235311 (cit. on p. 160).
- [48] L. Csepregi, E. F. Kennedy, J. W. Mayer, and T. W. Sigmon. "Substrate-orientation dependence of the epitaxial regrowth rate from Si-implanted amorphous Si". In: *Journal of Applied Physics* 49 (1978), pp. 3906–3911. DOI: 10.1063/1.325397 (cit. on pp. 160, 161).
- [49] B. E. Weir, B. S. Freer, R. L. Headrick, D. J. Eaglesham, G. H. Gilmer, J. Bevk, and L. C. Feldman. "Low-temperature homoepitaxy on Si(111)". In: *Applied Physics Letters* 59 (1991), pp. 204–206. DOI: 10.1063/1.105966 (cit. on p. 161).
- [50] D. J. Eaglesham, H.-J. Gossmann, and M. Cerullo. "Limiting thickness h_{epi} for epitaxial growth and room-temperature Si growth on Si(100)". In: *Phys. Rev. Lett.* 65 (1990), pp. 1227–1230. DOI: 10.1103/PhysRevLett.65.1227 (cit. on p. 161).

- [51] C. W. Teplin, D. H. Levi, E. Iwaniczko, K. M. Jones, J. D. Perkins, and H. M. Branz. "Monitoring and modeling silicon homoepitaxy breakdown with real-time spectroscopic ellipsometry". In: *Journal of Applied Physics* 97, 103536 (2005), p. 103536. DOI: 10.1063/1.1903110 (cit. on pp. 162, 163, 165).
- [52] S. H. Wolff, S. Wagner, J. C. Bean, R. Hull, and J. M. Gibson. "Hydrogen surface coverage: Raising the silicon epitaxial growth temperature". In: *Applied Physics Letters* 55 (1989), pp. 2017–2019. DOI: 10.1063/1.102149 (cit. on p. 162).
- [53] D. J. Eaglesham, F. C. Unterwald, H. Luftman, D. P. Adams, and S. M. Yalisove. "Effect of H on Si molecular-beam epitaxy". In: *Journal of Applied Physics* 74 (1993), pp. 6615–6618. DOI: 10.1063/1.355101 (cit. on p. 162).
- [54] J. F. Nützel, P. Brichzin, and G. Abstreiter. "RHEED investigations of surface diffusion on Si(001)". In: *Applied Surface Science* 102 (1996), pp. 78–81. DOI: 10.1016/0169-4332(96)00024-4 (cit. on p. 162).
- [55] K. Alberi, I. T. Martin, M. Shub, C. W. Teplin, M. J. Romero, R. C. Reedy, E. Iwaniczko, A. Duda, P. Stradins, H. M. Branz, and D. L. Young. "Material quality requirements for efficient epitaxial film silicon solar cells". In: *Applied Physics Letters* 96, 073502 (2010), p. 073502. DOI: 10.1063/1.3309751 (cit. on pp. 163, 168).
- [56] I. Kuzma-Filipek, K.V. Nieuwenhuysen, J.V. Hoeymissen, M.R. Payo, E.V. Kerschaver, J. Poortmans, R. Mertens, G. Beaucarne, E. Schmich, S. Lindekugel, and S. Reber. "Efficiency (>15%) for thin-film epitaxial silicon solar cells on 70 cm² area offspec silicon substrate using porous silicon segmented mirrors". In: *Progress in Photovoltaics* 18 (2010), pp. 137–143. DOI: 10.1002/pip.953 (cit. on p. 163).
- [57] M. Reuter, W. Brendle, O. Tobail, and J. H. Werner. "50 μm thin solar cells with 17.0% efficiency". In: *Solar Energy Materials & Solar Cells* 93 (2009), pp. 704–706. DOI: 10.1016/j.solmat.2008.09.035 (cit. on p. 163).
- [58] M. Moreno and P. Roca i Cabarrocas. "Ultra-thin crystalline silicon films produced by plasma assisted epitaxial growth on silicon wafers and their transfer to foreign substrates". In: *PV Direct* 1 (2010), p. 10301. DOI: 10.1051/pvd/2010001 (cit. on pp. 163, 164).
- [59] R. Cariou, M Labrune, and P. Roca i Cabarrocas. "Thin crystalline silicon solar cells based on epitaxial films grown at 165°C by RF PECVD". In: *Accepted for publication in Solar Energy Materials & Solar Cells* (2011). DOI: 10.1016/j.solmat.2011.03.038 (cit. on pp. 165, 168).
- [60] P. Roca i Cabarrocas, S. Kumar, and B. Drévilon. "In situ study of the thermal decomposition of B₂H₆ by combining spectroscopic ellipsometry and Kelvin probe measurements". In: *Journal of Applied Physics* 66 (1989), pp. 3286–3292. DOI: 10.1063/1.344122 (cit. on p. 171).

- [61] R. W. Collins. "In situ study of p-type amorphous silicon growth from $B_6H_6:SiH_4$ mixtures: Surface reactivity and interface effects". In: *Applied Physics Letters* 53 (1988), pp. 1086–1088. DOI: 10.1063/1.100029 (cit. on p. 171).
- [62] G. Masetti, M. Severi, and S. Solmi. "Modeling of carrier mobility against carrier concentration in arsenic-, phosphorus-, and boron-doped silicon". In: *Electron Devices, IEEE Transactions on* 30 (1983), pp. 764–769. DOI: 10.1109/T-ED.1983.21207 (cit. on pp. 172, 176).
- [63] Yassine Djeridane. "Synthèse de nanocristaux par plasma froid et leur rôle dans la croissance de couches minces de silicium microcristallin: Application aux transistors". PhD thesis. École Polytechnique, 2008 (cit. on p. 174).
- [64] J. Y. W. Seto. "The electrical properties of polycrystalline silicon films". In: *Journal of Applied Physics* 46 (1975), pp. 5247–5254. DOI: 10.1063/1.321593 (cit. on pp. 174, 175).
- [65] V. Suendo, A. V. Kharchenko, and P. Roca i Cabarrocas. "The effects of RF plasma excitation frequency and doping gas on the deposition of polymorphous silicon thin films". In: *Thin Solid Films* 451-452 (2004), pp. 259–263. DOI: 10.1016/j.tsf.2003.11.019 (cit. on p. 175).
- [66] M. Yoshimi, T. Sasaki, T. Sawada, T. Suezaki, T. Meguro, T. Matsuda, K. Santo, K. Wadano, A. Nakajima, and K. Yamamoto. "High efficiency thin film silicon hybrid solar cell module on 1 m²-class large area substrate". In: *Proceedings of 3rd World Conference on Photovoltaic Solar Energy Conversion, Osaka, Japan*. 2003. DOI: 10.1109/WCPEC.2003.1306226 (cit. on p. 176).
- [67] G. Parascandolo, G. Bugnon, A. Feltrin, and C. Ballif. "High-rate deposition of microcrystalline silicon in a large-area PECVD reactor and integration in tandem solar cells". In: *Progress in Photovoltaics* 18 (2010), pp. 257–264. DOI: 10.1002/pip.961 (cit. on p. 176).
- [68] X. Xu, T. Su, D. Beglau, S. Ehlert, G. Pietka, D. Bobela, Y. Li, K. Lord, G. Yue, J. Zhang, B. Yan, C. Worrel, K. Beernink, G. DeMaggio, A. Banerjee, J. Yang, and S. Guha. "High efficiency large area multi-junction solar cells incorporating a-SiGe:H and nc-Si:H using MVHF technology". In: *IEEE Photovoltaic Specialists Conference, Philadelphia, PA, June 7-12*. 2009. DOI: 10.1109/PVSC.2009.5411410 (cit. on p. 176).
- [69] S. Guha, J. Yang, T. Glatfelter, K. Hoffman, and X. Xu. "Progress in multijunction amorphous silicon alloy-based solar cells and modules". In: *Solar Energy Materials and Solar Cells* 34 (1994), pp. 329–337. DOI: 10.1016/0927-0248(94)90057-4 (cit. on p. 176).
- [70] W. Guter, J. Schöne, S. P. Philipps, M. Steiner, G. Siefer, A. Wekkeli, E. Welser, E. Oliva, A. W. Bett, and F. Dimroth. "Current-matched triple-junction solar cell reaching 41.1% conversion efficiency under concentrated sunlight". In: *Applied Physics Letters* 94, 223504 (2009), p. 223504. DOI: 10.1063/1.3148341 (cit. on p. 177).

- [71] J. F. Geisz, D. J. Friedman, J. S. Ward, A. Duda, W. J. Olavarria, T. E. Moriarty, J. T. Kiehl, M. J. Romero, A. G. Norman, and K. M. Jones. "40.8% efficient inverted triple-junction solar cell with two independently metamorphic junctions". In: *Applied Physics Letters* 93, 123505 (2008), p. 123505. DOI: 10.1063/1.2988497 (cit. on p. 177).
- [72] P. Wickboldt, D. Pang, W. Paul, J. H. Chen, F. Zhong, J. D. Cohen, Y. Chen, and D. L. Williamson. "Improved a-Si_{1-x}Ge_x:H of large x deposited by PECVD". In: *Journal of Non-Crystalline Solids* 198-200 (1996), pp. 567–571. DOI: 10.1016/0022-3093(95)00765-2 (cit. on p. 177).
- [73] W. A. Turner, S. J. Jones, D. Pang, B. F. Bateman, J. H. Chen, Y.-M. Li, F. C. Marques, A. E. Wetsel, P. Wickboldt, W. Paul, J. Bodart, R. E. Norberg, I. El Zawawi, and M. L. Theye. "Structural, optical, and electrical characterization of improved amorphous hydrogenated germanium". In: *Journal of Applied Physics* 67 (1990), pp. 7430–7438. DOI: 10.1063/1.344533 (cit. on p. 177).
- [74] W. Shockley, M. Sparks, and G. K. Teal. "*p* – *n* Junction Transistors". In: *Phys. Rev.* 83 (1951), pp. 151–162. DOI: 10.1103/PhysRev.83.151 (cit. on p. 177).
- [75] Charles Kittel. *Introduction to Solid State Physics, 7th edition*. Wiley, 1995 (cit. on p. 177).
- [76] A. G. Aberle. "Surface passivation of crystalline silicon solar cells: a review". In: *Progress in Photovoltaics: Research & applications* 8 (2000), pp. 473–487. DOI: 10.1002/1099-159X(200009/10)8:5<473::AID-PIP337>3.0.CO;2-D (cit. on p. 177).
- [77] B. Jenichen, V. M. Kaganer, R. Shayduk, W. Braun, and A. Trampert. "Heteroepitaxial growth of lattice matched films on GaAs(001)". In: *physica status solidi (a)* 206 (2009), pp. 1740–1743. DOI: 10.1002/pssa.200881582 (cit. on p. 177).
- [78] R.A. Outlaw and P. Hopson Jr. "Free-standing thin Ge single crystals grown by plasma-enhanced chemical vapor deposition". In: *Journal of Applied Physics* 55 (1984), pp. 1461–1463. DOI: 10.1063/1.333401 (cit. on p. 177).
- [79] J. H. Parker, D. W. Feldman, and M. Ashkin. "Raman Scattering by Silicon and Germanium". In: *Phys. Rev.* 155 (1967), pp. 712–714. DOI: 10.1103/PhysRev.155.712 (cit. on pp. 178, 182).
- [80] D. Bermejo and M. Cardona. "Raman scattering in pure and hydrogenated amorphous germanium and silicon". In: *Journal of Non-Crystalline Solids* 32 (1979), pp. 405–419. DOI: 10.1016/0022-3093(79)90085-1 (cit. on pp. 178, 179).
- [81] A. V. Kolobov. "Raman scattering from Ge nanostructures grown on Si substrates: Power and limitations". In: *Journal of Applied Physics* 87 (2000), pp. 2926–2930. DOI: 10.1063/1.372279 (cit. on p. 178).

- [82] B. Drévilion and C. Godet. "In situ investigation of the microcrystalline germanium nucleation and growth processes". In: *Journal of Applied Physics* 64 (1988), pp. 145–151. DOI: 10.1063/1.341447 (cit. on p. 179).
- [83] G. E. Jr. Jellison, M. F. Chisholm, and S. M. Gorbatkin. "Optical functions of chemical vapor deposited thin-film silicon determined by spectroscopic ellipsometry". In: *Applied Physics Letters* 62 (1993), pp. 3348–3350. DOI: 10.1063/1.109067 (cit. on p. 181).
- [84] D. E. Aspnes and A. A. Studna. "Dielectric functions and optical parameters of Si, Ge, GaP, GaAs, GaSb, InP, InAs, and InSb from 1.5 to 6.0 eV". In: *Phys. Rev. B* 27 (1983), p. 985. DOI: 10.1103/PhysRevB.27.985 (cit. on p. 181).

CONCLUSION

Thermal oxide is the natural passivation scheme for crystalline silicon but during this PhD thesis, we have investigated various passivation schemes based on a-Si:H materials elaborated by low temperature plasma processes ($\approx 200^\circ\text{C}$) and applied them to heterojunction solar cells. Having demonstrated the negative effect of the epitaxial buffer layers, we have investigated various ways to hinder it and grow purely amorphous silicon films on any silicon orientations.

i) Low temperature depositions, down to 100°C , coupled to post-deposition annealings, up to 250°C , have demonstrated a great potential in terms of passivation but failed to yield sufficient passivation in the case of (i/p) a-Si:H stacks.

ii) Plasma treatments of the silicon surface by argon or ammonia plasmas have proved to prevent epitaxial growth but to be either not sufficient to achieve the lowest surface recombination (argon) or to hinder the hole collection by the nitridation of the interface (ammonia).

iii) Alloying a-Si:H with carbon in the early stages of the deposition was the most robust, simple and reproducible way to hinder epitaxial growth while allowing to reach surface recombination velocities as low as $2\text{ cm}\cdot\text{s}^{-1}$, that none of the two first experiments could attain.

Based on that we have been able to optimize (n) a-Si:H and (p) a-Si:H in terms of surface passivation and solar cell characteristics. (n) a-Si:H layers were much less troublesome than (p) a-Si:H which had to be grown in argon dilution to allow for the lowest surface recombination velocities. Incorporated into solar cells, these layers resulted in V_{oc} above 710 mV and allowed to obtain efficiencies exceeding 17%. There is still room for improvement and for the study of other materials of smaller absorption coefficient. For instance, our reactor allows us to investigate (p) a-SiC_x:H or (p) a-SiO_x:H materials. It should be noted that some studies were performed on (p) $\mu\text{c-Si:H}$ layers that gave promising results in passivation but resulted in S-shaped characteristics due to the presence of incubation layers. A successful implementation of such layers would require further optimization to reduce the incubation layer phase without damaging the (i) a-Si:H buffer layer and the interface. Such optimization could be based on the use of a different chemistry, for instance based on SiF₄ for which large grain (p) $\mu\text{c-Si:H}$ layers can be grown with no incubation phase. It can also be thought of (p) $\mu\text{c-SiC:H}$ films which have already been used for efficient a-Si:H p-i-n by the Jülich group.

These processes could be transferred, with efficiency losses, to multicrystalline silicon substrates. However, the outsourced cleaning of the surface was identified as the step limiting the efficiency. Also, on (p) c-Si wafers, solar cells with back point-contacts realized by the laser firing of an aluminium film through an a-SiC_x:H layer have shown interesting po-

tential on highly doped p-type wafers. Finally, replacing the native oxide removal done by the conventional HF-dip by a plasma etching based on SiF_4 was successfully implemented, resulting in solar cells with a best V_{oc} of 698 mV. This goes beyond the proof of concept and opens the way to completely dry, one pump-down process, for heterojunction solar cells. A future cluster tool, equipped with in-situ ellipsometers will allow further optimization of this process based on real-time ellipsometry. It could also be considered to grow a-Si:H films from SiF_4 , diluted H_2 and Ar gas mixtures, so that a process entirely based on SiF_4 could be developed. Finally, a transfer to textured wafers is still to be achieved.

In parallel to that, this PhD thesis was also devoted to the study of the epitaxial growth of silicon and germanium films on (100)-oriented silicon substrates. Spectroscopic ellipsometry, Raman spectroscopy and Transmission Electron Microscopy could provide a comprehensive picture demonstrating the single crystal nature of our films. Silicon films could also be doped p-type successfully and n-type with less ease. Carrier mobility and concentration were studied by Hall effect measurements. Such films could be incorporated in epitaxial solar cells in the case of undoped films where they acted as the epitaxial absorber, grown on highly p-doped wafers used as contacts, and demonstrated an efficiency of 7% for a 2.4 μm thick epitaxial absorber layer. On (n) c-Si, we could grow a p-type homojunction emitter that resulted in a 14.2% cell efficiency. These promising results can provide the basis for future works including the fabrication of epitaxial germanium solar cells, or the implementation of an entire homojunction solar cell with passivation schemes based on a-SiN_x:H. Little imagination is required to consider the possibility of making multi-junction solar cells. However, making them efficient will require strong research efforts in coming years and one PhD thesis has already started on this topic.

LIST OF PUBLICATIONS

Peer reviewed publications

- [1] R. Chouffot, A. Brezard-Oudot, J.-P. Kleider, R. Brüggemann, M. Labrune, P. Roca i Cabarrocas, and P.-J. Ribeyron. "Modulated photoluminescence as an effective lifetime measurement method: Application to a-Si:H/c-Si heterojunction solar cells". In: *Materials Science and Engineering: B* 159-160 (2009), pp. 186–189. ISSN: 0921-5107. DOI: 10.1016/j.mseb.2008.10.038.
- [2] J.-P. Kleider, R. Chouffot, A.S. Gudovskikh, P. Roca i Cabarrocas, M. Labrune, P.-J. Ribeyron, and R. Brüggemann. "Electronic and structural properties of the amorphous/crystalline silicon interface". In: *Thin Solid Films* 517.23 (2009). Proceedings on the Sixth Symposium on Thin Films for Large Area Electronics, pp. 6386–6391. ISSN: 0040-6090. DOI: 10.1016/j.tsf.2009.02.092.
- [3] M. Moreno, M. Labrune, and P. Roca i Cabarrocas. "Dry fabrication process for heterojunction solar cells through in-situ plasma cleaning and passivation". In: *Solar Energy Materials & Solar Cells* 94 (2010), pp. 402–405. ISSN: 0927-0248. DOI: 10.1016/j.solmat.2009.10.016.
- [4] M. Labrune, M. Moreno, and P. Roca i Cabarrocas. "Ultra-shallow junctions formed by quasi-epitaxial growth of boron and phosphorous-doped silicon films at 175°C by rf-PECVD". In: *Thin Solid Films* 518 (2010), pp. 2528–2530. ISSN: 0040-6090. DOI: 10.1016/j.tsf.2009.09.143.
- [5] W. Favre, M. Labrune, F. Dadouche, A. S. Gudovskikh, P. Roca i Cabarrocas, and J.-P. Kleider. "Study of the interfacial properties of amorphous silicon/n-type crystalline silicon heterojunction through static planar conductance measurements". In: *physica status solidi (c)* 7 (2010), pp. 1037–1040. DOI: 10.1002/pssc.200982800.
- [6] J.-P. Kleider, J. Alvarez, A.V. Andkudinov, A.S. Gudovskikh, E.V. Gushina, M. Labrune, O. Maslova, W. Favre, M.-E. Gueunier-Farret, P. Roca i Cabarrocas, and E.I. Terukov. "Characterization of silicon heterojunction for solar cells". In: *Nanoscale Research Letters* 6 (2011), p. 152. DOI: 10.1186/1556-276X-6-152.
- [7] R. Cariou, M. Labrune, and P. Roca i Cabarrocas. "Thin crystalline silicon solar cells based on epitaxial films grown at 165°C by RF PECVD". In: *Solar Energy Materials & Solar Cells* 95 (2011), pp. 2260–2263. DOI: 10.1016/j.solmat.2011.03.038.

- [8] I. Martín, M Labrune, A Salomon, P. Roca i Cabarrocas, and R. Alcubilla. "Laser fired contacts applied to the rear surface of heterojunction silicon solar cells". In: *Accepted for publication in Solar Energy Materials & Solar Cells* (2011).

Patent filed

- [9] M. Labrune and P. Roca i Cabarrocas. "Cellule photovoltaïque hétérojonction à contact arrière". French. Pat. 0958922. 2010.

Conference proceedings

- [10] M. Labrune, P. Roca i Cabarrocas, R. Chouffot, A. Brezard-Oudot, J.-P. Kleider, P.-J. Ribeyron, A. Vandeneynde, and R. Brüggemann. "Polymorphous/crystalline silicon heterojunction solar cells: optimization on monocrystalline silicon". In: *23rd European Photovoltaic Solar Energy Conference, 1-5 September, Valencia, Spain*. 2008.
- [11] S. Amtablian, M. Labrune, P. Carroy, J. Dupuis, E. Fourmond, A. Kaminski, A. Fave, P. Roca i Cabarrocas, P.-J. Ribeyron, and M. Lemiti. "a-Si:H/c-Si heterojunction solar cells on 50 μm thick wafers with rear point contacts". In: *23rd European Photovoltaic Solar Energy Conference, 1-5 September, Valencia, Spain*. 2008.
- [12] T. Desrues, P.-J. Ribeyron, A. Vandeneynde, A.-S. Ozanne, F. Souche, Y. Veschetti, A. Bettinelli, P. Roca i Cabarrocas, M. Labrune, D. Diouf, J.-P. Kleider, and M. Lemiti. "New process intergration for interdigitated back contact (IBC) a-Si:H/c-Si heterojunction solar cells". In: *23rd European Photovoltaic Solar Energy Conference, 1-5 September, Valencia, Spain*. 2008.
- [13] P.-J. Ribeyron, T. Desrues, A. Vandeneynde, F. Souche, A.-S. Ozanne, M. Labrune, P. Roca i Cabarrocas, R. Chouffot, and J.-P. Kleider. "Silicon heterojunction solar cells: surface passivation quality on large area n type and p type monocrystalline silicon". In: *23rd European Photovoltaic Solar Energy Conference, 1-5 September, Valencia, Spain*. 2008.
- [14] A. Datta, M. Rahmouni, P. Roca i Cabarrocas, M. Labrune, and P. Chatterjee. "Influence of the amorphous/ crystalline band discontinuity on hole transport in P-a-Si:H/ N-c-Si front heterojunction solar cells". In: *Proceedings of the 18th International Photovoltaic Science and Engineering Conference, 19-23 January, Kolkata, India*. 2009.
- [15] J. Damon-Lacoste, M. Labrune, S. Granata, D. Daineka, and P. Roca i Cabarrocas. "Crystalline silicon solar cells with doped epitaxial silicon films obtained at low-temperature by PECVD". In: *35th IEEE Photovoltaic Specialists Conference, Hawaii, 20-25 June*. 2010.
- [16] M. Labrune, J. Damon-Lacoste, D. Daineka, and P. Roca i Cabarrocas. "Epitaxial growth of doped crystalline silicon films (n and p-type) on crystalline silicon wafers at low substrate temperatures by RF-PECVD". In: *25th European Photovoltaic Solar Energy Conference, 6-10 September, Valencia, Spain*. 2010.

- [17] A. Salomon, M. Labrune, J. Damon-Lacoste, M. Moreno, and P. Roca i Cabarrocas. "In-situ cleaning for high efficiency silicon heterojunction solar cells". In: *25th European Photovoltaic Solar Energy Conference, 6-10 September, Valencia, Spain*. 2010.
- [18] W. Favre, M. Labrune, F. Dadouche, A.S. Gudovskikh, P. Roca i Cabarrocas, and J.-P. Kleider. "Study of the interfacial properties of amorphous silicon/n-type crystalline silicon heterojunction through static planar conductance measurements". In: *23rd ICANS, Utrecht, The Netherlands*. 2010.
- [19] W. Favre, C. Pareige, J.-P. Kleider, M. Labrune, P. Roca i Cabarrocas, T. Schutz-Kuchly, and Y. Veschetti. "Optical and electrical characterization of silicon heterojunctions with n-type multicrystalline substrate: towards a low cost heterojunction solar cell". In: *25th European Photovoltaic Solar Energy Conference, 6-10 September, Valencia, Spain*. 2010.

Abstract

This thesis presents a work which has been devoted to the growth of silicon thin films on crystalline silicon for photovoltaic applications by means of RF PECVD. The primary goal of this work was to obtain an amorphous growth on any c-Si surface in order to provide an efficient passivation, as required in heterojunction solar cells. Indeed, we demonstrated that epitaxial or mixed phase growths, easy to obtain on (100) Si, would lead to poor surface passivation. We proved that growing a few nm thin a-Si_{1-x}C_x:H alloy film was an efficient, stable and reproducible way to hinder epitaxy while keeping an excellent surface passivation by the subsequent deposition of a-Si:H films. Process optimization mainly based on Spectroscopic Ellipsometry, Effective lifetime measurements (Sinton lifetime tester) and current-voltage characterization led us to demonstrate that it was possible to obtain a-Si:H/c-Si heterojunction solar cells with stable V_{OC} of 710 mV and FF of 76 % on flat (n) c-Si wafers, with solar cells of 25 cm² whose metallization was realized by screen-printing technology. This work has also demonstrated the viability of a completely dry process where the native oxide is removed by SiF₄ plasma etching instead of the wet HF removal. Last but not least, the epitaxial growth of silicon thin films, undoped and n or p-type doped, on (100)-oriented surfaces has been studied by Spectroscopic Ellipsometry and Hall effect measurements. We have been able to fabricate homojunction solar cells with a p-type emitter as well as p-i-n structures with an undoped epitaxial absorber on a heavily-doped (p) c-Si wafers.

Keywords: amorphous silicon, crystalline silicon, surface passivation, heterojunction, epitaxy, PECVD

Résumé

Cette thèse est le résultat d'un travail dédié à la croissance par PECVD de couches minces de silicium sur des substrats de silicium cristallin pour des applications photovoltaïques. L'objectif premier était d'obtenir une croissance amorphe sur toutes les orientations cristallines possibles afin de passiver efficacement les surfaces de silicium, prérequis indispensable à l'obtention de cellules solaires à hétérojonction efficaces. Nous avons en effet montré qu'une croissance épitaxiale, ou microcristalline, très faciles à obtenir sur (100) conduisait à une piètre passivation. Nous avons aussi montré que faire croître une couche de quelques nanomètres seulement d'alliage a-Si_{1-x}C_x:H permettait d'éviter, de manière robuste et reproductible la croissance épitaxiale, tout en permettant d'obtenir des passivations excellentes en déposant ensuite des couches minces d'a-Si:H. Une optimisation principalement basée sur des mesures d'ellipsométrie spectroscopique, de durée de vie effective (Sinton) et de caractéristiques courant-tension, nous ont permis d'obtenir des cellules à hétérojonctions a-Si:H/c-Si de 25 cm² avec des V_{CO} et des FF stables de 710 mV et 76 % respectivement sur des substrats lisses de (n) c-Si, dont les contacts étaient réalisés par sérigraphie de pâtes d'aluminium à basse température. Ce travail a aussi permis d'apporter la preuve du concept de cellules entièrement réalisées par voie sèche, i.e. dont l'oxyde natif est gravé par un plasma de SiF₄ au lieu d'une trempe HF. Enfin, la croissance épitaxiale de couches de silicium, non-dopé et dopé n et p, sur des surfaces orientées (100) a été étudiée par ellipsométrie et mesures par effet Hall. Nous avons été en mesure de produire des cellules cristallines dont l'émetteur de type P était épitaxié ainsi que des cellules de type p-i-n dont l'absorbeur était constitué par une couche non-dopée épitaxiée de silicium, déposé sur un substrat (100) très dopé au bore.

Mots-clés : silicium amorphe, silicium cristallin, passivation de surface, hétérojonction, épitaxie, PECVD